THE UNIVERSITY OF HULL

Performance Assessment and Optimisation of a Novel Guideless Irregular Dew Point Cooler using Artificial Intelligence

being a Thesis submitted for the Degree of Doctor of Philosophy

at the University of Hull

By

Yousef Golizadeh Akhlaghi

November 2020

TABLE OF CONTENTS

PUBLICATIONS

Journal publications

1. **Golizadeh Akhlaghi Yousef**, Aslansefat K, Zhao X, Sadati S, Badiei A, Xiao X, et al. Hourly performance forecast of a dew point cooler using explainable Artificial Intelligence and evolutionary optimisations by 2050. Appl Energy 2021;281:116062. https://doi.org/10.1016/j.apenergy.2020.116062.

2. **Golizadeh Akhlaghi Yousef**, Badiei A, Zhao X, Aslansefat K, Xiao X, Shittu S, et al. A constraint multi-objective evolutionary optimization of a state-of-the-art dew point cooler using digital twins. Energy Conversion and Manage. 2020;211:112772. doi:10.1016/j.enconman.2020.112772.

3. **Golizadeh Akhlaghi Yousef**, Zhao X, Shittu S, Badiei A, Cattaneo MEGV, Ma X. Statistical investigation of a dehumidification system performance using Gaussian process regression. Energy Build 2019;202:109406. doi:10.1016/j.enbuild.2019.109406.

4. **Golizadeh Akhlaghi Yousef**, Ma X, Zhao X, Shittu S, Li J. A statistical model for dew point air cooler based on the multiple polynomial regression approach. Energy 2019;181:868–81. doi:10.1016/j.energy.2019.05.213.

5. Badiei A, **Golizadeh Akhlaghi Yousef**, Zhao X, Li J, Yi F, Wang Z. Can whole building energy models outperform numerical models, when forecasting performance of indirect evaporative cooling systems? Energy Convers Manag 2020;213. https://doi.org/10.1016/j.enconman.2020.112886.

6. Liu Y, **Golizadeh Akhlaghi Yousef**, Zhao X, Li J. Experimental and numerical investigation of a high-efficiency dew-point evaporative cooler. Energy Build 2019;197:120–30.

https://doi.org/10.1016/j.enbuild.2019.05.038.

7. Badiei A, **Golizadeh Akhlaghi Yousef**, Zhao X, Shittu S, Xiao X, Li J, et al. A chronological review of advances in solar assisted heat pump technology in 21st century. Renew Sustain Energy Rev 2020;132. doi:10.1016/j.rser.2020.110132.

8. Lu Y, Li G, **Golizadeh Akhlaghi Yousef**, Xuan Q, Pei G, Ji J, et al. Effect of grid and optimization on improving the electrical performance of compound parabolic concentrator photovoltaic cells. Sol Energy 2020;196:607–15. https://doi.org/10.1016/j.solener.2019.12.065.

9. Fan Y, Zhao X, Li J, Li G, Myers S, Cheng Y, Badiei A, Yu M, **Yousef Golizadeh Akhlaghi**, Shittu S, Ma X. Economic and environmental analysis of a novel rural house heating and cooling system using a solar-assisted vapour injection heat pump. Appl Energy 2020;275:115323. doi:10.1016/j.apenergy.2020.115323.

10. Sohani A, Naderi S, Torabi F, Sayyaadi H, **Golizadeh Akhlaghi Yousef**, Zhao X, et al. Application based multi-objective performance optimization of a proton exchange membrane fuel cell. J Clean Prod 2020;252:119567. https://doi.org/10.1016/j.jclepro.2019.119567.

11. Li G, Lu Y, Xuan Q, **Golizadeh Akhlaghi Yousef**, Pei G, Ji J, et al. Small scale optimization in crystalline silicon solar cell on efficiency enhancement of low-concentrating photovoltaic cell. Sol Energy 2020;202. https://doi.org/10.1016/j.solener.2020.03.094.

12. Shittu S, Li G, Xuan Q, Xiao X, Zhao X, Ma X, **Golizadeh Akhlaghi Yousef**. Transient and non-uniform heat flux effect on solar thermoelectric generator with phase change material. Appl Therm Eng 2020;173:115206. https://doi.org/10.1016/j.applthermaleng.2020.115206.

13. Shittu S, Li G, Zhao X, Ma X, **Yousef Golizadeh Akhlaghi**, Ayodele E. High performance and thermal stress analysis of a segmented annular thermoelectric generator. Energy Convers Manag 2019;184:180–93. doi:10.1016/j.enconman.2019.01.064.

14. Shittu S, Li G, Zhao X, **Akhlaghi YG**, Ma X, Yu M. Comparative study of a concentrated photovoltaic-thermoelectric system with and without flat plate heat pipe. Energy Convers Manag 2019;193:1–14. doi:10.1016/j.enconman.2019.04.055.

15. Shittu S, Li G, Zhao X, Ma X, **Akhlaghi YG**, Ayodele E. Optimized high performance thermoelectric generator with combined segmented and asymmetrical legs under pulsed heat input power. J Power Sources 2019;428:53–66. doi:10.1016/j.jpowsour.2019.04.099.

16. Shittu S, Li G, **Akhlaghi YG**, Ma X, Zhao X, Ayodele E. Advancements in thermoelectric generators for enhanced hybrid photovoltaic system performance. Renew Sustain Energy Rev 2019;109:24–54. doi:10.1016/j.rser.2019.04.023.

17. Li G, Diallo TMO, **Akhlaghi YG**, Shittu S, Zhao X, Ma X, et al. Simulation and experiment on thermal performance of a micro-channel heat pipe under different evaporator temperatures and tilt angles. Energy 2019;179:549–57. doi:10.1016/j.energy.2019.05.040.

Conference publications

1. **Yousef Golizadeh Akhlaghi**, Ali Badiei, Xudong Zhao , "A Novel Mathematical Model of the Solar Assisted Dehumidification and Regeneration Systems, Kuala Lumpur, 18th International Conference on Sustainable Energy Technologies (Kuala Lumpur, Malaysia, 20-22 August 2019)

2. **Yousef Golizadeh Akhlaghi**, Xudong Zhao, Xiaoli Ma, "Development of an analytical model for a counter flow dew point cooler", 17th International Conference on Sustainable Energy Technologies (Wuhan, China, 21-23 August 2018)

3. Yi Fan, Xudong Zhao, Jing Li, Guiqiang Li, Min Yu, Yuanda Cheng, **Yousef Golizadeh Akhlaghi** "ENERGY, ECONOMIC AND ENVIRONMENTAL PERFORMANCE ANALYSIS OF A NOVEL SOLAR-POWERED ZERO-BILL RURAL HOUSE SPACE HEATING SYSTEM", International Conference on Applied Energy 2019, Aug 12-15, 2019, Västerås, Sweden.

ACKOWLEDGEMENT

ABSTRACT

Air Conditioners (ACs) are a vital need in modern buildings to provide comfortable indoor air for the occupants. Several alternatives for the traditional coolers are introduced to improve the cooling efficiency but among them, Evaporative Coolers (ECs) absorbed more attention owing to their intelligible structure and high efficiency. ECs are categorized into two types, i.e., Direct Evaporative Coolers (DECs) and Indirect Evaporative Coolers (IECs). Continuous endeavours in the improvement of the ECs resulted in development of Dew Point Coolers (DPCs) which enable the supply air to reach the dew point temperature. The main innovation of DPCs relies on invention of a M-cycle Heat and Mass Exchanger (HMX) which contributes towards improvement of the ECs' efficiency by up to 30%. A state-of-the-art counter flow DPC in which the flat plates in traditional HMXs are replaced by the corrugated plates is called Guideless Irregular DPC (GIDPC). This technology has 30-60% more cooling efficiency compared to the flat plate HMX in traditional DPCs.

Owing to the empirical success of the Artificial Intelligence (AI) in different fields and enhanced importance of Machine Learning (ML) models, this study pioneers in developing two ML models using Multiple Polynomial Regression (MPR), and Deep Neural Network (DNN) methods, and three Multi Objective Evolutionary Optimisation (MOEO) models using Genetic Algorithms (GA), Particle Swarm Optimisation (PSO), and a novel bio-inspired algorithm, i.e., Slime Mould Algorithm (SMA), for the performance prediction and optimisation of the GIDPC in all possible operating climates. Furthermore, this study pioneers in developing an explainable and interpretable DNN model for the GIDPC. To this end, a game theory-based SHapley

ABSTRACT

Additive exPlanations (SHAP) method is used to interpret contribution of the operating conditions on performance parameters.

The ML models, take the intake air characteristic as well as main operating and design parameters of the HMX as inputs of the ML models to predict the GIDPC's performance parameters, e.g., cooling capacity, coefficient of performance (COP), thermal efficiencies. The results revealed that both models have high prediction accuracies where MPR performs with a maximum average error of 1.22%. In addition, the Mean Square Error (MSE) of the selected DNN model is only 0.04. The objectives of the MOEO models are to simultaneously maximise the cooling efficiency and minimise the construction cost of the GIDPC by determining the optimum values of the selected decision variables.

The performance of the optimised GIDPCs is compared in a deterministic way in which the comparisons are carried out in diverse climates in 2020 and 2050 in which the hourly future weather data are projected using a high-emission scenario defined by Intergovernmental Panel for Climate Change (IPCC). The results revealed that the hourly COP of the optimised systems outperforms the base design. Moreover, although power consumption of all systems increases from 2020 to 2050, owing to more operating hours as a result of global warming, but power savings of up to 72%, 69.49%, 63.24%, and 69.21% in hot summer continental, arid, tropical rainforest and Mediterranean hot summer climates respectively, can be achieved compared to the base system when the systems run optimally.

NOMENCLATURE

A	area, m^2
C_p	specific heat capacity, kJ/(kg°C)
COP	coefficient of performance
dp	dew point
Dh	hydraulic diameter, m
De	Equivalent diameter, m
en	Latent heat, kJ/kg
G	Channel gap, m
h	Convection coefficient, W/(m²°C)
h_m	mass transfer coefficient, m/s
H	channel height, m
hum	humidity ratio, kg/kg
i	enthalpy, kJ/kg
Le	Lewis number
Nu	Nusselt number
N_L	number of layers
P	pressure, Pa
$Q_{cooling}$	cooling capacity, W
Q	heat transfer, W
Q_m	mass flow rate, kg/s
Re	Reynolds number
RH	relative humidity
dry	dry channel

T	temperature, °C
air	air
U	air velocity, m/s
dp	dew point
Subscripts	
W	electric power, kW
fan	fan
in	inlet
out	outlet
pump	pump
s	surface
steam	water steam
vap	evaporated water
water	water
wet	wet channel
w	wall
wb	wet bulb
Greek symbols	
λ	Thermal conduction coefficient, kW/(m °C)
σ	Surface wettability factor
φ	working air fraction over the intake air
ε	efficiency
ρ	density, kg/m^3
Le	Lewis number
Δ	difference between two states

λ_f	coefficient of friction resistance
ξ	coefficient of local resistance
ξ	coefficient of local resistance

Abbreviations

AC	Air conditioning
AI	Artificial intelligence
COP	coefficient of performance
DC	Data centre
DEC	Direct evaporative cooler
DNN	Deep neural network
DPC	guideless irregular dew point cooler
EC	Evaporative cooler
EO	Evolutionary optimisation
GA	Genetic algorithm
GIDPC	Guideless Irregular Dew Point Cooler
HMX	Heat and mass exchanger
HVAC	Heating, Ventilation, and Air-Conditioning
IEC	indirect evaporative cooling
IPCC	Intergovernmental Panel for Climate Change
ML	Machine learning
MOEO	Multi objective evolutionary optimization
MPR	Multiple polynomial regression
MSE	Mean square error
MVC	Mechanical vapour compression
PSO	Particle swarm optimisation

SHAP	SHapley Additive exPlanations
SMA	Slime mould algorithm

LIST OF FIGURES

LIST OF TABLES

CHAPTER 1: INTRODUCTION

1.1. Background

Thermal comfort of occupants in all types of buildings, particularly in residential and industrial buildings has become an indispensable research field over the recent years. To provide comfortable indoor condition, air conditioners are the commonly used devices in modern buildings which are responsible for the major part of the energy supplied to the buildings, i.e., up to 50% [1]. For instance, as shown in **Figure 1.1,** the air conditioners are the leading energy consumers in office buildings. Additionally, **Figure 1.2** shows the energy consumption in buildings across Europe which indicates the big share of space heating in total energy consumption in the countries where the detailed data are available.
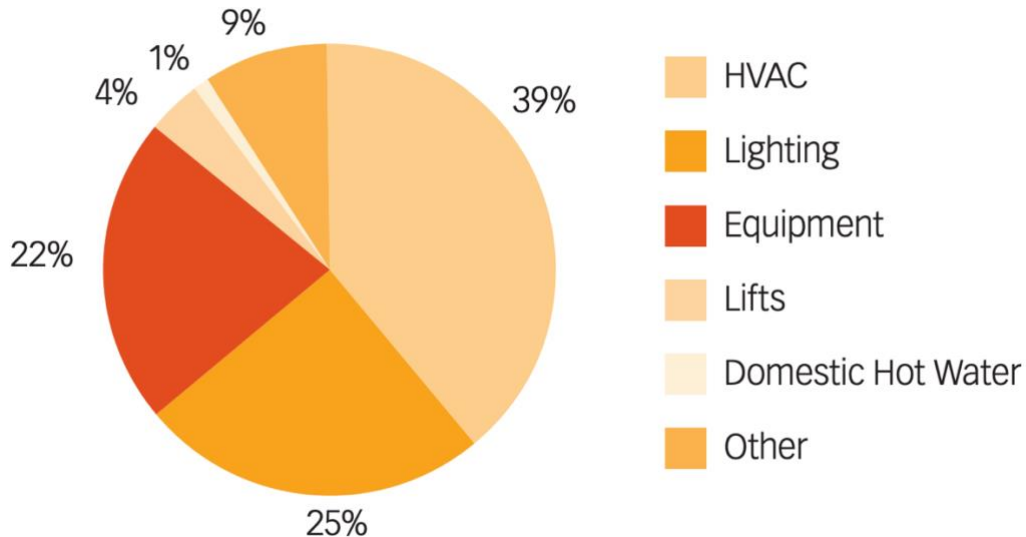
Figure 1.1: Energy consumption breakdown in office buildings [2]

It has been estimated that the total energy consumption in buildings will be increased by 34% until 2035 [3]. This can lead to more greenhouse gases emissions as a result of more energy supply to the buildings. Out of six major greenhouse gases, the CO_2

has the largest share among the other five gases which is needed to be managed by imposition of restricting measures. This was the main objective of the 2015 Paris agreement (2015 United Nations Climate Change Conference) [4], [5] in which the global warming was aimed to be controlled by limiting the temperature increase to less than 2°C. Although, the inevitable temperature increase will result in more demand for Heating, Ventilation, and Air-Conditioning (HVAC) systems but in advance restriction measures can pave the path towards the development of environmentally friendly HVACs.
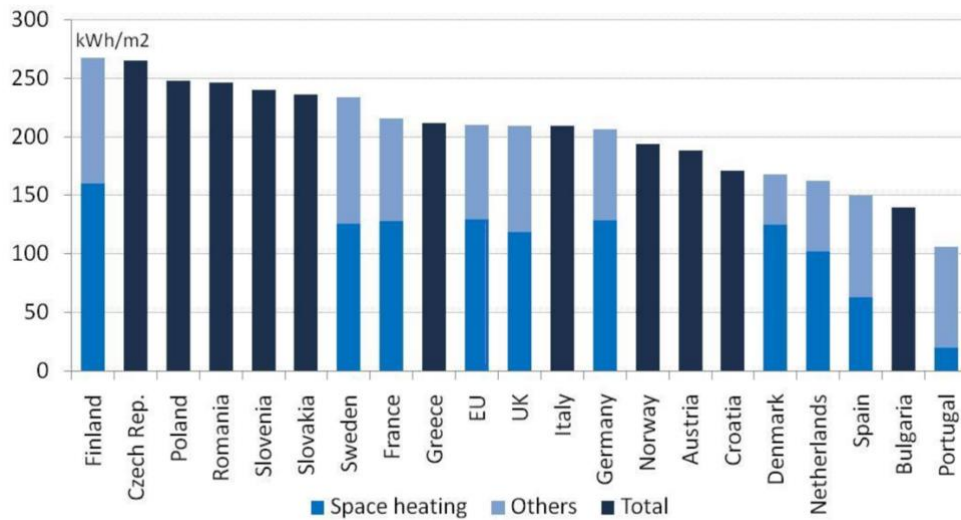
Figure 1.2: Energy consumption in buildings in European countries in 2012 [6]

In order to achieve the UK net zero carbon emission target by 2050, the implementation of efficient Air Conditioning (AC) systems are required to pave the path to make the determined objective attainable. **Figure 1.3** illustrates the share of global energy consumption and CO_2 emission by sector in 2015. The buildings account for 30% of energy consumption and 28% of CO_2 emission globally. Although the ACs account for 10% of the total electricity consumption around the world but demand for the ACs is estimated to increase over the next decades which will make the ACs top energy electricity consumers. The statistics and the estimations revealed

that the cooling market will substantially grow over the years in which it is expected to grow up to £20 billion in 2024. In a similar manner, the Dew Point Coolers (DPCs), as the latest Evaporative Coolers (ECs), market is expected to grow up to £6 billion in 2024. **Figure 1.4** shows the global growth of the ECs and in particular DPCs annually [7]. As a consequence, in addition to the essence of constructing more efficient buildings, the current ACs are needed to get optimised by the aim of operating in their full potential.
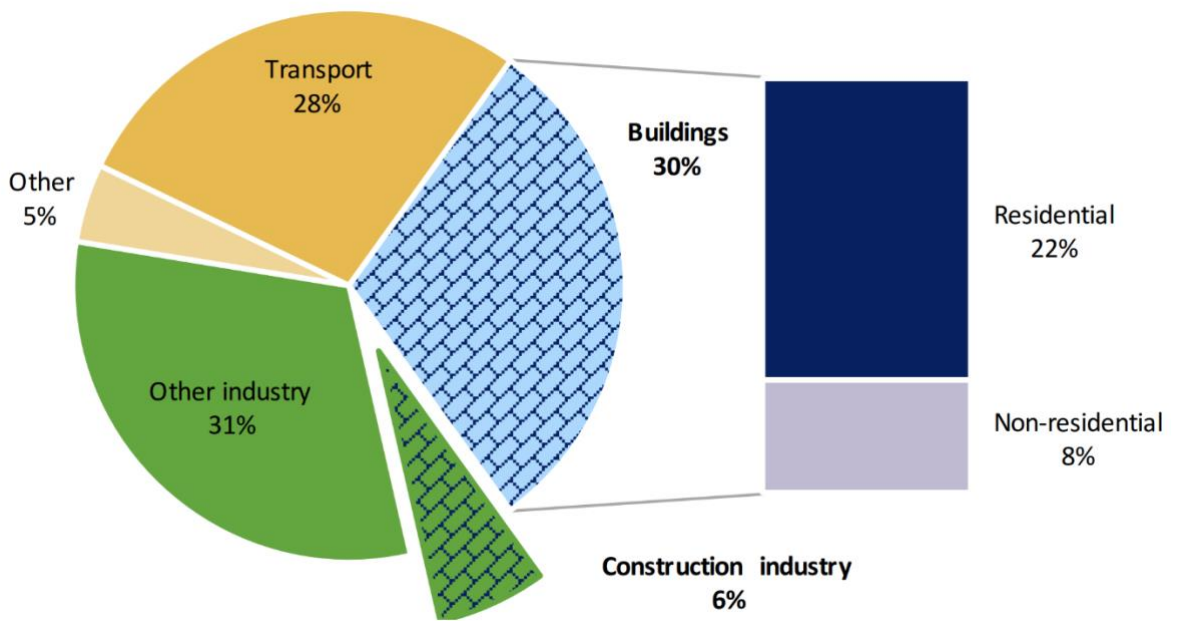
(a)
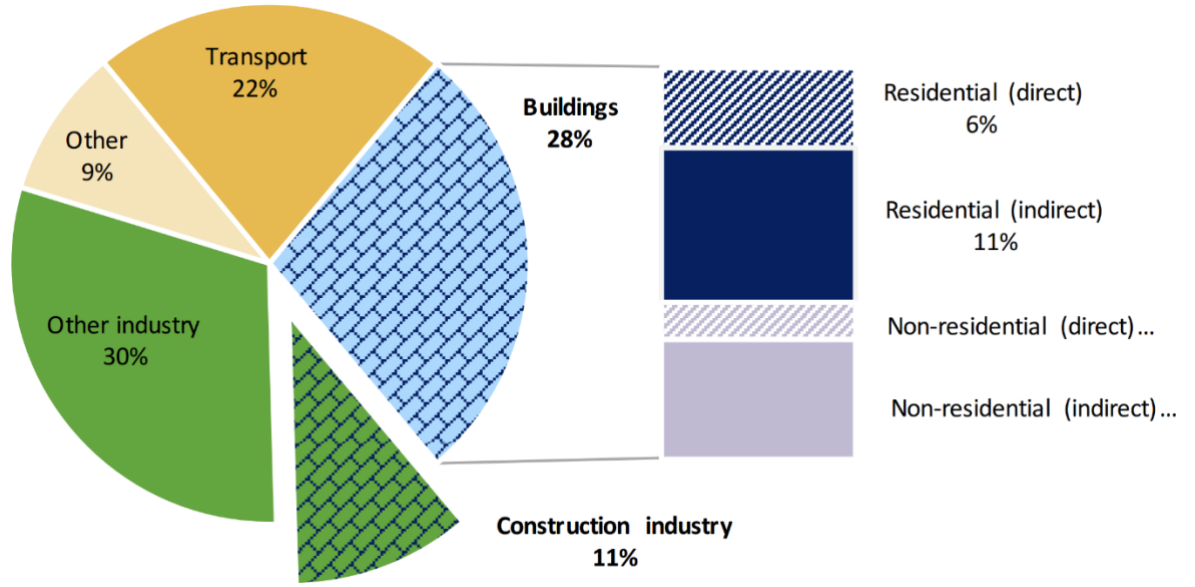
(b)

Figure 1.3: (a): Share of global energy consumption; (b): Share of global CO$_2$ emission [8]**.**
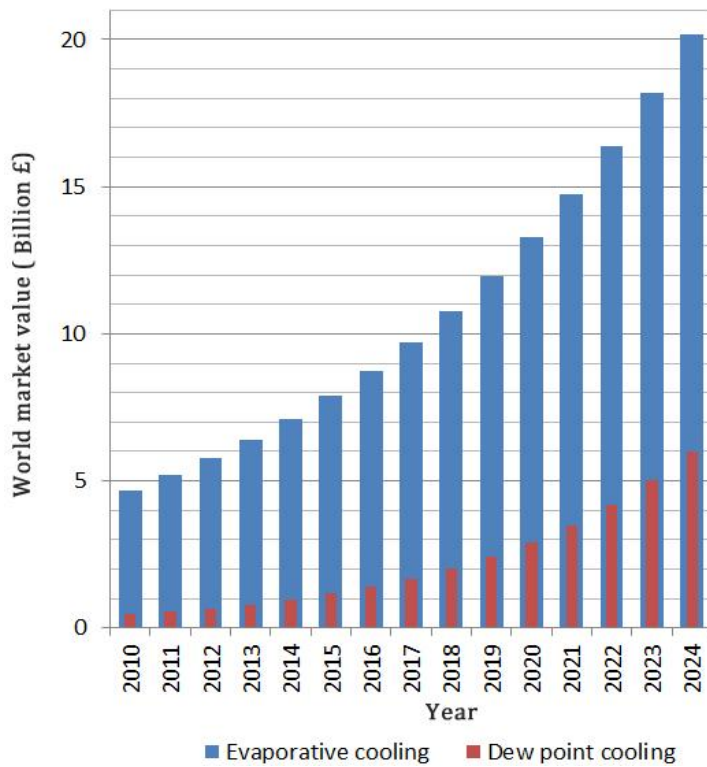
Figure 1.4: Cooling market growth from 2010 to 2024 [9]**.**

Energy intensiveness of the conventional Mechanical Vapour Compression (MVC) systems [7], plays a key role in energy intensiveness of the current cooling systems

with COP in the range of 2-4 [10]. MVCs comprise an evaporator, a condenser, a compressor and an expansion valve and a refrigerant which circulates within the system as a coolant fluid. Among which the energy intensive compressor results in an inefficient cooling system. Absorption and adsorption cooling system is introduced as the first replacement for the MVCs which operates needless of energy intensive compressors. However, requiring high temperature water or vapour and expensive chemicals are the undesirable features of the technology. This technology comprises a desiccant absorber, regenerator, condenser, evaporator, expansion valve and piping connections.

ECs with direct (DEC) and Indirect (IEC) types, were introduced as an environmentally friendly replacement cooling systems in the past decades [11], [12]. The ECs are simple in structure and working principle of them is based on water evaporation in which the sensible heat in the air is converted to the latent heat in an enthalpy-constant process. The heat transfer is done without energy intensive devices e.g., compressors, which makes the process efficient. These advantages have led to a significant leap forward in the efficiency of the cooling systems with an improved COP to the range of 15-20 [7]. The IECs are more preferred owing to their superior design structure in extracting the humidity from the cooled air which is supplied to the indoor environment [13], [14], whereas the DECs keep the water in direct contact with the supplied air which leads to a wetter environment.

One outstanding limitation that restricts the efficiency of the IECs, is the temperature of the intake air which can only be cooled down to the wet-bulb temperature. However, the efficiency can further be improved if the humidity of the intake air decreases substantially.

A continuous need for more efficient cooling systems resulted in development of DPCs. DPCs remove the aforementioned limitations with a remarkable potential in cooling down the intake air temperature to its dew point temperature [15], [16]. The M-cycle Heat and Mass Exchanger (HMX) was the core initiative of this technology which caused a significant decrease in dew point and wet-bulb temperatures of the air in the wet channel leading to up to 30% higher cooling efficiency [17]. DPC has two main types: cross flow and counter-flow [18]. **Figure 1.5** shows a cross flow heat exchanger while **Figure 1.6** shows a heat exchanger for a counter-flow DPC in which the flow direction within the HMX is the key difference. Different types of studies are in progress to improve the performance of the DPCs in order to improve the efficiency of the technology. To this end, a novel counter-flow Guideless Irregular DPC (GIDPC) was introduced in which the corrugated plates were replaced with the flat plates which led to the best performance in terms of COP value i.e., 52.5 [18, 19]. Moreover, airflow resistance is decreased by up to 56% and the heat transfer area is increased by up to 40% as a result of implementing the corrugated plates. Xu et al. [18] pioneered in introducing the technology through the numerical and experimental studies [19]. In this study, the aforementioned state-of-the-art DPC, which is called GIDPC, is considered as the main cooling system.
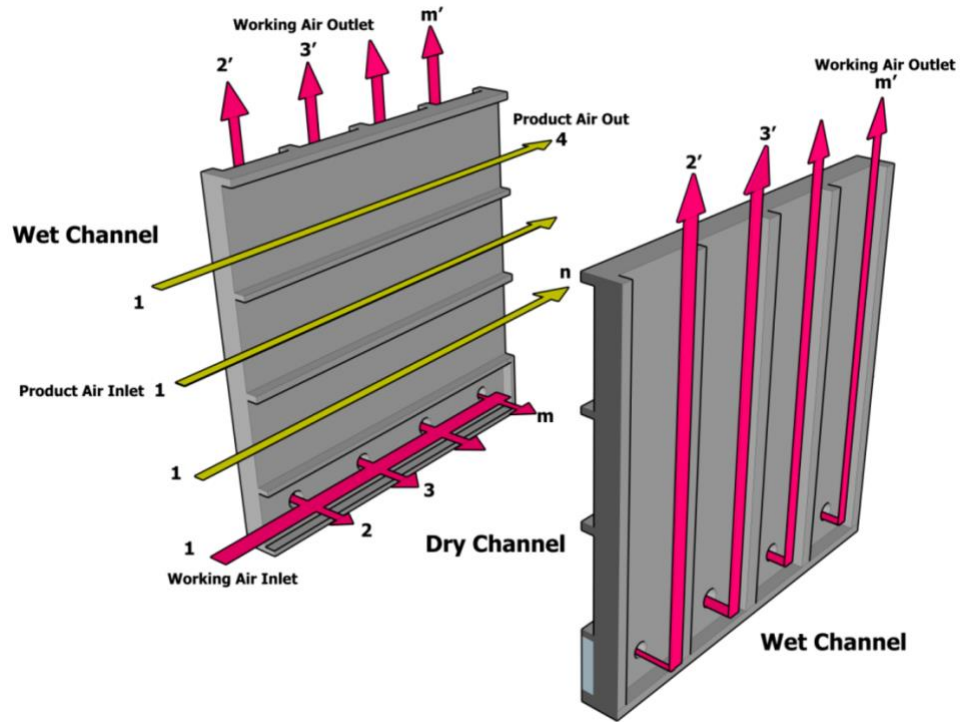
Figure 1.5: Cross flow DPC [19]
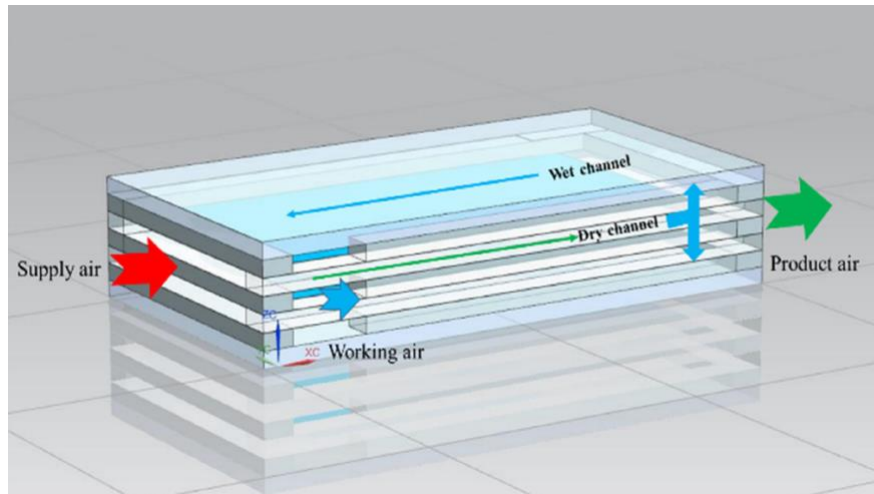
Figure 1.6: Counter-flow DPC [20]

1.2. Artificial Intelligence in Energy Systems

The Artificial Intelligence (AI) is a fast-growing smart area that has been an interesting topic for the research studies in different fields including energy technologies. In general, AI is inspired from the human brain's smart functionality which is able to solve the complex problems by reducing the burden of manual operations. In energy

systems, AI can be implemented to learn from previous performance of a particular system with the aim of predicting its behaviour through different mathematical algorithms [21]. The AI is used in various fields such as accounting, engineering, politics, production, medicine, and image recognition to make use of the historical informative data with the aim of developing data-driven predictive models. In addition, the necessity of presenting the full potential of the energy systems has led to the implementation of the optimisation algorithms to design and operate the systems optimally. Evolutionary Optimisation (EO) algorithms such as Genetic Algorithm (GA), and Particle Swarm Optimisation (PSO) are the most popular algorithms which have been used in different fields to optimise the system's performance in different operational circumstances. The success and impact of AI in its early trials have made the leading tech companies such as Google, Facebook and Apple to shift their research focus towards the AI models to assure the optimum and efficient operation of their systems. Apart from utilisation of the AI in different sectors, the endeavours in developing new algorithms and improving the existed methods are in progress which entail the consideration and investigation of the latest methods in new studies.

In this research, different AI based algorithms will be used for the GIDPC to firstly develop data-driven predictive models for the technology and additionally, to ensure the efficient and optimum design and operation of the system in different operating conditions.

1.3. Justification of research

Over the past decade, AI is brought into the energy systems which has led to outstanding success in the field but the cooling technology still suffers from a lack of data driven predictive models. Studies on DPC are mostly concentrated on the numerical and experimental approaches. However, the experimental models are cost-

intensive and limited to a single prototype with fixed dimensions. This situation has largely obstructed the wide and rational application of DPC technology in practical engineering where multiple parameters vary simultaneously across the wide ranges of data. Even though the numerical models are economical but it is often time-consuming to process the numerical models as they generally comprise complex differential equations. Apart from the aforementioned constraints, analysing the DPC in non-optimal conditions can restrict the potential of the technology. As a consequence, continuity of these issues will lead to a significant gap between the research findings and engineering application of this advanced technology.

To overcome the aforementioned limitations, it is essential to have a robust, economical and comprehensive model which can predict the system performance in any random operating conditions. In addition, to demonstrate the ultimate potential of the system it is essential to identify the optimum operating and design parameters.

To date, there has been little endeavour in developing the AI based models for the ECs and in particular for the DPC technology. Therefore, this study pioneers in developing different AI and optimisation models for the state-of-the-art EC, i.e., GIDPC, to mainly:

i. Construct a big dataset comprising the key operating and design parameters for a GIDPC using experimental data and validated numerical model.

ii. Train data-driven predictive models using the created dataset with the aim of performance prediction and analysis of the GIDPC.

iii. Develop optimisation models with the aim of identifying optimum operational conditions and design parameters of the GIDPC technology.

1.4. Aim and objectives of the research

The main aim of the research is mainly to develop several data-driven predictive models based on the Machine Learning (ML) algorithms and several optimisation models based on the metaheuristic algorithms which can be capable of predicting the system performance and identifying the optimum operational conditions and design parameters. To meet such targets, the research is scheduled by the following specific objectives:

1) Dataset development: Conducting an experimental study to construct part of the big dataset and to evaluate the performance of the prototype in diverse climates. Use a numerical model validated by the experimental data to complete the construction of the big dataset which will include the identified key operating, design and performance parameters of the GIDPC.

2) ML model development: Train different data-driven models to demonstrate and compare their performance in predicting the GIDPC performance in any random operational and design conditions.

3) Optimisation model development: Develop different Multi Objective Evolutionary Optimisation (MOEO) models to identify the optimum operating and design parameters of the GIDPC by shifting the focus towards analysing the effect of optimum conditions on system performance improvement.

4) Performance assessment: Comparing the performance of the developed models by expressing the energy saving potential of the optimised GIDPCs by shifting the concentrations towards the operation of the GIDPC in diverse climates in 2020 and 2050 by considering the impact of climate change.

1.5. Research methodologies

The constructed big dataset using an experiment and the validated numerical model is used to train the ML models using two algorithms, i.e., Multiple Polynomial Regression (MPR), and Deep Neural Network (DNN), which are selected after a primary performance evaluation of several algorithms. The pros and cons of each trained model in terms of accuracy, comprehensiveness, flexibility and training time are compared. The second major objective of the study which is optimising the GIDPC performance is accomplished through three optimisation models based on the Genetic Algorithm (GA), Particle Swarm Optimisation (PSO), and Slime Mould Algorithm (SMA). Moreover, the performance of the optimised systems is compared with the base model in order to present the energy saving potential of the optimised GIDPCs. This is achieved by comparing the performance of the systems in diverse climates.

1.6. Research novelties

This is to date the first endeavour in developing the data-driven models based on the selected algorithms, i.e., MPR and DNN, accompanying with three MOEO models in which the novel SMA is used along with the common GA and PSO algorithms for the state-of-the-art EC, i.e., GIDPC. The GA and PSO are selected as the commonly used methods in different applications while the SMA is introduced for the very first time for an engineering application. In addition, a new eXplainable AI (XAI) is used for the DNN model to interpret the developed black-box DNN model. The aforementioned approaches will be a leap forward in improving, analysing and evaluating the performance of the GIDPC technology. The developed data driven models will be trained to predict the performance of the system in any random operational conditions (with diverse design and in various climates) using the key operating and design parameters only. This will be followed by identifying the unique

optimum conditions in all possible climates around the world by each optimisation method. Ultimately, the optimised models developed in this study will assist in deployment of the novel DPC system by demonstrating the energy saving potential of the technology when it operates in various climates in 2020 and 2050 considering the impact of climate change.

1.7. Structure of the thesis

- **Chapter 1** summarises the necessity of conducting the current research by introducing the selected GIDPC and the required ML and optimisation models in order to fill the existed gaps.

- **Chapter 2** presents the literature review conducted for the ECs by shifting the focus towards the DPCs and the ML based studies. This chapter covers the detailed review of all numerical, experimental and data-driven models with their key outcomes for the DPCs.

- **Chapter 3** overviews the construction of the big dataset. This includes an experiment which is conducted to build the foundation of the big dataset and the validated numerical model which is used to produce the operating conditions (data points) of the big dataset.

- **Chapter 4** covers the ML methods which have been used in this study. The chapter overviews the methodologies and training process of the models as well as explaining the XAI model.

- **Chapter 5** overviews MOEO methods used in this research which covers the selection of the decision variables, objectives and results derived from the models.

- **Chapter 6** presents a representative application for each ML model by shifting the focus towards presenting the energy saving potential of the optimised systems in diverse operating climates in 2020 and 2050 by considering the impact of climate change.

- **Chapter 7** mainly summarizes the key outcomes of this research by overviewing the results driven by the developed models.

CHAPTER 2: LITERATURE REVIEW

2.1. Introduction

This chapter includes the comprehensive review on development of the ECs including the theory, concept, classification, evaluation metrics, experimental, numerical and evolving AI based studies which are conducted over the past years. However, the chapter is mainly focused on technological and research progress of EC technology which has led to development of the Dew Point Coolers (DPCs). This is followed by shifting the focus towards the AI based studies for the DPCs in which the optimisation-based models are covered as well. The chapter starts by description of the theory and concept of the ECs and the performance metrics that are used for performance assessment of the technology. Afterwards, the chronological research progress for ECs is overviewed in which the breakthrough in introducing the DPCs are prioritised. Eventually, the chapter provides the research progress in AI based models (data-driven and optimisation) for the ECs with a further focus on DPCs. This section is bolded by detailed discussion and gap extraction over the AI based studies conducted for the technology. The justification of the current study is then provided by outlining the lack of ML and MOEO models for the state-of-the-art DPC which is GIDPC.

2.2. Concept, theory and classifications of air conditioning systems

2.2.1. Concept and theory

It is worth mentioning that over the past decades, a substantial increase in energy consumption within the building sector has led the focus of sustainable energy researchers to design and implement more efficient appliances. According to the latest statistics, the buildings consume 30-40% of the world total energy which has resulted

in similar proportion in greenhouse gases emissions [10]. HVAC systems are the major energy consumers in the buildings which account for around 50% of the energy delivered to the buildings. This indicates that the buildings are the largest end-users in European countries which is followed by transport, industry and agriculture which are responsible for 32%, 26% and 2% total energy consumption respectively.

AC systems are considered as an essential need for all types of buildings e.g., Data Centres (DCs), offices, supermarkets, health centres, hospitals and other public infrastructures. This is because of the growing global warming which has increased the need for ACs in the hot and arid regions e.g., the Middle East and North America. In addition, the need for ACs in mild climates, e.g., UK, has also grown rapidly over the past decade [22]. Continuous operation of the current energy intensive ACs is considered as one of the main reasons for experiencing the common grid cut-offs in some regions such as China [23]. The aforementioned issues in effectiveness of the existing commercial ACs have trigged the research studies on developing more efficient ACs and reduction in carbon emissions by an increased attention to utilisation of the natural and renewable sources.

2.2.2. Classifications of air conditioning systems

The chapter is followed by introducing various types of common ACs as follows:

Mechanical Vapour Compression (MVC): The AC market is currently dominated by the MVC systems. The MVC operational scheme is based on the heat transfer within a dynamic refrigerant (refrigeration cycle) [24]. Generally, the technology has an evaporator, a condenser, a compressor and an expansion valve. The heat transfer phenomena in MVCs are based on phase change between liquid and gaseous states. In

a refrigeration cycle, heat is absorbed and rejected through a liquid refrigerant. As seen in **Figure 2.1**, the refrigerant enters the compressor as a saturated vapour and leaves it with higher pressure and temperature. Then the hot vapour which is in a superheated vapour state, is condensed via water or air by flowing across the coils in the condenser. This is when the heat is rejected and moved away by the water cooler or air cooler. Then the condensed liquid refrigerant is gone through the expansion valve in which the pressure of the liquid decreases. This process also resulted in temperature decrease leading to a cold refrigerant. The cold refrigerant is then flown into an evaporator where the refrigerant absorbs heat. As a result of heat absorption, the saturated refrigerant vapour is ready to enter the compressor. The cycle is illustrated in a pressure-volume diagram in **Figure 2.2**.

The refrigeration cycle has been known for a long period and the production of the MVCs was made in large scales with the following advantages: long life, stability, and cost effectiveness at the time. However, its disadvantages i.e., low COP values in the range of 3 to 5 [25], high energy consumption which is mainly because of the compressor, and running independent of renewable sources have made the researchers to look for efficient alternatives.
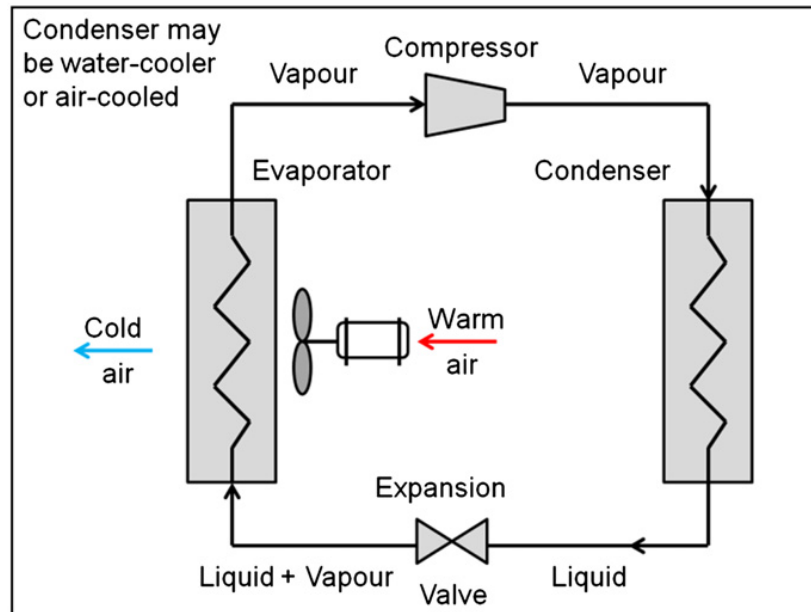
Figure 2.1: Refrigeration cycle [26]
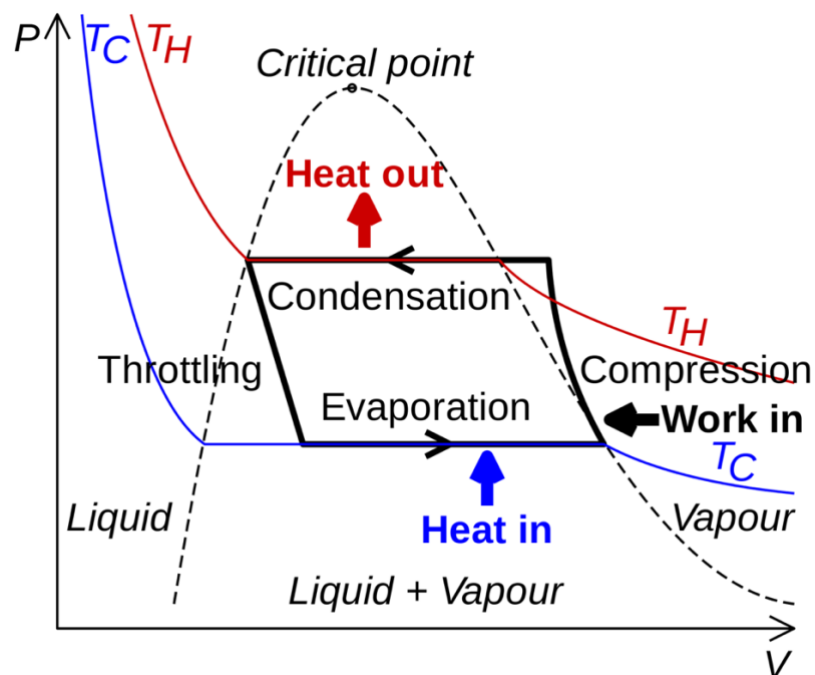
Figure 2.2: Pressure-volume diagram in a refrigeration cycle [26]

Absorption and adsorption cooling systems:

The Absorption Cooling System (ACS) is based on the liquid sorption such as water

or the corrosive lithium bromide while the Adsorption Cooling System (ADCS) is

based on solid sorption such as a non-hazardous or corrosive silica gel [27]. This is the main difference between these two systems which were introduced as a potential replacement for the MVCs [28]. In ACS, the absorption and desorption of a working fluid which is known as refrigerant determines the working principle of the system. As shown in **Figure 2.3**, the ACS working cycle starts by vaporising the refrigerant from a high absorbent concentration which is transferred into a condenser to generate heat ($Q_{cooling}$). The refrigerant leaves the condenser for an expansion valve with the aim of pressure decreasing. Then it enters an evaporator in order to get vaporised through receiving heat. Afterwards, the generated vapour is absorbed by absorbent in the generator which results in heat dissipation to the environment. Eventually, the combined refrigerant and absorbent are transferred back to generator to start another cycle.

Figure 2.4 demonstrates the working principle of the ADCS in which the components are same as the ACS. However, the cooling process can be carried out in two separate phases. In the first phase, the refrigerant vapour is transferred from the evaporator into the absorber while the heat is removed from the liquid. The vapour refrigerant is absorbed by the absorbent bed. The desorption process is triggered by warming up the refrigerant bed in order to remove the refrigerant from the absorbent bed. Afterwards, the vapour goes into the condenser and the condensed liquid leaves it to enters the evaporator. The existence of two beds in ADCS ensures the continuous operation of the absorption and desperation processes.

Although the absorbent system, removes the need for energy intensive compressors, but it adds high pressure vapour or water requirements. To fulfil the aforementioned requirement, an expensive and metal-corrosive chemical are needed for the system to

operate. In addition, the need for heat source, low COP value, i.e., 0.4-1.2, and complex system configuration are another main disadvantages of this technology [29].
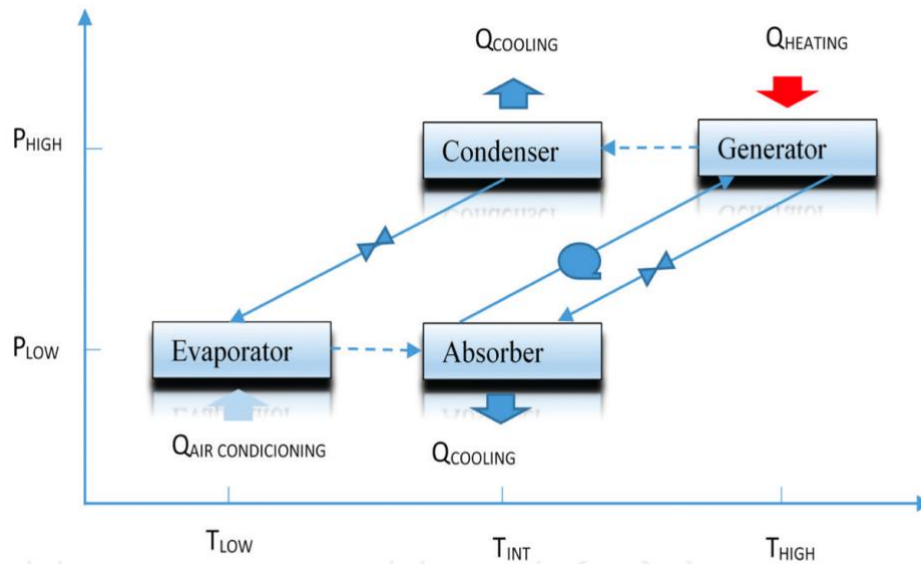
Figure 2.3: Schematic of ACS [27]
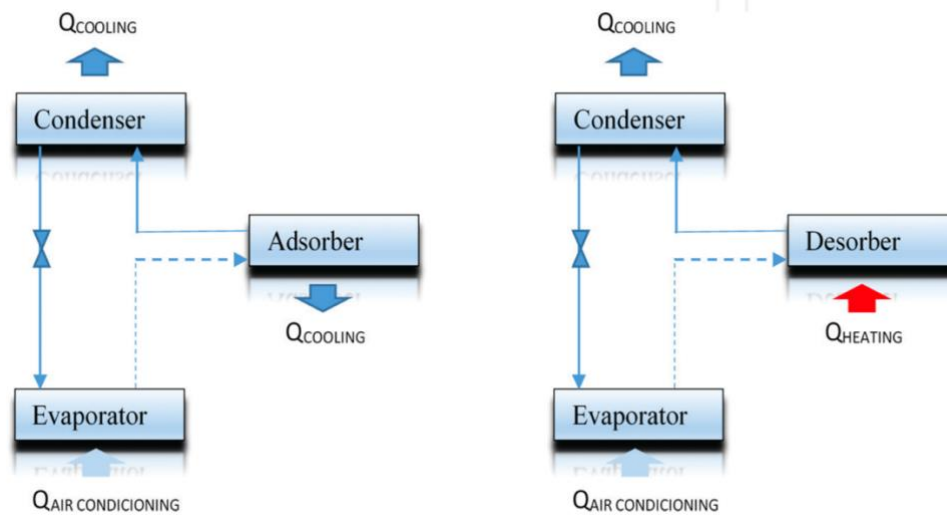
Figure 2.4: Adsorption cycle [27]

2.2.3. Evaporative Coolers

To overcome the aforementioned disadvantages, Evaporative Coolers (ECs) have been introduced [30]–[32]. Working principle of the ECs is based on the water evaporation which enables the heat transfer and heat absorption. Owing to this feature, ECs have a simple structure and use the natural sources which are attractive to researchers. In addition, the improved COP values (15-20) [7] compared to the MVCs, ACSs, and ADCSs have increased the popularity of the ECs among the users.

Classification of the ECs: In general, the ECs are classified into two main categories, i.e., air-side and water-side coolers. The main difference between these two categories is the source of latent heat that contribute to the evaporation process. Many different sources can be used to provide the latent heat but the most common source is air. However, water is another common latent heat source that both are used to trigger the evaporation process. Basically, the latent heat is the main source of energy that is used to evaporate the water which is transferred from the air. This helps the air to lose its heat and as a consequence, it leads to the temperature drop in the air which is the primary goal of the ECs.

ECs have been introduced with two types of Direct (DEC) and Indirect (IEC) systems [33]. However, in some cases a hybrid EC comprising two mentioned types are also used. **Figure 2.5**, shows all types of ECs which are going to be described in details as follows:

Direct Evaporative Cooling (DEC): DECs keep the supply air in direct contact with the evaporated water which helps the air to lose its heat. The water absorbs the heat from the intake air, and then as a consequence of evaporation, adds moisture to the air. This direct contact increases the humidity level of the air and results in uncomfortable wetter supply air which can annoy the residents and the equipment of the supplied

area. The process continues until the air reaches the saturation point which is normally when the air is reached to its wet-bulb temperature.
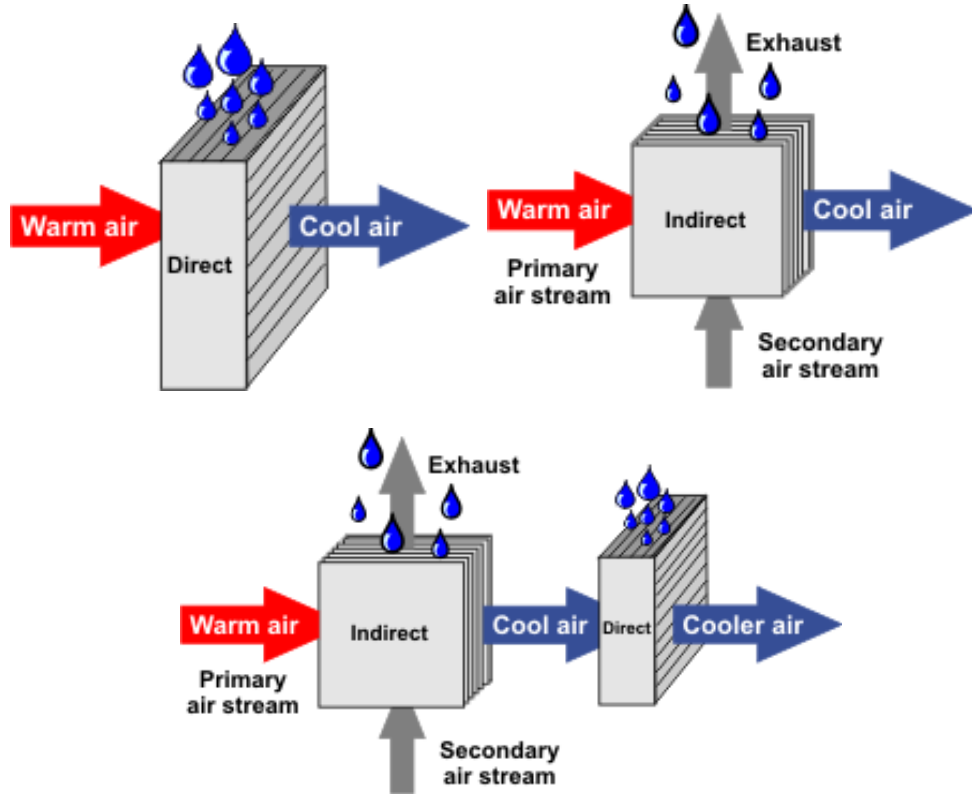
Figure 2.5: DECs, IECs, and combined ECs [34]–[36]

Indirect Evaporative Cooling (IEC): Owing to separating plates, the IECs are more preferred as the supply air is separated from the water and the heat transfer takes place in separated sections through the heat exchanging plates [37]. As shown in **Figure 2.5**, the heat exchanging plates create several separated channels in which the supply air flows in a dry channel and the working air flows within the adjacent wet channel where the water evaporation occurs. The water evaporation leads to temperature decrease in the wet side of the plate and the as a result, the achieved temperature difference between two sides of the plate in wet and dry channels causes the heat transfer from the supply air in the dry channel to the working air in the wet channel. Having completed the heat transfer, the wet and warm working air leaves the wet channel. As

a consequence, the intake air is cooled without being in direct contact with water which resulted in a cold and dry supply air. This is considered as a big advance in ECs as the quality of the supply air is improved. One outstanding disadvantage of the IECs is their high dependency on the outdoor environment. The difference between the dry bulb and wet bulb temperatures has the key role in performing the ECs. This difference is limited to small amounts in some climates, e.g., humid climate which leads to low cooling capacities. Moreover, instability of the outdoor air conditions can lead to poor performance of the ECs.

Hybrid indirect/direct Evaporative cooling (IDEC): Although this type is not very popular but it is designed to mainly increase the efficiency of the ECs. As shown in **Figure 2.5**, the intake air is first cooled in the IEC and then it is directed into the DEC. Although it is proved that the temperature of the supply air is decreased more in the hybrid system but the disadvantages of both individual systems are still in existence in the hybrid systems. As a consequence, the necessity of a novel method was needed to increase the efficiency of the ECs. This is done by introducing the Dew Point Coolers (DPCs) in which the aforementioned disadvantages of the existing ECs are aimed to be resolved.

Dew Point Cooler (DPC): The DPC is introduced by aiming to achieve higher cooling efficiency. The research studies on previous EC technologies revealed that the maximum wet-bulb cooling efficiency is only 60% [38]. Therefore, the temperature of the supply air must be decreased more in order to reach higher cooling capacities. This can be achieved by implementing an idea in which a proportion of the supply air is transferred to a separated wet channel where the water evaporation takes place. This proportion of air is then called working air which helps the intake air to reach the lower temperature levels. This new cycle is called M-cycle which is shown in **Figure 2.6**

[35]. The M-cycle was claimed to reduce the temperature of the intake air down to the dew point temperature. Therefore, the term "Dew Point Cooler" is also used to represent the M-cycle cooling systems. The early-stage research showed that the cooling efficiency of the DPC is much better than the previous technologies. Over an experimental study, the wet-bulb efficiency of 80% is achieved which is 20% higher than the previous technologies [17]. In addition, it is reported that the wet-bulb efficiency of the DPC can reach the outstanding value of 50% under the identified ideal operating conditions [17]. As a consequence, the M-cycle absorbed the attention of the researchers and the engineers which has led to many further studies on the DPCs.

4. The product fluid traveled the length of the dry (green) channels, transferring its heat to the working fluid. The product fluid is now dry and close to the dew point temperature of the entering fluid.

3. Working fluid that was fractioned off into the wet channels. Heat from the product fluid has been transferred into the working fluid and is rejected as exhaust.

2. Working fluid that has been cooled is fractioned off into the wet (gray) channels repeatedly across the exchanger.

1. Product fluid enters the heat and mass exchanger here.

Figure 2.6: Schematic of the M-cycle HMX [34]

2.2.4. Performance evaluation metrics of ECs

Despite having ECs as the main cooling systems over the last century, the review of standards for IECs, as the most popular ECs, revealed that there is no unique international standard for the performance evaluation of the technology. However, several national standards have been released so far as follows:

   I.   ANSI/ASHRAE Standards (133-2008/143-2015) [39], [40]

II.   AS/NZS 2913-2000 (Australia) [41]

III.   Labelling Program (Iran) [42]

IV.   IS3315-1974 (India) [43]

V.   C22.2 No. 104 (Canada) [44]

VI.   GB/T25860-2010(China) [45]

Although all the aforementioned national standards are valuable in performance evaluation of the IECs but the Australian and American standards are considered as leading and popular standards in the world of cooling systems. International standards are vital needs for any technology to let the researchers, designers and end-users have a single reference for performance evaluation of that technology. However, having one internationally accepted standard is an essence in improvement and efficient operation of the technology. In this regard, the Australian standard, i.e., AS 2913 Evaporative Air Conditioning Equipment, was firstly introduced in 1987 in which the performance of the ECs was being assessed in terms of few key parameters such as airflow, power consumption and water evaporation efficiency [46].

American Society of Heating, Refrigerating and Air-Conditioning Engineers (ASHRAE) standards are the most common and globally accepted criteria for performance evaluation of the ECs. The ASHRAE standards have been updated over the years and are considered as comprehensive standards which provides useful suggestions for testing and assessment of the ECs. The Standard "143-2015 Method of Test for Rating Indirect Evaporative Coolers" provides the performance evaluation metrics for the IECs. Its accuracy has been proved through different tests in which the following performance parameters are provided as the performance indicators [47]:

Temperature drop: This simply represents the temperature difference between the intake and supply air. This shows how much the cooler has reduced the temperature of the intake air which is the primary factor in evaluating the system performance at first glance. In addition, it is the principle of calculating other important performance parameters.

Wet-bulb depression: It indicates the difference between the wet-bulb and dry-bulb temperatures which is normally measured by the psychometric chart. It is used to measure the Relative Humidity (RH) of air. For instance, when the RH is 100%, the wet-bulb depression is equal to zero as the wet and dry-bulb temperatures becomes identical.

Dew point depression: This expresses the difference between dew point and dry-bulb temperatures. It is used to indicate how wet the air is, in which the higher dew point depression values mean that the air is dry and the lower dew point depression means the air is quite wet.

Total power consumption: It is equal to the power consumption by the electrical components such as pumps, fans, etc.

Cooling capacity: The cooling capacity simply determines the IEC's capacity in removing heat which is normally expressed in Watt unit. It is the sensible cooling of the supply air which is highly dependent on the temperature drop. The cooling capacity can be expressed by Eq. (2.1):

$$Q_{cooling} = C_p(T_{dry,in} - T_{dry,out})(1 - \varphi)Q_{m,dr,in} \qquad (2.1)$$

where $Q_{cooling}$ is cooling capacity, C_p is the specific heat capacity, $T_{dry,in}$ is the intake air temperature in dry channel, $T_{dry,out}$ is the outlet air temperature in the dry channel which is identical with the supply air temperature, φ is the working air fraction over the intake air and, $Q_{m,dr,in}$ is mass flow rate of intake air in dry channel.

Coefficient of Performance (COP): The COP is a common evaluation metric for the heat pumps and air conditioning systems in which the ratio of the sensible cooling/heating to the conducted work is considered. For the ECs, the COP represents the ratio of the cooling capacity to the consumed power by fans and pumps and other power consuming components. The COP value is normally more than 1 as the system needs to be efficient and economical to operate when the heat removal capacity is more than the required work. The COP is a metric that considers the technical and economic aspects of the EC simultaneously which can be calculated using the following Eq. (2.2):

$$COP = \frac{Q_{cooling}}{W_{fan} + W_{pump}} \qquad (2.2)$$

Where W_{fan} and W_{pump} are the electrical power consumed by the fan and the pump respectively.

Wet-bulb efficiency: is the ratio of the temperature drop to the wet-bulb depression which can be expressed using Eq. (2.3):

$$\varepsilon_{wb} = \frac{T_{dry,in} - T_{dry,out}}{T_{dry,in} - T_{dry,in,wb}} \tag{2.3}$$

Where ε_{wb} is the wet bulb effectiveness and $T_{dry,in,wb}$ is the wet-bulb temperature of the intake air in dry channel.

Dew point efficiency: It is the ratio of the temperature drop to the dew point depression which can be expressed by Eq. (2.4):

$$\varepsilon_{dp} = \frac{T_{dry,in} - T_{dry,out}}{T_{dry,in} - T_{dry,in,dp}} \tag{2.4}$$

where ε_{dp} is the dew point effectiveness and $T_{dry,in,dp}$ is the dew point temperature of the intake air in dry channel.

Pressure drop: It refers to the pressure decrease which takes place along the airflow path within the ducting systems. The pressure drop takes place mainly due to the friction and velocity which can be powered by the air fans within the EC systems. The pressure drop is proportional with power consumed by the fans and is normally expressed in kPa as Eq. (2.5):

$$\Delta P = (\xi + \lambda_f \frac{1}{Dh}) \frac{\rho U^2}{2} \tag{2.5}$$

Where ΔP is pressure drop, ξ is coefficient of local resistance, λ_f is coefficient of friction resistance where it can be calculated using $\lambda_f = (64/Re)$ for the laminar flows, D_h is hydraulic diameter, ρ is air density and U is the air velocity.

Water evaporation/consumption rate: Water evaporation and the corresponding water usage is a big concern for all the users particularly to those who live in dry climates/regions. The water evaporation rate is an important factor that takes place when the water absorbs the heat of the intake air and exits the cooling system as the exhaust air which can be calculated by the following Eq. (2.6):

$$V_{evp} = \frac{1000 V_2 \rho_{a,2}}{\rho_w} (w_2 - w_1) \tag{2.6}$$

Where V_{evp} represents the water evaporation [L/h], V_2 is the working airflow rate [m3/h], $\rho_{a,2}$ is mean density of the secondary airflow [kg/m3], ρ_w represents the density of the water, w_1 represents the inlet humidity ratio of the working air [kg/kg], and w_2 represents the outlet humidity ratio of the working air [kg/kg]. It is estimated that 1.5 L water is needed to produce 1kWh cooling in an efficient EC [9].

Working air ratio: As mentioned earlier, in an IEC the intake air is separated into two parts in which one part is diverted to the adjacent wet channel which is called working air and the rest leaves the cooler as the supply air. The more working airflow leads to a higher evaporation rate. The working air ratio is also called secondary to primary air ratio in which the primary air represents the intake air and the secondary airflow represents the working air. The working air ratio can be calculated by the following simple Eq. (2.7):

$$\varphi = \frac{V_{EA}}{V_{IA}} \tag{2.7}$$

Where φ represents the working air ratio, V_{EA} represents the airflow rate of the exhaust air [m3/h], and V_{IA} represents the airflow volume of the intake air [m3/h].

2.3. Research progress on IECs

The continuous studies and progress in EC technology and in particular the huge breakthrough in cooling efficiency improvement by invention of the M-cycle cooling systems, the IECs gained more popularity and attention in cooling market and among the researchers. This is highlighted particularly when the cooling performance and energy consumption of the M-cycle cooling systems outperform the previous traditional cooling systems. This importance achievement resulted in numerous research studies on IECs which can mainly be classified as follows:

1. Methodology based studies in which the new methods and theories are implemented.

2. Technological based studies in which the new technical progress are discussed.

3. The hybrid studies in which the IEC technology is combined with other technologies with the aim of achieving better efficiency.

4. Application based studies in which the main purpose of these studies is to investigate the applicability of IECs in various fields.

5. Comparison based studies in which the energy saving potential and performance of different ECs are presented. In addition, these studies often include economic and/or environmental analysis.

6. Detailed HMX based studies in which the structure of the HMX, as well as the flow patterns within the HMX are the mainly discussed topics.

7. Over the past decade, new research studies based on Artificial Intelligence (AI) are being popular in all fields. The AI based models are mainly developed to provide data driven smart models for the technology in order to predict the performance parameters of the system using the selected key operating parameters. These studies gain more popularity among the researchers as they remove the need for expensive experiments and complex and time-consuming numerical studies.

8. Similar to the AI based studies, the optimisation-based studies are conducted to operate the technologies in their full potential. Various optimisation algorithms are developed to identify the optimum operating and design parameters of the technology in diverse applications which will contribute to reduction of the carbon emissions and power consumption. This is simply achieved by determining the objectives for the optimisation algorithm. For instance, one potential objective for the IECs can be maximising the COP.

In this section, firstly, it is aimed to review the theoretical progresses that have been conducted for the ECs and then the related research studies, including material-based, experimental and numerical studies, which eventually led to the introduction of M-cycle cooling systems (DPCs). Eventually, the AI based studies which are conducted for the IECs are reviewed to extract the existing gap in the research studies for the DPCs in order to justify the development of current study.

2.3.1. Theoretical progress

The common methods to simulate the IECs' performance is based on the thermodynamic first and second laws by taking the entransy dissipation and exergy destruction into account [31]. These approaches are applied to mainly analyse and investigate the system efficiency.

An approach is introduced in 2010, based on the entransy theory [31] which is provided to mainly handle the coupled heat and mass transfers and in addition, to optimise and analyse the system efficiency. Moreover, new methodologies such as Moisture Entransy Dissipation based Thermal Resistance (TRMED) are introduced. Moreover, a new thermal resistance metric is introduced which was mainly used to assess the performance of the ECs. This new metric is identical with the ratio of dissipation rate over the output rate of squared refrigerating effect.

In another study in 2011, Chen et al. [32] carried out an application-based study in which a similar metrics other than enthalpy, i.e., moisture entransy and TRMED, are introduced which could affect the performance of the ECs including both DECs and IECs. The application proved that the lower TRMED values will lead to superior cooling efficiency.

Another application-based study is conducted [48] in which a new method, called global optimisation, is introduced in which the cooling efficiency of the IECs was aimed to be improved. The method was mainly based on the detailed investigation of the process irreversibility and it is assessed based on the entransy dissipation. The optimisation is conducted by providing a theoretical relationship between the

requirement of the users and the operating and design parameters of the HMX. The case study revealed that the system optimum operation is mainly based on the global optimisation than the parametric analysis.

The exergy analysis is used by Santos et al. [49], for the first time along with the energy analysis for performance simulation of the ECs. The authors provided a new method by opposing the previous traditional methods in which the supplementary mass and energy analysis, the introduced exergy analysis with thermodynamic second law are suggested to be used for the performance evaluation of the ECs. Eventually, the results revealed that it is essential to include both energy and exergy analyses when the performance of the ECs are investigated.

The exergy analysis is then implemented in an experimental study [50] for three different ECs, i.e., a DEC, an IEC, and an IDEC. The experiment is carried out in diverse climates in Iran in which the process irreversibility and exergy efficiency are considered through the exergy analysis. The results revealed that considering both thermodynamic first and second laws in evaluating the performance of the ECs is essential. Additionally, the best performance of the ECs in different climates are identified which led to introduction of optimal climate conditions for the three selected cooling systems.

In a comparison-based study, Caliskan et al. [51], compared the performance of different cooling systems using the energy and exergy analyses. The considered systems were a M-cycle and three conventional IECs. A new metric was introduced to assess the sustainability of the considered cooling systems. The new metric which

was called sustainability metric, was related to the energy consumption and exergy destruction of the systems. Both exergy analysis and new sustainability index proved that the M-cycle outperforms the other three IECs in terms of exergy and sustainability.

In another attempt in improving the performance evaluation methods for the cooling systems, Zhang et al. [52], provided a novel evaluation tool by investigating the similarities and differences between the exergy and entransy analyses. The relationship between diverse operating parameters is identified through the exergy destruction and entransy dissipation. This is achieved by identifying the factors with a negative impact on cooing performance of the considered system in which the results revealed that reducing the exergy reduction and entransy dissipation will lead to a poor cooling performance by the system. Moreover, new theoretical parameters are also recommended for the technical processes that take place in system performance.

Two studies conducted by Zhang et al. [53], [54] are aimed to further investigate the EC performance by utilising the exergy and entransy analyses. These analyses are conducted within the humid air handling process for the evaporation and dehumidification. The case studies revealed that in order to improve the moisture evaporation, increasing the water temperature is a better way compared to increasing the air temperature value.

In summary, based on the conducted research studies on evaluating the diverse theoretical methods for performance evaluation of the ECs, the following issues are the focal areas worthy of intensive investigation:

- Irreversibility of the heat and mass transfer

- Impact of exergy destruction

- Impact of entransy dissipation

In summary, it is tried to provide a comprehensive method for performance evaluation and optimisation of the IECs by implementing the thermodynamic first and second laws simultaneously. Although the proposed methods are proved and discussed by the authors in order to prove the applicability of the newly proposed methods but numerous detailed investigations are needed to consider them as common methods/index.

2.3.2. Technical progress

Having reviewed the theoretical progress, this section will shift the focus towards the studies that are mainly focused on technical progress of the IECs. For instance, the material-based studies are considered as one of the main research topics in which choosing the HMX material that has a key role in determining the evaporation rate, heat transfer rate, and cooling efficiency of the system. In addition, the research studies in forms of numerical and experimental studies which investigate the system performance to mainly improve the cooling efficiency as well as to reduce the construction and operation costs of the technology are taken into consideration.

In a research study conducted by Xie and Jiang [55], a constructed IEC in which the water was cooled in a terminal AC, it is aimed to improve the cooling efficiency by water instead of airflow. This research is especially suitable for systems which are operated in public buildings of dry and hot climates. The schematic of the constructed water side IEC is illustrated in **Figure 2.7**, in which the intake air is firstly cooled in a

heat exchanger and then the cooled intake air is sprayed by water to the paddling tower to produce the desired cold water through the evaporation. The experiments revealed that the water can be cooled below the wet-bulb temperature of the intake air. In addition, it is established that the COP of the system reaches a value of 9.1. Although the system is efficient and the results are promising but there are few studies on this technology.

Figure 2.7: A water-side IEC [49].

The evaporation process in IECs can take place separately which keeps the supply air separate from the working air. This can happen via a solid wall in a tube in a tubular exchanger. An experimental research study is carried out on an IEC system in which the water film freely moves within the horizontal tubes [56]. This study is considered as the primary work on the IECs with tubular HMX. The results revealed that the different water flow rates result in different patterns which are droplets, columns, and

liquid sheet. The cooling performance of the system is calculated using a developed empirical equation which was based on the experiment.

In another tubular based research study, a semi-indirect evaporative refrigerator is developed by Martinez et al. [57], [58]. As shown in **Figure 2.8**, the system was constructed using the standing solid porous ceramic pipes. The water moves towards the down of the ceramic wall which separates the primary and secondary airflows and then evaporates within inner wall where the primary air flows along the outer surface. The system can efficiently be operated in hot and humid climates.
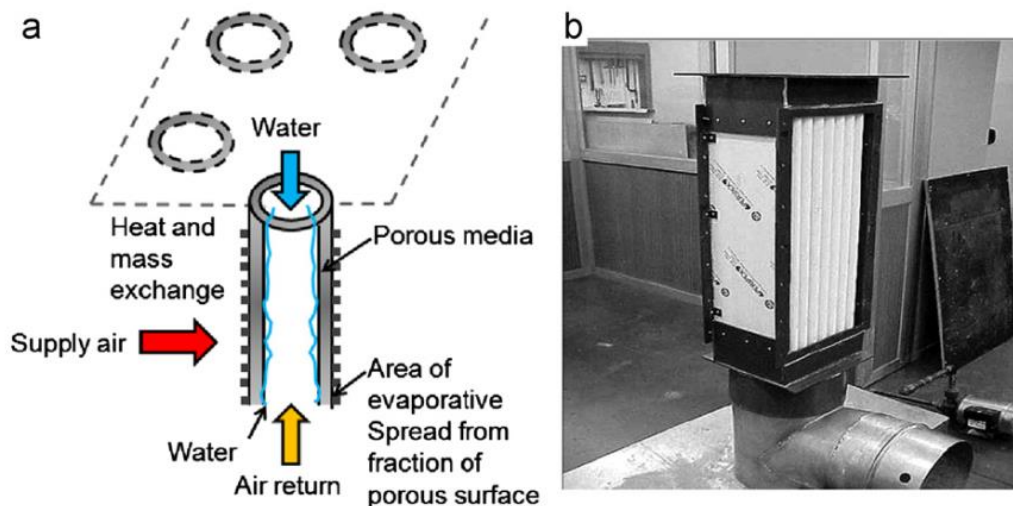
Figure 2.8: A semi-indirect tubular evaporative refrigerator [57]

The remarkable progress in performance of the IECs, have made the researchers not only to focus on sole operation of the IECs but also on hybrid applications of the technology. The hybrid operation of the system is considered in order to improve the cooling efficiency of the system in diverse applications [15], [59]–[67]. Majority of the hybrid systems are the combination of the IECs with desiccant systems. However, there are some other hybrid systems in which the IECs are combined with other

technologies such as heat pipes [45], [68], gas turbines [69], radiative cooling [70], and cooling/reheating treatment [71] which all have led to superior cooling performance. In addition, other hybrid systems such as the desiccant-enhanced evaporative air conditions (DEVap) are gained increasing popularity over the past years. These systems are operated as pre-treatment tools for the inlet air flows within the IECs by creating a chance for the cooling system in order to improve the cooling potential in the working channel. The DEVap has three main classifications as follows:

-   Membrane dehumidification [72]–[76]

-   Solid desiccant hybrid systems [77]–[80]

-   Liquid desiccant hybrid systems [81], [82], [91]–[94], [83]–[90]

The liquid desiccant hybrid system is the most common hybrid cooling system in which the commonly used liquids are: calcium chloride, lithium chloride, etc. During the operation, the pre-humidification is completed when the moisture of the intake air is absorbed by the desiccant, which is mainly because of the partial pressure difference between the air and the liquid. The wet desiccant is then regenerated through a regeneration process in which the moisture of the desiccant is decreased with the help of external heat source. Then the air is dehumidified by the help of a desiccant dehumidifier. In addition, the temperature of the air is reduced via the evaporative cooler.

Superiority of the liquid desiccant hybrid systems and their potential in efficient cooling deserve more attention which will lead to a significant contribution to mitigate

the restriction of using IECs in wet climates. This will provide the residents with comfortable air quality and efficient cooling systems in wet climates.

2.3.3. Materials for evaporating surface

Several different studies are conducted to improve the IECs cooling efficiency and decrease the operational and construction cost of the technology. However, one important way to improve the system performance, is employing appropriate wet surface materials [95]–[102]. The properties of a suitable wet surface material can improve the moisture diffusion and evaporation rate which will result in more evaporation and consequently more heat and mass transfer within the wet channel of the IECs. The major properties of the materials which can hugely affect the performance of the system are moisture wicking ability, diffusivity and evaporation rate.

Different material types have been used and tested for the heat and mass exchanger of the IECs in order to find the most effective material. The used materials can be classified in different categories as follows:

- Metals: This category includes different types of plates, tubes, etc.

- Fibres: In this category, the most common fibre-based materials are paper boards, woods, glasses, etc.

- Ceramics: The most common ceramic-based materials are silicon carbide and the related composites, zirconia ceramics, aluminium oxide, polystyrene composites, zirconia toughened aluminium, aluminium nitride, etc.

- Zeolite: The most common zeolites are synthetic polymers, molecular sieves, porous ceramics, carbon fibres, etc.

- Carbons: The common suitable carbon-based materials are carbon fibres, carbon composites, activated carbons, etc.

The first ever material that was suggested for the IECs was plastic. Although, the material is less-corrosion and extremely light but its poor thermal conductivity which is a vital feature in operation of the IECs, has limited the usage of plastic in the technology [103]. Over the years of research, the fibre materials were introduced as potential replacements for the plastic [101], [104]–[106]. The fibre has an acceptable level of permeability which lets the water to distribute across the surface of the exchanger plate in the wet channel and increase the probability of the heat transferring and water evaporation.

In an experimental study, which is conducted by Bruno [95], a new material for the wet side of an IEC is used aiming to increase the cooling efficiency of the technology. The used material for the wet surface had high water retention and wickability specifications. This resulted in improved cooling efficiency.

In a study conducted by Zhao et al. [97], by considering the effect of the materials on performance of the IECs. The results revealed that the thermal properties of the selected materials have small impact on amount of heat and mass transfer. Therefore, it is concluded that thermal conductivity and water retaining capacity, also called porosity, cannot be considered as key player parameters in selecting the materials for heat and mass exchanger. However, the key player factors are the compatibility with waterproof coatings, formation and durability and the material cost.

A few studies have conducted by considering the natural fibres as the material for the heat exchanger of the IECs. For instance, Maurya et al. [98], conducted comparative research in which three different materials, i.e., aspen fibre, cellulose, and coconut coir, are considered. The study was undertaken to investigate the performance of the

IECs in Bhopal, India to report the system performance in summer. The results revealed that the performance of the aspen is the best among the other materials in terms of saturation efficiency, i.e., 80.99%, when the air velocity was 0.5 m/s. The cellulose is located in the second place by the saturation efficiency of 69.58% and eventually, the coconut aspen has the weakest performance by the saturation efficiency of 68.15%. In addition, it was observed that the cellulose and coconut coir have similar performance in terms of water soaking. In another endeavour, Kulkarni et al. [99], considered different configuration (or shapes) and materials for the heat exchanger. The considered shapes were the rectangular, cylindrical and hexagonal shaped evaporative coolers while the considered materials were, cellulose, aspen, paper, polyethylene. The thorough comparison of the aforementioned options revealed that the hexagonal system with aspen material outperforms the other systems with saturation efficiency of 91% while the performance of the rectangular shaped cooler made from cellulose held the lowest saturation efficiency, i.e., 72.4%. In another similar study [100], pressure drop and cooling efficiency of an IEC with high-density polyethylene, rice husk, and commercial wetted pads, are compared. It was revealed that the rice husk pas with saturation efficiency of 55.90% outperforms the high-density polyethylene with saturation efficiency of 29.10%. However, the commercial wetted pas outperforms the other two types in terms of pressure drop by holding a lower value. The performance of various materials such as jute, luffa and palm fibre are all compared with the commercial aspen-wood excelsior wetted pas as the commonly used material in ECs [101]. The cooling efficiency of all systems is compared in which the jute material showed the best performance with cooling efficiency of 62.1%. This is followed by luffa and commercial systems by holding the values of 55.1% and 49.5% respectively. Eventually, the palm fibre system had the

worst performance by the efficiency of 38.9%. However, considering the Cloth fabrics, which exhibits large capillary force and avoid bacterial growth with proper treatment, are potentially highly effective media for evaporative cooling. However, relatively few reports of this type of materials can be found in evaporative cooling applications. In another material-based studies, experimental research is conducted to evaluate the performance of a cooling system made from raw cotton fabric and a curtain fabric [102]. The experiments showed that the saturation efficiency of the curtain fabric made system, i.e., 54.8%, outperforms the raw cotton fabric made system with saturation efficiency of 33.2%. In addition, it is reported that the temperature drops for the curtain fabric system was 2.9°C and for the raw cotton fabric was 1.7°C. In another comprehensive experimental study [107], six different cloth fabrics and a kraft paper as materials of the heat and mass transfer in an IECs, are compared for performance evaluation. The comparison was made to reveal the best material based on four factors, i.e., evaporation rate, wicking ability, diffusion rates and wetted areas. The results showed that some fabrics outperform the kraft paper in terms of moisture wicking, diffusivity and evaporation ability. In addition, some fabrics are failed to satisfy the authors mainly because of low immediate diffusion ability. Moreover, some fabrics are also failed to perform well due to distortion. Eventually, it was reported that the best materials for the system in terms of cooling efficiency are Coopass bird eye mesh fabric and Bamboo charcoal Coolmax active fabric. However, it is reported that Bamboo Charcoal Coolmax active fabric is more economic choice than Coopass bird eye mesh fabric. Use of aforementioned selected materials has led to improvements of up to 182%, 37% and 20% in vertical wicking rate, diffusion rate and evaporation rates respectively.

It can be concluded that the materials used for exchanger plates in IEC play a key role in performance of the systems. This is mainly because the heat and mass transfer in wet channel is in direct interaction with the sensible heat exchange between the wall and air in the adjacent dry channel. The material of the wet channel must be able to keep and distribute the water on its surface to support the water evaporation. This feature will facilitate the water evaporation and simultaneous heat transfer between two sides of the plate in wet and dry channels. Several studies have been conducted to test, compare and eventually find the appropriate material for the IEC's exchanger plates.

In summary, the chosen material must have the properties which can facilitate the heat and mass transfer as much as possible and let the water evaporation to cool down the supply air by enabling the heat transfer between the supply air and working air.

2.3.4. Review of the analytical studies

Apart from the material-based studies, the experimental and analytical/numerical models are the core studies which have been conducted in research studies on IEC technology. The analytical/numerical studies are carried out to establish the mathematical expressions (equations) which can reflect the heat and mass transfer occurring within the heat exchanger of the IECs. This approach will contribute to analysing the role of all operational and design characteristics including the effect of different climates, various shape and dimension of heat exchangers, etc., on the performance of the system. Generally, the analytical models employ the thermo-fluid theories to develop relationship-based equations between the performance and operating parameters of the technology.

Maclaine-cross and Banks [108] developed the first analytical model for an IEC in which the efficiency of the model was 20% higher than the experimental data. The main reasons for the resulted differences are originally coming from the assumptions made to develop the analytical model, i.e., it was assumed that the wet surface in the wet channel was fully saturated, water was evenly distributed over the wet surface and was fed to have continuous evaporation, and Lewis relation was fully applied. In another attempt, Stoitchkov and Dimitrov [109], a method is proposed for a cross-flow flat-plate heat exchanger to calculate the cooling effectiveness. The model was developed based on analysing the mean temperature of the flowing water. In addition, an equation is developed to calculate the proportion of the total to sensible heat. The recorded errors compared to the experimental data was in the range of 2-4% which was much lower than first model. Another numerical model was developed for a cross-flow flat-plate heat exchanger IEC in which the calculation of the energy consumption and thermal performance of the system was possible [110]. Additionally, identification of the optimum geometrical dimensions as well as the configuration were considered in the model. The maximum difference of 0.54 °C in supply air temperature between the model prediction and the experimental data was recorded [111]. Erens and Dreyer [112] carried our another early study on developing the analytical models for the IECs by shifting the focus towards the comparison of the new model with previously developed models. It was concluded that:

- Poppe method [113], [114] is accurate enough when it is assumed that the working air is supersaturated with water vapour.

- Merkel method [115] which is simplified of Poppe method has lower accuracy because the number of assumptions was high (Lewis factor is constant, water temperature is constant, the working air is saturated).

The developed simple model by Erens and Dreyer, with much higher discrepancy, is only suitable for initial assessment of the small sized systems.

The commons assumption in developing the analytical/numerical models were the main reasons for the discrepancies [7]. The main assumptions are:

I. The heat transfer along the airflow is ignored (the heat transfer occurs only vertically between the separating plates).

II. Ait flow always has the uniform behaviour along the channels.

III. Water transfer from wet side of the plate to the working air occurs vertically only.

IV. The wet side of the exchanger plate in the wet channel is saturated with water.

V. Air is considered as an incompressible gas.

Several studies are conducted to reduce the discrepancy of the developed models. For instance, Kettleborough and Hsieh [116], proposed a one-dimensional numerical model for a counter flow flat-plate heat exchanger IEC. To increase the accuracy, this study takes the water behaviour such as temperature change during the operation into account which has led to reduced error of 14%. Guo and Zhao [117] developed a numerical model for cross-flow IEC in which the effect of various operating parameters i.e., air velocities, channel width, relative humidity, etc., on the performance of the system was studied. This led to valuable results which could lead to an improved performance by the system. For instance, it is found that a system with a lower relative humidity of working air and channel width will have higher efficiency. New model for a cross and counter flow IECs is proposed by Ren and Yang [118] in which the coupled heat and mass transfer equations were solved together (two-dimensional). In addition, instead of common assumptions, the effect of Lewis factor,

evaporation, water temperature and saturation condition of the wet surface were all considered. This led to low discrepancy values as follows: 0.17% for the supply air temperature, 0.64% for the working air temperature and 0.24% for the working air temperature. It is also concluded that performance of the counter flow systems is superior to the parallel IECs.

Hettiarachchi et al. [119] employed the NTU method to develop a model for investigating the effect of longitudinal heat transfer on the performance of flat-plate cross flow IEC. The results revealed that the cooling efficiency of the system is 10% less than conservative conditions.

There are some more similar analytical/numerical studies for the IECs in which slight improvement can be seen in some models. However, no significant novelty was found in reports.

2.3.5. Review of the experimental studies

The experimental studies are normally done to practically observe the performance of the system under various conditions. In addition, the experimental data are the key source for validating the developed numerical models. Moreover, the experiments can be carried out to investigate the effect of different parameters on performance of the system. The experiments contribute to identifying the optimum operating conditions. One more superiority of the experimental studies is that the system performance can be evaluated without any simplifying assumptions which are normally made in analytical/numerical models. Generally, various performance parameters of the system i.e., cooling capacity, COP, efficiencies, pressure drop, and temperature drop are analysed to evaluate the performance of the system. A number of experimental studies have been carried out in the IECs which are addressed below:

Tulsidasani et al. [120] experimented a tube type IEC in Indore city to study the effect of air velocities on the system COP. The studies revealed that the maximum COP of 22 was achieved when the velocity of the intake air is 3.5 m/s and the velocity of the working air is 3 m/s. This occurred when the temperature drop had an acceptable value of 10.4 °C. To improve the efficiency, performance of a two-stage IEC with a flat-plate heat exchanger and two evaporative cooling chambers, is tested by Jain [121]. This innovative system is designed to enhance system performance in wet environments with low indoor air temperature values. The experiment revealed that the temperature drop was in the range of 8-16 °C when the relative humidity was 90%. In addition, the cooling efficiency of the novel system was 20-30% higher than the single IEC. A polycarbonate-made IEC was tested under two operating conditions by Velasco Gomez et al.[96]. In this first case, the exhaust air of a climate chamber is used as the working air of the IEC system, and in the second case, a water spraying is added to the exhaust air. The results showed that the performance of the system in terms of cooling capacity and cooling effectiveness is better in second case. Moreover, the system had better performance when the outdoor air temperature and airflow rate were both higher. Jiang et al. [55] used an IEC to provide the cooling water of the HVAC system in a building. The test showed that the COP of the system was ranged from 0.4 to 0.8 while the outlet water temperature was 14 to 20°C cooler than the inlet air wet bulb temperature.

Over another experimental study, the effect of various operating parameters e.g., outdoor air temperature, airflow rate, water flow rate, etc., on the performance of an IEC is studied by Costelloe and Finn [122]. This study helped the researchers to identify the optimum operational rate of the fan and pump system.

2.4. Technological breakthrough in IECs

Continuous endeavours in developing efficiency of the IECs resulted in an evolutionary breakthrough. As mentioned earlier, the heat and mass exchanger in IECs is core of the technology in which the heat transfer and evaporation take place. As a consequence, studies focus on improving the exchanger in order to achieve more efficient systems.

2.4.1. M-cycle Heat and Mass Exchanger

Dr. Maisotsenko [18], as one of the pioneers in IEC technology, introduced the M-cycle HMX which was the main initiative of the new technology which is called Dew Point Cooler (DPC). The main advantage of the new technology was proposing huge temperature drop compared to the previous IECs. The proposed system can be categorized into two types based on the airflow distribution, i.e., cross flow and counter-flow. The DPC is the state-of-the-art IEC which is able to reduce the temperature of the intake air to its dew point temperature which can end up with 30% more cooling efficiency [16].

Figure 2.9 shows the structure of the novel M-cycle HMX and airflow configuration for the DPC. As can be seen, the middle section of the surface in dry channel is allocated for the working air to flow and the rest of the surface is allocated for the product air (supply air) to flow. Both airflows are flown in a direct path using the parallel guided flow channels. Numerous tiny holes are designed on the surfaces to allow a certain amount of working air to divert to the wet channel. This innovative idea lets the working air to be cooled before entering the wet channel as it flows in the dry channel and loses heat to the adjacent wet channel. This will lead to more heat absorption be the working air in the wet channel mainly because of its lower temperature compared with the air streams in adjacent dry channels. As a result, the

cooling efficiency of the novel DPC will be higher than the traditional IECs. The psychrometric chart is provided as shown in **Figure 2.10**, to illustrate the various terms which are being used in performance evaluation of the DPCs. As seen, reaching the dew point temperature can significantly increase the temperature drop and lead to better cooling efficiency in the IECs.
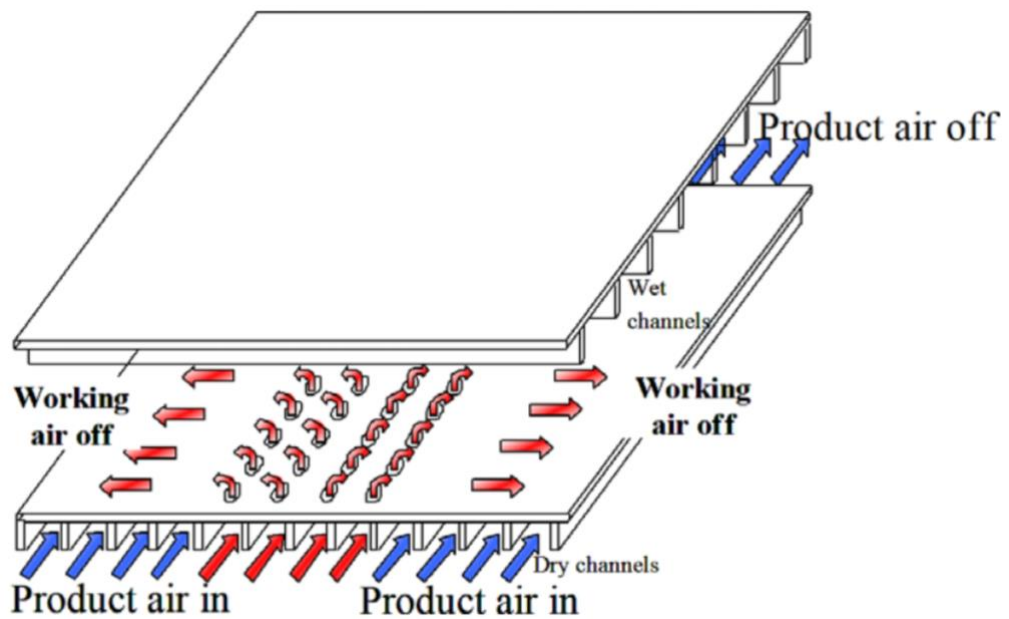
Figure 2.9: Structure of the HMX in DPC [34]**.**
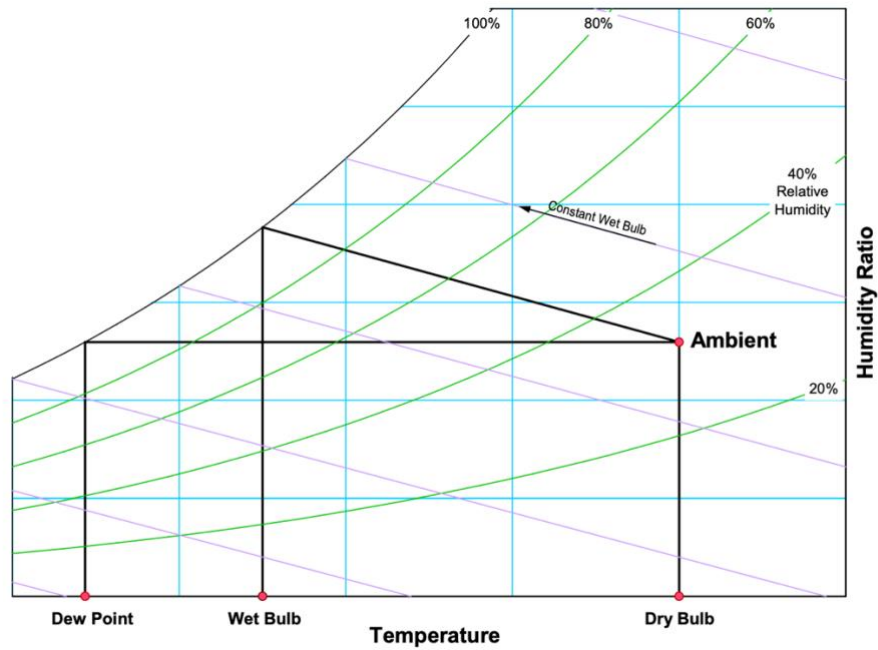
Figure 2.10: Temperatures in Psychrometric Chart

2.4.2. Research progress on DPC

The first ever research study for the novel DPC was an experimental work which is done in Coolerado® project in USA (see **Figure 2.11**) [17]. The test is conducted to evaluate the performance of the 2005 model Coolerado cooler in which the heat exchanger was inspired from the novel cross flow M-cycle design. The test results based on the ASHRAE standards revealed that the wet-bulb and dew-point efficiencies could reach the 80% and 50%, respectively.
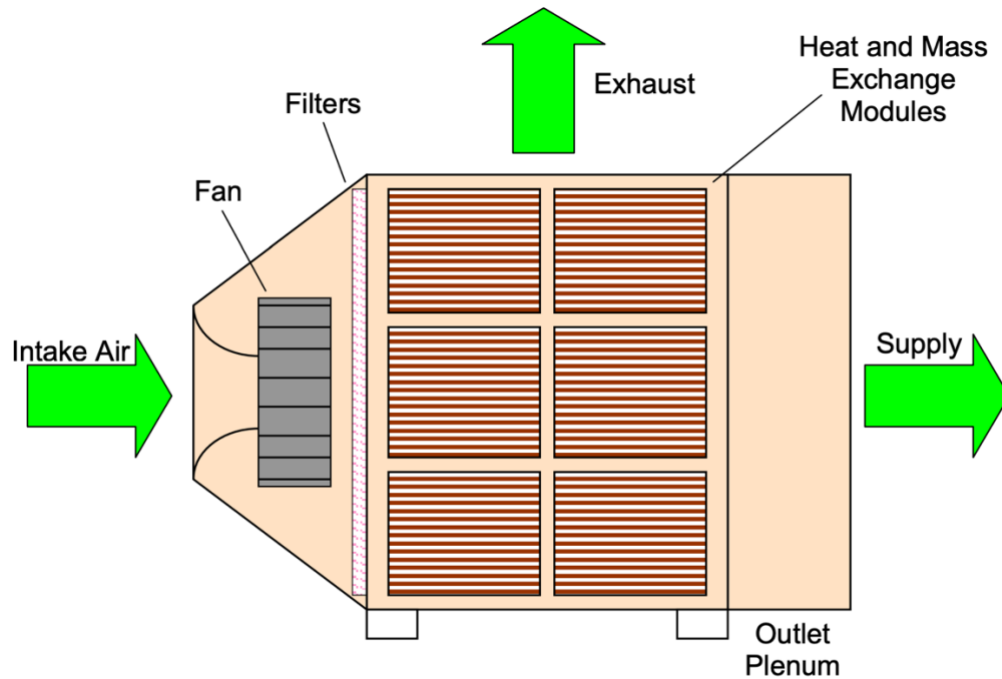
Figure 2.11: Coolerado indirect evaporative cooling [123]

Zhao et al. [12] carried out a study to investigate the feasibility of the DPC operation in buildings of China. The study focused on climates of different regions in China and availability of water for operation of the DPC. The analysis results revealed that the northern and west regions of China are the most suitable regions for the system as the weather was warm enough in summer season in these regions. Additionally, integrating the silica-gel dehumidification to the DPC system to dehumidify the wet conditions is highly recommended as the lower humidity will lead to higher cooling efficiency.

Riangvilaikul and Kumar [124] test a DPC in diverse operating conditions, representing dry, temperature and humid climates. The continuous operation of the system showed that the wet-bulb and dew point efficiencies were 102%, and 76%, respectively. Bruno [95] conducted an experimental study on a counter flow DPC prototype to mainly investigate the system performance in both commercial and residential buildings. Operation of the system in commercial buildings revealed that

the cooling performance of the system increases sharply in hot and dry climates. In addition, an energy saving of up to 56% was achieved when the system is used to cool down the outside air for ventilation purpose of the buildings. Jradi et al. [125] developed a numerical model with experimental validation for operation of a cross flow DPC in buildings. Moreover, a parametric study is conducted to identify the optimum operating conditions of the system. The results showed that the wet-bulb efficiencies of 70–117% with supply airflow rate of 300–1500 m3.h^{-1} can be achieved. It was also reported that the higher intake air temperature will lead to higher cooling efficiencies. On contrary, the increase of intake air velocity, channel height and working air ratio have a negative effect on system performance. Pandelidis et al. [126] compared the performance of a novel plate-fin exchanger with M-cycle systems by focusing on effect of inlet air parameters. It was revealed that the arrangement of the holes on the surface of the dry channels and the amount of working air ratio has a key impact on the performance of the both systems. In addition, the effect of operating parameters on was indispensable.

Xu et al. [127] introduced a novel heat and mass exchanger for the DPCs. As shown in Figure 2.12, the new exchanger is constructed by irregular plates which in comparison to the traditional flat-plate heat exchangers, is able to achieve higher heat transfer rate owing to the increased heat transfer area in the corrugated plates. In addition, the air resistance is decreased owing to removal of the triangular supporting guides. The results revealed that
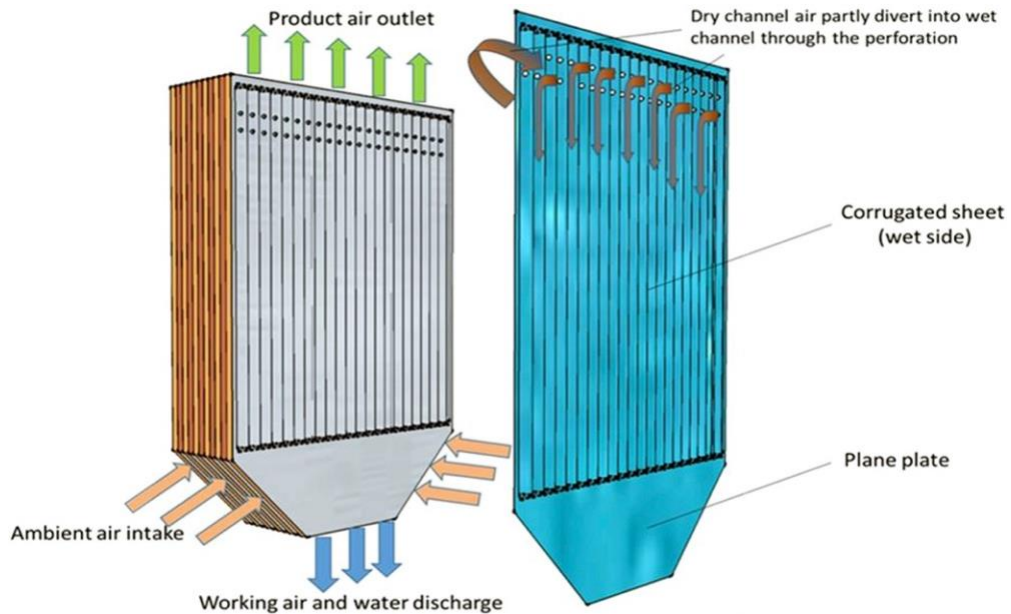
Figure 2.12: Novel heat exchanger introduced by Xu et al. [127]

Lin et al. [128], [129] carried out two studies in which the mathematical models are developed and converted to dimensionless equations for a counter-flow DPC. The developed models were able to predict the transient and steady-state performance of the system with maximum error of 8%. It is also found that the local Nusselt number and Sherwood number are stable in fully developed regions which were in the range of 8.67-9.95 and 8.17-8.67 respectively.

In another comparison-based study, Wan et al. [130], compared the cooling efficiency and temperature drop of two DPCs in which they were distinguished by their airflow configurations. Another study is conducted for a hybrid membrane liquid desiccant was integrated with the DPC. The results derived by a thermodynamic analysis revealed that the supply air temperature was in the range of 20-28°C while the maximum humidity ratio was 12 g/kg [131]. Wan et al. [132] developed a two-dimensional CFD model based on the NTU-Le-R method for a counter flow DPC in which the behaviour of the temperature and humidity ratio is studied. In addition, different operating and design parameters on the performance of the system are

analysed. Liu et al. [133] conducted a study for a counter flow dew point cooler in which the wet-bulb efficiency and COP increased by 29.3% and 34.6% respectively. It is also reported that the DPC have 10% higher cooling efficiency than a flat-plate DPC. In addition, it is also concluded that the cooling efficiency can be improved by increasing the channel length and cross-sectional area of the channel entrance, and by decreasing the channel width and channel gaps. Liu et al. [134] developed a numerical model for a counter flow DPC in which the effect of different operating parameters on the performance of the system studied by shifting the focus towards the comparison of the model results with three other developed models in the literature. The model with accuracy of 5% showed that the most important factor in improving the cooling efficiency of the system is the intake air temperature. A few more similar studies are conducted as well but no significant achievements are reported.

2.5. AI and optimisation in energy systems

The empirical success of Artificial Intelligence (AI) in various fields, as well as its capability in predicting the behaviour of the diverse technologies, have led to its increasing popularity in research and real-time applications. As a result, the benefits of applying AI in engineering applications, particularly in research studies on energy systems should not be underestimated. AI will pave the path in simplifying the engineering tasks which were difficult, time consuming or impossible to achieve in the past. Although AI was introduced in 1956 for the first time but the substantiality of its impact has been discovered over the past decade where it is used in wide ranges of fields including engineering. This is mainly because of the remarkable progress in computer sciences, in particular the computer hardware. AI can facilitate the tasks which were previously required human intelligence by learning and mutating human

intelligence [135]. ML is a subset of AI in which a machine/system learns by processing the data derived from the previously recorded behaviour of the system through different mathematical methods which contributes to predicting the behaviour of the system in any unforeseen operating conditions. AI is being gradually replaced by the sophisticated machines by taking over the smart production lines and manufacturing tasks over time. AI will contribute to design and simulation of the engineering products. It also can fully handle the low-value tasks and let the human to handle the higher-value tasks.

Optimisation algorithms are generally used in AI applications with the aim of optimising the behaviour/performance of the system to discover the full potential of the technology. The optimisation has a key role in determining the best and optimal value for the decision variables which affect the performance of the system [136]. For instance, it can have a wide range of objectives such as minimising the power consumption or cost, maximising efficiency, productivity, product quality or profit, etc. Mathematical optimisations fulfil these objectives through the sophisticated programming and mathematical tools to overcome the highly nonlinear problems in real applications [137].

2.5.1. Practical applications

The AI, in particular ML, has been a leading research subject in various engineering applications. For instance, ML is used in building energy [138] and building structural engineering [139] studies for diverse prediction purposes such as predicting the space heating and cooling loads of residential buildings. The growing popularity of the ML studies in building life cycle is proved in which the building design accounts for 44%, control for 28%, and operation and maintenance for 16% of the total studies [140].

The phase change materials integrated cooling systems including centralised and distributed cooling systems, is another area in which the ML algorithms are commonly used [141]. In addition, improving the power efficiency in Data Centres (DCs) by ML tools has become a common research topic. Growth in employment of cloud-based systems, internet-based services and hardware availability has led to the emergence of large DCs which are embedded with challenging operational concerns [142]. One of the complicated challenges is energy consumption management which has a direct impact on energy costs and environmental related issues. The AI-based methods such as neural network are generally implemented to predict the Power Usage Effectiveness (PUE) of the DCs. For instance, a model which is validated at Google DC is capable of accurately predict the PUE of a DC [143].

AI is actively used in big tech companies such as Facebook and Google. Apart from the nature of the tech companies in employing AI in their products and services, it is widely used in their DCs where huge amount of data are needed to be stored safely. For instance, Google uses its DeepMind AI unit to control the power consumption of the cooling systems through robust predictions [144]. This effort has resulted in 40% less power consumption by the cooling systems in Google's DCs which is considered as a major breakthrough by Google. This is done by recognising the hidden pattern in the historical data including the key affecting parameters such as temperature, pump speeds, etc. **Figure 2.13** shows how google tried to reduce the power consumption in its DC by controlling the Power Usage Effectiveness (PUE) through a developed ML recommendation. This DC consumes 0.01% of the total energy consumption globally, i.e., 260 million watts. This amount is identical with the power usage of 200,000 homes.
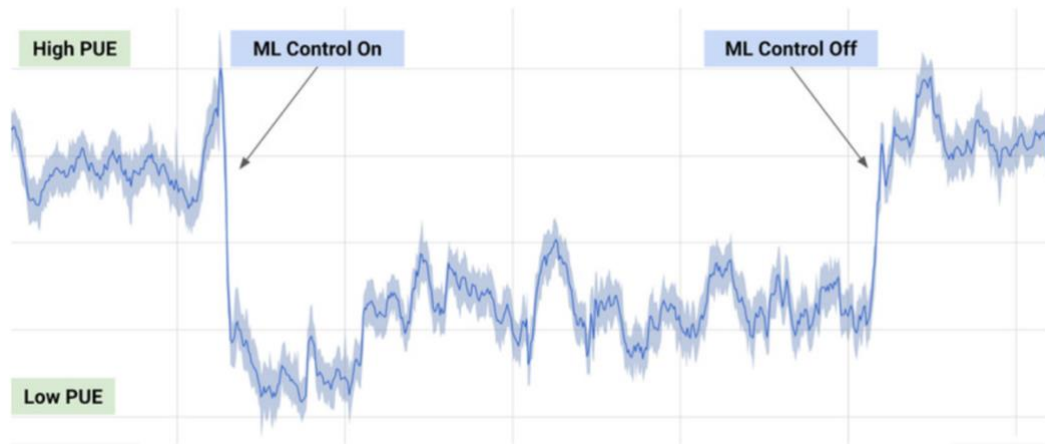
Figure 2.13: PUE prediction in Google's data centre using machine learning control tool [145]

The performance of the cooling systems as vital need of different buildings and their habitants, is needed to be predicted accurately in order to control and optimise the power consumption of the technology. For instance, ML models for the ECs, as the most common cooling systems, would be beneficiary. It would be invaluable to have a smart model that can predict and optimise the system behaviour in a world that time, energy consumption and intelligent application are growing swiftly. The AI based research studies on buildings and HVAC systems are risen over the past decade which are mainly conducted to provide the users with smart buildings as well as to intervene the detrimental impact of greenhouse emissions originated from the buildings and HVAC systems. For instance, an adaptive ML based building study [146] is conducted by the aim of building automation. The developed building model is updated by an online building data using a dynamic neural network-based model. In addition, an optimisation model is embedded in the system to optimise indoor thermal comfort and power consumption. The model is operated by controlling/optimising the ACs and mechanical ventilation systems which led to 36-58% energy saving in the considered building.

Similar to AI, the optimisation algorithms are needed in similar sectors ranging from business planning to engineering applications as it is vital to design the systems as economical as possible which can deliver the assigned duties in a short period of time. Tool in the optimisation algorithms can be applied to various energy technologies such as thermal components, heat exchangers, refrigeration systems, heat pump systems, fuel cell systems, renewable energy-based systems, power plants, cogeneration and trigeneration systems, multi generation systems, etc. [136].

2.5.2. Artificial Intelligence and Optimisation in IEC

Like other technologies, although very few, but AI is also implemented in the EC technology. As ECs are evaluated based on numerous parameters so that employing the ML algorithms, as a subset of AI, are beneficial for this technology. It is worth mentioning that ML is mainly employed to learn from the existed data, produced from the numerical models and laboratory tests, for performance/behaviour prediction of the technology by estimation of the common performance metrics, e.g., cooling capacity, COP, efficiency, pressure drop, temperature drop, etc. In addition, some attempts are tried in optimising the EC performance through the optimization algorithms which helps the engineers to identify the optimum design and operating conditions for the system. However, due to the quick developments in the field of AI, a lot of efforts are required to investigate the effectiveness and performance of all algorithms on ECs. However, to best of the author's knowledge, to date all of the AI related studies are on the DPCs which are the most advanced IEC.

In one of the early ML-based studies, Pandelidis and Anisimov [147] developed a ML model using the Response Surface Methodology (RSM) for a cross-flow DPC to predict the system performance using the four selected performance parameters. The

selected performance parameters were COP, cooling capacity, supply air temperature and dew point efficiency. Five operating parameters as the operating parameters, i.e., intake air temperature and humidity, mass flow rate of the supply air, working air ratio, heat capacity ratio and relative width of the exchanger in dry channel for working air, are selected as the inputs of the RSM model. The model has acceptable accuracy and showed that most effective parameters on system performance are supply air mass flow rate and intake air properties. In one other early attempt, Sohani et al. [148], employed the Group Method of Data Handling-type neural network (GMDH) to predict the supply air properties for a cross flow DPC using the intake air properties and channel length. The results revealed that apart from the model good fitting, its accuracy was 1.76% compared to the experimental data. Afterwards, the developed GMDH model is used in a Multi Objective Optimization (MOO) to maximise the COP and cooling capacity of the system by identifying the system optimum operating conditions. This is undertaken for the selected climates in which on average, the COP and cooling capacity is improved by 8.1% and 6.9% respectively. Similarly, as shown in **Figure 2.14**, Jafarian et al. [149] used the GMDH and NSGA-II algorithm-based MOO for a counter flow DPC with almost the same purposes, i.e., to find the optimized conditions in cities of Yazd, Masjed-Soleiman and Ahvaz. The MOO resulted in improved COP and specific surface area in all selected regions. The GMDH method produces some mathematical equations which comprising numerous terms for each performance parameter including all of the selected inputs. In another study, Sohani et al. [150], selected two DPCs, which one is called counter-regenerative DPC and the other one was a cross flow DPC. The optimum operating conditions are identified for both technologies and the performance of them were compared based on the water consumption, annual COP and life-cycle cost. The results revealed that the

counter-regenerative DPC has better performance compared to the cross flow DPC. In addition, the optimisation results revealed that the water consumption can be improved by up to 86.4%. The similar improvement is seen for the annual COP which was improved by 1,039%. Eventually, the results also reported that the life cycle cost of the systems can be improved by 64.4%. In another optimization-based study, Sohani et al. [151] also presented an hourly optimizations method for the DPCs employing Hourly Optimization Strategy (HOS) in which the performance of the system was tracked and optimized hourly. The results revealed that the annual water consumption was reduced by 19.6%. Additionally, it is concluded that the derived optimization conditions led to 17.8% more COP and 36.2% less operating cost.
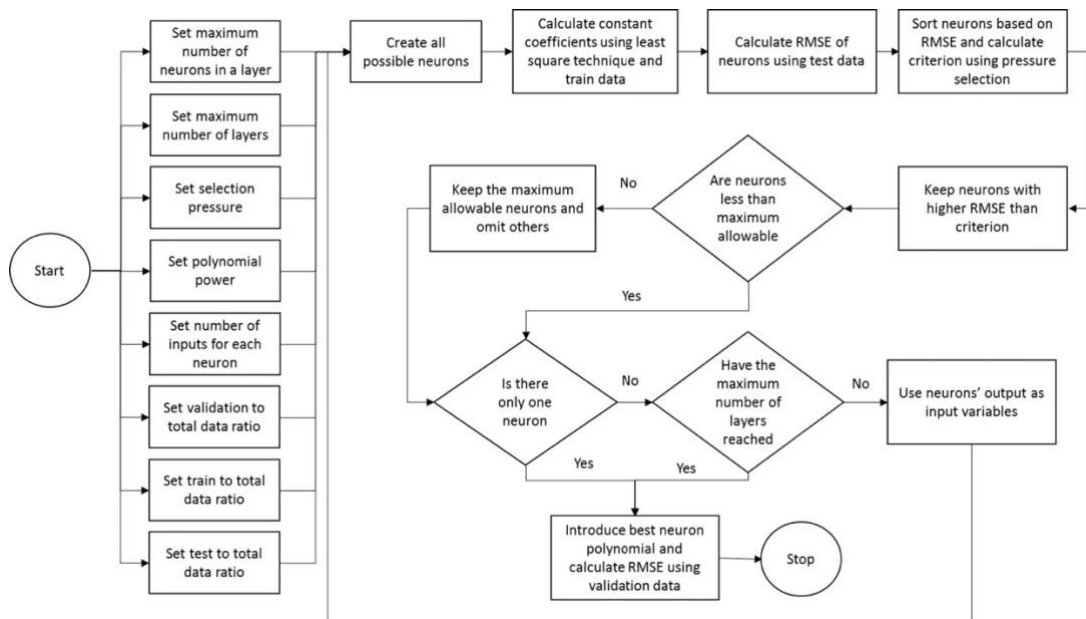
Figure 2.14: Flow chart of GMDH used in [149]

Pakari and Ghani [152] employed three regression models using RSM method for a counter flow DPC in which four operating parameters i.e., intake air properties, extraction ratio, channel length and channel width, to predict the supply air temperature and relative humidity as well as wet-bulb efficiency of the system. The

results revealed that the maximum discrepancies are less than 10%. Similar to the GMDH method, mathematical equations with numerous terms is produced for each of the performance parameters. An optimization-based study [153] used Genetic Algorithm (GA) based multi-to-single-objective and MOO to optimize the performance of a counter-flow DPC by taking the dew point efficiency, COP and cooling capacity as the objectives. The results showed that the multi-to-single-objective method outperforms MOO in terms of simplicity and operating time. The optimal channel length and working ratio for the considered DPC were 0.50m and 0.40 respectively. Moreover, the COP was 36% - 92% higher in the optimized system compared with the base system.

2.6. Research Gap and Scientific Challenges

Review of the existing literature showed that the studies on DPCs have been mostly concentrated on the traditional flat plate HMXs. However, a novel counter-flow Guideless Irregular Heat and Mass Exchanger (GIDPC) has the best performance in terms of COP value i.e., 52.5 [38], [127] under an ideal operating condition. Xu et al. [127] pioneered in introducing the GIDPC through the numerical and experimental studies. However, to the best knowledge of the author, there is not any attempt in developing the ML based models for the system. In addition, the lack of optimization models for the GIDPC is another outstanding gap which limits the full potential of the GIDPC.

The work in this thesis, mainly focuses on employing various ML algorithms and different optimization methods in order to:

    I.   Construct a big and comprehensive dataset for the GIDPC using a validated numerical model which is developed in Engineering Equation Solver (EES) software by inspiring from the experimental data.

II.   Develop different AI models in R, MATLAB and Python using novel ML algorithms for the performance prediction of the technology. The models will be compared and the best model will be introduced

III.   Develop different MOEO models using various algorithms to identify the optimum operating and design conditions of the GIDPC.

IV.   Present and compare the performance of the optimised systems in diverse climates in 2020 and 2050 by considering the impact of climate change.

2.7. Summary

This chapter carried out an extensive literature review focusing on the invention and improvement of the ECs. The focus of the chapter is then shifted towards the IECs after describing the outperformance of this technology over the DECs. Then the chronological review over the research findings for the IECs is discussed in details. It is mentioned that the continuous endeavours led to performance improvement of the technology and eventually ended up with an evolutionary breakthrough by introducing the DPCs. The overview is then continued by a detailed discussion on research works conducted for the DPCs. The introduction of GIDPC as the state-of-the-art DPC was a turning point in the EC technology as it is able to minimise the power consumption without sacrificing the cooling efficiencies.

However, to date, there is no effort in bringing the AI including ML and optimisation to further improve the performance of the GIDPC, which is identified as a clear research gap requiring an innovative solution. The rising popularity and success of AI in engineering applications have entailed this PhD study to conduct AI and optimisation-based study for the GIDPC. This approach fills the aforementioned gap by developing two ML models and three optimisation models for the performance

prediction and optimisation of the GIDPC. In summary, it can be concluded that this chapter contributed to illustrating the basic theory and concept of the ECs, reviewing the research progress made on IECs, identifying the opportunities to further improve the performance of the DPCs using the state-of-the-art methods, and eventually to building the structure and justification of the thesis.

CHAPTER 3: BIG DATASET FOR MACHINE LEARNING ALGORITHMS

3.1. Introduction

Data are the fundamental need of AI and in particular ML algorithms in the training process for the ultimate aim of prediction. Dataset plays a key role in efficiency, accuracy and applicability of the ML models in predicting the behaviour and/or performance of the considered system in any unforeseen and random situation. In this chapter, the methods used for construction of the big dataset as well as the sources of data, which will be used to train the ML models for the performance prediction of the GIDPC are explained in details. The dataset construction mainly comprises the selection of the various key parameters including operational, design and performance parameters of the GIDPC. The selection criteria and identification processes of the aforementioned key parameters which enable the investigation of the system behaviour, are detailed in the chapter. The aforementioned parameters are classified as the input and output variables of the ML models and the corresponding operating ranges of the input variables are also determined. In addition, data points creation based on the aforementioned input and output variables are included in this chapter. Eventually, common data pre-processing methods are explained which are used occasionally in training processes to enhance the efficiency of the models. In summary, the major works addressed in this chapter are:

- Selecting the operational, design and performance parameters of the GIDPC for prediction, assessment and optimisation purposes of the technology.

- Defining the operational ranges for the input variables to avoid creation and consideration of unreal operational conditions in the big dataset.

- Explaining the method used to construct the big dataset based on the created data points.

- Explaining the methods used for data pre-processing to improve the efficiency of the ML models.

3.2. Principles of data preparation

In the predictive data-driven ML based tasks, i.e., classification and regression, data preparation is an essential step. The data volume is substantially increased over the past decade owing to the significant and continuous advances in smart technologies [154]. However, 80% of the created data are unstructured [155]. It is predicted that an increase of up to 4300% in data creation will occur annually by 2020. It is identical to the individual data production of 1.7 megabytes by each person in the globe [156]–[158]. Basically, the emergence of the AI and in particular ML and any data driven algorithms are all reasons of data production in a huge scale. This sometimes becomes challenging to prepare the proper data quickly and accurately. It is vital to make sure that the data is clean, consistent and accurate enough before using them in any ML algorithm.

The primary step in developing the ML models is to construct a comprehensive and/or big dataset. This is because the ML models are based on data-driven algorithms which are aimed to get the required information through the data to analysis, extract the hidden patterns and eventually learn from them to finally establish a model which can predict the system's behaviour in any random and unforeseen operational condition. As a consequence, the dataset creation is very sensitive and requires a deep understanding of the considered system to hold and transfer the correct and sufficient information to the ML algorithm. The dataset which is used to train the ML model can

either properly build the model or can destructively confuse it. Thus, the destructiveness of a bad dataset should not be underestimated.

Therefore, it is aimed to summarise the key steps in preparing the dataset in this section. It can be defined as the process of transforming raw data into a form that is suitable for training the ML algorithms. Although the data preparation is highly dependent on the type of data but the following essential steps are needed in all applications:

Data collection: This is the primary step in constructing the big dataset. The probable challenges that can happen during the data collection must be handled properly. For instance, in a csv (common-separated) file, the relevant attributes must be determined. Converting the highly nested data structures, e.g., XML, JSOM, etc., must be analysed and converted to the tabular format for better analysing [159], [160]. The data collection step requires the full definition of the problem comprising the objectives and/or applications of the ML model.

Data exploration: The data exploration is an important step in building a big dataset. It should be undertaken once the data is collected. This step is necessary to assess the condition of the collected data. This assessment process should identify any missing value as well as any incorrect value among the collected data [161]. This is a vital step as the ML algorithm will capture all the provided information within the dataset. Giving incorrect information to the algorithm will affect the accuracy of the model and thus results in completely inaccurate models.
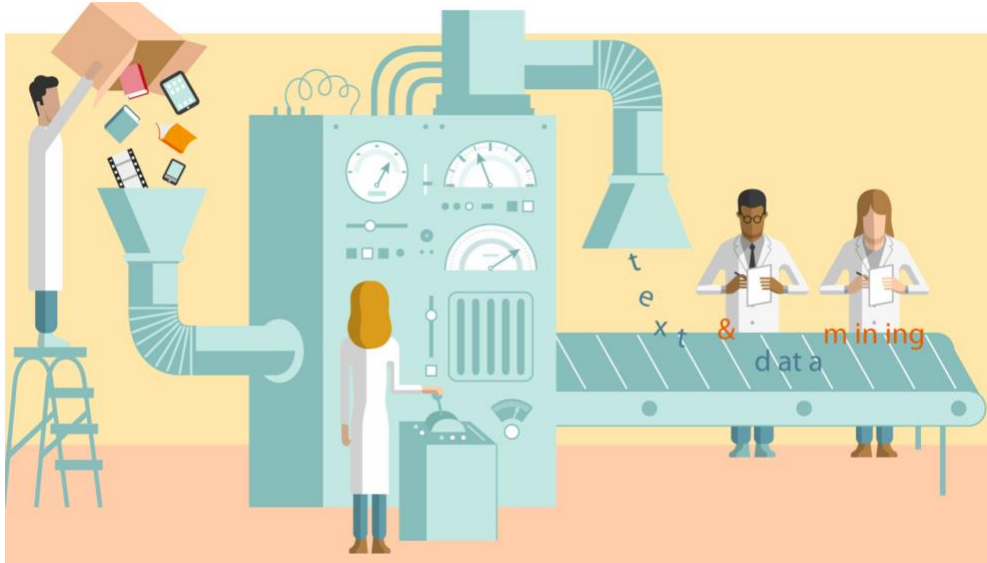
Figure 3.1: Graphical demonstration of data mining

Formatting: The next important step is to control the format of the collected data to ensure that they are in a suitable form to be employed and analysed by the ML algorithm [162]. This problem occurs when the data are collected from different sources. For instance, in the current study, the sources of data are experimental data and the analytical data where the format of some data, e.g., RH= 50% versus RH= 0.5, can be different. In addition, for instance, if a parameter is calculated by aggregating multiple sources, it is essential to make sure that the formats of all sources are same and correct.

Data quality check: The collected data must be controlled in order to increase the quality of data. For instance, it must be ensured that the collected data are in the required range. For example, for the GIDPC, when the data is collected from the numerical model, the parameters of the collected data should fall into the GIDPC's predefined ranges. Another quality check would avoid any repetitive or similar data which hold the same information. Having repetitive data, would lead to an inaccurate model which is unable to represent the true predictions. In summary, any outlier must be removed to increase the quality of the collected data [163], [164]

66

Feature engineering: Although it is said that the data is the fuel of ML models but this statement is more accurate when data is considered as the crude oil for the ML model which is needed to be refined. The feature engineering is used to prepare the inputs of the ML algorithm by transforming the raw data into features that suit the method [163], [165]. In addition, like other steps, it is undertaken to improve the information given to the algorithm.

Dataset split: The final constructed dataset should be split into two main subsets, i.e., training data and testing data [168]–[170]. The training data would simply be used to train and develop the model while the testing data would be used to assess the performance of the developed model. It must be ensured that the split data are not overlapped. In addition, it is important to split the data in a way that the algorithm can observe all the required data.

In this study, the main operational and design parameters of the GIDPC which practically affect the system performance and can vary simultaneously in different operational conditions, e.g., various climates, are considered only. This is because the main purpose of this study is to provide the models which can predict/assess the system performance when it is in real operation under various conditions. As a consequence, it is not necessary to involve all of the parameters in energy and mass transfer which are integrated with heat and mass transfer and fluid flow characteristics. This is an important advantage of data-driven models which are able to predict the performance of a system by knowing the major parameters only which simultaneously change in system's real operation. This results in development of more applicable models which could possibly be commercialised. The operating ranges are necessary for both operating and design parameters as they are needed to let the model and users know the upper bound and lower bound of the inputs. It prevents the model from

considering the unreal values (operating conditions) which can complicate the model structure and also can significantly add to the training and prediction time of the model. In addition, considering the unreal operating conditions causes the ML model to learn the conditions which do not exist in system's real time operation. Therefore, the operating ranges for each of the following operating and design parameters are the essential needs which are provided based on the rational assessment and real operation of the GIDPC in experiments.

Choosing the parameters as input/output variables of the ML models is the most important stage in data-driven models. Therefore, a careful analysis and thorough knowledge on system behaviour and theory are needed to select the appropriate parameters. It is aimed to choose the parameters which are touchable by the manufacturers and consumers. It should be noticed that choosing the same or similar parameters with relatively same scientific meaning can be considered as an outstanding disadvantage for the ML models. The reason for the negative impact mainly lies in the fact that considering the same/similar parameters will astronomically increase the time of training and will lead to more complex models. In addition, in some cases due to existence of excessive data points, weak algorithms will not be able to find an accurate model ever. The literature review shown in Chapter 2 revealed that considering various parameters with same/similar scientific interpretation can provide the readers with more information but in the ML models, the parameters selection should consider the independency of the parameters by focusing on the major parameters. In this chapter, the main parameters of the GIDPC system which can simultaneously change in system operation, are chosen. The importance and impact of each parameter on the GIDPC performance are explained in details and the corresponding operating ranges are disclosed accordingly.

3.3. Operating parameters

Based on the literature [33], [171], and experimental studies overviewed and explained in Chapter 2 of this research, it is identified that the common operating parameters for all types of ECs are mainly: intake air characteristics, flow rate (or velocity) of the air streams and a parameter which defines the proportion of intake and working airflows. These parameters play a key role in determining the system efficiency in terms of cooling capacity and power consumption.

3.3.1. Intake air temperature

Temperature is the first characteristic of the air which is considered as one of the most effective parameters on performance of the GIDPCs [127]. Temperature of the intake air is in direct link with the principal purpose of the GIDPC which is decreasing the temperature of the intake air. In addition, the intake air temperature is considered as a major factor in assessing the efficiency of the cooling systems. Therefore, temperature of the intake air [T_{in} (°C)], as one of the operating parameters of the GIDPC system, is selected as the first input for the ML models. Based on the literature, the system is efficient when the intake air temperature is in the range of 25 to 45 (°C). This means that when the temperature is below 25 C°, the natural air can be used to cool down the area.

3.3.2. Intake air relative humidity

The relative humidity is another parameter which has a key role in the efficient operation of the GIDPC. It is the second characteristic of air which is defined as the amount of water vapour that is held by air. In general, when the temperature of the air rises, the relative humidity decreases as the amount of water vapour that can be held by air is increased. Therefore, the relative humidity of the intake air [RH_{in} (%)] is considered as the second input variable for the ML models. Based on numerous studies

and the conducted experiments, it is concluded that the wet conditions (i.e., RH above 50%) will lead to poor system performance [127] as it leads to lower cooling capacity and COP. Consequently, using a dehumidifier in wet conditions is highly recommended in studies [168]. However, in the current study, a comprehensive operating range for the intake air relative humidity, i.e., 10-80 (%), is considered.

3.3.3. Velocity of the intake air

The intake air velocity is a factor which has a remarkable impact on system performance as it directly affects the cooling capacity, and rate of heat and mass transfer within the HMX. In addition, it is a key player in determining air flow rates and power consumption of the GIDPC in various operating conditions. Higher velocity provided by fans is associated with larger pressure drop which results in more power consumption and consequently lower COP values which are not desirable for the GIDPCs. As a consequence, the air velocity of the intake air [U_{in} (m/s)], is selected as the third input of the ML models. Similar to the previous input parameters, the operational range is inspired from the literature and real operation of the system which is decided to be in the range 0.3 to 3.3 (m/s) for the ML models in this research study.

3.3.4. Working air ratio

The working air ratio is defined as the ratio of the exhaust air to the total intake air. It plays a key role in system performance where higher working air ratio will lead to less supply air flow and consequently more temperature drop will occur in intake air which flows inside the HMX dry channels. As a result, at a very high working air ratio, the dew point efficiency will increase but it will lead to lower COP and cooling capacity values. In addition, the low supply air flow will remain as an unfavourable issue. Thus, the working air ratio [φ] is selected as the fourth input parameters for the ML models in this study. Numerous experimental and numerical studies [17], [38] have revealed

that the operating range for the working air ratio is 0.1-0.9. The selection of proper value for the working air ratio is widely dependent on the operating conditions (temperature and relative humidity in particular) and a simultaneous trade-off is needed to reach the best possible value for the system.

3.4. Design parameters

The dimension of the HMX, as the core part of the GIDPC, affects the performance of the system. Therefore, the most effective geometrical parameters of the HMX are selected as the design parameters of the ML models. The dimension of the HMX specifies the system cooling capacity and it plays a key role in determining the performance parameters of the system. So that it is crucial to include the design parameters in the big dataset for the ML models. In addition, the appropriate ranges for each of the selected design parameters are inspired from the literature. The selected design parameters are HMX height, channel gap and number of layers. The HMX width is not considered since: 1) The heat transfer in width direction is ignored; 2) To avoid time consuming and complex model by ignoring the less important parameters.

3.4.1. HMX height

Height of the HMX is a factor which has the most significant impact on efficiency of the GIDPC which is needed to be selected carefully. The larger HMX height normally results in a better GIDPC performance [127] in terms of cooling capacity as it provides more heat transfer area through the HMX layers but on the contrary it leads to a higher pressure drop along the heat exchanger, higher fan power, larger surface area and higher construction costs simultaneously [172]. The importance of this factor has led us to choose it as the fifth input variable for the ML models. The height of the HMX is largely dependent on the application of the GIDPC and the required cooling capacity. However, through numerous conducted studies, it is revealed that the GIDPC

can perform effectively when the height of the HMX [H(m)] is in the range of 0.8-3.3 (m) [33].

3.4.2. Channel gap

Channel gap is another design parameter which is defined as the distance between two adjacent layers in the HMX. This parameter has a key role in system performance as smaller channel gap will cause a higher pressure drop and consequently will result in higher fan power and lower COP values. To the contrary, the larger channel gap will lead to a higher mass flow rate and higher cooling capacity. As a consequence, it is vital to include the channel gap in the big dataset and consider it as one of the inputs for the ML models. Thus, the channel gap G(m) is selected as the sixth input variable for the ML models which is generally in the range of 0.004-0.008 (m). The ranges for the channel gap is specified based on the numerous experiments and the modelling studies conducted for the DPCs.

3.4.3. Number of layers

A number of layers in HMX is another important factor which can affect the performance of the system. It plays a key role in determining the production cost so that is vital to take into account the pros and cons of different number of layers in the structure of the HMX. More layers can be considered as an important factor in increasing the pressure drop, surface area and construction cost. In addition, an increase of these parameters will lead to more evaporation area and more heat transfer from dry channel to wet channel. The importance of this factor in dimension and performance of the system is made the author select it as the seventh input variable in ML models. It has been concluded that the number of layers, $[N_L]$, varies between 100 and 200. This range is identified through the comprehensive review of the experiments and modelling studies conducted for the DPCs.

The summary diagram for the selected inputs variables which are classified as operating and design parameters are shown in **Figure 3.2**. Moreover, the operating ranges of all input variables are listed in **Table 3.1**.
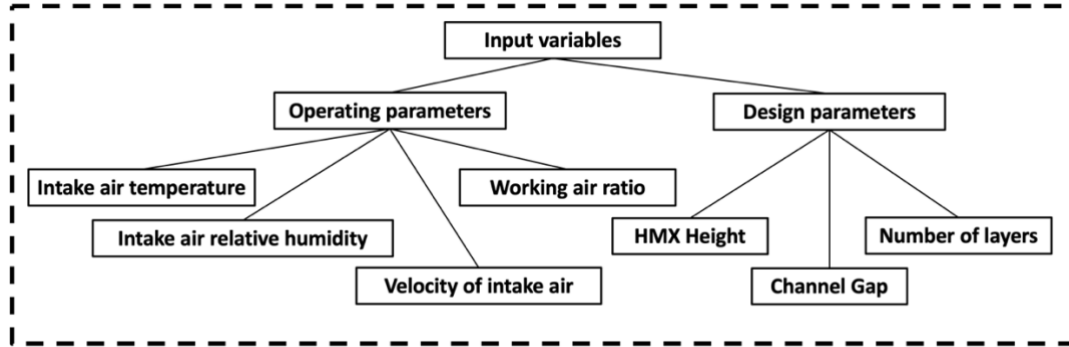
Figure 3.2: Selected operating and design parameters

Table 3.1: Operating ranges of the input variables

Type of parameters	input parameters	Minimum	Maximum
	$T_{dry,in}$ (°C)	25	45
Operating parameters	$RH_{dry,in}$ (-)	0.10	0.80
	$U_{dry,in}$ (m/s)	0.30	3.30
	φ (-)	0.10	0.90
	H (m)	0.80	3.30
Design parameters	G (m)	0.004	0.008
	N_L (-)	100	200

3.5. Performance parameters

Generally, the IECs performance is assessed by their ability in decreasing the temperature of the intake air which is called temperature drop. The temperature drop is the core parameter in evaluating the performance of the ECs. However, apart from the thermal performance of the system, it is vital to know how efficient the EC is in terms of power consumption. These aspects can be evaluated by common metrics, i.e.,

cooling capacity and COP which are defined by ASHRAE [47] in which the cooling capacity is responsible to report the system performance in terms of heat removal and COP is the ratio of the cooling capacity to the required power. However, there are several other metrics which can be used to further assess the performance of the system in depth. For instance, wet-bulb and dew point efficiencies, pressure drop and surface area of the HMX layers are other performance parameters. The selected performance parameters of the GIDPC as the output (target) variables of the ML models are followed in this section.

3.5.1. Cooling capacity

The cooling capacity is one of the key performance parameters which expresses the amount of energy produced by the system. The cooling capacity is identical to the capacity/ability of the system in removing heat from the space which its increasing was one of the principal objectives of the research studies. The parameter uses the temperature drop as the core term in its formula as Eq. (3.1):

$$Q_{cooling} = C_p(T_{dry,in} - T_{dry,out})(1 - \varphi)Q_{m,dry,in} \tag{3.1}$$

Where $Q_{cooling}$ is cooling capacity, C_p is the specific heat capacity, $T_{dry,in}$ is the intake air temperature in dry channel, $T_{dry,out}$ is the outlet air temperature in the dry channel, φ is working air ratio, and $Q_{m,dry,in}$ is mass flow rate of intake air in dry channel. Therefore, the cooling capacity , [$Q_{cooling}$ (kW)], is selected as the first main output for the ML models.

3.5.2. Coefficient of Performance

Coefficient of Performance (COP) is another key performance parameter of the EC which is identical to the ratio of the produced energy by the system (cooling capacity) to the amount of energy used by the system. In the GIDPC structure, the supply air fan, exhaust air fan and water pup are responsible for the main power consumers. Huge efforts are made in research for the ECs to improve the COP value by decreasing the power consumption by choosing the efficient fans/powers. In addition, increasing the cooling capacity result in improved COP values which was the focus of most studies. The COP can be expressed as Eq. (3.2):

$$
\begin{cases}
\text{COP} = \dfrac{Q_{cooling}}{W_{fan} + W_{pump}} \\
W_{fan} = (U_{dry})(Chord)\left(\dfrac{G}{2}\right)(m)(\Delta P)/(e_f) \\
W_{pump} = f(water\ flow\ rate, H)
\end{cases}
\qquad (3.2)
$$

Where, W_{fan} and W_{pump} are the electrical power consumed by the fans and the pumps respectively, chord is a parameter that defines corrugations of the plates in HMX, m is number of channels in the HMX structure, ΔP is pressure drop and e_f represents efficiency of the fan. The power consumption values are correlated with the GIDPC's design parameters. As a consequence, COP is selected as the second main output for the ML models.

3.5.3. Thermal efficiency

Thermal efficiencies demonstrate the ability of the system in decreasing the temperature of the intake air to some specific levels. In general, thermal efficiency includes two terms, i.e., wet bulb efficiency and dew point efficiency. Wet bulb

efficiency assesses the system ability in decreasing the intake air temperature to the wet bulb temperature while the dew point efficiency evaluates the system performance in decreasing the intake air temperature to the dew point temperature. Scientifically, both aforementioned performance parameters represent the thermal efficiency of the system and the only difference is the comparing factor. In most of the reviewed literature in Chapter 2, both wet bulb and dew point efficiencies are considered as the performance parameters as it was intended to give the authors more information regarding the temperature drop occurred by the system operation where the trend/behaviour of both parameters was exactly the same. The definition of these parameters is shown in the following Eq. (3.3):

$$
\begin{cases}
\varepsilon_{wb} = \dfrac{T_{dry,in} - T_{dry,out}}{T_{dry,in} - T_{dry,in,wb}} \\
\varepsilon_{dp} = \dfrac{T_{dry,in} - T_{dry,out}}{T_{dry,in} - T_{dry,in,dp}}
\end{cases}
\tag{3.3}
$$

Where, ε_{wb} is the wet bulb efficiency and $T_{dry,in,wb}$ is the wet-bulb temperature of the intake air in dry channel, ε_{dp} is the dew point efficiency and $T_{dry,in,dp}$ is the dew point temperature of the intake air in dry channel. As a consequence, the wet bulb efficiency, $[\varepsilon_{wb}]$, and dew point efficiency, $[\varepsilon_{dp}]$, were selected as potential outputs (third and fourth) for the ML model.

3.5.4. Pressure drop

The pressure drop is another performance parameter which is created when the air flow is distributed within the HMX. The main reasons for pressure drop occurrence within the HMX are velocity and friction. Pressure drop can have positive and negative effects on the system performance and the heat transfer process. Excessive pressure drop is considered as a negative impact as it adds up the requirement for the air velocity which leads to more power consumption by fans and low COP values. To the

contrary, it is vital to overcome the air resistance alongside the flowing channel. The pressure drop can be expressed as Eq. (3.4):

$$\Delta P = (\xi + \lambda_f \frac{1}{Dh}) \frac{\rho U^2}{2} \qquad (3.4)$$

where ΔP is pressure drop, ξ is coefficient of local resistance, λ_f is coefficient of friction resistance, Dh is hydraulic diameter, ρ is density and U is the air velocity. Therefore, the pressure drop, $[\Delta P(kPa)]$, is considered as another potential output for the ML models.

3.5.5. Surface area of the HMX layers

All of the aforementioned performance parameters have focused on the technical performance of the system. Although the COP takes the economic aspect into consideration but another parameter is needed to represent the material cost used in the core part of the system (HMX). Surface area of the layers is a parameter that represents the area of all layers used in structure description of the HMX. It is chosen to mainly control the cost which can be calculated using the following Eq. (3.5):

$$A_s = (N_L)(H)(w) \qquad (3.5)$$

Where A_s is the surface area, N_L is the number of layers, H is height of the HMX and w represents the width of the surface. Although the surface of the area, $[A_s\ (m^2)]$, is not a key performance parameter, it is still considered as one of the potential outputs (sixth) in the ML models. Although lower surface area values are desired but higher surface area values can astronomically increase the cooling capacity of the GIDPC.

3.6. Experimental performance of the GIDPC

An experiment on a 4-kW GIDPC prototype is conducted by simulating various operating conditions in the lab environment. The main objectives of this experimental study is: 1) to provide a set of experimental data to validate a numerical model which

will be used to create data for the ML algorithms; 2) to present the superior performance of the GIDPC in diverse simulated operating conditions.

3.6.1. Guideless irregular dew point cooler prototype

A 4-kW counter-flow GIDPC prototype, as shown in **Figure 3.3**, was operated to show the performance of the GIDPC in diverse operating conditions. The prototype is mainly constituted of three components:
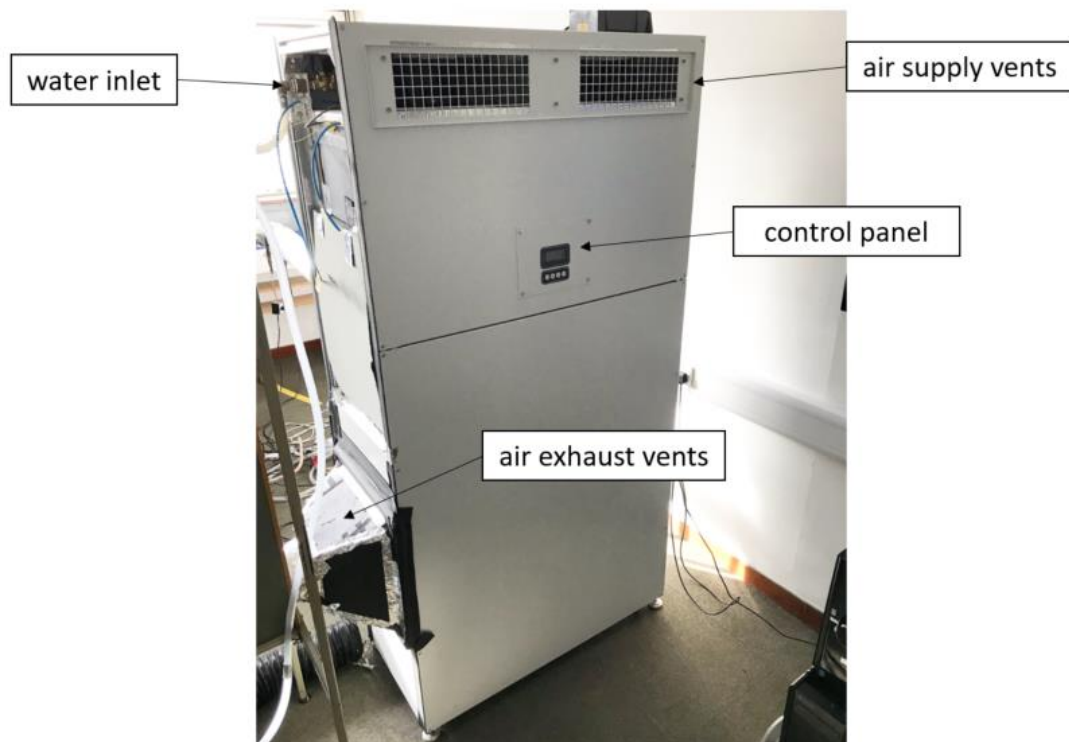
Figure 3.3: Counter-flow GIDPC prototype

A novel guideless irregular HMX: The guideless irregular HMX as the principal component of the GIDPC is shown in **Figure 3.4**, which is formed of 160 layers. The HMX dimensions are 1000mm (height) $\times$ 360mm (width) $\times$ 800mm (length). To divert the inlet airflow from dry channels to wet channels, a number of small holes (with a diameter of 5mm) are placed on top side of the HMX (**Figure 3.4(a)**). The number of holes (perforations) in the prototype is 118. Generally, the effect of perforation numbers is considered in the pressure drop calculations through the local resistance.

Considering the dimension and corrugated structure of the HMX, the total heat transfer area includes the corrugated are, i.e., 341032 mm^2, and the lower flat section area, i.e., 41760 mm^2, which results in the total heat transfer area of 380479 mm^2.

(a)

(b)

(c)
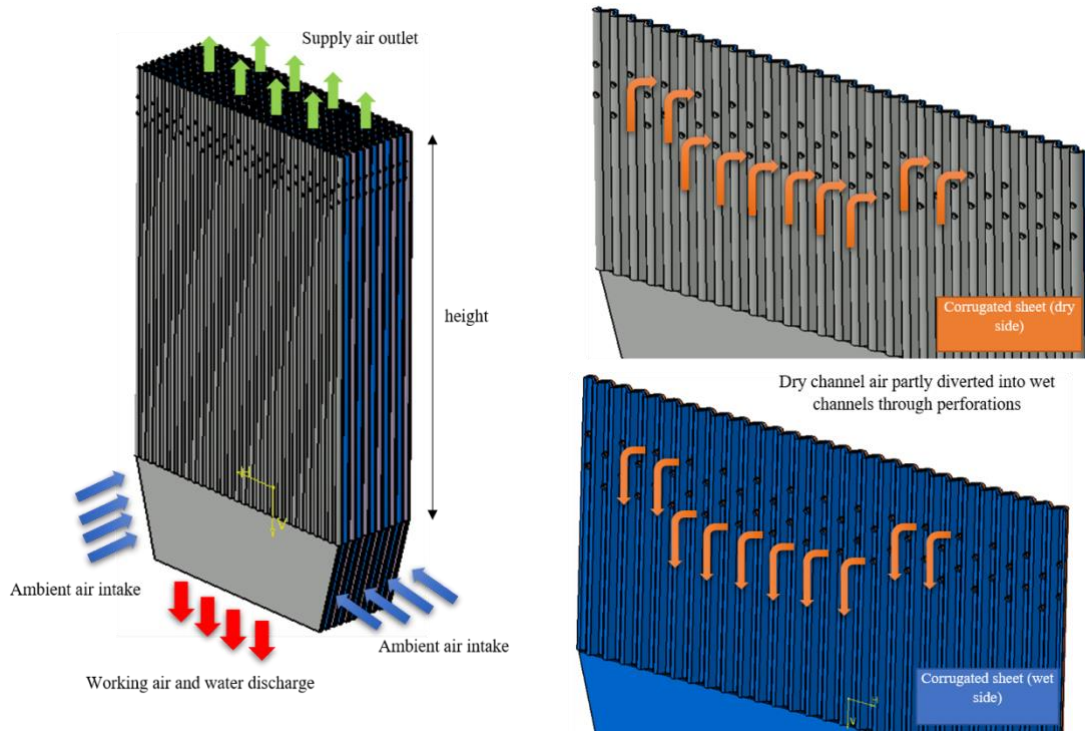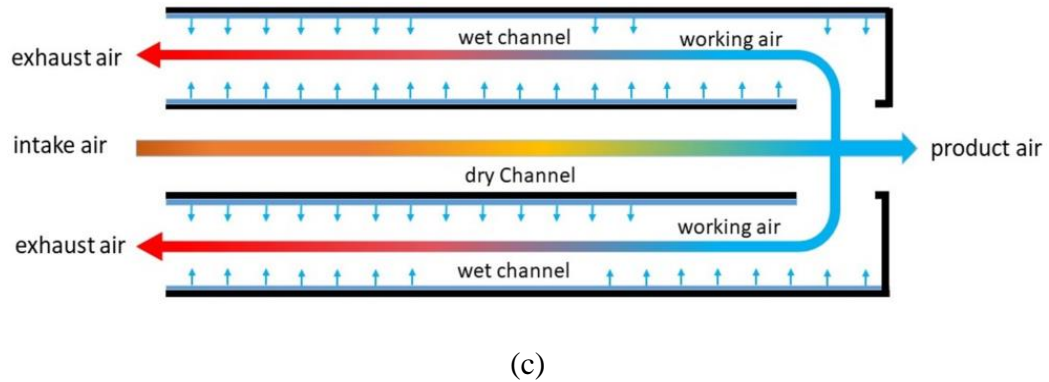
Figure 3.4: Schematic of heat and mass exchanger (HMX) as used in the DPC: (a): front view of a corrugated sheet [33]**; (b): wet and dry channel layers; (c): air distribution within HMX.**

As shown in **Figure 3.5**, the materials used to construct the sheets within the HMX are specific aluminium and Coolmax fibre in which the aluminium side has made the dry channel and the Coolmax fibre side has made the wet channel which has high water diffusivity and evaporation capacity [107].
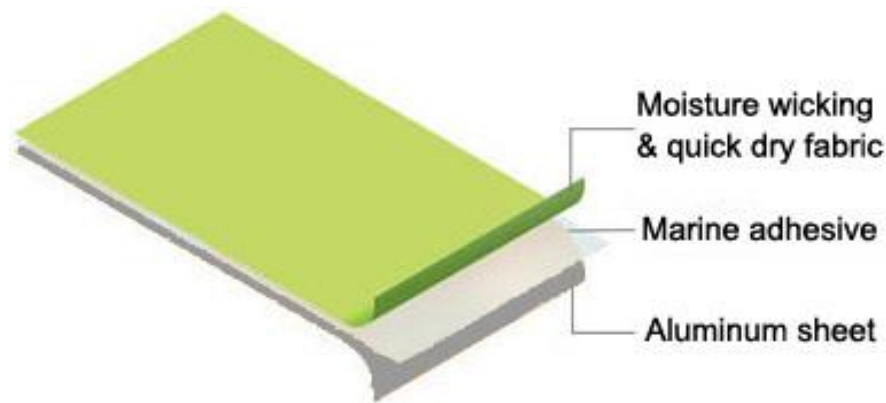
Figure 3.5: Material of the layers in HMX [107]

Water supply/distribution system: Owing to the advanced absorption capacity of fibrous material in the wet channels, the periodic water supply design was used by a dedicated water distribution system [38], which reduces the amount of used water as well as water pump power consumption. The water distributer is composed of a water pump, a water header, a water sink, and water distributor tubes which enable the even

distribution of water over the surface of wet channels. **Figure 3.6**, demonstrates the water distribution systems which is then embedded within the HMX.
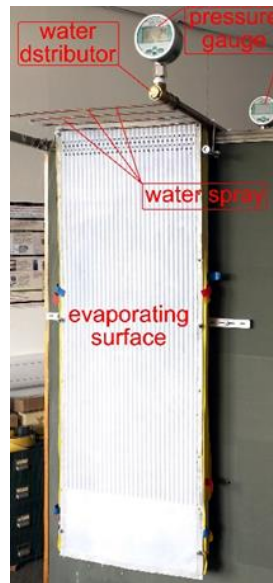
Figure 3.6: Test and demonstration system of water distributing [38]**.**

When the water sink underneath the HMX is empty, the water is supplied with a flow rate of 6.85 L.min^{-1} for 15 seconds with 10 minutes intervals, and when the tank is full, the water is supplied with flow rate of 2.45 L.min^{-1} for 60 seconds with 10 minutes intervals. Moreover, temperature of the running water is kept at the range of 16-20˚C to ensure efficient cooling. In order to apply the aforementioned scheme, the dedicated controllers are used within the GIDPC unit. A time relay is employed to control and adjust the running time of the water pump to ensure the timely water circulation within the HMX. In addition, the pressure of the feeding water could be controlled by a pressure gauge and the air pressure sensors in order to follow the desired water spray scheme which is quite important to make the evaporation process continue all along the experiment.

Product and exhaust air fans: Two fans for supply air, two fans for exhaust air, and one water pump together with fan/pump controller are placed inside the DPC unit to

control the air flow and water circulation during the experiment. The specifications of

the aforementioned components are listed in **Table 3.2**. The speed of the fans could

be changed and adjusted manually through the fan controllers which could be

displayed on the control panel.

Table 3.2: Technical specifications of the DPC components

Component	Specifications
Supply air fan	R3G225-RE07-03, 705 m^3.h^{-1}, 458 Pa, 160 W
Exhaust air fan	R3G225-RE07-03, 705 m^3.h^{-1}, 458 Pa, 160 W
Water pump	DH40H-24110, 24 V/1.2 A DC, 11mH2O, 450 L/hr
Fan controller	980-CAS11007 – TMS Controller, ebm-papst Ltd
Pump controller	DH48S-S, Xinling Electrical Co. Ltd

During the system operation, the intake air flows along the guideless layers of the dry

channel with relatively high temperature and a certain value of relative humidity. The

heat transfer is triggered owing to the temperature difference between the intake air

and the neighbour wet channel. Part of the cooled intake air is diverted to the

neighbour wet channel when it approaches the holes on the layers, while rest of it

leaves the dry channel as the supply air. The diverted air, called the working air in the

wet channel, is to absorb and carry the transferred heat and the moisture out as the

exhaust air.

3.6.2. Integrated experimental rigs

Figure 3.7 shows the complete experimental instruments and schematic of the

experiment. The experimental rigs alongside the GIDPC unit were all integrated in the

laboratory to carry out the experiment. An intake air regulating system comprising an

electrical heater to adjust the temperature, a humidifier and a dehumidifier to adjust

the humidity, are used to imitate the weather condition of the selected climates in each

month. The heater was adjustable which enabled the flexibility of adjusting the required air temperature. The humidity of the air with the required temperature is adjusted by the dehumidifier/dehumidifier and is transferred to the GIDPC as the intake air through the spiral ducts. The humidifier/dehumidifier was mixing the wet air with the air coming from the heater to achieve the required humidity. Spiral ducting with several embedded dampers are installed to construct the airflow distribution system for the GIDPC with ability of controlling the rate and direction of the airflow. The relatively long ducts are used in front of the intake, supply and exhaust air vents to overcome the pressure drop along the flow direction. In addition, small auxiliary fans are also embedded inside the intake/supply air ducting systems to maintain the zero-static pressure of the flowing air inside the ducts which were being controlled continuously by the measurement devices during the experiment. Furthermore, several other measurement instruments (i.e., temperature and humidity sensors, and flow meters) were used to measure the temperature and humidity and flow rate of flowing air during the experiment. Moreover, power meters were used to measure the power consumption of the fans and a water pump, and a water flow meter was used to measure the water flow rate, a pressure gauge was used to measure the water pressure, and eventually, a fan controller system was used to adjust the fan speed during the experiment. In addition to the manual controls, all of the measured data were transferred through a USB port and embedded sensors to a screen located next to the experimental rigs and were compared with the manually recorded measurement data. The top view of the lab environment with the fully integrated rigs and their locations are shown in **Figure 3.7 (b).** The schematic top view reveals the location of the unit and the corresponding test rigs in the lab room.
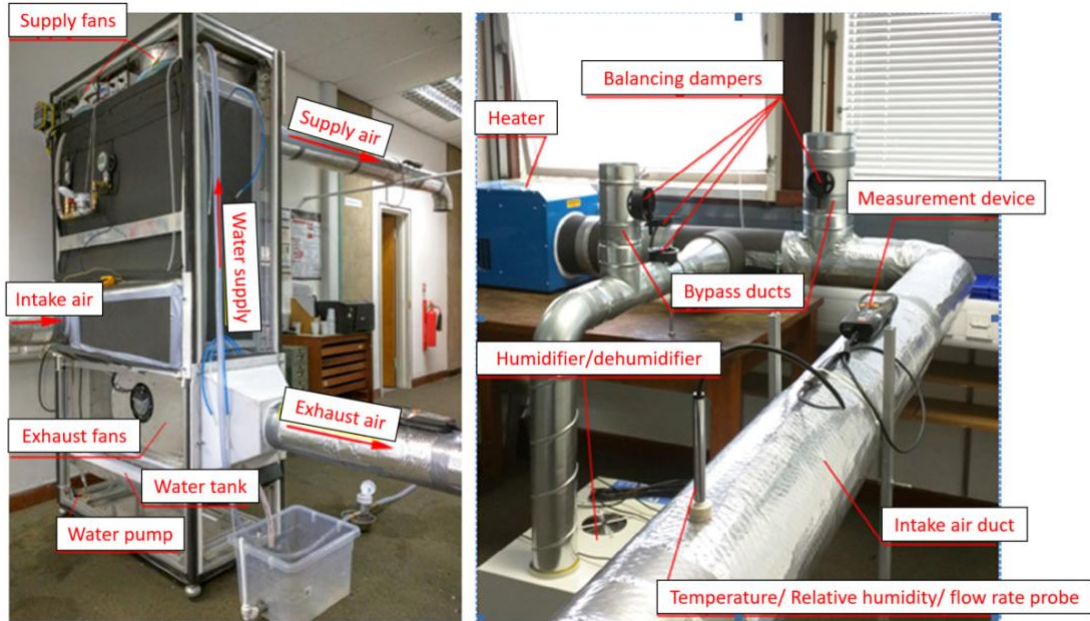
(a)
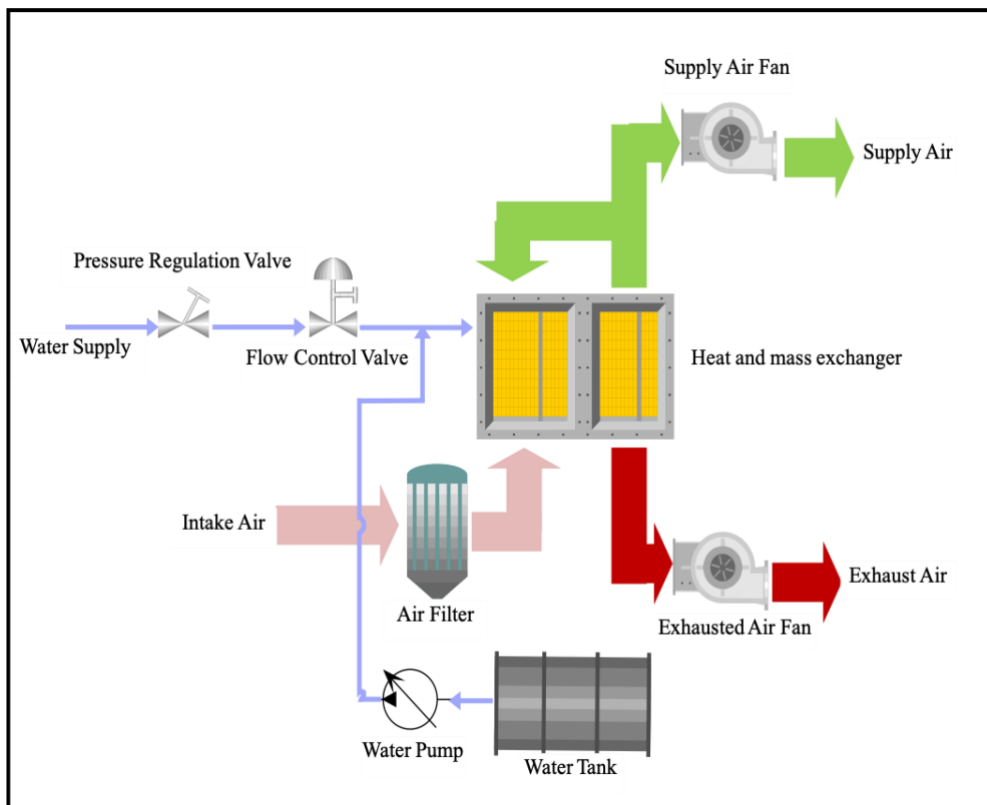
(b)

Figure 3.7: (a): Fully integrated experimental set-up; (b): Schematic of the experiment

3.6.3. Experiment procedure

During the experiment the considered weather conditions in the laboratory were simulated by the dedicated heater and humidifier/dehumidifier (as shown in **Figure 3.7(a)**). The GIDPC was run for 180 minutes for each simulated condition in which the first quarter of the experiment was allocated for the system stabilizing which is mainly because of the water to distribute over the wet channels' surfaces to have better evaporation. It also helps the intake air to reach the target temperature and relative humidity of the considered weather; as adjusting the relative humidity and temperature is time consuming where the simulated air needs enough time to reach the GIDPC unit and then to get distributed within the system. During the experiment, the temperature and the relative humidity were being monitored continuously by the humidifier/dehumidifier within the laboratory and also through the measurement devices to avoid any change. Then, the system performance parameters, i.e., cooling capacity, COP, wet-bulb and dew point efficiencies which were displayed on the screen, were recorded every 15 minutes and eventually at the end of the experiment the average values of each performance parameter were calculated and reported. The experiment for each operating condition is repeated twice and the average of the results were calculated. This is carried out mainly to decrease or minimise any error and inaccuracy which could occur during the experiment. Because the whole experiment comprised numerous components including sensitive sensors, so that the error sources could arise from the components such as sensors or even by the human. In addition, the delayed response and other probable error sources made us repeat each operating condition twice.

To maximize the energy saving potential of the GIDPC, optimum operational proportion of the supply and exhaust air were adjusted by the corresponding fans. It

was experimentally established that the best cooling performance of present GIDPC achieves when the working air ratio over the intake air is 0.37 [38]. This value could have been achieved by different supply and exhaust air flow rates but examining different values revealed that some flow rates lead to more efficient cooling. Therefore, it is decided to have the optimum supply air and exhaust airflow rates of 602 and 364 $m^3.h^{-1}$, respectively, which were kept constant throughout the experiment. This is undertaken to have the comparable results in all diverse weather conditions. Under these circumstances, the fans' power consumption, which varies by supply and exhaust airflow rates, is measured as 89 W by fan power meter in the working air ratio of 0.37. The water pump power consumption is measured as 1.5 W by a power meter leading to the total GIDPC power consumption of 90.5 W. It is worth mentioning that all of the power units in this study are electrical watts or kilowatts per unit time which represent the rate of power consumption instead of amount of power.

3.6.4. Climate pre-treatment

A developed numerical model for a solar/waste energy driven dehumidification/regeneration cycle with a solid adsorbent bed by authors [168] is used to pre-treat the wet climates by reducing the humidity of the intake air prior to its entrance into the GIDPC. In actual real-life scenarios, the intake air from extremely hot and humid climates needs to initially go through a dehumidifier for pre-treatment purposes of the wet conditions in order to achieve the operating ranges of GIDPC, which leads to a massive improvement in performance efficiencies of GIDPCs. These ranges indicate that the intake air temperature of GIDPC should be in the range of 25-45°C and the relative humidity should be less than 50%. The reason for having such a limited relative humidity range is that the intake air with high relative humidity will

have less chance to lose its heat to the adjacent wet channel. The reason for this is because a part of the intake air will be diverted to the wet channel in which the evaporation takes place to absorb the heat from the initial intake air in the dry channel. The wet intake air which enters the wet channel will have less capacity in absorbing the water and consequently the heat transfer rate will be decreased. As a consequence, the wet conditions should be pre-treated to decrease the relative humidity level of the GIDPC intake air. Real operation of GIDPC in such conditions will be accompanied by a dehumidification system, but in current experimental study, the focus is on the GIDPC prototype, and no dehumidification system is used. Instead, a verified auxiliary model is used as a replacement. Therefore, the model is used to pre-treat the air parameters of wet conditions only (Mediterranean and humid continental) prior to their entrance to the GIDPC.

The model is developed for a solar/waste energy driven dehumidification/regeneration cycle with a solid adsorbent bed as shown in **Figure 3.8** to solve the energy conservation and mass conservation laws. The corresponding equations are applied to the selected control volumes, i.e., flowing air and desiccant bed particles, in the dehumidifier. Generally, a number of assumptions are made in dehumidifier models [173] to mainly simplify and accelerate the simulation without sacrificing accuracy. These assumptions are: temperature and moisture content of the air and absorbent in the vertical direction are uniforms which result in one dimensional heat and mass transfer; heat transfer via conduction is not considered in the flow direction which is mainly because of the small thermal conductivity of the air; heat and mass transfer coefficients are considered to be unchanged between air and desiccant; it is assumed to have the identical solar radiation in the regeneration process; it is assumed to have an unchanged air state at inlet and outlet of both cycles.

dehumidification process
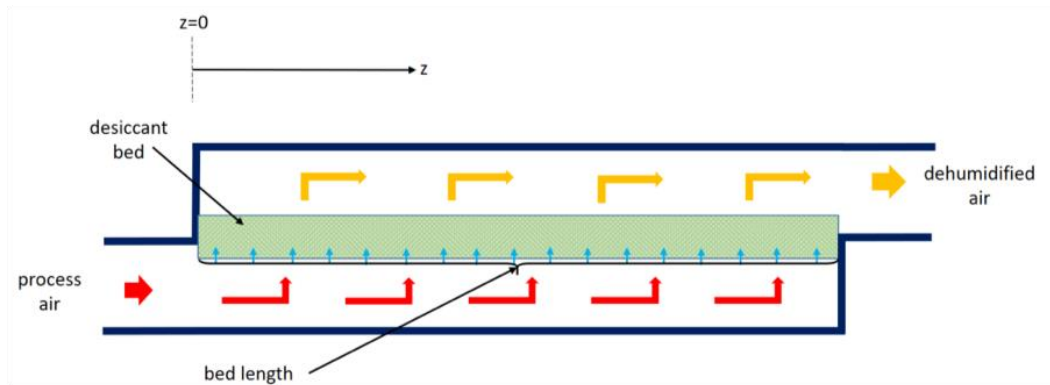
regeneration process
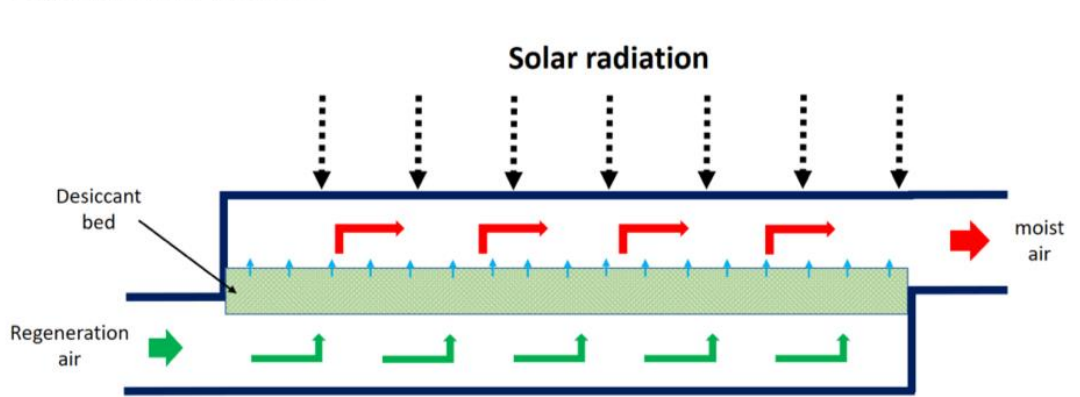
Figure 3.8: Solar/waste energy driven dehumidification and regeneration cycle

MATLAB is used to simulate and analyse the performance of the system employing the energy and mass balance equations. It is worth mentioning that the finite element method is used to implement the simulation. The mass balance for the flowing air stream is given as Eq. (3.6):

$$\rho_a fA \left(\frac{\partial d_a}{\partial t} + u \frac{\partial d_a}{\partial z} \right) = K_y C(d_d - d_a) \tag{3.6}$$

Where, ρ_a represents density of the air, f represents ratio of the air to entire channel, A represents cross-sectional area , d_a and d_d represent the absolute humidity ratios for air and desiccant, respectively, u represents flow rate, K_y represents the coefficient of

mass convection, C represents the perimeter of the section where air flows, t represents time, and eventually, z represents the flow direction.

The mass balance within the absorbent bed is given as Eq. (3.7):

$$\rho_a\varepsilon(1-f)A\frac{\partial d_d}{\partial t} + \rho_d(1-\varepsilon)(1-f)A\phi\frac{\partial W}{\partial t}$$

$$= \rho_a\varepsilon(1-f)A\,D_G\frac{\partial^2 d_d}{\partial z^2} + \rho_d\varepsilon(1-\varepsilon)(1-f)AD_s\frac{\partial^2 W}{\partial z^2} + K_y C(d_a - d_d) \tag{3.7}$$

where ε is porosity, ρ_d represents the density of desiccant, ϕ is volume ratio of desiccant while W stands as the dry base water content. In addition, D_G represents the gas phase diffusivity, eventually, D_s stands as the surface diffusivity.

The energy balance within the flowing air stream is given as Eq. (3.8):

$$\rho_a\left(c_{p,a} + d_a c_{p,v}\right)fA\left(\frac{\partial T_a}{\partial t} + u\,\frac{\partial T_a}{\partial z}\right) = \alpha C(T_d - T_a) + K_y c_{p,v} C(d_d - d_a)\,(T_d - T_a) \tag{3.8}$$

Where, $c_{p,a}$ and $c_{p,v}$ stand as the specific heat capacities of air and water vapour respectively while α represents the convective heat transfer coefficient. Additionally, T_a and T_d stand as the temperature of air and desiccant bed, respectively. The energy balance of the absorbent bed is represented as Eq. (3.9):

$$\rho_d c_{p,d}(1-f)A(1-\varepsilon)\left(\frac{\partial T_d}{\partial t} - \frac{k_d}{c_p \rho_d}\frac{\partial^2 T_d}{\partial z^2}\right)$$

$$= \alpha C(T_a - T_d) + K_y c_{p,v} C(d_d - d_a)(T_a - T_d) + K_y C(d_d - d_a)q_s + I.\,A/L \tag{3.9}$$

Where, $c_{p,d}$ represents the specific heat capacity of the desiccant bed while k_d stands as the thermal conductivity of desiccant. Moreover, I represents the solar radiation intensity where it is only used for regeneration purpose, and eventually L represents the thickness of the absorbent bed.

It is assumed that the flowing air and desiccant have a constant initial temperature which is equal to the initial temperature of inlet air. In addition, it is assumed that the corresponding humidity ratios are equal to the inlet air humidity ratios. The initial condition of the desiccant bed should be dry enough to trigger the dehumidification process so that the initial water content of the desiccant is assumed to have a small value of 0.015 [kg.kg^{-1}]. In the inlet of both dehumidification and regeneration process it is assumed to have constant boundary temperature and humidity ratios for each time step. Moreover, the gradient of the temperature and moisture content at desiccant boundaries are taken as zero. The heat transfer coefficient is given as Eq. (3.10):

$$\alpha = \frac{(Nu)(k)(C)}{4A} \tag{3.10}$$

Where Nu is nusselt number, k is thermal conductivity. The mass transfer coefficient is also presented as Eq. (3.11):

$$K_y = \rho_a \frac{(Sh)D_0 C}{4A} \tag{3.11}$$

Where Sh is Sherwood number and D_0 is ordinary diffusivity.

3.6.5. Climate simulation

Out of seven existed climate classifications, four different climates are identified as suitable operating conditions for the GIDPC. In this regard, a representative city for each climate is chosen to carry out the experiment. This is the first endeavour ever in investigating the monthly performance of the GIDPC in different climates. These climates and representative cities are: Las Vegas, USA, for the subtropical hot desert climate; Rome, Italy for the Mediterranean climate; Beijing, China for the humid continental climate; and Riyadh, Saudi Arabia for the hot desert climate. The GIDPC operating conditions are simulated in laboratory under the aforementioned climates to record the monthly performance of the system. The operating months of the GIDPC in each selected city are recognized based on the temperature and relative humidity requirements. It means that in those months that the temperature and relative humidity of the considered city fall out of the defined ranges, the GIDPC will not operate as the natural weather condition is cold enough.

As a consequence, the weather information of each selected city is listed in **Table 3.3** [174] for all the year round. As seen, some relative humidity values are fallen out of the defined range for operating of the GIDPC ($0 \leq RH \leq 50\%$). In these conditions, the intake air properties are needed to modify for the GIDPC operation. Therefore, a pre-treatment is needed to modify the humidity of those cities. Thus, the auxiliary dehumidifier model is used for wet conditions to reduce the humidity levels. As a result, as can be seen in **Table 3.3**, the pre-treatment is conducted in Rome and Beijing where their conditions were out of the GIDPC's operation ranges whereas Las Vegas and Riyadh are needless of any pre-treatment.

It is found out that the GIDPC is only needed from April to October in two cities, i.e., Beijing and Las Vegas; and from March to October in Riyadh; and from May to

October in Rome. For rest of the year, the outdoor air can be directly used without being cooled by GIDPC. The temperature and relative humidity before treatment in Beijing range from 20 to 31˚C and from 45% to 78%, respectively which were beyond the defined humidity for GIDPC. However, after treatment, the temperature ranges from 23.68 ˚C to 36.75 ˚C and the relative humidity level reduced to the acceptable range of 16-42.31%. The trend is similar in Rome, where the temperature and relative humidity before the treatment ranged from 23 to 28 ˚C and from 73 to 76%, respectively; whereas after the treatment the temperature is in the range of 27.25 to 33.22 ˚C and the relative humidity has decreased to an acceptable range of 35 to 40% for GIDPC operation. Temperature in Las Vegas and Riyadh are in range of 25-40˚C and 27-44 ˚C, and the relative humidity are in ranges of 18-30% and 16-37%, respectively. Therefore, subtropical hot desert climate and hot desert climate are well in the range of GIDPC predefined ranges, and no pre-treatment is needed for them. As a consequence, all of the weather conditions are now within the operating ranges of the GIDPC.

Figures 3.9 (a)-(d) illustrate the target and experiment values of the monthly temperature and relative humidity in operating months for each city. Target values are the real monthly weather conditions of the cities which are listed in **Table 3.3** while the experiment values are those simulated by the heater and the dehumidifier/humidifier in the laboratory. These are presented to show how accurate was the weather simulations in the experiment.

The measurements revealed that the maximum relative errors between target and experiment temperature values in Beijing, Rome, Las Vegas, and Riyadh were 5.15%, 3.43%, 5.55% and 5.95%, respectively, and the relative humidity errors were 6.25%, 3.07%, 4.76%, and 7.89%, respectively. Therefore, the weather conditions in each city

are simulated with high accuracy. However, the main reasons for the slight errors are: delayed response in sensors and adjustment limits in the electrical heater, humidifier and dehumidifier, as well as likely prototype's inherent errors.

Table 3.3: Average monthly weather conditions

Month	Beijing				Rome				Las Vegas		Riyadh	
	Before treatment		After treatment		Before treatment		After treatment		No treatment needed			
	T(˚C)	RH(%)	T(˚C)	RH(%)	T(˚C)	RH(%)	T(˚C)	RH(%)	T(˚C)	RH(%)	T(˚C)	RH(%)
January	2	44	-	-	12	77	-	-	15.4	43	20	50
February	5	44	-	-	13	77.2	-	-	17.05	39.8	23.90	40
March	12	45	-	-	15	73	-	-	19.7	34	27	37
April	20	45	23.68	16	17.5	73	-	-	25	25	31	35
May	26	53	30.84	22.53	23	75	27.25	39	30	21	38	21
June	30	60	35.58	23.48	26	74	30.84	35	37	18	42	16
July	31	75	36.75	23.81	28	73	33.22	38	40	20	44	17
August	30	78	35.58	42.31	28	75	33.22	39	39	27	42	19
September	27	69	32.03	34.94	27	75	32.03	39	33	26	42	19
October	20	60	23.68	27.98	23	76	27.25	40	27	30	35	23
November	10	58	-	-	16	78.8	-	-	18.5	37	24.60	38
December	4.5	50	-	-	14	79	-	-	15	43	23	47
Average in operating months	-	-	31.31	27.02	-	-	30.68	32.13	32.67	24.01	37.35	23.05
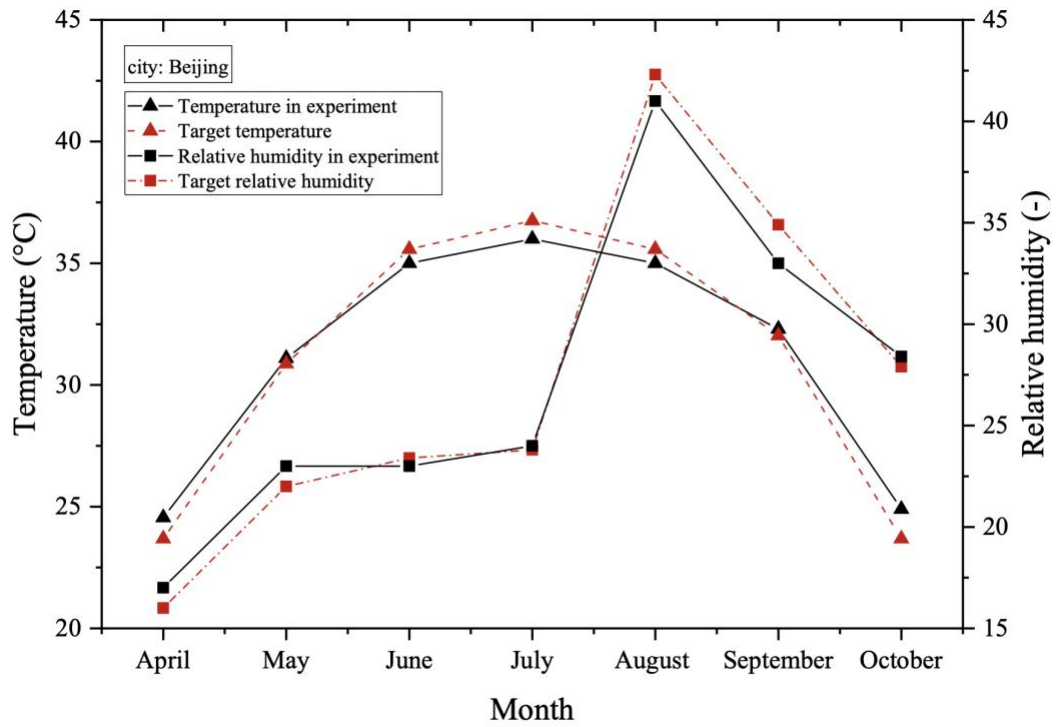
(a)
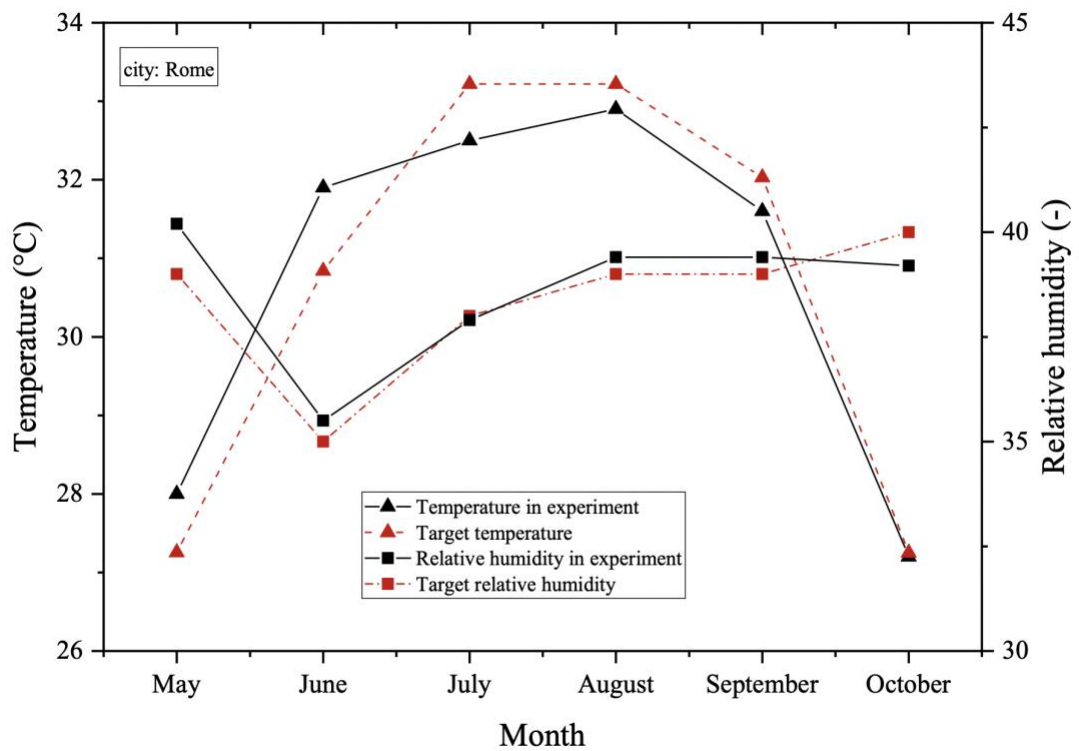
(b)
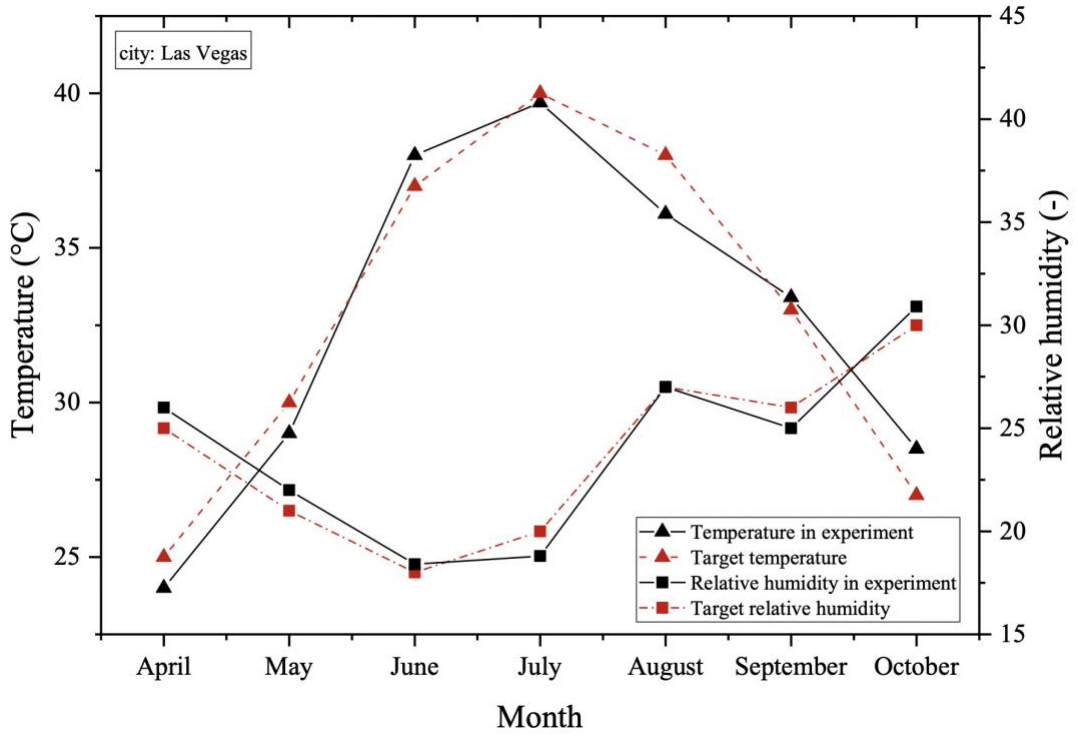
(c)
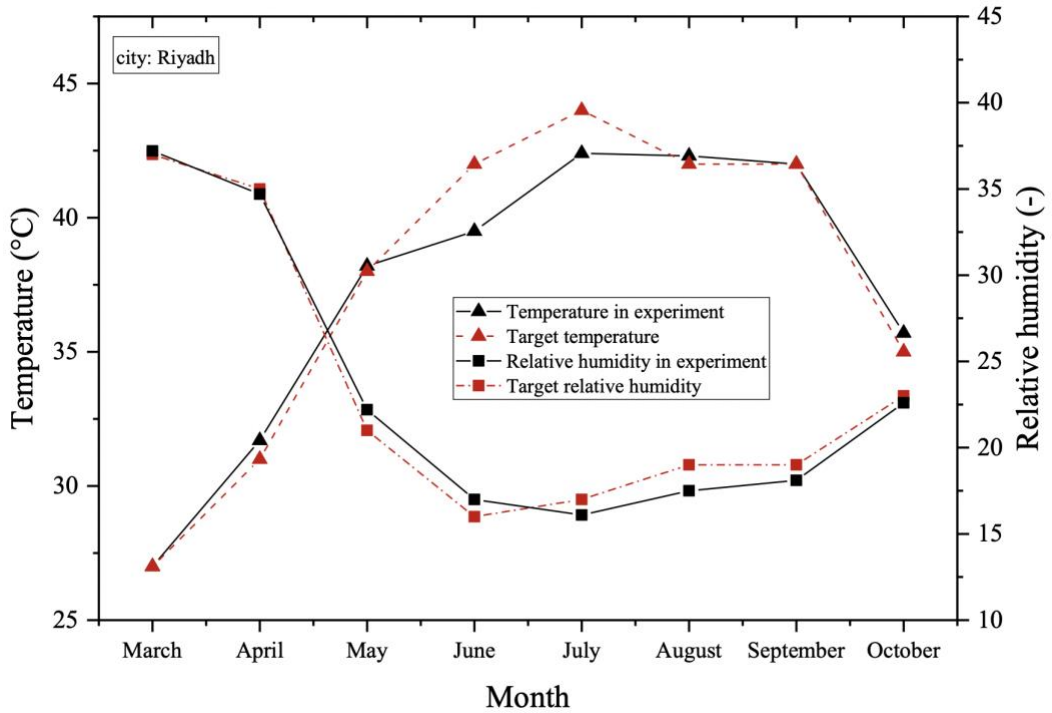
(d)

Figure 3.9: Monthly target and experiment weather conditions in various climates. (a) Beijing

(b) Rome (c) Las Vegas (d) Riyadh

3.6.6. GIDPC performance in diverse climates

The performance of the GIDPC in the aforementioned simulated operating conditions is reported using the common performance parameters i.e., cooling capacity, COP, wet-bulb and dew point efficiencies in each of the identified operating months for the four representative cities. The results revealed that the performance of the system varies in each month where the temperature and the relative humidity play the key roles in having the various performance values while other key operating and design parameters of the system such as working air ratio, airflow rates, and the dimensional parameters were all same.

The monthly results are shown through the **Figures 3.10-3.13** in which big differences in GIDPC performance can be observed. This proves how different operating conditions can affect the system efficiency. For instance, **Figure 3.10** shows monthly cooling capacity values of the system which are in the range of 1.6 - 4.65 kW. The monthly COP values are also given in **Figure 3.11** which are in the range of 17.7 – 51.38. The COP is a principal factor in decision-making as it considers both economic and technical aspects of the system. The maximum value of COP for the current GIDPC (52.5) was reported previously [38]. The reason for high COP values is mainly because of the novel guideless irregular heat and mass exchanger which has created 40% more heat transfer area and 50% less flow resistance along the flow direction within the channels.

The COP in Beijing ranges from 30.07 in April to 40.2 in July, and the cooling capacity is in the range of 2.72 kW in April to 3.63kW in July. The reason for the minimum values in April is due to the relatively cold and dry conditions (the pre-treated experiment temperature and relative humidity are 23.68 ˚C and 16% respectively), which lead to the lowest cooling capacity and consequently the lowest COP in April.

Contrarily, the maximum values in July are mostly owing to the warm weather condition, where the pre-treated experiment temperature rises to 36.75 ˚C. In Rome, the COP value ranges from 24.6 in May to 43.06 in August, and the cooling capacity is in the range of 2.22-3.89 kW. Due to the wet Mediterranean climate in Rome, temperature is the principal factor affecting system performance. Therefore, the lowest experiment temperature values observed in May (27.25 ˚C), and the highest experiment temperature values observed in August (33.22 ˚C), have caused the corresponding minimum and maximum COP and cooling capacity values. The experiment relative humidity was constant at 39% in both months.

Similarly, in subtropical hot desert climates, due to the dry condition, the temperature has the pivotal role in performance of GIDPC in Las Vegas, where the experiment temperature varies from 25 ˚C in April to 40 ˚C in July. Accordingly, the minimum COP and cooling capacity values occur in April, i.e., 17.7 and 1.6 kW, respectively, and the maximum values occur in July i.e., 50.57 and 4.57 kW, respectively. Meanwhile, the experimental relative humidity was 25% in April and 20% in July.

In hot desert climate, the GIDPC displays its highest potential in saving energy. This is mainly because of the warm and dry conditions throughout the summer where the experiment temperature and relative humidity were in the narrow ranges of 39.5-42.4 ˚C and 16.1-18.1%, respectively. The COP in Riyadh reached 51.38, 51.06, 50.93 and 49.66 in September, July, June, and August, respectively, and the lowest value, i.e., 26.6 occurred in March. Similarly, the cooling capacity was as high as 4.65 kW, 4.62 kW, 4.6 kW and 4.49 kW in September, July, June, and August, respectively, and the lowest value, i.e., 2.4 kW happened in March.

Wet-bulb and dew point efficiencies of the GIDPC are shown in **Figures 3.12** and **Figure 3.13** respectively. These efficiencies show how close the GIDPC prototype

can reduce the temperature of the intake air to the wet-bulb and dew point temperatures. The experiment results revealed that the wet-bulb efficiency is in the range of 68.57–126.47%, and the dew point efficiency varied between 35.29% and 90.2%.

In Beijing, the highest wet-bulb and dew point and efficiencies are 126.47% and 90.20% respectively, which happened in August while the lowest values of 103.61% and 69.6% occurred in April. It means that the temperature difference between the dew point and the supply air temperatures in August when the supply air temperature is recorded as 22.1˚C, is less than April when the supply air temperature is recorded 12.7 ˚C. This trend is also same for the temperature difference between the wet-bulb and supply temperatures. Similarly, the maximum dew point and wet-bulb efficiencies for Rome occurs in August, and in both Las Vegas and Riyadh occur in July, and the minimum values occur in May, April and March for Rome, Las Vegas, and Riyadh, respectively.
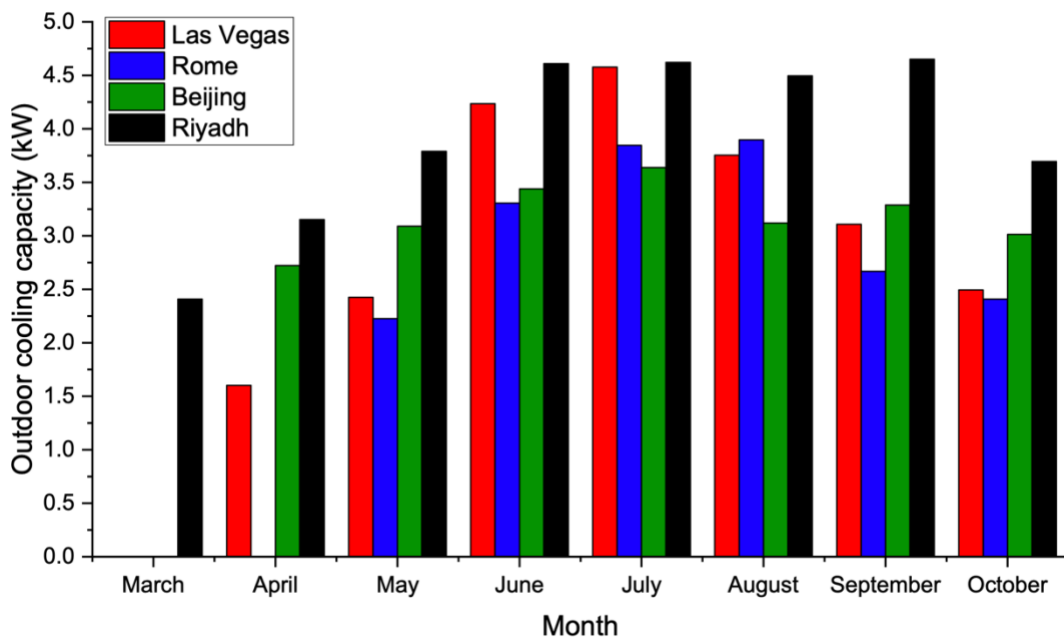
Figure 3.10: Monthly cooling capacity of GIDPC
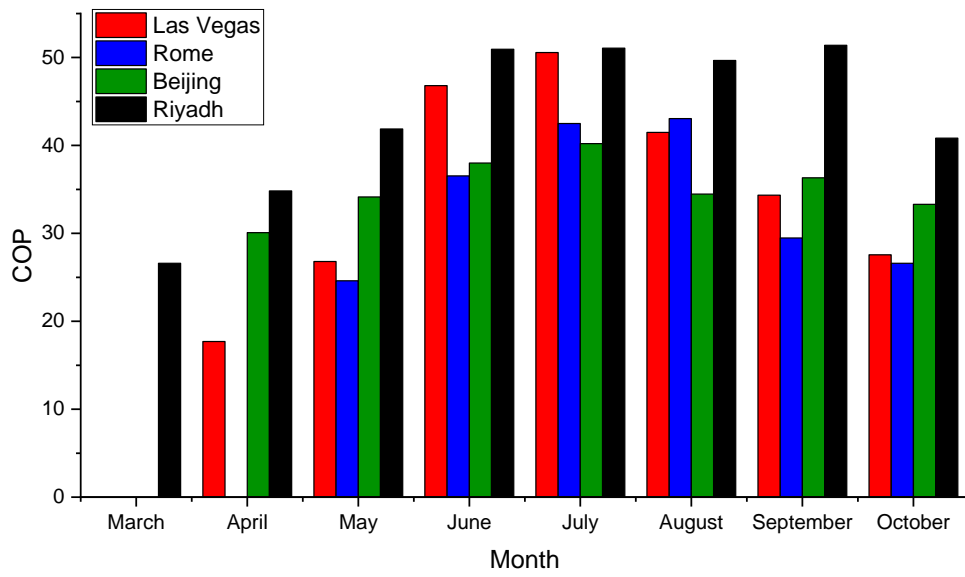
Figure 3.11: Monthly COP of GIDPC
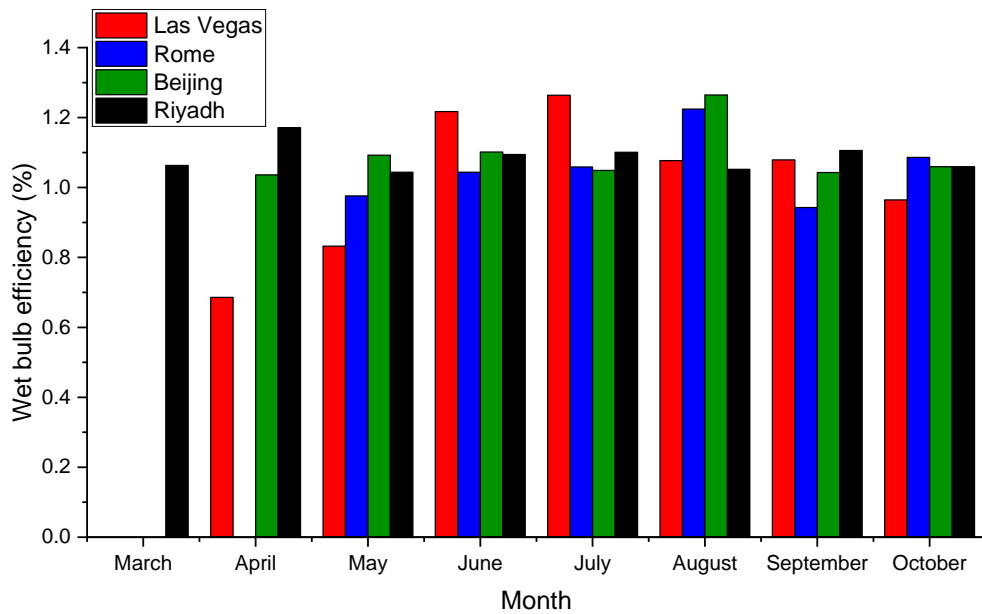
Figure 3.12: Monthly wet-bulb efficiency of GIDPC
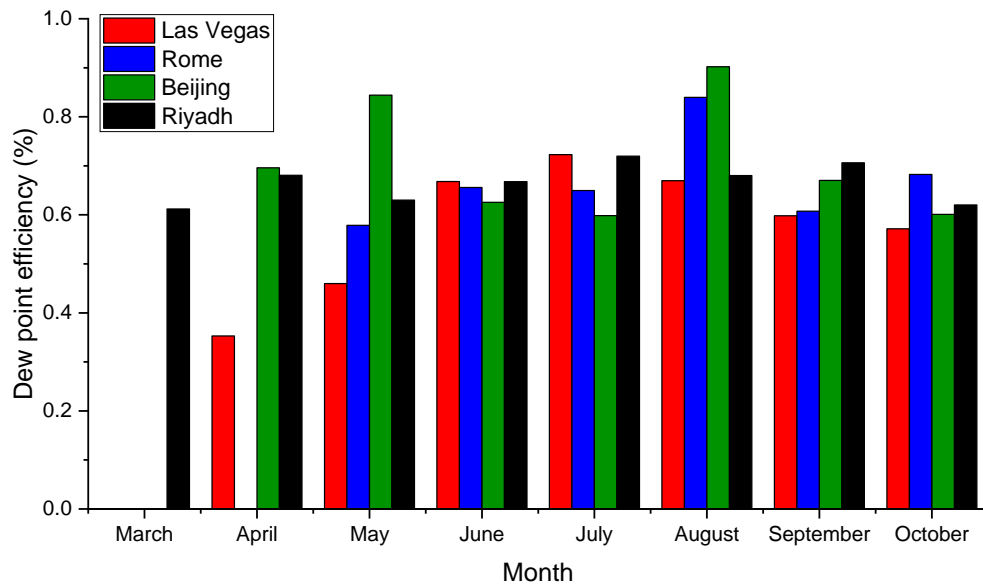
Figure 3.13: Monthly dew point efficiency of GIDPC

3.7. Review of a validated numerical model for data production

3.7.1. Model development

Before getting into the details of the big dataset construction, it is vital to go through a validated numerical model [125] which is widely used to produce data. The sources of data in this research are mainly the aforementioned experiment and the numerical model.

The common finite element [175]–[179] method is employed to treat the traditional mass and energy equations differentially, and the Newton iteration [180] is applied to each considered element to pursue the equilibrium state in heat and mass transfer phenomena with some simplifying assumptions as follows:

- Heat transfer between the HMX and surrounding was ignored.

- Heat and mass transfer were assumed to occur in steady state.

- The convective heat transfer in the walls of the channels was in vertical direction only.

- The walls were also considered to be impenetrable, thermal resistance of walls was ignored, and air within the channels was considered to be an incompressible gas.

The numerical model was developed by applying the following equations to each of the selected computational elements along the channels:

The air enthalpy difference between the inlet and outlet of the dry element is equal to the total heat transfer between the airflow in the dry element and channel walls as Eq. (3.12):

$$\Delta i_{dry} = C_P \cdot Q_{m,dry} \cdot \Delta T_{dry} = h_{dry} \cdot \left(T_{dry} - T_w\right) \cdot \Delta A \tag{3.12}$$

Where C_P is specific heat capacity of air, $Q_{m,dry}$ is the mass flow rate of air in dry channel, T_{dry} is the air temperature in dry channel, T_w is the temperature of the wall and ΔA is the heat and mass transfer area of computational element.

The difference of humidity ratio (HR) between the inlet and outlet of the wet element is equal to the amount of water evaporated across the wet surface as shown in Eq. (3.13):

$$\Delta hum_{wet} = h_m \cdot \rho_{air,wet} \cdot \left(hum_w - hum_{air,wet}\right) \cdot \sigma \cdot \Delta A \tag{3.13}$$

Where h_m is the convective mass transfer coefficient between the working airflow and wet channel surface, $\rho_{air,wet}$ is density of the air in wet channel, *hum*_w and *hum*_{air,wet} are the humidity ratio of the working air at the wet wall temperature and wet channel air temperature respectively and σ is the wettability of the surface material. The convective mass transfer coefficient between the working airflow and wet channel

surface is expressed as a function of the convective heat transfer coefficient and the Lewis number ($h/h_m = \rho \cdot C_P \cdot Le^{1-n}$) where n=1/3. The convective heat transfer coefficient between the airflow and the channel wall mainly depends on the flow regime (which is laminar in this study i.e., $52.31 < Re_{dry} < 1209$ and $5.38 < Re_{wet} < 1131$) and can be calculated as Eq. (3.14):

$$h = \frac{Nu \cdot \lambda}{De} \qquad\qquad (3.14)$$

Where Nu is the Nusselt number which depends on the airflow regime, λ and De (m) are the thermal conductivity and the equivalent diameter respectively.

The energy balance of air in the wet channel is, shown by Eq. (3.15), considered by calculating the difference of air enthalpy between the inlet and outlet of a wet element through the following expression which is equal to the sum of the heat transferred from the dry to wet elements and the change of airflow enthalpy in the wet element because of the evaporation.

$$\begin{cases} \Delta i_{wet} = C_P \cdot Q_{m,wet} \cdot \varphi \cdot \Delta T_{wet} = \Delta Q_{wet} + \Delta i_{steam} \\ \Delta Q_{wet} = h_{wet} \cdot (T_w - T_{wet}) \cdot \Delta A \\ \Delta i_{steam} = h_m \cdot \rho_{air,wet} \cdot (hum_w - hum_{air,wet}) \cdot C_{P,steam} \cdot T_{wet,out} \cdot \sigma \cdot \Delta A \end{cases} \qquad (3.15)$$

Where $Q_{m,wet}$ is mass flow rate in wet channel and φ is the working air fraction over the intake air.

As shown in the following Eq. (3.16), the amount of water evaporated from the wet element surface is equal to variation of the water flow rate between the inlet and outlet of the computational wet element.

$$\Delta Q_{m,water} = h_m \cdot \rho_{air,wet} \cdot \left(hum_w - hum_{air,wet}\right) \cdot \sigma \cdot \Delta A \tag{3.16}$$

Water enthalpy difference between the inlet and outlet of a wet element is caused by heat transfer between the water and airflow in the dry/wet channels as well as the latent heat of the evaporated water as expressed as Eq. (3.17):

$$\begin{cases} \Delta Q_{dry} = \Delta Q_{wet} + \Delta Q_{vap} + \Delta i_{water} \\ \Delta i_{water} = \left(Q_{m,water,out} \cdot Tw_{out} - Q_{m,water,in} \cdot Tw_{in}\right) \cdot C_{P,water} \\ \Delta Q_{vap} = h_m \cdot \rho_{air,wet} \cdot \left(hum_w - hum_{air,wet}\right) \cdot en_{steam} \cdot \sigma \cdot \Delta A \\ en_{steam} = 2446 + 1.86 T_{water} \end{cases} \tag{3.17}$$

Where en_{steam} , is the latent heat of the evaporated water.

The model is then used an algorithm to solve the aforementioned equations (including the performance parameters' equations) using the finite element and Newton iteration methods in the EES software to enable the heat and mass transfer processes within different channels (elements) [125].

3.7.2. Numerical model validation

Although the validity of the numerical model and consistency of the results with the considered 4-kW GIDPC were proven [125], but it is worth ensuring that the results derived from the latest experimental data, which are presented in this chapter, are comparable. The comparison is made by verifying the monthly COP values in Riyadh. It is worth repeating that the experiment is carried out when the working air ratio was 0.37 and velocity intake air was 3.3 (m/s). In addition, the HMX height was 1(m), the gap was 0.005 (m) and the number of layers was 160 in the experiment. These parameters as well as the monthly temperature and relative humidity values in Riyadh,

are all applied to the numerical model to conduct the comparison. The results, as shown in **Figure 3.14**, revealed that the maximum relative error between the experimental and numerical results is 5.24%.
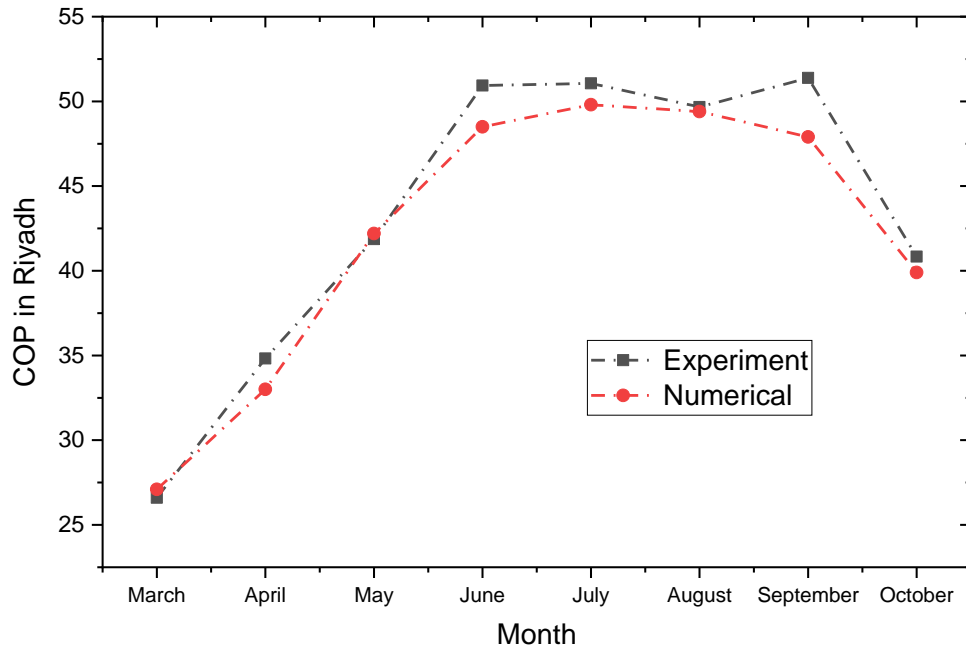
Figure 3.14: Validity of the proposed numerical model: COP values in Riyadh

3.8. Big dataset construction

3.8.1. Dataset structure

The needed parameters, i.e., operating, design and performance parameters are all explained in which the operating and design parameters will be considered as input variables and performance parameters will be considered as output variables of the ML models. The big dataset will be constructed based on the aforementioned parameters considering the defined operating ranges. The dataset is considered as the backbone of the ML models so that it is essential to choose the appropriate parameters which are considered as the key players in performance of the GIDPC. In general, as seen in **Figure 3.15**, the dataset is divided into two subsections, i.e., training and testing datasets. The training data is used to train the model and let the model learn

and memorize the behaviour of the data for future prediction. It means that the training dataset is the only source which can be used as an input for the ML model which will help the model to learn from the data and predict the unforeseen conditions and makes up majority of the big dataset, i.e., more than 60%. The validation dataset is used to tune the hyper-parameters of the ML model which is often done in model training process. But the testing data is used to test/evaluate the model performance in predicting the output variables.
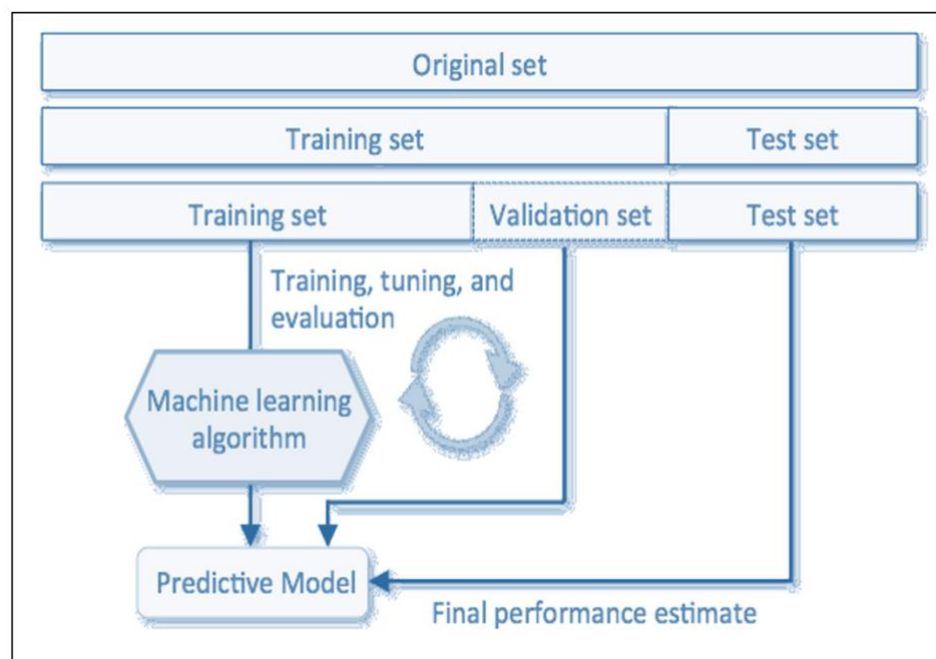
Figure 3.15: Breakdown of big dataset

The dataset size and number of parameters can vary from one model to another model. This is mainly because the size of dataset is significantly important in training process of the ML models. The size of the dataset can be determined by answering two questions:

- How much data is needed to approximate the underlying correlation between the input and output variables?

- How much data is needed to evaluate the performance of the developed model?

It is a common statement in ML that too little data can result in poor and inaccurate models. In addition, it can cause the model to be an optimistic and high variance. It is also a fact that the over-constrained model will underfit the little dataset and under-constrained model will overfit the dataset. Overfitting occurs when a function is too closely fit to a limited set of data points. It means that model learns too much from the training dataset which can results in low error values but the model cannot be generalized. But the underfitting occurs when the model has not learned enough from the training dataset which will cause the model to be unreliable and inaccurate. Therefore, it is vital to train the model faster, reduce the overfitting and increase the accuracy by choosing the appropriate dataset.

Both training and testing datasets comprise the input and output variables with plenty of data points. A data point or an observation is a group of single or multiple measurements that represent the specific unit of observation. In this study, the data point refers to unit of observation which comprises a group of separated integers which each of them represents each input variables. Every single group of input variable will be used by the numerical model to calculate the performance parameters which will represent the output variables in ML model.

It is necessary to have an organized dataset in which comprehensive information about the system performance can be provided. It is vital for the model to be aware of all possible operating conditions to learn and predict efficiently. As a consequence, the number of data points and the way they cover the comprehensiveness of all possible operating conditions are substantial.

In this research, firstly, a number of discrete values, which basically defines the size of dataset, for each input variables are created. The evenly distributed discrete values for each input variable considering the corresponding lower bounds and upper bounds,

are generated. The number of discrete values for each parameter is totally dependent on ML algorithm and the power of the method which can vary from one method to another one. Therefore, the distance between the discrete values are selected based on the performance and ability of the ML models. In this study, different discrete values will be selected for each ML model to increase the accuracy of the model as well as to avoid the unnecessary and big datasets. Having generated the evenly distributed discrete values for each input variable, it is time to generate the numerous data points which can cover all possible operating conditions of the GIDPC. As demonstrated in **Figure 3.16**, all possible combination method is used to generate the data points. This method generates all possible combinations of the discrete values. The number of data points depends on the number of discrete values for each input. The number of discrete values will be decided for each ML model in chapter 4 based on the model robustness and performance. One way to improve the model accuracy would be increasing the number of discrete values to cover more data and train a more comprehensive model. Therefore, the total number of data points will be determined once the number of discrete values is set. Having created all data points which represent the operating conditions, the validated numerical model is used to calculate the corresponding performance parameters for all data points. Eventually, the big dataset is created once the created data points (as input variables) and performance parameters (as output variables) are put together.
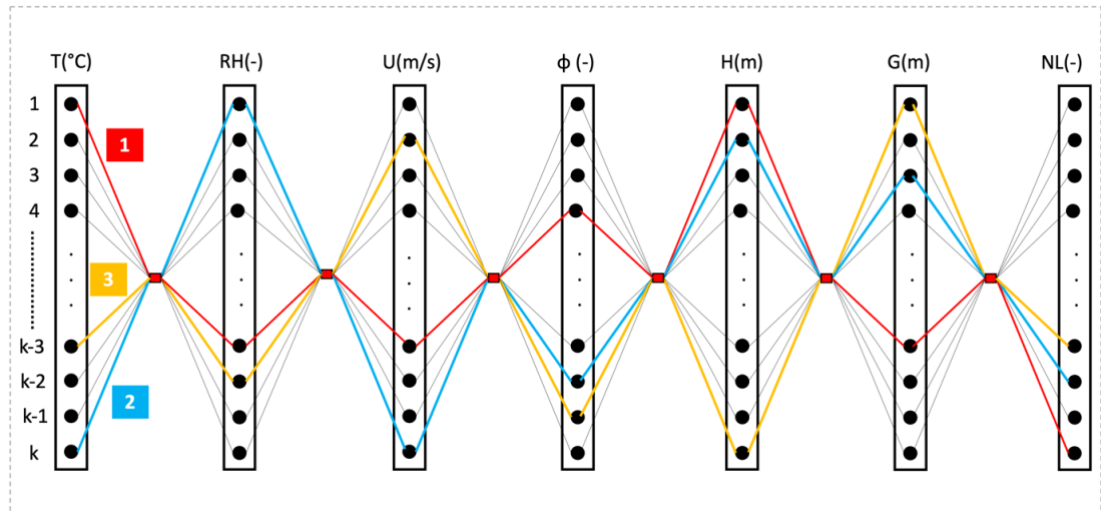
Figure 3.16: Demonstration of all possible combination method

3.8.2. Dataset pre-processing

Once the data points are created and big dataset is established, it is time to conduct the pre-processing steps [181]–[183]. Data pre-processing is a data mining technique that is used to make the raw data understandable for the ML models. Raw data is sometimes incomplete and inconsistent. In addition, it may lack data or include some wrong data. Therefore, data pre-processing is needed to clean up the raw data and resolve all the issues within the raw dataset to let the ML model train better. As demonstrated in **Figure 3.17**, data pre-processing has three major steps which are data cleaning, data transformation and data reduction.
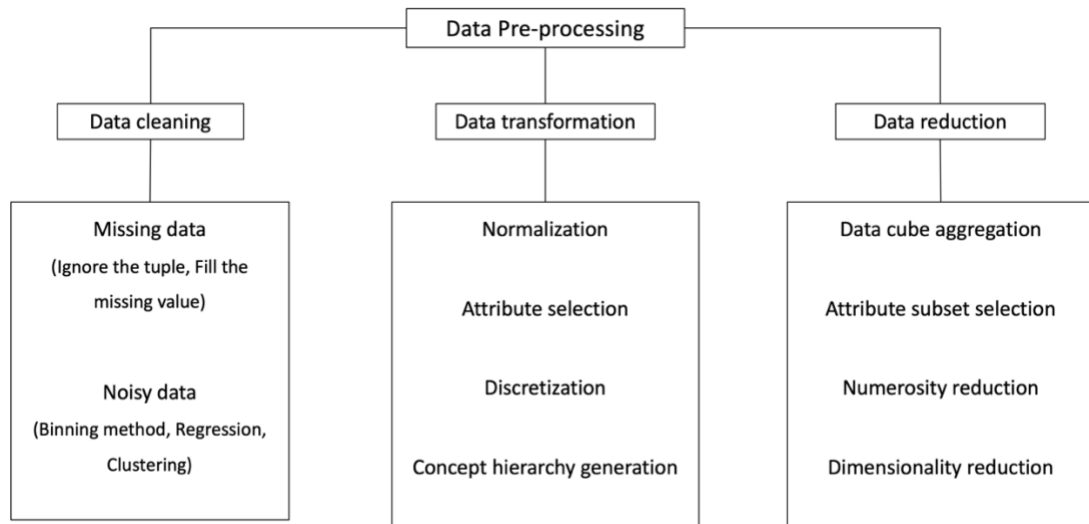
Figure 3.17: Data pre-processing types

Data Cleaning: dataset can have missing, error or irrelated values which are needed to be cleaned up and replaced by proper data. These processes are done in data cleaning step in which can be handled by different methods as follows:

For missing data in the big dataset, the common methods are as follows:

- **Ignore the tuple:** In large dataset, when a group of data is missed, ignoring those data can be one option.

- **Filling the missing values:** In a big dataset, some values can be missed which for this study can mainly be the weird operating condition for the GIDPC where the numerical model is not able to solve that. In this circumstance, the missing values can be filled with different values, e.g., mean value of that variable, most probable value, or simply a constant value. In a large dataset, the impact of these fillings will be ignorable.

Some data are not missed but they are incorrect and not definable for the models. The main origins of these kinds of errors are incomplete and faulty data that are collected by mistake which has resulted in meaningless data. In this case, the following methods can be taken:

- **Binning method:** data binning or discrete binning is a method that replaces the wrong data with a value which stands as the representative of the wrong data interval. Generally, the central value of the original data interval is selected to replace the wrong data.

- **Regression:** a linear or multiple regression can be used to fit the data to a regression function. This method will provide the logical values for the wrong data as replacement.

- **Clustering:** grouping the data with same characteristics can be another way to refine the dataset. Data clustering has different methods such as partitioning method, hierarchical method, density-based method, grid-based method, the model-based method, and the constraint-based method.

Data transformation: data transformation is basically undertaken to change the format/structure of the data in order to make it suitable for data mining process. Data transformation can be conducted by various simple and complicated methods based on size of the dataset and the ML model, by the following methods:

- **Normalization:** The normalization is made to simply scale the values of the parameters in a particular range. This will contribute the ML model in training process and in some cases can lead to better results. However, better results are not always guaranteed.

- **Feature selection:** The feature selection is implemented to select a subset of the related inputs (features) to train the model. It means that the number of input variables is decreased in order to reduce the computational cost and training time of the model and sometimes to improve the model accuracy and performance [184].

- **Discretization:** Most of the ML algorithms perform better when input variables have standard probability distribution. However, due to the outliers in data, highly exponential distributions, etc., input variables have non-standard distribution. The discretization changes the input variables to have the standard distributions to make them suitable for ML algorithms.

Data reduction: As it can be guessed from the name of the method, data reduction, is used to simply reduce the size/amount of data in order to improve the ML model accuracy and reduce the CPU and GPU computational working hours. Although big data sets have massive amounts of data but there are significant number of errors, noise and missing values in the data set so that the data reduction is needed to keep the useful data for training the ML models.

- **Data cube aggregation:** Data cubes can be built to reduce the volume of data without losing any information in order to decrease the computational time. Data cubes include multidimensional aggregated information in which each cell holds aggregated values which stand for data points in multidimensional space [185].

- **Attribute Subset Selection:** In most cases, data set have an excessive number of attributes which some of them can be unrelated or ineffective on the model accuracy or performance. The main purpose of attribute subset selection is to find the useful attribute subsets to increase the speed of model training and decrease the cost and time of data analysis.

- **Numerosity Reduction:** The numerosity reduction replaces the original data by smaller data as representative of the original data. There are two main methods for numerosity reduction, i.e., parametric and non-parametric.

- **Dimensionality reduction:** It is simply a process of reducing the size of inputs to make the data handling easier for the ML algorithm. There are different methods to conduct the dimensionality reduction in which the linear transformations, i.e., Principal Component Analysis (PCA), Factor Analysis, and Linear Discriminant Analysis (LDA), are more popular.

3.9. Summary

In this chapter, all GIDPC parameters included in the big dataset are explained. The big dataset as the backbone of the ML models, comprises all operating, design and performance parameters of the GIDPC system in which the input variables include the operational and design parameters of the system while the output variables include the performance parameters of the system. In addition, the operating ranges of all input variables which are necessary for considering the real operating conditions of the GIDPC, are defined. The operating ranges contribute the ML model to consider and learn the real operating conditions and ignore the unreal operating conditions. An experiment is conducted to demonstrate the superiority of the GIDPC in diverse climates and in order to ensure the validity of the numerical model which is used to create a big dataset. It is explained that discrete values are needed for each of the input variables to form the data points (operating conditions). The discrete values are selected within the lower and upper bound of the defined operating ranges in which the number of discrete values is dependent on the performance of the ML models. All possible combinations method is used to create the data points or operating conditions of the system. The created comprehensive operating conditions are used to calculate each of the selected performance parameters of the GIDPC using the validated numerical model. The big dataset will be formed once the created data points (input variables) and the corresponding calculated performance parameters (output

variables) are put together. Eventually, a thorough review of the data pre-processing

methods are summarized which will be used in development processes of the ML

models in this study.

CHAPTER 4: DEVELOPMENT OF MACHINE LEARNING MODELS

4.1. Introduction

In this chapter the development of ML models is detailed. The theory of the algorithms used in this study, i.e., Multiple Polynomial Regression (MPR) and Deep Neural Network (DNN) as well as the mathematical development of the models are overviewed. Then, the dataset used for each model and the corresponding input variables (comprising the operating and design parameters of the GIDPC) and output variables (performance parameters of the GIDPC) are described. Moreover, the number of data points, the proportion of training and testing data, the used data pre-processing techniques are also provided. The chapter is then followed by explaining the tuning process of the models which is selecting the polynomial degrees for the MPR model, and improving the network structure in the DNN model. Furthermore, the fitting quality and accuracy of the trained models are analysed through the common accuracy metrics which are generally used in evaluating the ML models. This stage includes a comparison of different model structures, which were taken into consideration in development process of the final models, through robust trade-offs between the accuracy and complexity of the models. In addition, the new and evolving eXplainable AI (XAI) is used for the DNN model to interpret the effect of operating conditions on the performance parameters of the system. Eventually, the developed models are compared in terms of accuracy, training time, complexity and flexibility, to disclose the advantages and disadvantages of each algorithm.

4.2. Overview of Artificial Intelligence: Machine Learning

AI is a science by which the computer-based data driven tools, which are inspired by human intelligence, are developed [135], [186], [187]. AI enables the computers to think critically and comprehend deeply to decide without any intervention from a human. AI falls into three classifications based on their ability in simulating the human's behaviour and their applications. The first category is Artificial Narrow Intelligence (ANI) [188], also called weak AI, which is designed to fulfil a specific task in a very intelligent way. Despite the general description of AI, the ANI does not think like human but learn from a set of data to do the specific task only. Artificial General Intelligence (AGI) is called strong AI in which the trained machines can outperform the human by learning and properly acting in unforeseen circumstances [185]–[187]. Artificial Super Intelligence (ASI) is a superb type of AI in which the developed AI model is able to present substantially better intelligence than human [191]. Over the last century, as seen in **Figure 4.1**, endeavours in AI resulted in two major subsets, i.e., Machine Learning (ML) and Deep Learning (DL).
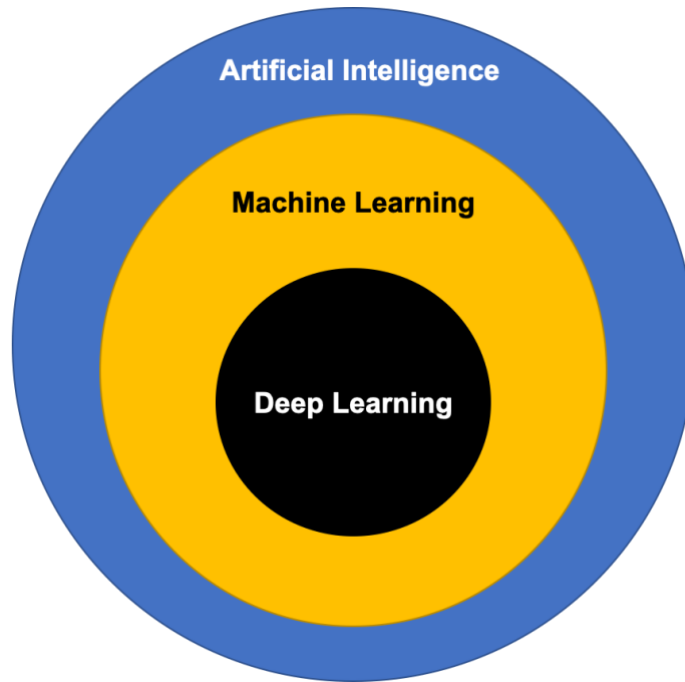
Figure 4.1: Illustration of AI and classified subsets

AI is a broad subject while ML as the subset of AI, deals with data to carry out the AI applications using the computers. ML uses numerous mathematical algorithms to fulfil the learning and data exploring processes which have resulted in discovery of DL [192]. Substantial high accuracy and success of DL models are mainly due to the major multi-layer Artificial Neural Network (ANN) structure which is the core algorithm used in the DL applications [193], [194]. **Figure 4.2** illustrates the evolution of AI over the past century with the general definition of each category. Since the algorithms used in this research study, are based on ML and DL so that the detailed explanations and classifications of both categories are provided in this chapter.
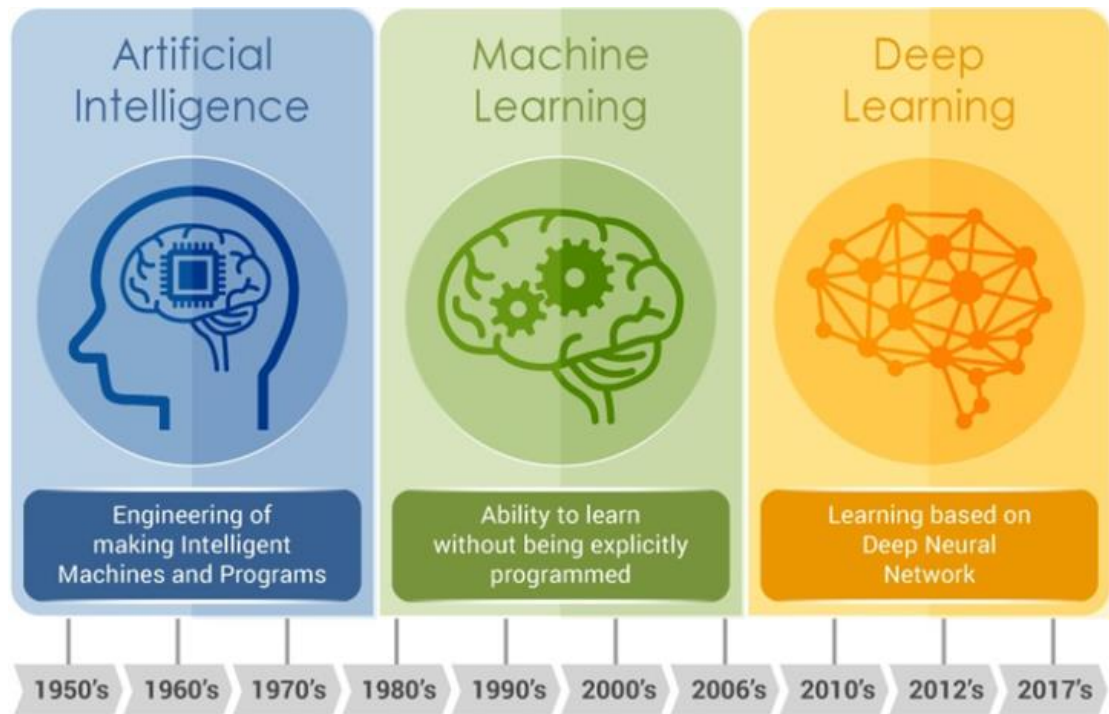
Figure 4.2: Evolution of AI [195]

ML is a subset of AI which is used to discover the hidden patterns and explore the distinctions within small to big datasets for the future prediction [196]. ML is based on statistical/mathematical algorithms to develop a program/model which can learn from the provided data to predict the behaviour of the system in unforeseen situations without explicitly programmed [167], [197], [198]. For instance, the recommendation systems on YouTube, Netflix, etc., which learn from a broad scope of data that are provided for them through the previous selections, are all based on ML algorithms. ML is generally classified into three subsections, i.e., supervised learning, unsupervised learning, reinforcement learning [199] .

4.2.1. Supervised Learning

In supervised learning labelled dataset including one or more independent variables (inputs) and the corresponding dependent variables (outputs) are scrutinized by the ML algorithm to extract the hidden relationship or pattern between the inputs and outputs [200]. The supervised ML will then be provided by a trained model to predict

the outputs for any unforeseen and random set of new inputs. Supervised ML is generally classified into two groups, i.e., regression and classification (see **Figure 4.3**) [200].

Regression: In regression supervised ML, the algorithm is aimed to provide a function which can predict continuous numerical output variables by taking the input variables [201]. Therefore, the output variables are in the form of integers to let the regression algorithms predict the quantities. Numerous regression algorithms are in existence in which the linear regression, Support Vector Regression (SVR), polynomial regression and regression trees are among the most popular ones [202].

Classification: Despite regression, in classification algorithms, the mapping function tries to estimate the discrete parameters and categorise the output variables. It means that in classification, the algorithm tries to separate the data into different classes. For instance, the detection of spam emails is one of the common classification problems that we can see. Common classification supervised ML algorithms are: K Nearest Neighbours, logistic regression, decision trees, Naïve Bayes, random forest classification and Kernel SVM [203].

Classification   Regression
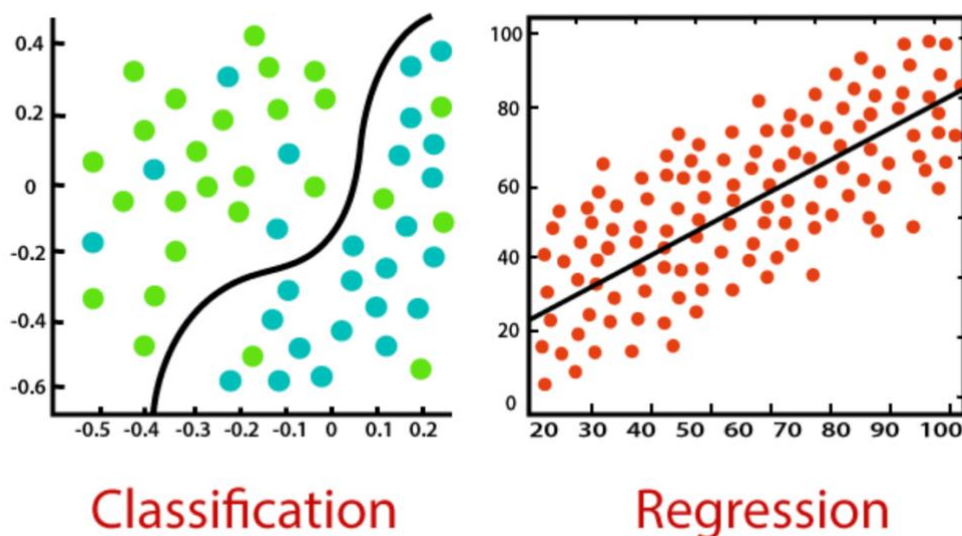
Figure 4.3: Illustration of classification and regression supervised ML algorithms [204]

4.2.2. Unsupervised Learning

The unsupervised ML is trained using unlabelled data. It means that in unsupervised ML the relationship (pattern) between the input and output variables is inferred without knowing the output variables [205], [206]. The algorithm investigates data and finds the hidden patterns within data itself. This is why it is called unsupervised as the algorithm is on its own to find and discover the relationships and provides the users with useful information. In general, the unsupervised ML is categorized into two subsets, i.e., clustering and association, which are illustrated in **Figure 4.4**.

Clustering: In the clustering unsupervised ML, the set of similar data are grouped together. The clustering is a common algorithm which can be seen in many different subjects. For instance, grouping similar context in Twitter, YouTube, news articles or books can be considered as examples of clustering.

Association: In association unsupervised ML, associations among data in a big dataset is established which is all based on discovering the relationship among the variables in a dataset. For instance, it is predicted that the people who buy a car will probably look for insurance to buy as well.
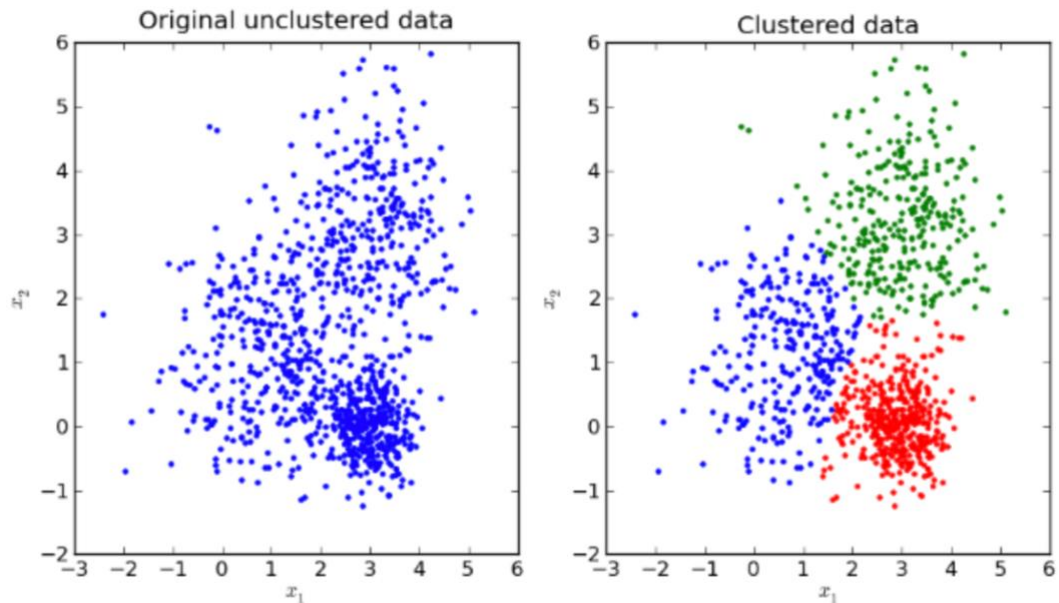
Figure 4.4: Illustration of data in clustering and association unsupervised ML [207]

4.2.3. Reinforcement Learning

In the reinforcement ML, the algorithm learns from continuous interaction with the environment in which an agent is in trial and error by receiving feedback from the previous interactions [208], [209]. It is based on rewards and punishment which the agent is awarded by correct interactions and is punished by incorrect interactions. The model is simply trained by getting implicit rewards or punishments by trial and error. The agent makes a decision after observing the environment and if the observation is not satisfactory, the weights of the system are adjusted to gain a different decision in next observation. It is based on getting the greatest reward which can be changed in different systems.

4.2.4. Deep Learning

DL is a subset of ML in which the algorithms are inspired from structure of human brain in which it is called Artificial Neural Network (ANN) that learns swiftly and accurately from examples [210]. The main distinction of the DL is that it employs an ANN with plenty of hidden layers which are stacked together one another. DL is also

referred to a large and complex neural network in which a huge amount of data is processed. As demonstrated in **Figure 4.5**, DL is the first class of algorithms that are scalable in a way to gradually and continuously improve it by feeding more data into the model. The value of the DL which is understood recently, is mainly because of the supervised ML which is trained through the labelled data.

As seen in **Figure 4.6**, our brains are complex network-based systems in which billions of neurons are connected to each other which makes the neural network in the mind connected to nervous systems. Although owing to the progress in neuroscience it is known that each neuron receives electrochemical signals but still, it is not clear how the brain's neurons work. ANN is inspired from the brain network which includes a number of layers with neurons to learn from the received inputs and make a prediction. Image classification, handwriting recognition, speech recognition, and autopilot devices are all inspired by ANN.
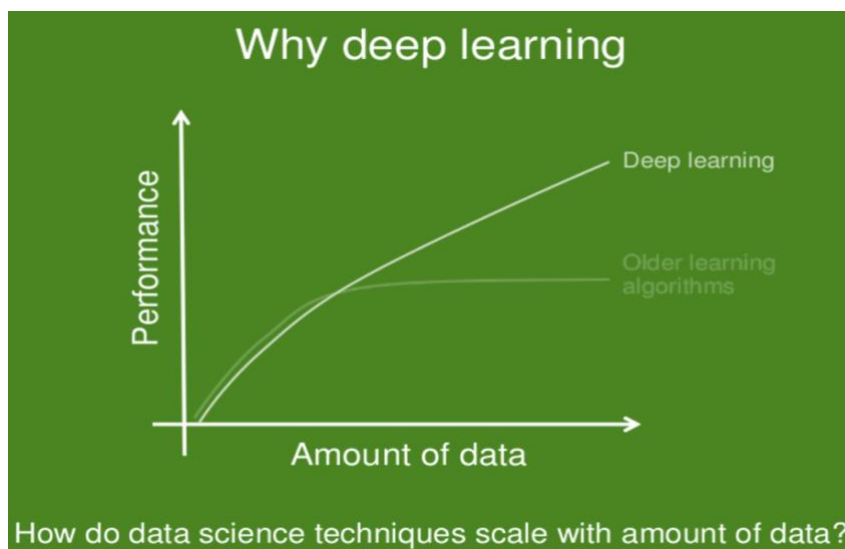
Figure 4.5: Superiority of deep learning over other old algorithms

The simplest ANN, as seen in **Figure 4.6**, is a network with several core sections. Input node(s) which can hold any numerical value, and connections which are weighted through real numbers needed to get optimized through number of

iterations, are brought together as a weighted sum. The weighted sum goes through the activation function to produce the value of the output node.
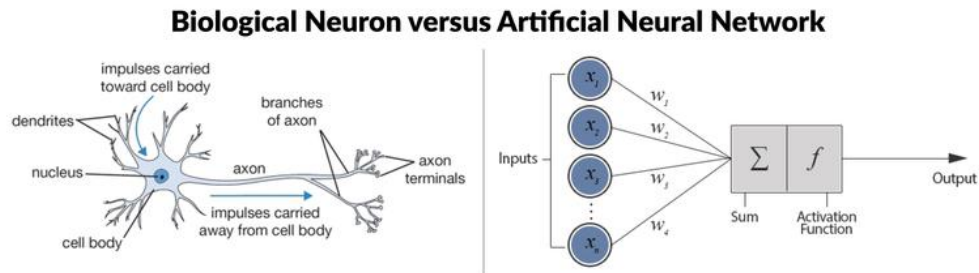
Figure 4.6: Artificial Neural Network (right) and Biological Neurons (left) [211]

Depth is a factor that distinguishes the Deep Neural Networks (DNNs) from the simple ANNs. The depth refers to more than one hidden layer where powerful computers are needed to fulfil the forward or backward weight optimization processes. **Figure 4.7** shows the difference in configuration of the simple and DL neural networks in which the number of hidden layers is the key difference. There are different DL neural networks. The main categories of the DL methods are explained below.
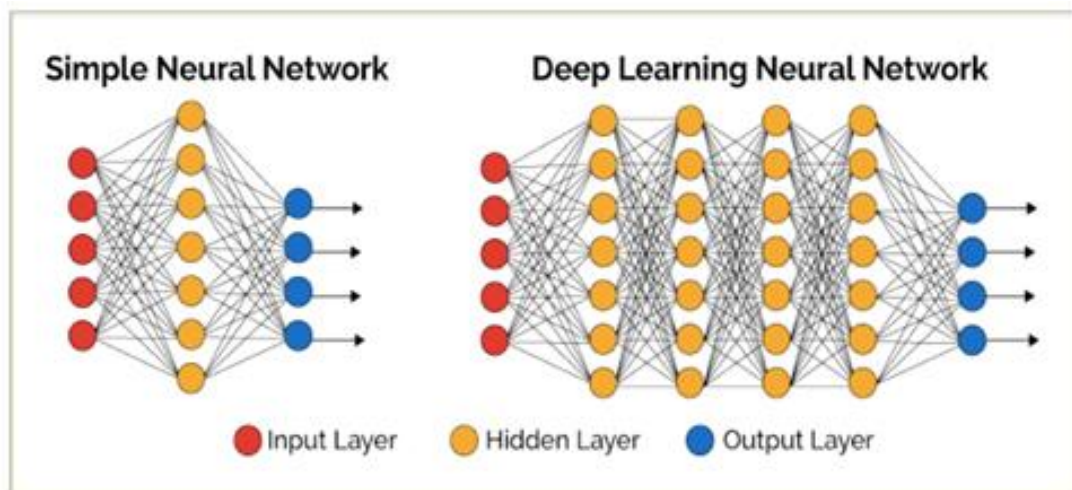
Figure 4.7: DL neural network versus a simple neural network [195]

Convolutional Neural Network (CNN): CNNs are one of the common DL methods which are generally used in image recognition. They are used in face identifications

[212], street signs and all the applications with visual data. Each image with three dimensions, i.e., width, height and depth, are sent to the network as an input. Resolution of the images is described by width and height while the depth is used to specify the colour of the image. The model will learn from thousands of images in big dataset and will optimise the weights by continuous calculation of loss function and back propagation. **Figure 4.8** shows an example of CNN for recognising the vehicle type.

Recursive (recurrent) Neural Network (RNN): The RNN is the general form of ANN with internal memory. It means that a dynamic learning process takes place by feeding the output from the previous step to the network as an input of the current step. The key distinguish of RNN is the hidden state which remembers the information of the previous iteration.
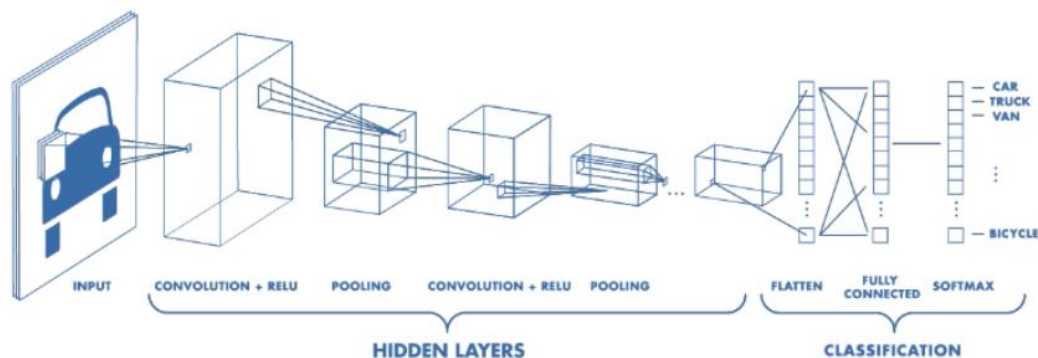
Figure 4.8: Example of a CNN application

Having reviewed the concept and definition of AI and its categories, it can be concluded that the appropriate model should be chosen after the problem definition and objective determination. The following sections will describe two methods which is used for development of the ML models for the GIDPC.

4.3. Method I: Multiple Polynomial Regression (MPR)

Polynomial regression is a subset of the regression ML which is under the category of supervised ML. The definition of the regression can be inspired by the general concept of ML in which the models are trained to find a relationship between the input and outputs. The inputs of the regression models are often called independent variables as their value are not dependent on other parameters, and the outputs are often called dependent variables as their values are highly dependent on the inputs. Regression can be defined as a relationship between the input and output variables that is identified by a best fitting line, as shown in **Figure 4.9**, or a mathematical equation to make a prediction.
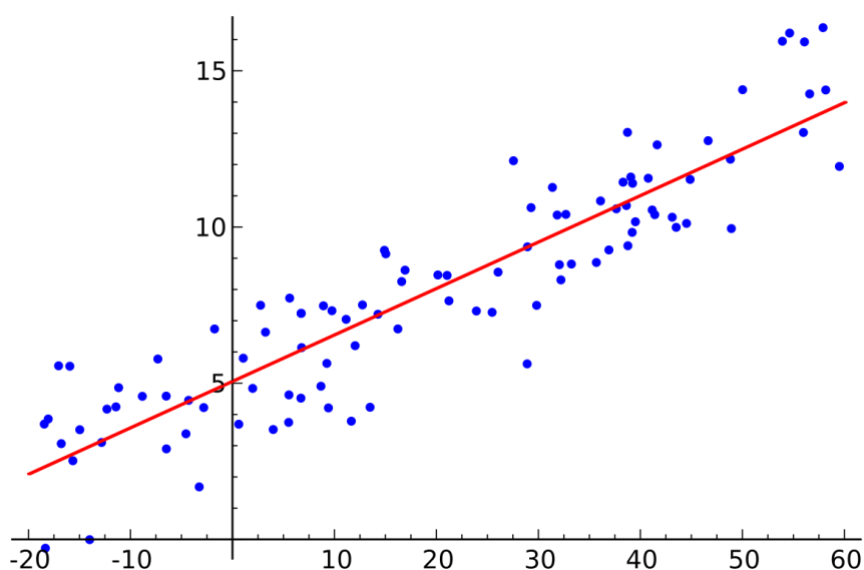
Figure 4.9: Fitting line in regression

There are various types of regression such as linear regression, polynomial regression, logistic regression and stepwise regression which are summarised in **Table 4.1**. However, in this chapter, the polynomial regression is used as the first ML algorithm to develop a data driven predictive model for the GIDPC. To fully comprehend the polynomial regression, firstly, the linear regression as the basic regression algorithm is overviewed and then the polynomial regression will be described.

Table 4.1: Various classifications of regression analysis

Type of Regression	Definition
Univariate / Multivariate	Only one/ two or more quantitative dependent variables
Simple / Multiple	Only one / two or more independent variables
Linear	All parameters appear in the equation linearly
Nonlinear	The relationship between the dependent variable and some of the independent variables is nonlinear
Polynomial Regression	The relationship between the dependent variable and independent variable can be expressed by a polynomial function
Stepwise regression	Builds a model by adding or removing the predictor variables, generally via a series of T-tests or F-tests
Logistic Regression	It is used to predict the probability of an event where the result is binary that is either yes or no

4.3.1. Overview of Linear Regression

The primary objective of linear regression is to find out a relation between one or multiple independent variables and continuous dependent variables [213]. As listed in Table 4.1, the linear regression with more than one independent variable is called multiple linear regression while it is called simple linear regression when there is only one independent variable. Therefore, the linear regression is represented by general expression as Eq. (4.1):

$$Y = \beta_0 + \beta_1 X_1 + \beta_2 X_2 + \cdots + \beta_n X_n \tag{4.1}$$

Where,

- Y is the dependent variable or predicted (also called target) value.

- β_0 is the model bias.

- $\beta_1, \beta_2, \dots, \beta_n$ are the regression coefficients.

- $X_1, X_2, \dots, X_n$ are the independent variables.

125

Which can also be represented as Eq. (4.2):

$$Y = \beta^T X \tag{4.2}$$

Where,

- β is the regression vector

- X is the independent variables vector in which the $X_0 = 1$, i.e., $\{1, X_1, X_2, \dots, X_n\}$.

When the independent variables are observed, the linear regression has to find the appropriate regression coefficients which can enable the model to fit the observed independent variables. As shown in **Figure 4.10**, the regression line will continuously search for a line in which the difference between the predicted values through the equation and the real values is minimal. The error between the real value and the predicted value is called residual.
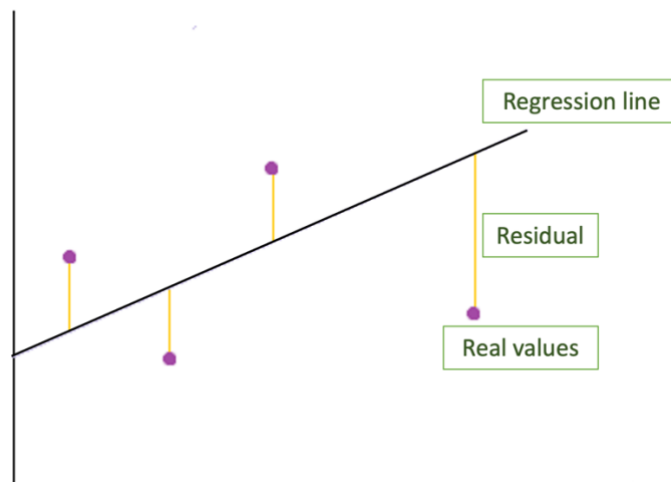
Figure 4.10: Regression line

A cost function is needed to represent the error values that normally is the sum of squares of the residuals as Eq. (4.3):

$$C(\beta) = \frac{\sum_{i=1}^{N}(Y(i) - y_i)^2}{2N} \tag{4.3}$$

Where N is the number of total data points.

In order to find the regression coefficients, the gradient descent is used to find the minimum cost function [214]. The gradient descent is a common generic optimisation which performs in a way to minimise the cost function via iterative steps as follows:

1) The regression coefficients are randomly initialized in a process called random initialization.

2) In order to minimise the cost function, the partial derivatives of the function are taken with respect to the regression functions as Eq. (4.4)-(4.6):

$$\frac{\partial C(\beta)}{\partial \beta_0} = \frac{\sum_{i=1}^{N} Y(i) - y_i}{N} \tag{4.4}$$

$$\frac{\partial C(\beta)}{\partial \beta_1} = \frac{\sum_{i=1}^{N} Y(i) - y_i}{N} X_{1,i} \tag{4.5}$$

$$\frac{\partial C(\beta)}{\partial \beta_n} = \frac{\sum_{i=1}^{N} Y(i) - y_i}{N} X_{n,i} \tag{4.6}$$

All of partial derivatives can be calculated through the following Eq. (4.7):

$$\begin{bmatrix} \frac{\partial C(\beta)}{\partial \beta_0} \\ \frac{\partial C(\beta)}{\partial \beta_1} \\ \vdots \\ \frac{\partial C(\beta)}{\partial \beta_n} \end{bmatrix} = \frac{X^T (Y - y)}{N} \tag{4.7}$$

Having calculated the derivatives, the regression parameters will be updated as Eq. (4.8)-(4.9):

$$\beta_0 = \beta_0 - \frac{\alpha}{N} \sum_{i=1}^{N} (Y(i) - y_i) \tag{4.8}$$

$$\beta_1 = \beta_1 - \frac{\alpha}{N} \sum_{i=1}^{N} (Y(i) - y_i) X_{1,i} \tag{4.9}$$

Where,

- α is called learning parameter.

All the regression coefficients can be updated using the following Eq. (4.10):

$$\begin{bmatrix} \beta_0 \\ \beta_1 \\ \vdots \\ \beta_n \end{bmatrix} = \begin{bmatrix} \beta_0 \\ \beta_1 \\ \vdots \\ \beta_n \end{bmatrix} - \alpha \begin{bmatrix} \dfrac{\partial C(\beta)}{\partial \beta_0} \\[2mm] \dfrac{\partial C(\beta)}{\partial \beta_1} \\[2mm] \vdots \\ \dfrac{\partial C(\beta)}{\partial \beta_n} \end{bmatrix} \tag{4.10}$$

The above steps will be processed through numerous iterations until the cost function is minimised. **Figure 4.11** illustrates an example for minimizing the cost function in which the cost function has reached the minimum value after roughly 100 iterations. In the iteration process, the α value plays a key role. The high learning parameters will cause the model to overshoot the best fit line. To the contrary, in the low learning parameters, the gradient descent needs more time to find the best fit. So, it is vital to choose an appropriate value for the learning parameter.
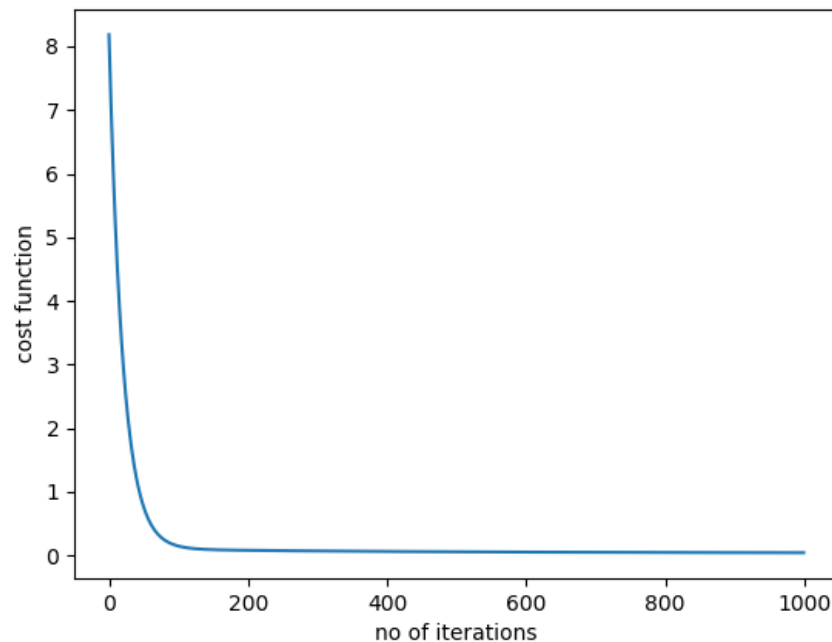
Figure 4.11: Cost function versus number of iterations

4.3.2. Regression evaluation

Regression models are evaluated through different metrics in which few of them are more common. In the current study, we will use coefficient of determination (R^2), Mean Square Error (MSE) and Maximum Relative Error (MRE). R^2 reveals how close the predicted data are to the real dependent variables which is defined by proportion of the variance for the dependent variable. Its value is between 0 and 1 in which:

- "0" means none of the dependent variables is explained by the regression line.

- "1" means that all of the dependent variables are explained by the regression line.

MSE represents average of squares errors which is calculated by average square difference between the predicted value and real value of the independent variables. The MSE and R^2 are defined by the following Eq. (4.11)-(4.12) [171]:

$$MSE = \frac{SSE}{N} = \frac{\sum_{i=0}^{N}(Y_i - y_i)^2}{N} \tag{4.11}$$

$$R^2 = 1 - \frac{SSE}{SST} = 1 - \frac{\sum_{i=0}^{N}(Y_i - y_i)^2}{\sum_{i=0}^{N}(\overline{Y}_i - y_i)^2} \tag{4.12}$$

Where,

- SSE is sum square of errors

- SST is sum square of total

- $\overline{Y}$ is the mean of predicted values

4.3.3. Polynomial Regression

Polynomial Regression is needed when the relationship between data cannot be defined by a straight line [171]. It means that in this case, the proposed linear equation by the linear regression cannot represent the relationship in data. Thus, as seen in **Figure 4.12**, the data should be fitted through a curved regression line. The curved

regression line covers data in a better and more comprehensive way compared to the linear regression.
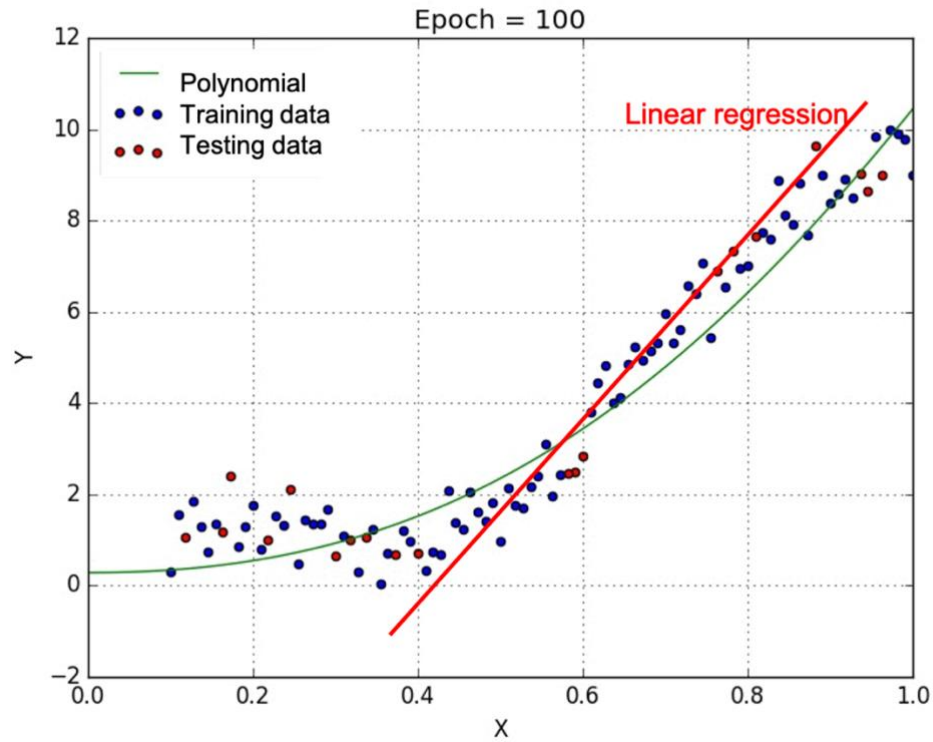
Figure 4.12: Fitting line in polynomial and linear regressions [215]

The general polynomial regression can be expressed by the following Eq. (4.13):

$$Y = \beta_0 + \beta_1 X + \beta_2 X^2 + \cdots + \beta_n X^n \tag{4.13}$$

Where

- "n" represents the polynomial degree of the equation

- Y is the dependent variable or predicted (also called target) value.

- β_0 is the model bias.

- $\beta_1, \beta_2, \dots, \beta_n$ are the polynomial coefficients.

- X is the independent variable.

More complex data need more complicated curves to fit the data. In this case, polynomial fitting curve can be adjusted by the polynomial degrees. When the polynomial curve does not properly cover or fit the data, under fitting happens so that

it is needed to overcome the under fitting by making the model more complex through increasing the polynomial degrees. However, it is an important step as further increasing of the polynomial degree will result in over fitting. Over fitting means that the regression curve captures most of the data including noises which will result in unrealistic and inaccurate predictions. **Figure 4.13** shows different fitting lines to demonstrate the most desirable fitting line. For the selected sample data, it is revealed that a fitting line with degree of 3, can be the correct fitting while the model with degree 1 results in under fitting and the model with degree 20 leads to over fitting. One efficient way to prevent the over fitting is providing the model with more data to allow the algorithm to learn more and become generalized. Although it is a challenging step to adjust the polynomial degree but it can be overcome by identifying the appropriate bias and variance. It should be noted that high bias leads to under fitting and high variance results in over fitting. As a consequence, the appropriate model should have low bias and low variance but as seen in **Figure 4.14**, it is not feasible to reach ideal bias and variance simultaneously. Therefore, an accurate trade-off is needed to select the best model which can be general as well as accurate enough in prediction.

The advantages of using the polynomial regression are listed below:

- Can outperform the linear regression in accurately representing the relationship between the independent and dependent variables.

- Functions applicability is broad which can result in better regression fitting and consequently accurate predictions.

- Can cover complex data distributions with numerous numbers of curvatures.

However, there are some features which can leave a negative impact on performance of polynomial regression as listed below:

-   Existing of outliers can severely lead to inefficient models.

-   It is almost impossible to detect the effect of outliers by the validation tools.
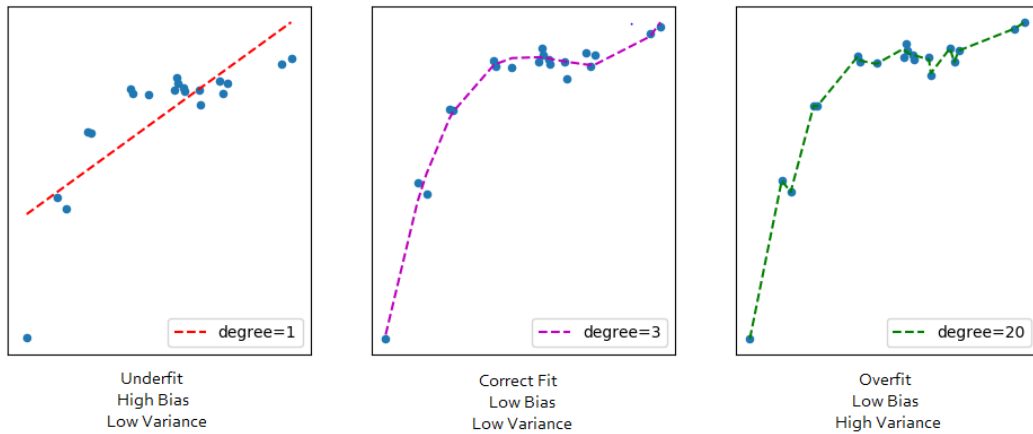
Figure 4.13: Fitting line in polynomial and linear regressions [215]
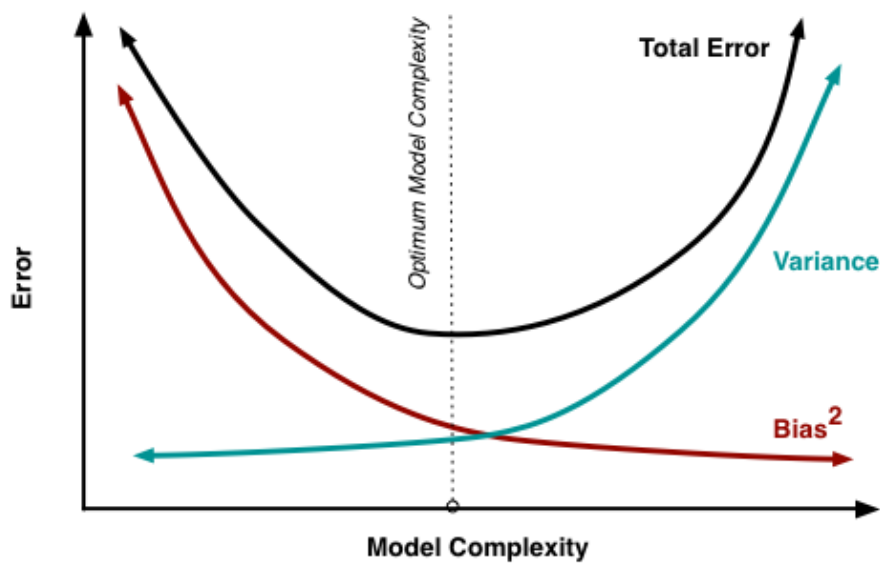
Figure 4.14: Optimum model selection in regression

4.3.4. Associated dataset for MPR

The comprehensive dataset constructed based on the methodology described in chapter 3 and is divided into two sub-sets: 1) training set; 2) testing set. 80% of the comprehensive dataset is selected as the training set and 20% is testing set. The

training set is used to train and develop the model and testing set is used to test and evaluate the developed model. Each set comprises two different parts: 1) Operating parameters; 2) Performance parameters. The required evenly distributed discrete values of the operating parameters are selected to construct the dataset. For polynomial regression, it is decided to have seven operating and design parameters, i.e., temperature of the intake air, relative humidity of the intake air, velocity of the intake air, working air ratio, height of the HMX, gap and number of layers within the HMX. The existence of numerous input variables causes the regression-based model to be called MPR. As performance parameters (dependent variables), cooling capacity, COP, pressure drop, wet bulb and dew point efficiencies are selected.

All possible combinations of the selected operating parameters which represent all possible operating conditions for the selected discrete values are produced for each set. All possible combinations take all of the probable combinations of the discrete operating parameters into consideration. Thus, making the model aware of any random operating conditions.

The total number of operating conditions which also represents number of data points is 7857 in the MPR model. Having created the all possible operating conditions, the performance parameters of the GIDPC for each created operating conditions are calculated using the numerical model, explained in Chapter 3, to finalise the construction of the dataset considering the constant parameters listed in **Table 4.2**.

Table 4.2: Geometric parameters and water status in numerical model

Parameters	Value
Height (m)	1
Width (m)	0.348
Gap (m)	0.004
Number of layers	200
Water temperature (°C)	16
Water flow rate (kg/s)	18

The reason for creating the dataset based on the constant geometrical/design parameters is that the MPR was unable to process the big comprehensive dataset. To overcome this issue, different geometric sets are defined and a dataset is created for each of the twelve geometric sets. In addition, because in real operating conditions, the geometric variables are unchanged, thus it would be sensible to have a separate and organized dataset for each geometric set. As shown in **Table 4.3**, each geometric set has constant geometric parameters including channel height, channel gap and the number of layers. As a consequence, the polynomial regression will be used for each geometric set to identify 12 sets of polynomial equations with different polynomial coefficients. It is worth mentioning that the geometric sets are created based on the evenly distributed discrete data using the all possible combination method described in chapter 3.

Table 4.3: Discreet values of geometric characteristics for each geometric set

No. of sets	1	2	3	4	5	6	7	8	9	10	11	12
H(m)	1	1	1	1	2	2	2	2	3	3	3	3
G(m)	0.004	0.004	0.008	0.008	0.004	0.004	0.008	0.008	0.004	0.004	0.008	0.008
L	100	200	100	200	100	200	100	200	100	200	100	200

The analysis of the big dataset revealed that the created dataset for MPR is in good condition. All of values are checked and it is ensured that the values are correct and sensible. However, a few values were missing which are filled by manually rerunning the numerical simulation model in EES. Apart from this issue, no significant problem is observed.

4.3.5. MPR development process

Figure 4.15 shows the visual relationship between the operating and performance parameters which discloses a reason for choosing the polynomial regression than the linear regression. It can be observed that the behaviour of the operating conditions versus each of the performance parameters cannot be covered by a straight line. This means that a curve can be a solid solution to represent the pattern among operating and performance parameters. As a consequence, the MPR with flexibility in controlling the complexity of the model and the fitting curve, can be an appropriate ML algorithm.

The MPR method was carried out in an open source R software. The general MPR mathematical expression for GIDPC is based on the general polynomial equation (Eq. 4.13) which correlates the flow characteristics with the performance parameters of the system. The regression coefficients vary for each geometry sets and thus considers the impact of geometric characteristics. Eq. (4.15) is the general form of the statistical model which is based on the MPR:

$$Y = \beta_0 + \beta_1 \times (T^{n_{1,1}} \times RH^{n_{2,1}} \times U^{n_{3,1}} \times \varphi^{n_{4,1}}) + \beta_2 \times (T^{n_{1,2}} \times RH^{n_{2,2}} \times U^{n_{3,2}} \times \varphi^{n_{4,2}}) + \cdots + \beta_m \times (T^{n_{1,m}} \times RH^{n_{2,m}} \times U^{n_{3,m}} \times \varphi^{n_{4,m}}) \tag{4.15}$$

Where,

- Y represents the performance parameters

- T, RH, U and φ represent the intake air temperature, relative humidity, airflow velocity and working air fraction over the intake air respectively.

- $\beta_1, \beta_2, ..., \beta_m$ represent the regression coefficients.

- Power of each independent variable is represented by n in which n_1 is for intake air temperature, n_2 is for intake air relative humidity, n_3 is for the airflow velocity, n_4 is for the working air fraction over the intake air and the second subscript for n which is shown by m is the number of the coefficients.
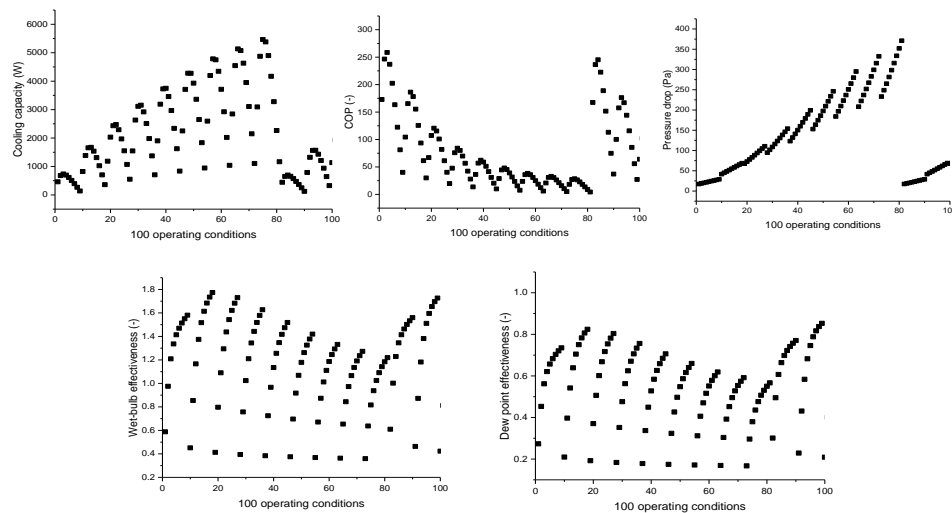
Figure 4.15: Relationships between the data points and the corresponding performance parameters

Nine MPR models with different degrees, i.e., 1st, 2nd, …, 9th, are considered and compared in order to choose the optimum one, in terms of complexity and accuracy, for performance analysis and design of the GIDPC.

These models' accuracy and performance are compared through two general methods:

    I. Changing degree of the polynomial model.

    II. Assessing the model performance by different metrics.

Model complexity in MPR is controlled by polynomial degrees. Larger degrees lead to more complex prediction functions and better fitting quality. However, it does not necessarily lead to better predictions. Thus, three common metrics [216], MSE, R^2 and MRE, are selected to evaluate the performance of the models with different level of complexities. Five predicted performance parameters are compared with those from the numerical simulation.

Firstly, the model results are assessed by R^2 to investigate the level of correlation fitting. As shown in **Figure 4.16(a)**, the R^2 value has sharply increased by increasing the polynomial degrees and has reached the superior value of 1 for all of the performance parameters from 5th degree onwards. Although R^2 of 1 indicates the good level of fitting, but it does not always lead to a good model. This is because R^2 gets higher values by covering more operating parameters so that other metrics are considered in model assessment to ensure the model accuracy.

As shown in **Figure 4.16(b)**, the MRE decreases for all parameters by increasing the model complexity. The sharp declines show the contribution of the model complexity in enhancement of model accuracy. MSE of 10% is specified as an acceptable margin in this study and the accepted values are coloured in green as listed in **Table 4.4**. Thus, in terms of MSE, 7th degree for cooling capacity, 8th degree for COP, 3rd degree for pressure drop, 6th degree for dew point effectiveness and 5th degree for wet-bulb effectiveness can be selected. Therefore, in terms of MRE, increasing the model complexity from aforementioned acceptable degrees leads to a more complex model and does not contribute to model accuracy.

The trend is exactly the same for the MSE values. As can be seen from **Figure 4.16(c)**, MSE for all variables has declined by increasing the model degrees. For dew point and wet-bulb effectiveness, all of the studied models are in favour as the MSE values

are close to zero. However, the appropriate models for cooling capacity, COP and pressure drop are 8th degree, 6th degree and 2nd degree respectively as the MSE values have approached zero.
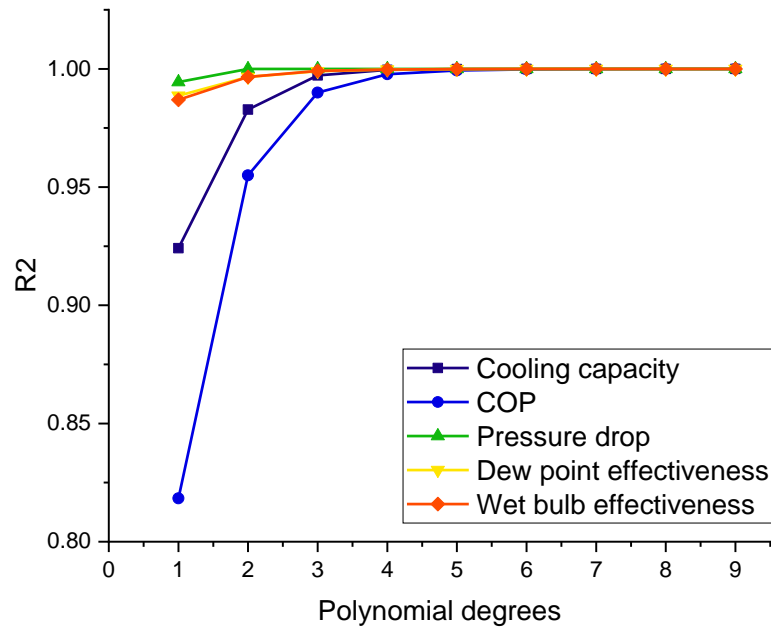
(a)
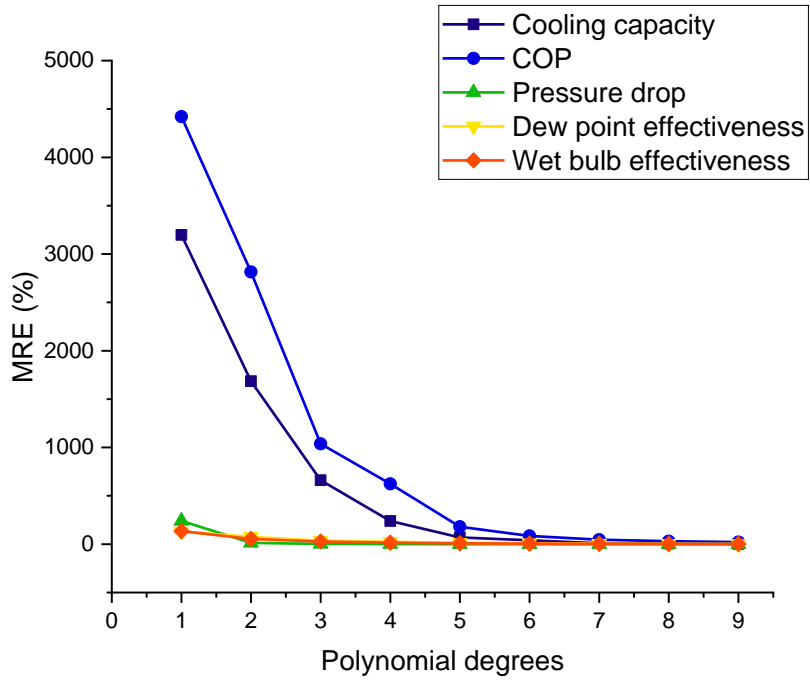
(b)
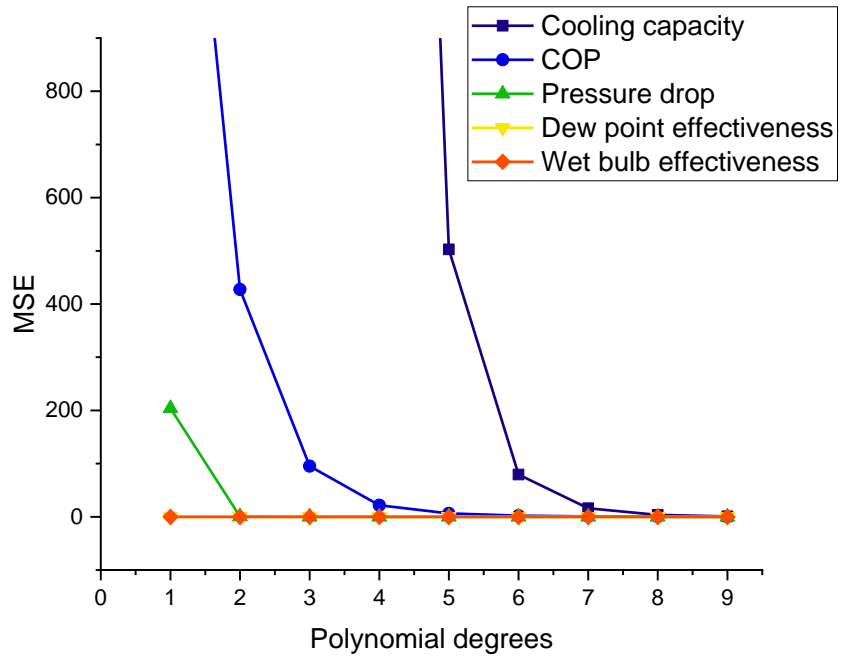
(c)

Figure 4.16: Influence of degrees on Metrics: (a): R2; (b): MRE; (c): MSE

Table 4.4: MRE of different MPR models

Performance parameters	MRE (%)								
	1st	2nd	3rd	4th	5th	6th	7th	8th	9th
Cooling capacity (W)	3197.36	1684.56	660.96	239.65	68.85	39.33	8.39	6.1	2.59
COP (-)	4421.66	2814.83	1038.02	623.98	180.78	85.83	46.46	7.54	2.9
Pressure drop (Pa)	241.04	14.34	2.42	0.6	0.21	0.12	0.086	0.07	0.07
Dew point effectiveness (%)	129.6	76.55	35.69	23.76	13.86	9.78	5.67	3.54	2.1
Wet bulb effectiveness (%)	135.71	53.53	27.98	15.18	8.95	6.43	4.30	2.53	1.16

Consequently, having done all of the aforementioned analyses, the accepted models for cooling capacity, COP, pressure drop, dew point and wet-bulb effectiveness are 8th, 8th, 5th, 6th and 5th respectively. All other models with higher degrees than the abovementioned accepted degrees are valid and more accurate. Therefore, in order to have a solid single model for all of the five performance parameters, the 8th degree MPR model is taken in next sections to carry out the validation and test parts. Therefore, R2 values and average relative error values for the selected 8th degree model are given in Table 4.5. Both R2 values (0.99-1) and average errors (less than 1.22%) indicate the quality and accuracy of the 8th degree model.

Table 4.5: Average errors and r-squared values of 8th degree MPR

Dependent variables	R2	Average error (%)
Cooling capacity (W)	1	0.09
COP (-)	1	1.22
Pressure drop (Pa)	1	0.01
Dew point effectiveness (%)	1	0.12
Wet bulb effectiveness (%)	0.99	0.11

It is worth mentioning that the dataset is once normalized through scaling all values in a particular range, e.g., [0,1], by the aim of observing the impact of normalization on MPR accuracy but no significant improvement is seen.

Cross Validation: In this section, cross validation is performed, firstly to validate the selected model and, secondly to check the model overfitting. In addition, the model has been generalized through the cross verification. It means that cross validation shows the validity of the proposed model for any new operating condition within the defined ranges. Comparison of the predicted values by 8th degree MPR for each performance parameter with corresponding values derived by numerical model are shown in **Figure 4.17.** The validation is carried out using the testing set and the constant values in Table 4.2. In addition, due to the high number of operating conditions, i.e., 1570 (20% of total dataset), only 20 operating conditions are demonstrated here. Channel width, water temperature and water flow rate which have less importance in operation of standard GIDPC are used to operate the numerical model only. As can be seen, predicted values by MPR are overlapped with the numerical simulation values whereas the maximum relative errors for cooling capacity, COP, pressure drop, dew point and wet-bulb effectiveness are 1.73%, 3.31%, 0.05%, 3.53% and 3.48% respectively. This indicates that MPR model has the satisfactory accuracy and is not over-fitted. Therefore, this regression model can be used to replace the previous numerical and experimental models to predict the performance of the GIDPC.
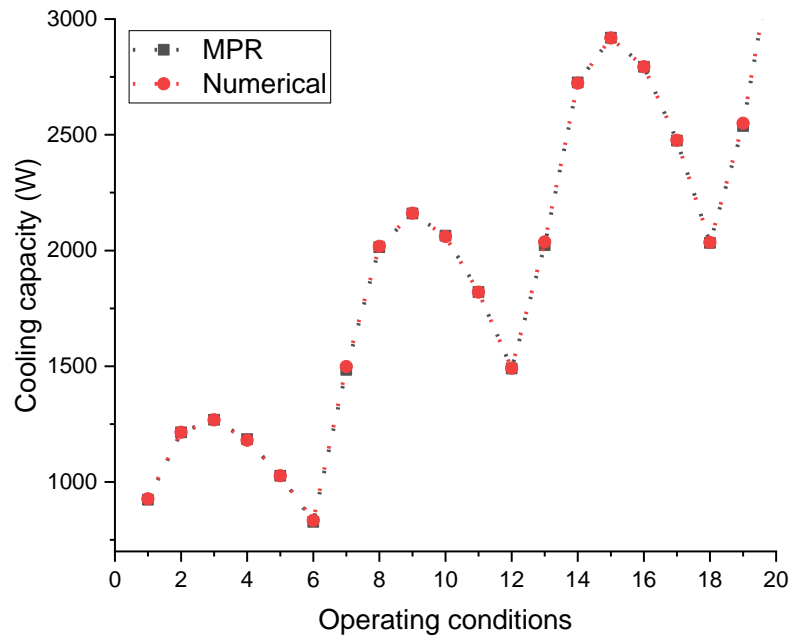
(a)
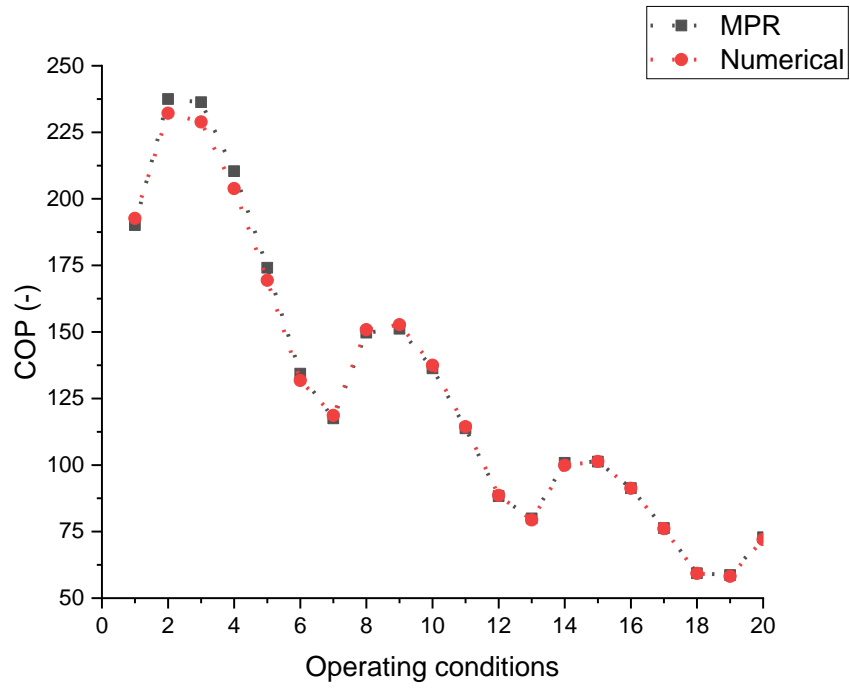
(b)
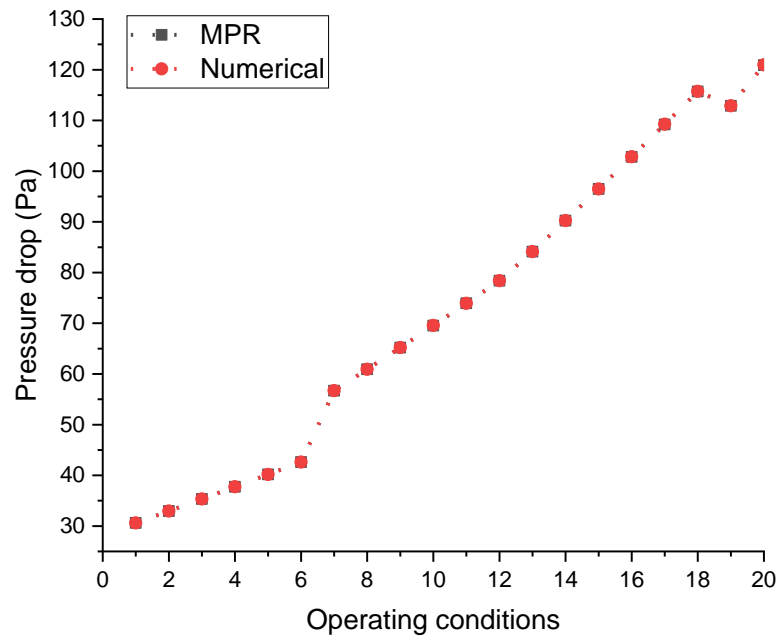
(c)
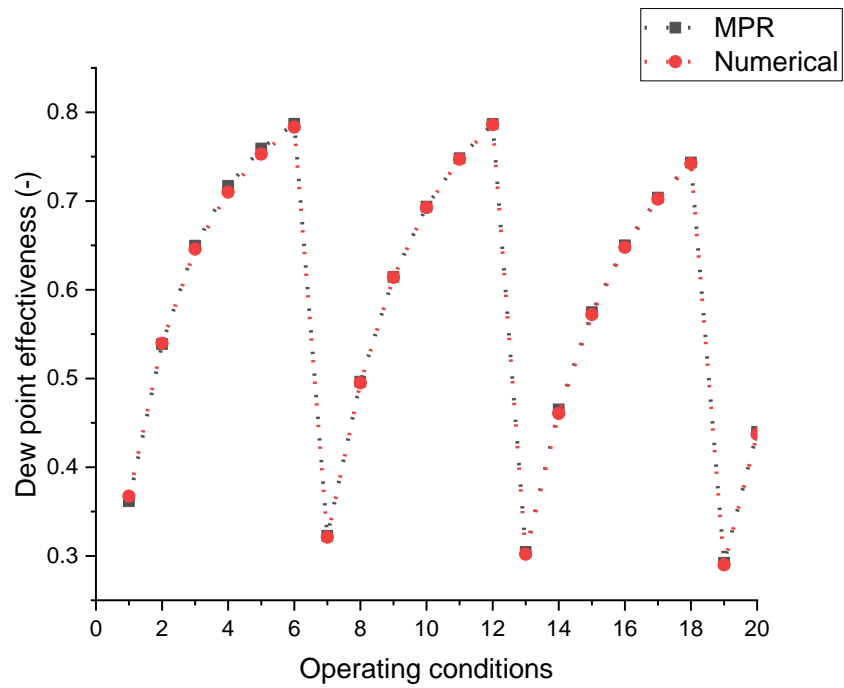
(d)
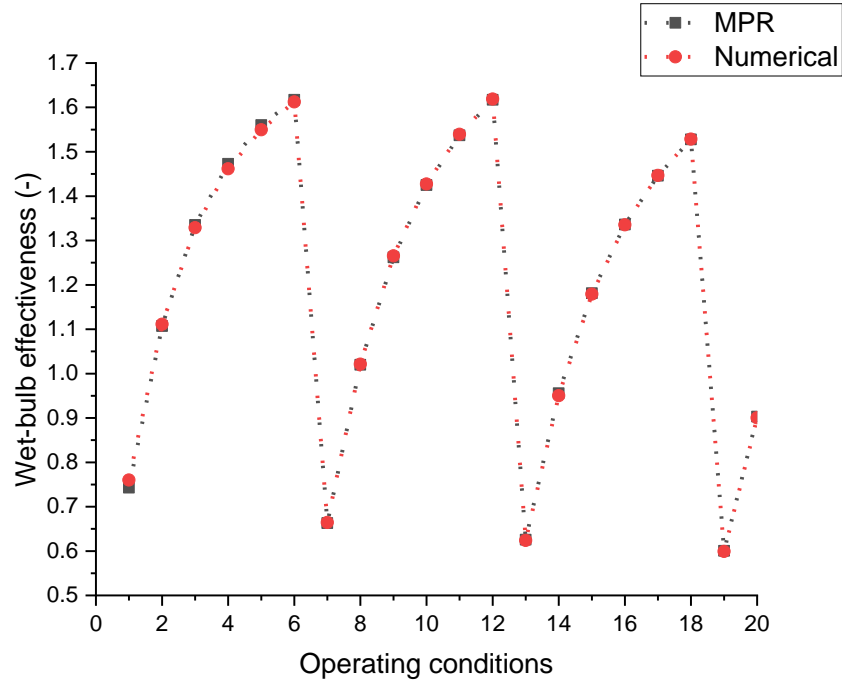
(e)

Figure 4.17: Cross validation: (a): Cooling capacity; (b): Pressure drop; (c): COP; (d): Dew-point effectiveness; (e): Wet-bulb effectiveness

4.3.6. Developed polynomial equations

The comprehensive MPR model obtained for the GIDPC is presented in Eq. (4.16), which is the generalized form of Eq. (4.15). The matrix on the left of equal sign represents the performance parameters and on the two first matrices on right side of equal sign, represent the regression/polynomial coefficients and third matrix represents the operating parameters. Power of each independent variable is denoted by n in which n_1 is for intake air temperature, n_2 is for intake air relative humidity, n_3 is for the airflow velocity, n_4 is for the working air fraction over the intake air and the second subscript for n which is shown by m indicates the number of coefficients. The number of coefficients for N^{th} degree polynomial with k variables is $\binom{k + N}{N} - 1$, which is 494 for 8th degree model with four operating parameters. It is important to

144

mention that the corresponding powers for each coefficient in general 8th degree polynomial are listed in **Table 4.6**.

$$\begin{bmatrix} Q_{cooling} \\ COP \\ \varepsilon_{wb} \\ \varepsilon_{dp} \\ \Delta P \end{bmatrix} = \begin{bmatrix} \beta_{0,1} \\ \beta_{0,2} \\ \beta_{0,3} \\ \beta_{0,4} \\ \beta_{0,5} \end{bmatrix} +$$

$$\begin{bmatrix} \beta_{1,1} & \beta_{1,2} & \beta_{1,3} & \cdots & \beta_{1,m} \\ \beta_{2,1} & \beta_{2,2} & \beta_{2,3} & \cdots & \beta_{2,m} \\ \beta_{3,1} & \beta_{3,2} & \beta_{3,3} & \cdots & \beta_{3,m} \\ \beta_{4,1} & \beta_{4,2} & \beta_{4,3} & \cdots & \vdots \\ \beta_{5,1} & \beta_{5,2} & \beta_{5,3} & \cdots & \beta_{5,m} \end{bmatrix} \begin{bmatrix} T^{n_{1,1}} \times RH^{n_{2,1}} \times U^{n_{3,1}} \times \varphi^{n_{4,1}} \\ T^{n_{1,2}} \times RH^{n_{2,2}} \times U^{n_{3,2}} \times \varphi^{n_{4,2}} \\ T^{n_{1,3}} \times RH^{n_{2,3}} \times U^{n_{3,3}} \times \varphi^{n_{4,3}} \\ \vdots \\ T^{n_{1,m}} \times RH^{n_{2,m}} \times U^{n_{3,m}} \times \varphi^{n_{4,m}} \end{bmatrix} \quad (4.16)$$

Table 4.6: Powers of general 8th degree polynomial equations

m	T	RH	U	ϕ
	$n_{1,m}$	$n_{2,m}$	$n_{3,m}$	$n_{4,m}$
1	1	0	0	0
2	2	0	0	0
3	3	0	0	0
$\vdots$	$\vdots$	$\vdots$	$\vdots$	$\vdots$
494	0	0	0	8

Table 4.7 gives all the regression coefficients to construct the 8th degree polynomial equations for different geometric sets. The equations for five performance parameters can be used by substituting the proper coefficients in Eq. (4.16) and thus the performance analysis of the GIDPC is possible for any operating conditions by considering the operating ranges. Since the total number of the coefficients for each performance parameter is 494, thus the table is summarized.

Table 4.7: Coefficients of 8th degree MPR model

Geometric set	Performance parameters	m=0	m=1	m=2	...	m=494
	Y	β_0	β_1	β_2	B_m	β_{494}
1	$Q_{cooling}$	3.807e+04	-9.006e+03	9.193e+02	...	-5.059e+04
	COP	-2.354e+03	5.113e+0	-4.893e+01	...	-3.128e+03
	ΔP	1.298e+03	-2.627e+02	2.284e+01	...	-1.718e+02
	ε_{dp}	3.483e+02	-8.201e+01	8.251e+00	...	-1.368e+01
	ε_{wb}	-4.996e+01	1.133e+0	-1.124e+00	...	-9.738e+00
2	$Q_{cooling}$	3.118e+03	1.048e+03	1.092e+02	...	-6.689e+04
	COP	-2.287e+03	5.186e+02	-5.254e+01	...	-4.727e+03
	ΔP	-1.661e+02	1.046e+02	-1.708e+0	...	5.501e+01
	ε_{dp}	3.661e+02	-8.634e+01	8.701e+00	...	-7.692e+00
	ε_{wb}	-3.839e+01	8.032e+00	-7.435e-01	...	-4.384e+00
3	$Q_{cooling}$	-4.378e+03	1.075e+03	-1.065e+02	...	-1.151e+05
	COP	-1.016e+03	2.057e+02	-1.946e+01	...	-7.906e+03
	ΔP	2.590e+02	-6.177e+01	6.359e+00	...	4.164e+01
	ε_{dp}	2.652e+02	-6.249e+01	6.297e+00	...	-1.895e+01
	ε_{wb}	-1.707e+01	3.785e+00	-3.788e-01	...	-2.939e+01
4	$Q_{cooling}$	-3.821e+02	-2.462e+02	8.092e+01	...	-2.372e+05
	COP	2.903e+03	-6.294e+02	6.052e+01	...	-7.800e+03
	ΔP	3.051e+03	-7.324e+02	7.660e+01	...	2.071e+02
	ε_{dp}	2.387e+02	-5.608e+01	5.630e+00	...	-1.610e+01
	ε_{wb}	-1.453e+01	3.461e+00	-3.493e-01	...	-2.125e+01
5	$Q_{cooling}$	1.351e+04	-3.454e+03	3.597e+02	...	8.692e+03
	COP	-6.549e+02	1.348e+02	-1.280e+01	...	-1.162e+03
	ΔP	1.026e+03	-2.475e+02	2.590e+01	...	3.402e+01
	ε_{dp}	3.906e+02	-9.235e+01	9.328e+00	...	9.135e+00
	ε_{wb}	2.461e+00	-7.326e-01	7.598e-02	...	2.712e+01
	$Q_{cooling}$	-1.248e+04	1.512e+03	-9.795e+01	...	1.076e+05
	COP	-1.485e+02	1.117e+01	-4.411e-01	...	-2.809e+03

6	ΔP	-2.296e+03	4.556e+02	-3.865e+01	...	9.069e+01
	ε_{dp}	1.017e+02	-2.411e+01	2.298e+00	...	2.107e+01
	ε_{wb}	-8.642e+00	1.014e+00	-4.549e-02	...	4.398e+01
	$Q_{cooling}$	-1.278e+04	3.001e+03	-3.134e+02	...	-1.183e+05
	COP	3.071e+03	-6.890e+02	6.563e+01	...	-6.401e+03
7	ΔP	-4.816e+03	1.144e+03	-1.172e+02	...	-8.053e+01
	ε_{dp}	3.157e+02	-7.450e+01	7.516e+00	...	-1.827e+01
	ε_{wb}	-5.186e+00	1.160e+00	-1.229e-01	...	-2.137e+01
	$Q_{cooling}$	-1.401e+04	3.315e+03	-3.284e+02	...	-2.136e+05
	COP	1.377e+03	-2.511e+02	2.489e+01	...	-1.714e+03
8	ΔP	2.640e+02	-3.346e+01	5.031e-01	...	7.573e+01
	ε_{dp}	3.337e+02	-7.868e+01	7.944e+00	...	-2.812e+00
	ε_{wb}	-1.621e+01	3.606e+00	-3.269e-01	...	2.961e+00
	$Q_{cooling}$	1.596e+04	-4.310e+03	4.504e+02	...	7.089e+04
	COP	1.765e+02	-7.621e+01	1.014e+01	...	-3.743e+02
9	ΔP	7.107e+03	-1.897e+03	2.157e+02	...	-6.753e+02
	ε_{dp}	4.144e+02	-9.783e+01	9.872e+00	...	2.994e+01
	ε_{wb}	2.766e+01	-7.527e+00	8.420e-01	...	6.029e+01
	$Q_{cooling}$	-1.251e+04	8.453e+02	-3.641e+01	...	2.437e+05
	COP	-6.748e+02	1.053e+02	-6.987e+00	...	-1.935e+03
10	ΔP	-6.303e+03	1.287e+03	-1.089e+02	...	-7.345e+02
	ε_{dp}	4.235e+02	-1.009e+02	1.025e+01	...	4.747e+01
	ε_{wb}	-3.157e+0	5.909e+00	-5.084e-0	...	8.068e+01
	$Q_{cooling}$	-3.305e+04	8.131e+03	-8.888e+02	...	-9.191e+04
	COP	5.614e+0	-1.372e+02	1.327e+01	...	-4.929e+03
11	ΔP	6.201e+02	-1.663e+02	1.865e+01	...	-2.395e+01
	ε_{dp}	3.404e+02	-8.030e+01	8.090e+00	...	-1.138e+01
	ε_{wb}	2.566e+01	-5.993e+00	6.013e-0	...	-1.016e+01
	$Q_{cooling}$	-1.920e+04	3.678e+03	-3.309e+02	...	-1.104e+05
	COP	-1.318e+0	1.283e+02	-1.574e+01	...	1.845e+03
12	ΔP	7.786e+03	-1.816e+03	1.850e+02	...	-1.772e+02
	ε_{dp}	3.655e+02	-8.615e+01	8.692e+00	...	1.182e+01

ε_{wb}	-1.285e+01	3.215e+00	-3.287e-01	...	1.825e+01

4.4. Method II: Deep Neural Network (DNN)

4.4.1. Overview of the mathematics

Digital Twins can be defined as a digital replication of a physical entity. It can also be combined with the Internet of Things (IoT) and/or augmented reality. However, in the simplest case, it would be just a system identification for different purposes such as abnormality detection and system optimization [217]. Black box, grey box and weight box models are three classes of the system identification known as the main part of digital twins. In this section, DNN is used as a black box and data-driven model to build the digital twins.

As explained in previous sections, the DNN is a complex type of ANN considered as a subset of DL. In this section, as a second ML model, the DNN is selected for performance prediction of the GIDPC. DNN is also have some other names such as Multilayer Perceptron (MLP) and Deep Feedforward network. Generally, these networks are known as supervised ML tasks in which data including independent and dependent variables are known and the task of the network is to find a function that can represent the relationship among the data for future prediction of the target/dependent variables. It is worth repeating that in ANN models, there is an input layer with number of neurons, one or more hidden layers with number of neurons and an output layer with a number of neurons. Each neuron in its layer is connected to all neurons in the next layer to transmit the information and data to the final output layer. The connections are assigned by weights which determine the importance of each connection in calculation of the final output value. The number of neurons in each layer is independent of other layers but normally, the number of neurons in hidden

148

layers is larger than the input neurons. **Figure 4.18** illustrates the general components

of a NN in which:

- "I" indicated the input nodes.

- "W" is the weight of connections

- "H" indicates the inactive nodes of hidden layer

- "HA" represents the activated nodes in hidden layers

- "O" represents the inactive output nodes in output layer

- "OA" is the activated output node in the output layer

- "B" is the bias of the layers.
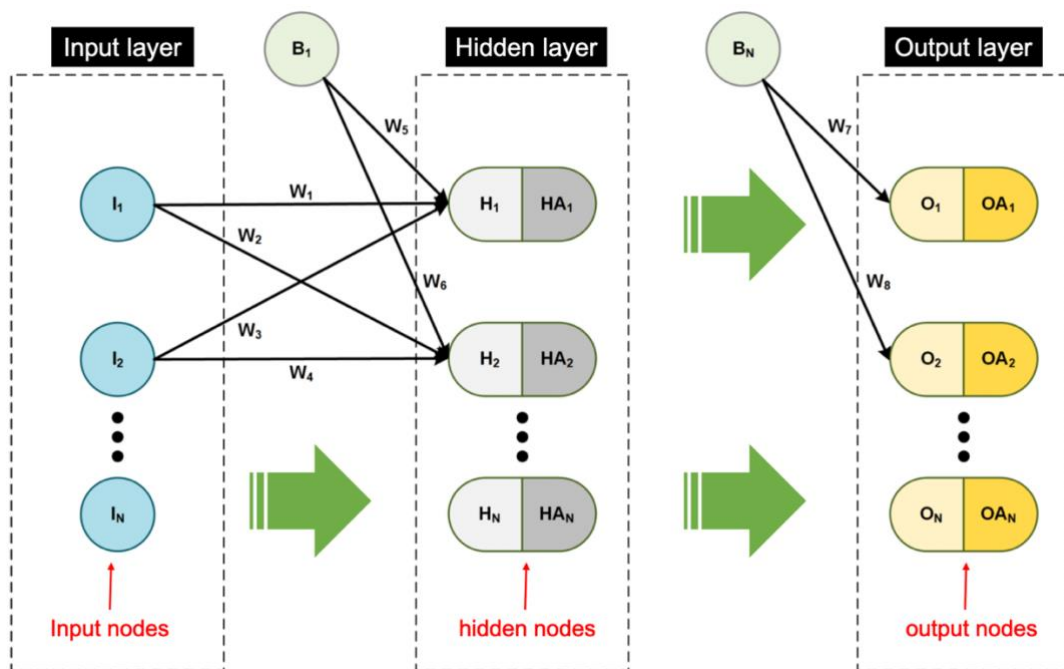
Figure 4.18: General structure of the Neural Network

The number of hidden layers and the associated number of neurons are all in hands of

the users and there is no rule for that. The users will increase or decrease the numbers

by considering the complexity and accuracy of the model. In order to be able to explain

the algorithm mathematically, the simple NN in **Figure 4.19**, with associated weight values is selected to explain the training steps of a NN model as follows:

Initialization: The first step in training the model will be initialization in which all the weights (W_1 to W_{12}) will get random values. In addition, bias nodes should get initial values which can be assumed 1 for simplicity.

Feed-forward: Once the dataset is given to the network, the hidden neuron values can be calculated as Eq. (4.17)-(4.18):

$$H_1 = I_1 W_1 + I_2 W_3 + B_1 W_5 \tag{4.17}$$

$$H_2 = I_1 W_2 + I_2 W_4 + B_1 W_6 \tag{4.18}$$
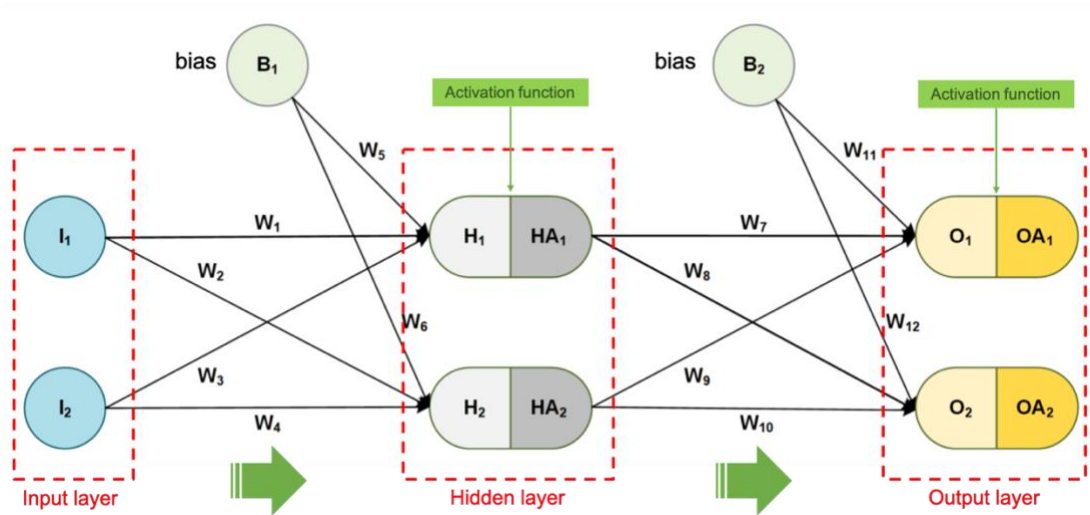
Figure 4.19: A sample Neural Network structure

The calculated hidden neuron values are inactive. An activation function, also called transfer function, is needed to activate the values. The activation functions are mathematical equations which calculate the output of each neuron and decide if the value of the neuron should be activated or not. It means that they decide if the considered neuron's value affect the model's final prediction or not. In addition, the activation functions normalise the output of each neuron to a value in ranges of (0,1)

or (-1,1) based on the type of activation function. In general, there are three types of activation functions:

1. **Binary step function:** It is a threshold-based function in which if only the input value is above a certain value, it transfers the same value to the next layer.

2. **Linear activation function:** As it can be realized from the name, it takes the input and multiply it by a certain coefficient and transfers it to the next layer.

3. **Non-linear activation function:** The most popular activation function in modern NNs are non-linear as it creates a complex mapping between the network inputs and outputs. Non-linear activation functions have two mains advantages over the binary and linear activation functions:

   - The backpropagation is possible as they have a derivative function which is related to the input values.

   - In addition, they enable using the multiple hidden layers which are essential in DNNs.

Different non-linear activation functions are in existence in which the common types are: Sigmoid/Logistic, Hyperbolic Tangent (TanH), Rectified Linear Unit (ReLU), Leaky ReLU, Parametric ReLU, Softmax, and Swish [218]. The most three common non-linear activation functions are shown in **Figure 4.20**. Further details about these functions are as follows:

   - **Sigmoid:** This type is smooth gradient and it creates the output values in a range of (0,1). In very high and low value inputs, there is no change in prediction due to the vanishing gradient. In addition, the outputs are not zero centred and it is computationally expensive.

- **TanH:** Despite the sigmoid activation function, TanH is zero centred and it creates the output values in a range of (-1,1).

- **ReLU:** It is computationally efficient as it leads to quick convergence and is suitable for backpropagation. The disadvantages of the ReLU is that when the input values are zero or negative, the gradient of the function is zero which causes the model to struggle in learning.

Function	Derivative
$$S(z) = \frac{1}{1 + e^{-z}}$$	$$S'(z) = S(z) \cdot (1 - S(z))$$
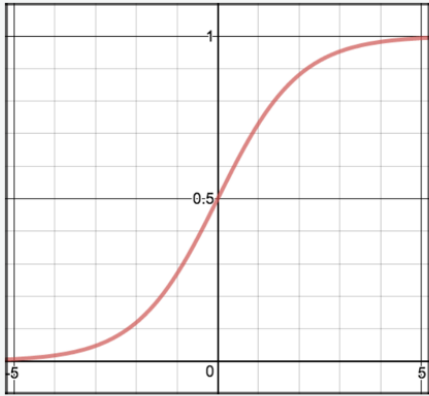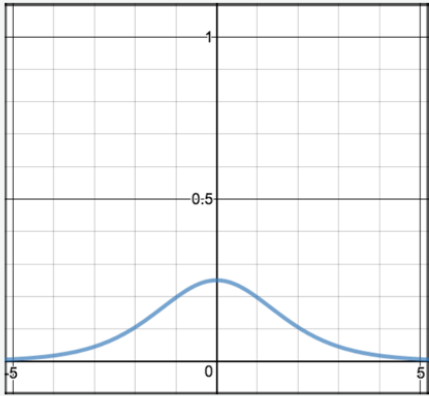

```
def sigmoid(z):
    return 1.0 / (1 + np.exp(-z))
```

```
def sigmoid_prime(z):
    return sigmoid(z) * (1-sigmoid(z))
```

(a)

Function	Derivative
$tanh(z) = \dfrac{e^z - e^{-z}}{e^z + e^{-z}}$	$tanh'(z) = 1 - tanh(z)^2$

```python
def tanh(z):
    return (np.exp(z) - np.exp(-z)) / (np.exp(z) + np.exp(-z))
```

```python
def tanh_prime(z):
    return 1 - np.power(tanh(z), 2)
```

(b)

Function	Derivative
$R(z) = \begin{cases} z & z > 0 \\ 0 & z <= 0 \end{cases}$	$R'(z) = \begin{cases} 1 & z > 0 \\ 0 & z < 0 \end{cases}$

```python
def relu(z):
    return max(0, z)
```

```python
def relu_prime(z):
    return 1 if z > 0 else 0
```
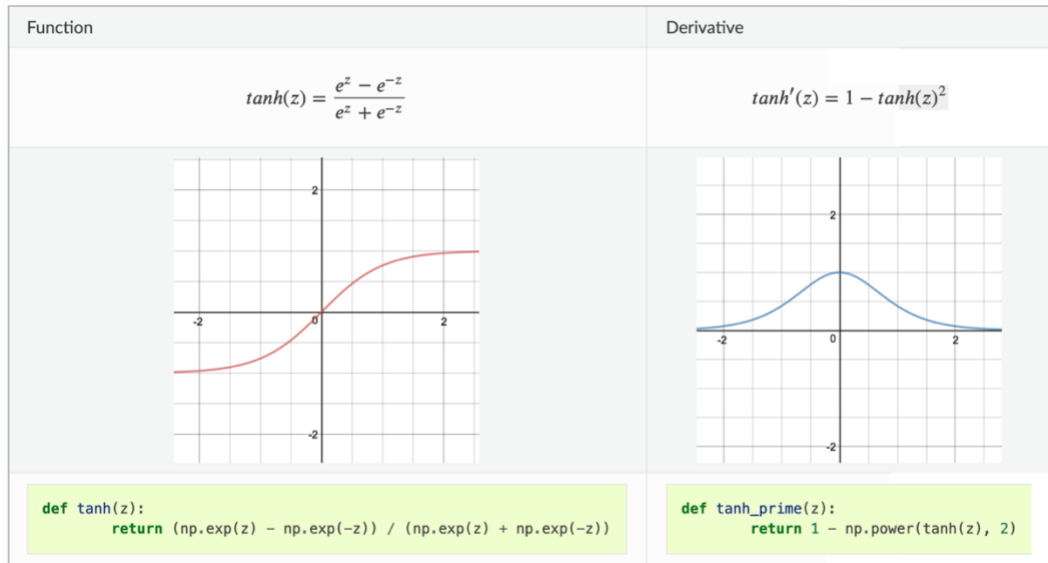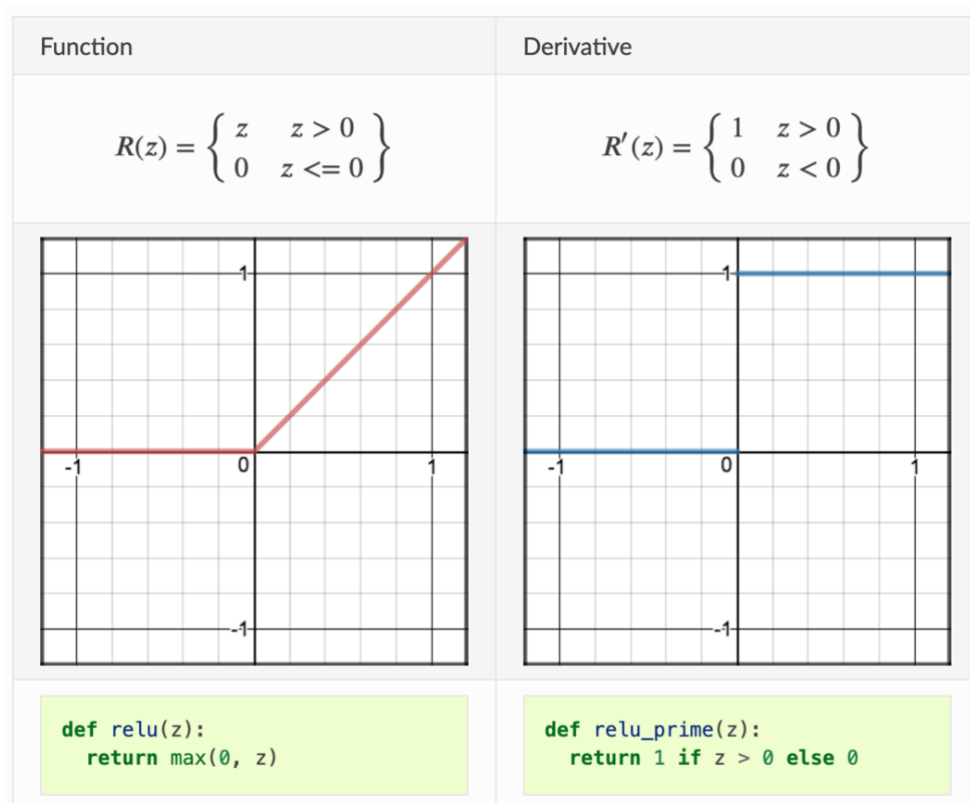
(c)

Figure 4.20: Common non-linear activation functions: (a): Sigmoid; (b): TanH; (c): ReLU

153

In the current example, the activation function is assumed to be Sigmoid function which can be expressed as Eq. (4.19):

$$A(x) = \frac{1}{1+e^{-x}} \tag{4.19}$$

Therefore, the calculated hidden neuron values can be activated as Eq. (4.20):

$$HA_1 = \frac{1}{1+e^{-H_1}} \tag{4.20}$$

$$HA_2 = \frac{1}{1+e^{-H_2}} \tag{4.21}$$

Having activated the hidden neurons, the value of the output neurons can be calculated as Eq. (4.22)-(4.23):

$$O_1 = HA_1 W_7 + HA_2 W_9 + B_2 W_{11} \tag{4.22}$$

$$O_2 = HA_1 W_8 + HA_2 W_{10} + B_2 W_{12} \tag{4.23}$$

Another activation function is needed in output layer to activate the output neurons. For instance, the following linear function, as shown by Eq. (4.24), is considered as the activation function of the output layer:

$$y = f(x) = x \tag{4.24}$$

Which results in following activated output values (Eq. (4.25)):

$$OA_1 = O_1 \tag{4.25}$$

$$OA_2 = O_2 \tag{4.26}$$

Having calculated the output values, the following expression, which represents the MSE, can be used to calculate the prediction error by Eq. (4.27).

$$e = \frac{1}{n}\sum_{i=1}^{2}(y_i - OA_i)^2 \tag{4.27}$$

If it meets the maximum considered error value, the OA can be considered as the predicted value. However, it is unlikely to reach an acceptable level of MSE in the first pass. Therefore, an iterative method called "backpropagation" is needed to adjust the weight values in order to decrease the error values.

Backpropagation: the backpropagation is used to optimise the weight values using "stochastic gradient descent" optimization method using the following Eq. (4.28):

$$W_i^{k+1} = W_i^k - \eta \frac{\partial e}{\partial W_i^k}$$
(4.28)

Where

- k represents the number of iterations

- η is the learning rate which is normally taken as a small number

- W_i^{k+1} represents the adjusted weight value

- $\frac{\partial e}{\partial W_i^k}$ shows the derivative of the total error regards to the weight.

For instance, the derivative of the error regards to the W_1 is as Eq. (4.29):

$$\frac{\partial e}{\partial W_1} = \left(\frac{\partial e}{\partial OA_1} \frac{\partial OA_1}{\partial O_1} \frac{\partial O_1}{\partial HA_1} \frac{\partial HA_1}{\partial H_1} \frac{\partial H_1}{\partial W_1} \right) + \left(\frac{\partial e}{\partial OA_2} \frac{\partial OA_2}{\partial O_2} \frac{\partial O_2}{\partial HA_1} \frac{\partial HA_1}{\partial H_1} \frac{\partial H_1}{\partial W_1} \right) = \left(\frac{\partial e}{\partial OA_1} \frac{\partial OA_1}{\partial O_1} \frac{\partial O_1}{\partial HA_1} + \right.$$

$$\left. \frac{\partial e}{\partial OA_2} \frac{\partial OA_2}{\partial O_2} \frac{\partial O_2}{\partial HA_1} \right) \left(\frac{\partial HA_1}{\partial H_1} \frac{\partial H_1}{\partial W_1} \right)$$
(4.29)

In which the calculation of each term is summarized in the following Eq. (4.30):

$$\begin{vmatrix} \frac{\partial e}{\partial OA_1} = -\frac{2}{n}(y_1 - OA_1) \\ \frac{\partial OA_1}{\partial O_1} = \frac{\partial O_1}{\partial O_1} = 1 \\ \frac{\partial O_1}{\partial HA_1} = W_7 \\ \frac{\partial HA_1}{\partial H_1} = \left(\frac{1}{1+e^{-H_1}} \right) \left(1 - \frac{1}{1+e^{-H_1}} \right) \\ \frac{\partial H_1}{\partial W_1} = I_1 \end{vmatrix}$$
(4.30)

This process should repeat for all weights to update their value with a new adjusted value. Once all of the derivatives for each weight is calculated, the following comprehensive gradient decent expression, as Eq. (4.31), can be used to update the value of all weights:

$$
\begin{bmatrix} W_1^{k+1} \\ W_2^{k+1} \\ \vdots \\ W_n^{k+1} \end{bmatrix} = \begin{bmatrix} W_1^{k} \\ W_2^{k} \\ \vdots \\ W_n^{k} \end{bmatrix} - \eta \begin{bmatrix} \dfrac{\partial e}{\partial w_1^k} \\ \dfrac{\partial e}{\partial w_2^k} \\ \vdots \\ \dfrac{\partial e}{\partial w_n^k} \end{bmatrix}
\tag{4.31}
$$

Based on the network configuration, the outputs can be calculated based on the iterative backpropagation method which is based on the stochastic gradient descent. For instance, for a network with three hidden layers as shown in **Figure 4.21**, the total derivative of error to the weight W_1 can be calculated by Eq. (4.32):
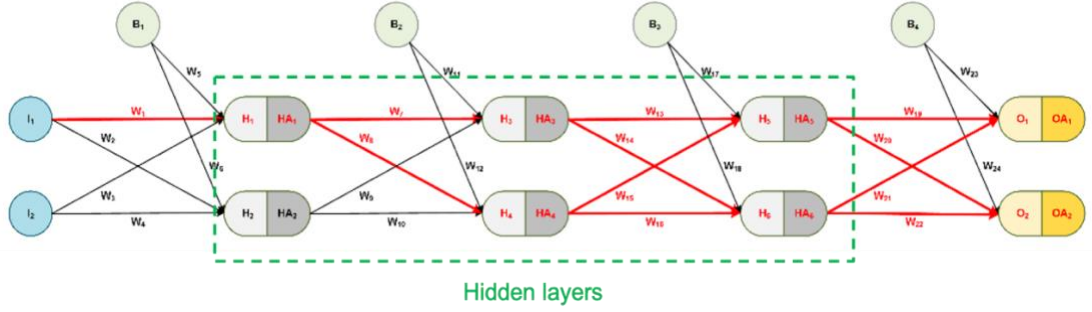
Figure 4.21: A deep neural network with three hidden layers

$$
\frac{\partial e}{\partial W_1} = \left(\frac{\partial e}{\partial OA_1} \frac{\partial OA_1}{\partial O_1} \frac{\partial O_1}{\partial HA_5} \frac{\partial HA_5}{\partial H_5} \frac{\partial H_5}{\partial H_3} \frac{\partial HA_3}{\partial H_3} \frac{\partial H_3}{\partial HA_1} \frac{\partial HA_1}{\partial H_1} \frac{\partial H_1}{\partial W_1} \right) +
$$

$$
\left(\frac{\partial e}{\partial OA_2} \frac{\partial OA_2}{\partial O_2} \frac{\partial O_2}{\partial HA_5} \frac{\partial HA_5}{\partial H_5} \frac{\partial H_5}{\partial H_3} \frac{\partial HA_3}{\partial H_3} \frac{\partial H_3}{\partial HA_1} \frac{\partial HA_1}{\partial H_1} \frac{\partial H_1}{\partial W_1} \right) +
$$

$$
\left(\frac{\partial e}{\partial OA_1} \frac{\partial OA_1}{\partial O_1} \frac{\partial O_1}{\partial HA_6} \frac{\partial HA_6}{\partial H_6} \frac{\partial H_6}{\partial HA_3} \frac{\partial HA_3}{\partial H_3} \frac{\partial H_3}{\partial HA_1} \frac{\partial HA_1}{\partial H_1} \frac{\partial H_1}{\partial W_1} \right) +
$$

$$
\left(\frac{\partial e}{\partial OA_2} \frac{\partial OA_2}{\partial O_2} \frac{\partial O_2}{\partial HA_6} \frac{\partial HA_6}{\partial H_6} \frac{\partial H_6}{\partial HA_3} \frac{\partial HA_3}{\partial H_3} \frac{\partial H_3}{\partial HA_1} \frac{\partial HA_1}{\partial H_1} \frac{\partial H_1}{\partial W_1} \right) +
$$

$$
\left(\frac{\partial e}{\partial OA_1} \frac{\partial OA_1}{\partial O_1} \frac{\partial O_1}{\partial HA_5} \frac{\partial HA_5}{\partial H_5} \frac{\partial H_5}{\partial HA_4} \frac{\partial HA_4}{\partial H_4} \frac{\partial H_4}{\partial HA_1} \frac{\partial HA_1}{\partial H_1} \frac{\partial H_1}{\partial W_1} \right) +
$$

$$
\left(\frac{\partial e}{\partial OA_2} \frac{\partial OA_2}{\partial O_2} \frac{\partial O_2}{\partial HA_5} \frac{\partial HA_5}{\partial H_5} \frac{\partial H_5}{\partial HA_4} \frac{\partial HA_4}{\partial H_4} \frac{\partial H_4}{\partial HA_1} \frac{\partial HA_1}{\partial H_1} \frac{\partial H_1}{\partial W_1} \right) +
$$

$$
\left(\frac{\partial e}{\partial OA_1} \frac{\partial OA_1}{\partial O_1} \frac{\partial O_1}{\partial HA_6} \frac{\partial HA_6}{\partial H_6} \frac{\partial H_6}{\partial HA_4} \frac{\partial HA_4}{\partial H_4} \frac{\partial H_4}{\partial HA_1} \frac{\partial HA_1}{\partial H_1} \frac{\partial H_1}{\partial W_1} \right) +
$$

$$
\left(\frac{\partial e}{\partial OA_2} \frac{\partial OA_2}{\partial O_2} \frac{\partial O_2}{\partial HA_6} \frac{\partial HA_6}{\partial H_6} \frac{\partial H_6}{\partial HA_4} \frac{\partial HA_4}{\partial H_4} \frac{\partial H_4}{\partial HA_1} \frac{\partial HA_1}{\partial H_1} \frac{\partial H_1}{\partial W_1} \right)
\tag{4.32}
$$

As seen when the number of hidden layers increases, calculating the derivatives becomes more complex and time consuming. This issue becomes outstanding for the big dataset as larger networks with more hidden layers and more neurons are needed to learn the patterns within the variables of the dataset. Therefore, the necessity of using computer programs is a vital need in training the neural network models.

In this research study, a DNN is developed in Python for the performance prediction of the GIDPC. As explained in chapter 3 of the current research study, the number of inputs and outputs which are represented by operating, design and performance parameters of the GIDPC, are numerous. As a consequence, a big dataset is required to train a model with acceptable accuracy. Therefore, it is decided to develop a DNN model for the performance prediction of the considered GIDPC which can learn from huge datasets.

The overall architecture of a DNN is depicted in **Figure 4.22** where each neuron within each layer is connected to every one of the neurons in the following layer. As explained in previous sections, initialization process triggers when each of the connections is weighted by a random value which will be updated during the training procedure to reach the best fit with the lowest possible error values. In addition, there is a bias parameter (shown in Eq. (4.33)) which is used to adjust the output values of the weighted sum of the inputs to the neuron. Bias is a random constant which helps the model in a way that it can fit best for the given data.

$$x_j = \sum_{i=1}^{i=n} w_i x_i + b_i \tag{4.33}$$

Where w_i represents the weight connecting the neuron x_i to neurone x_j in the next layer, n represents the number of the connections, and b_i is the corresponding bias.
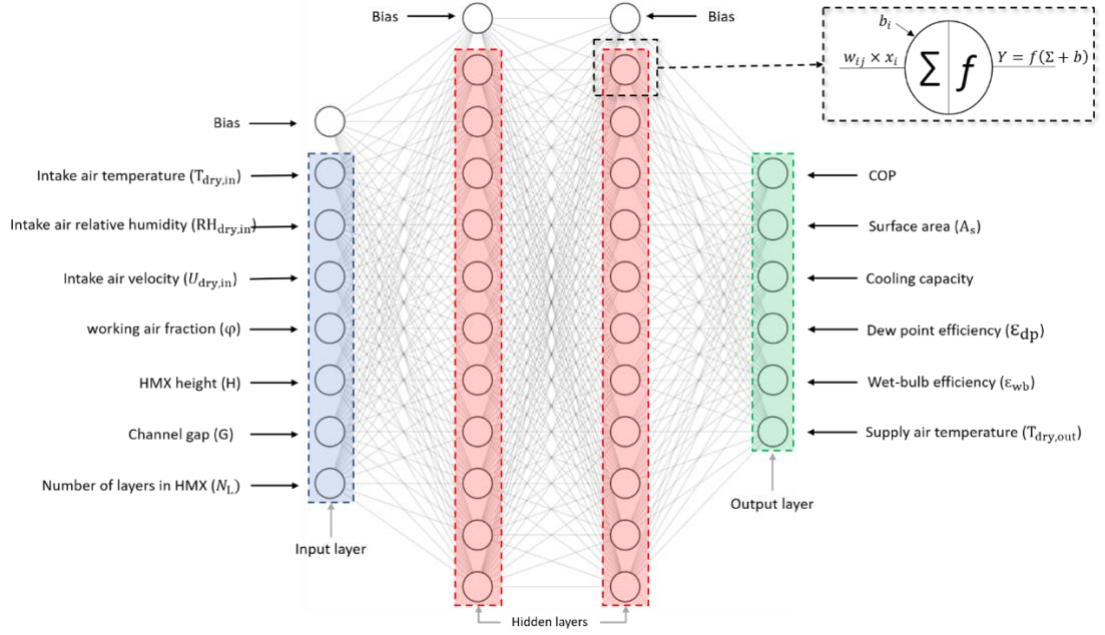
Figure 4.22: Structure of the DNN

Activation functions are needed to attach to each neuron and their role is to determine the importance of each neuron's input in prediction of the outputs and to normalize the output of the neurons. Different activation functions are compared and it is found that the performance of the network in terms of MSE is best when the activation function is hyperbolic tangent sigmoid for the current GIDPC big dataset which can be represented through the function below (Eq. (4.34)):

$$y_j = f(x_j) = \frac{e^{x_j} - e^{-x_j}}{e^{x_j} + e^{-x_j}} \tag{4.34}$$

Where y_j is the activated value of the neuron j.

Randomly selected weights and biases are iteratively optimized through back-propagation process until the considered evaluation metric, e.g., the MSE, is minimised. The back-propagation is an essential step in minimising the errors and maximising the model generalization [219]. The holdout cross-validation is used to divide the big dataset into three sources: a training data set (70%), a validation data set (15%), and a testing data set (15%). The training dataset is used to estimate the

network weights, while the validation dataset is used to monitor the network and calculate the minimum error during the iterations till network is stopped. The test dataset is unseen data by network and task of the test dataset is to decrease the bias and generate unbiased estimates for predicting future outcomes and generalizability. The test dataset is used at the end of the iteration process for evaluating the performance of the model from an independently drawn sample.

A Bayesian Regularization (BR) is used as a regularization method in optimizing the weight and bias values, which is the linear combination of Bayesian methods and NN to determine the optimal regularization parameters. BR technique implements certain prior distributions on the model parameters as follows (Eq. (4.35)) [220]:

$$F = \beta E_D(D|w, M) + \alpha E_w(w|M) \, ; \text{D=} \{X, Y\} \tag{4.35}$$

Where D represents the big dataset, i.e., X represents the inputs and Y represents the outputs, $E_D(D|w, M)$ is the sum of squared estimation errors, M represents the network structure, β and α are estimated hyper-parameters. $E_w(w|M)$ is sum of the weights' squares which intends to decrease the overfitting probability of the model [221]. Density function is used for updating the weights according to Bayes' rule. The posterior distribution of w given α, β, D, and M can be written as Eq. (4.36):

$$P(w|D, \alpha, \beta, M) = \frac{P(D|w, \beta, M)P(w|\alpha, M)}{P(D|\alpha, \beta, M)} \tag{4.36}$$

Where $P(D|w, \beta, M)$ is likelihood function of w, $P(w|\alpha, M)$ is the prior distribution of weights under M, which is the probability of observing the data given w and $P(D|\alpha, \beta, M)$ is a normalization factor or evidence for hyperparameters α and β.

4.4.2. Associated dataset for DNN

In this study, as listed in **Table 4.8**, main operating and design parameters i.e., temperature, relative humidity and velocity of the intake air, working air fraction,

HMX height and channel gap, and number of layers in HMX structure are all considered as input parameters. Additionally, main performance parameters i.e., supply air temperature, cooling capacity, COP, dew point efficiency, wet-bulb efficiency and surface area of the layers are considered as output parameters. The big data set is created using the defined operating ranges based on the literature [33], and with a purpose of covering wider ranges, by the validated numerical model [127]. Unlike the MPR, for the DNN model, all operating and design (geometric) parameters are included in a single huge dataset. 78125 data points (operating conditions) are created using the evenly distributed discrete values for each of the operating parameters and based on the all possible combination method described in chapter 3. In quite a similar manner to MPR dataset, no significant issue such as inconsistency or incorrect values is seen in the DNN model dataset so that, the normalization, as a common method in data pre-processing, is tested to observe its impact on the DNN model but no significant improvement in neither accuracy nor training time of the model are seen.

Table 4.8: Operating ranges of the input variables

Type of parameters	input parameters	Minimum	Maximum
	$T_{dry,in}$ (°C)	25	45
Operating parameters	$RH_{dry,in}$ (-)	0.10	0.80
	$U_{dry,in}$ (m/s)	0.30	3.30
	φ (-)	0.10	0.90
	H (m)	0.80	3.3
Design parameters	G (m)	0.004	0.008
	N_L (-)	100	200

4.4.3. DNN development process

DNN is mainly configured by two main hyperparameters that define the structure of the network, i.e., the number of layers and the number of neurons in each hidden layer. The most common method to spot the preeminent values of these hyperparameters for a specific problem is calibration by a robust test harness. Therefore, several models with different hyperparameters are constructed until the desired accurate model is identified. The model reconstruction stopped when no significant improvement in accuracy metrics i.e., MSE and coefficient of determination (R^2) is seen. As listed in **Table 4.9**, ten different configurations are compared in terms of MSE and R^2 values.

Table 4.9: Comparison of different DNN models

Model	Number of layers	Neurons No in 1st layer	Neurons No in 2nd layer	MSE	R2
1	1	10	NA	1483.89	0.98
2	1	20	NA	182.21	0.99
3	1	30	NA	112.33	0.99
4	2	30	10	12.86	1
5	2	30	20	6.74	1
6	2	40	30	2.39	1
7	2	40	40	1.19	1
8	2	45	40	0.9	1
*9**	*2*	*45*	*45*	*0.04*	*1*
10	2	50	45	0.03	1

Due to the relatively high number of operating conditions in the big dataset, i.e., 78125, firstly, the DNN model with a single hidden layer and 10 neurons is configured. The MSE value has revealed that more a robust configuration is needed in order to reduce the MSE and increase the accuracy of the network. Thus, the network complexity is increased gradually by increasing the number of hidden layers and

neurons until no significant improvement observed in the MSE value. Model number 9 with 2 hidden layers, and 45 neurons in each hidden layer is selected as the final network since it is accurate enough with MSE value of 0.04 to stop the robust test harness. However, one more model with a slight improvement, i.e., model number 10, is constructed to compare it with the selected model. It can be seen that, although the model was improved, i.e., with MSE of 0.03, but no significant accuracy added to the network. Hence, the model No. 9 is selected for the performance prediction of the GIDPC.

4.4.4. DNN model testing: comparison of the supply air temperature

The developed DNN model is tested by the validated numerical model for 4-kW GIDPC described in chapter 3. Although the DNN model is inherently validated by being trained and validated through the big dataset which was constructed by the numerical model but to test the performance of the model, the temperature of the supply air is predicted by the DNN and numerical models for the comparison purpose. The idea of selecting the temperature of the supply air, as a comparison factor, is based on the key role of this factor in system performance evaluation. Supply air temperature is directly considered in performance parameters calculations, e.g., cooling capacity, and its value is influenced by other key parameters such as intake air parameters, working air fraction and HMX dimensions [222].

Therefore, the predicted supply air temperature by the model is compared in four different climates and the results are shown in **Figure 4.23.** According to the Koppen–Geiger's climate classification [223] and considering the defined ranges, out of seven existed climates, warm periods of four different climates, i.e., Tropical rainforest climate (Miami), Arid (Doha), Mediterranean hot summer (Rome) and Hot summer continental (Beijing) are identified as suitable regions for the GIDPC operation. One

representative city for each climate is selected and, in each city, the warm months for the GIDPC operation are identified. The criteria for selection of the operating months is the commonly defined ranges of the temperature and relative humidity of the intake air. The climate data, i.e., temperature and relative humidity of four cities are inspired from a source for the comparison purpose only as listed in Table 4.10.

The comparison is made over the identified operating months by holding the key parameters unchanged, i.e., the air velocity, air working fraction, HMX height, channel gap and number of layers were kept at 3 (m/s), 0.44, 1 (m), 0.005 (m) and 160 respectively which are also defined as the base system parameters. The results revealed that the predictions made by two models are in good agreement in which the maximum discrepancies between the numerical and DNN models in Miami, Doha, Rome and Beijing are recorded as 0.32 ⁰C, 0.77 ⁰C, 0.21 ⁰C and 0.54 ⁰C respectively.
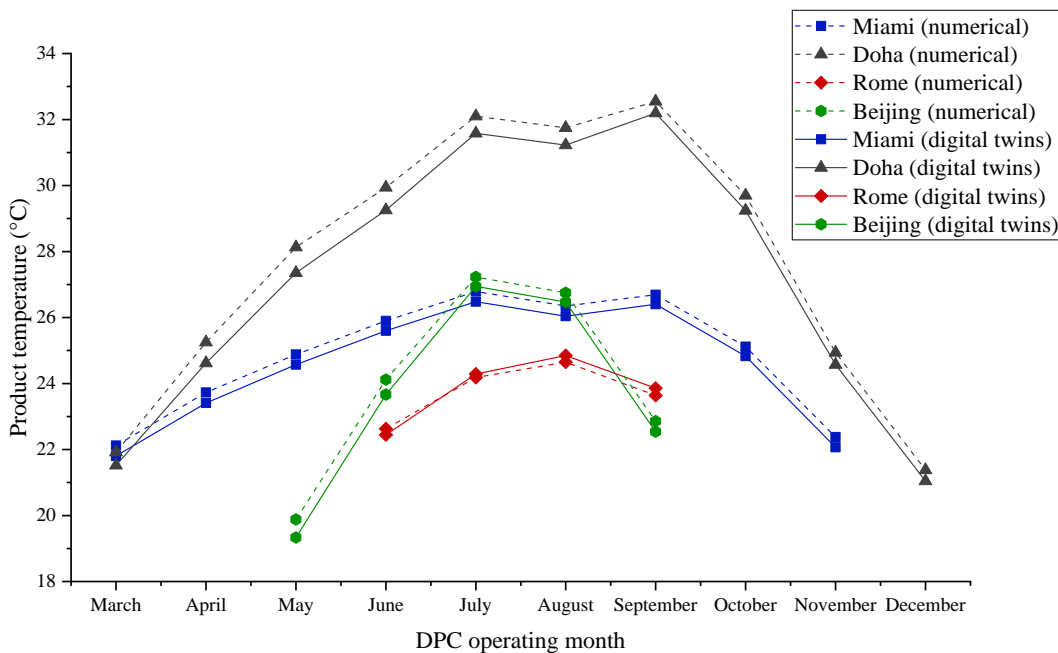
Figure 4.23: Comparison of the supply air temperature of the base system by numerical and DNN models in operating months

Table 4.10: Monthly and average weather data of each city [174]

Month	Miami		Doha		Rome		Beijing	
	T(ºC)	RH(-)	T(ºC)	RH(-)	T(ºC)	RH(-)	T(ºC)	RH(-)
January	24	0.74	22	0.72	12	0.76	2.5	0.44
February	24	0.73	23	0.7	13	0.76	5	0.44
March	26	0.70	27	0.62	15	0.75	12	0.44
April	28	0.69	33	0.52	18	0.75	20	0.45
May	29	0.71	39	0.43	22.9	0.75	26	0.53
June	30	0.72	42	0.41	26	0.74	30	0.60
July	31	0.72	42	0.50	27.90	0.73	31	0.75
August	30.50	0.72	40.50	0.54	28.10	0.75	30	0.78
September	30.40	0.75	39.50	0.62	27	0.75	27	0.69
October	28.50	0.76	36	0.63	22.90	0.76	19.90	0.60
November	26	0.72	29.90	0.66	17	0.79	20	0.58
December	23.90	0.74	25	0.71	12	0.79	5	0.50
Average in operating months	28.82	0.72	35.39	0.56	27.25	0.74	28.80	0.67

4.4.5. Explainable Artificial Intelligence

Owing to the empirical success of the ML models in complex computational tasks, the need for interpreting the black box models, e.g., a complex DNN model with numerous layers and parameters is increased [224]. The transparency of such models will contribute the experts with providing more detailed information about the model than a final accurate prediction [225]. Furthermore, it will lead to more trustable ML models in which the researchers can observe the evolving process of the model [224]. The aforementioned need for interpreting the complex ML models has led to appearance of eXplainable Artificial Intelligence (XAI) field. The newly evolving XAI has the ability to demonstrate the rationality of the results in different ways [226]. SHapley Additive eXplanations (SHAP) is based on a game theory which can be used as a XAI method to interpret the ML models [227]. In this study, the SHAP is used to

mainly show how the operating and design parameters of the GIDPC affect the performance parameters using the function provided by the developed DNN model. SHAP can demonstrate the contribution of each input to the predicted value using the calculated Shapley values which reveal how to distribute the predicted values (performance parameters) among the features (operating and design parameters). In SHAP, the Shapley value explanation is provided as an additive feature contribution [227]. In summary, SHAP describes the following three attributes (Eq. (4.37)-(4.39)):

1) Local accuracy:

$$f(x) = g(\acute{x}) = \varphi_0 + \sum_{i=1}^{N} \varphi_i \acute{x}_i \tag{4.37}$$

2) Missingness :

$$\text{if } \acute{x}_i = 0 \text{ then } \varphi_i = 0 \tag{4.38}$$

3) Consistency:

For any two different models f and $\acute{f}$:

$$\begin{cases} if: \acute{f}_x(\acute{x}) - \acute{f}_x(\acute{x}_{\backslash i}) \geq f_x(\acute{x}) - f_x(\acute{x}_{\backslash i}) \text{ where } (\acute{x}_{\backslash i} = (\acute{x}_i = 0)) \\ \qquad \qquad then: \varphi_i(\acute{f}, x) \geq \varphi_i(f, x) \end{cases} \tag{4.39}$$

Where g represents the explanation model, f is the mapping function, $\acute{x}$ represents the coalition vector, φ_i is the feature attribution for the input i, N is the maximum coalition size, $\acute{f}_x$ and f_x are the mapping functions which use the simplified input $\acute{x}$ to map the original input x.

In local accuracy, the requirement of the explanation model (g) which can match the main model (f) for the simplified input($\acute{x}$), is explained. The missingness simply says the contribution of missing input (feature) is zero. The consistency indicates when the model changes, the contribution of the feature will be higher and will stay same.

Shapley values are given by the following **Eq. (4.40)**which is the only set of values

that satisfies the three aforementioned conditions:

$$\varphi_i(f, x) = \sum_{\acute{z} \subseteq \acute{x}} \frac{|\acute{z}|!(N - |\acute{z}| - 1)!}{N!} \left[f_x(\acute{z}) - f_x(\acute{z}_{\backslash i}) \right] \tag{4.40}$$

in which the $|\acute{z}|$ in the group of non-zero values in $\acute{z}$, as the subset of $\acute{x}$.

The Shapley values can be visualized as forces to demonstrate the attribution of each

feature on the prediction [35, 36]. **Figure 4.24** shows the force plots for each of the

performance parameters in the developed DNN. Force plots show how each of the

input variables (features) contribute to the value of the performance parameters. Each

figure consists of two sub figures in which the first one is demonstrated for one

representative data point (operating condition) and the second one is demonstrated for

10 data points (out of 78125 data points used in DNN model) which are rotated 90

degrees and stacked together horizontally [230].

Each feature is considered as a force which either has a positive or negative effect.

The prediction for each performance parameter starts from the base value which is the

average value of the performance parameter in the training dataset used to train the

DNN which would happen if the effect of features (operating and design parameters)

was not considered. There is also an output value in each figure which is identical to

the predicted value by the DNN model. SHAP values are the arrows in red and blue

indicating how much contribution each feature has on the output value which results

in increasing or decreasing the prediction. There are positive contributions in red

colours which mean that the correspondent feature contributes to increasing the

performance parameter value from the base value to the actual predicted value by the

DNN whereas the negative contributions with blue colours contribute to decreasing

the value of the performance parameter from the base value to the actual predicted

value. As seen from **Figure 4.24**, the contribution of each data point is different which

is simply because of the different operating and design parameter values. These plots allow us to know the impact of each parameter on the predicted values in the desired data point. This information let the researchers observe the positive and negative contribution of each parameter and identify the appropriate operating condition for each performance parameter. This will eventually result in improved system performance and energy management. For instance, **Figure 4.24 (a)** shows the force plots for the cooling capacity in which the data point number 8 is selected as the representative. As seen, the base value is increased from 1.77 (kW) to the model predicted value of 3.59 (kW) in which four inputs in red colours have positive contribution while other three inputs i.e., gap, relative humidity and height have negative contributions. The force plots of other performance parameters are also provided for ten sample data points as demonstrated in **Figures 4.24 (b)-(f)**.
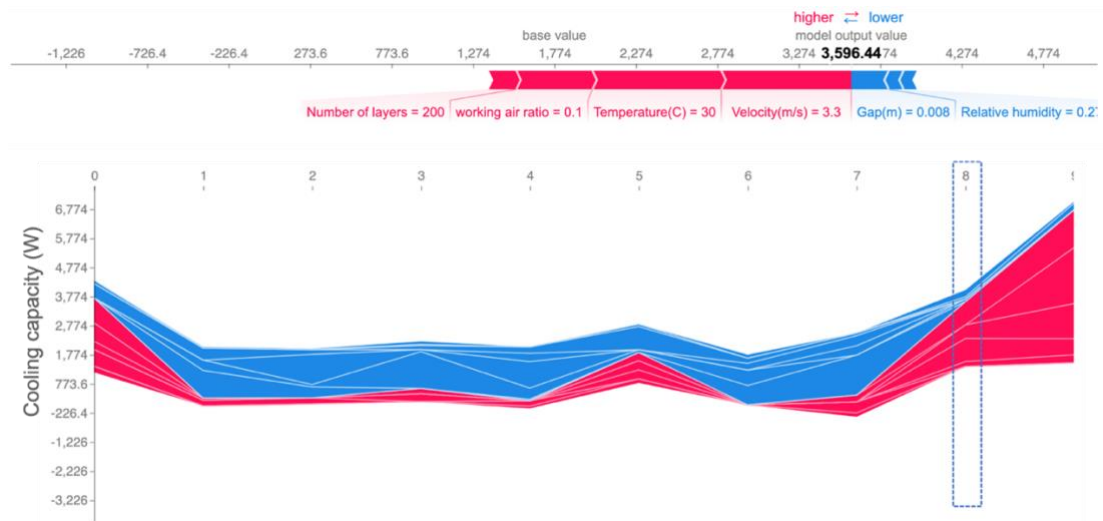
(a)
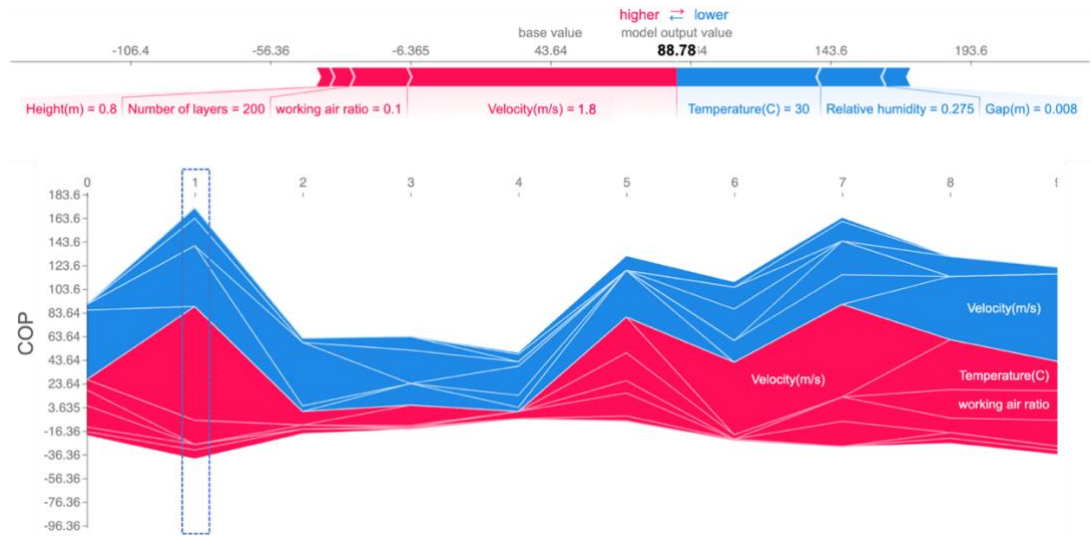
(b)
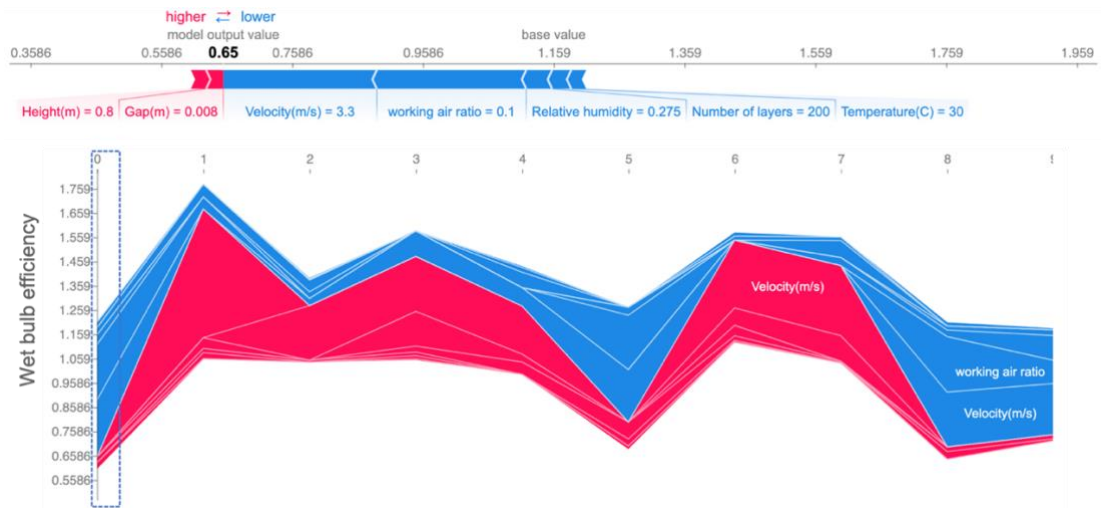
(c)
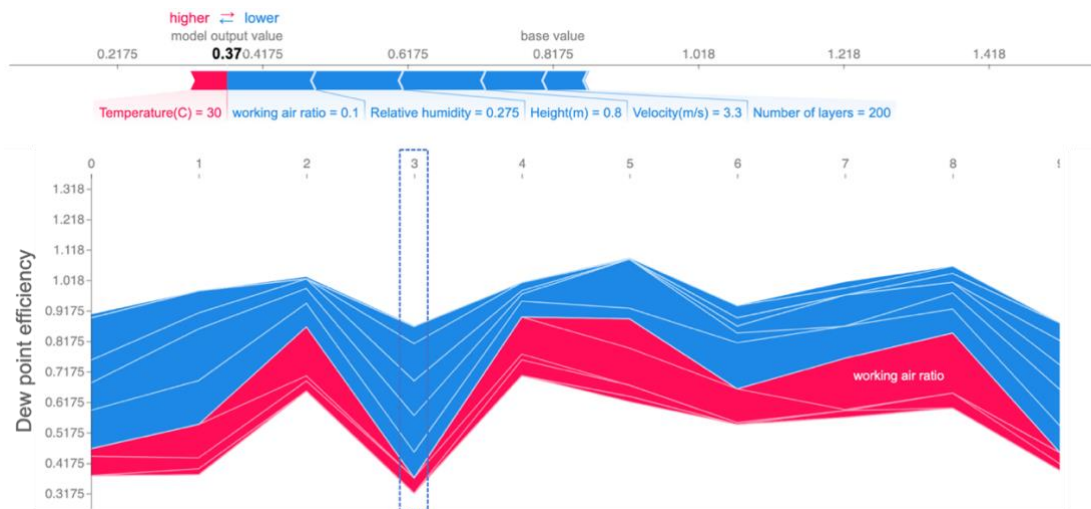
(d)
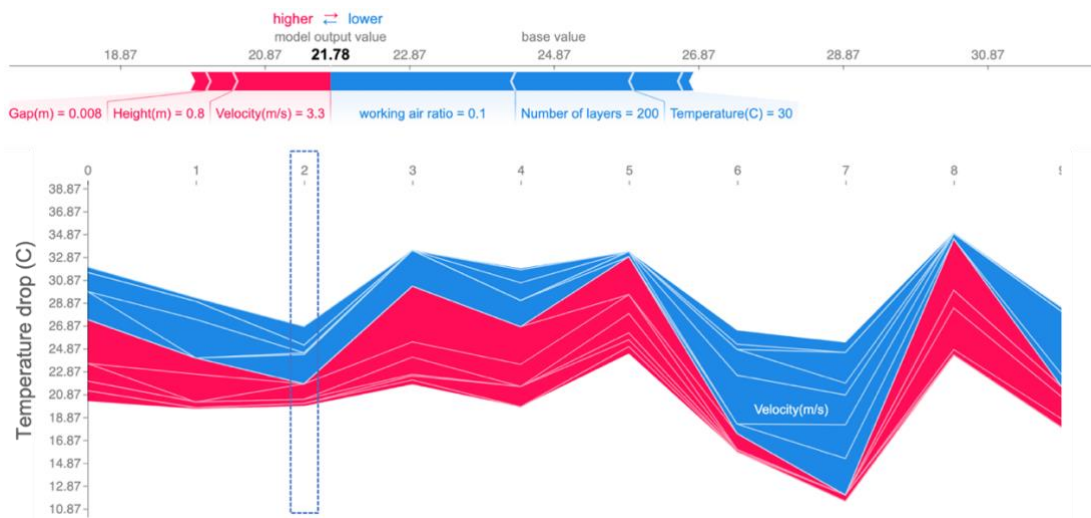
(e)
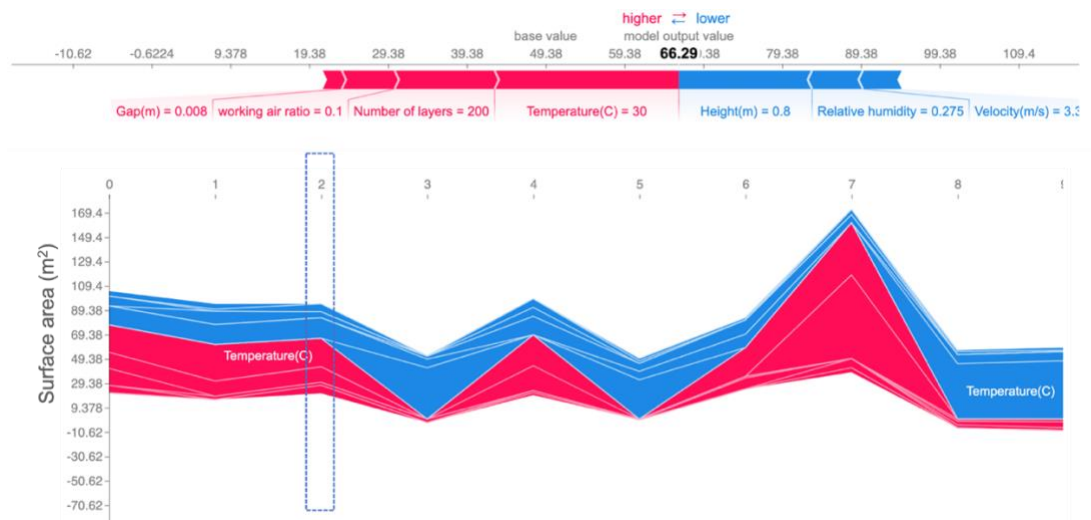
(f)

Figure 4.24: Force plots : (a): cooling capacity; (b): COP; (c): wet bulb efficiency; (d): dew point efficiency; (e): temperature drop; (f) surface area

4.5. Comparison of the developed models

In this section the performance of the developed MPR and DNN models are compared. The comparison factors are mainly based on the models' performance, accuracy, comprehensiveness and development processes. In addition, the flexibility of the model in prediction and dataset processing are the other comparison factors. The

comparison is made by considering the following advantages and disadvantages of the models:

MPR:

Advantages:

- Flexibility in increasing the model complexity in a gradual way: Increasing polynomial degrees is a way to control the complexity of the model and avoid developing unnecessary complex models.

- High R^2 value which indicates the good fitting capability: The fitting quality of the MPR model was quite satisfactory where it reached the value of 1 from the 5th degree polynomial equations.

- High accuracy: The accuracy of the selected 8th degree MPR is quite high where the MSE reached the minimum value of zero while the maximum average error was 1.2%.

Disadvantages:

- Higher possibility of over fitting: Although the gradual improvement by increasing the polynomial degrees can be considered as an advantage but in MPR, more complex models will lead to overfitted model by covering data noises.

- Unable to find an appropriate trade-off between the model accuracy and over fitting: It is a big challenge in MPR to find the best model in order to avoid overfitting without sacrificing the accuracy.

- The MPR was unable to provide a single model for the big dataset including all of the operating and design parameters. Therefore, one model for each design set (geometric set) is provided as the MPR couldn't discover the pattern

amongst all parameters. This led to numerous equations sets which are considered as the major disadvantages of the model.

DNN:

Advantages:

- Higher accuracy: The selected model has reached the MSE substantially close to zero which proves the high accuracy of the model.

- High R^2: Similar to MPR, in terms of fitting, the DNN model performs well with the R^2 value of 1.

- Capability in increasing the complexity and accuracy of the model without overfitting hazard: This can be considered as an outstanding advantage over the MPR model where the model complexity and accuracy can be increased without confronting the overfitting problem.

- The model could process the big dataset with all operating and design parameters and more performance parameters. Despite MRP, the DNN provided a single comprehensive model.

Disadvantages:

- Long training time: The only negative point of the DNN model compared to the MPR is its roughly high computational time. Increasing the model complexity leads to more computational time.

By taking all the aforementioned discussions into consideration, the DNN model is selected as the fitting function to be used in the optimisation models in the next chapter.

4.6. Summary

In this chapter, a detailed overview of AI and its subsets including ML and DL are conducted. It is mentioned that the ML is a broad subset of AI in which diverse algorithms are implemented to develop models which are capable of predicting particular systems behaviour through previously established performance data. As the models used in this chapter are based on the ML algorithms so that the focus of the introduction is shifted towards different ML algorithms. It is mentioned that the ML is mainly categorized in supervised and unsupervised ML. The supervised ML uses the labelled known data to learn and then extract the hidden pattern within the dataset by mapping a relationship between the independent and dependent variables while the unsupervised ML uses unlabelled data to extract the relationships among them. In addition, procedure of developing two models based on supervised ML are explained in details. MPR as one of the regression-based models is selected as the first method to find the relationship between the performance and operating parameters of the GIDPC. The development procedure and all steps in model development as well as the challenges in development process are explained. DNN based model was the second model that is used to predict the performance of the GIDPC using the operating and design parameters of the system. The developed models are used to demonstrate the applicability of them in predicting the system performance in diverse operating conditions. In addition, the XAI is used to interpret the developed DNN model by demonstrating how each of the input variables (features) contribute to the value of the performance parameters. Comparison of the two developed models has revealed that the DNN model outperforms the MPR model in different aspects. As a consequence, the DNN model is selected as the main ML function for the performance prediction of

the GIDPC. This model will be used in optimization models that will be explained in

the next chapter.

CHAPTER 5: DEVELOPMENT OF MULTI-OBJECTIVE EVOLUTIONARY OPTIMISATIONS AND ASSOCIATED RESULTS

5.1. Introduction

In this chapter, firstly traditional and nature-inspired optimisation algorithms and their classifications are overviewed. Then, the Multi-Objective Evolutionary Optimization (MOEO) methods are explained to reveal the importance and impact of the optimisation methods on engineering applications and in particular on energy systems over the recent decades. Then the chapter continues by introducing the selected MOEO algorithms that are used to find the optimum operating conditions for the GIDPC. The Genetic Algorithm (GA) and the Particle Swarm Optimisation (PSO) are two common optimisation methods that are used as the base optimisation methods and the state-of-the-art Slime Mould Algorithm (SMA) is introduced as a novel method for the performance optimisation of the GIDPC. The models' development procedures, mathematical approach and corresponding decision variables and objective functions are explained in details. In addition, it is justified that how the objectives of the optimisation are selected by explaining superiority of the MOEO over the single objective optimisation models. Eventually, the results of each method are presented in which the optimum operating and design parameters of the GIDPC are identified to maximise the cooling efficiency and minimise the operating and construction cost of the GIDPC. This is carried out for different identified operating climates in order to propose a single optimized unit for each climate. Eventually, the advantages and disadvantages of each method are presented.

5.2. Optimisation algorithms

5.2.1. Concept

Optimization is simply contributed to maximising the performance of a system. This is undertaken by identifying the optimum conditions for the desired system which will lead to efficient and economic performance of the technology. In general, optimization includes a process in which a particular function is maximised or minimised by finding appropriate inputs. The function/parameter which is aimed to get maximal/minimal figures is called objective of the optimization and the inputs being identified are called decision variables of the optimisation. An optimisation problem is unconstrained when the objective is achieved without any predefined constraints while it is called constrained when additional limitations and constraints are imposed on the decision variables [231].

The simplest optimisation problem is an unconstrained optimisation in which a single variate function is maximised or minimised as Eq. (5.1):

$$\max or \min f(x), \quad x \epsilon \mathbb{R} \tag{5.1}$$

In the unconstrained optimisation, a point with the condition $f'(x) = 0$ can be an optimal solution. However, it can be a local maximum when $f''(x) < 0$, and a local minimum when $f''(x) > 0$. Therefore, to find the global minimum and maximum it is required to go through all of the local minimums and maximums. The local/global maximum and minimum values are illustrated in a sample function in **Figure 5.1**.
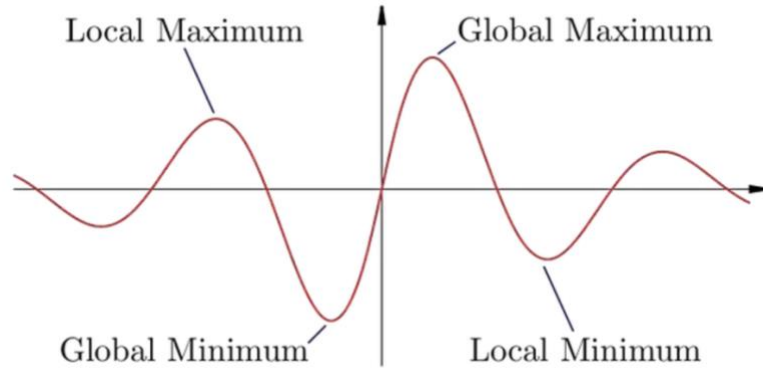
Figure 5.1: Illustration of global and local maximum/minimum

Although the theory of the optimisation is simple but using the simple analytical methods can only be applicable in small/simple problems. Thus, to overcome the complexity in finding the optimal solution in complex problems such as highly nonlinear and multimodal problems, the numerical optimisation algorithms are needed. Generally, the optimisation for a problem with multiple decision variables can be expressed by the following constrained Eq. (5.2):

$$minimize \ f(x), \quad x = (x_1, x_2, x_3, \dots, x_n)^T \ \epsilon \ \mathbb{R}^n \tag{5.2}$$

In which the $\mathbb{R}^n$ represents the n-dimensionality of vector x that is constructed by real numbers. The constraints are represented by the following Eq. (5.3) and (5.4):

$$h_i(x) = 0, (i = 1, 2, \dots, I) \tag{5.3}$$

$$g_j(x) \leq 0, (j = 1, 2, \dots, J) \tag{5.4}$$

In which h_i and g_j are considered as the constraints of the optimisation problem. In case of having nonlinear functions in the optimisation problem, solving them will be challenging and requires robust optimisation algorithms. For the linear functions, the optimisation problem can either take integer or continuous input values which are called a Mixed Integer Programming (MIP), which also requires numerical optimisation algorithms to be solved [232]. The optimisation problems are generally

classified by their functions, and their complexity is determined by the linearity and nonlinearity of them. There are numerous types of optimisation problems which require different solving techniques, i.e., linear/quadratic programming, conjugate gradient, trust region method, etc. [233].

The gradient based methods are the most common methods in which the gradient of the objective function is foundation of the calculations. In general, the gradient methods are based on an iterative process where information derived from the gradient of the objective functions are used to solve the problem. Basically, to minimise the function, the following Eq. (5.5) is followed during the iteration processes:

$$x^{k+1} = x^k + \alpha g(\nabla f, x^k) \tag{5.5}$$

Where k represents the number of iterations, g is a function based on the gradient ∇f and the current step, and α stands for the step size value in which type of the function g is varied in different methods. It is worth mentioning that the step direction in searching for the global minimum in minimisation problems is towards the negative gradient direction $(-\nabla f)$. The iteration continues until the determined maximum iteration number reached or when the difference between two last values reached zero. Having explained the principle of the optimisation, the chapter continues by introducing some common traditional optimisation algorithms.

5.2.2. Newton's Method

The Newton's method is a derivative based method in which the optimum solution of a continuously differentiable and single variable function, f, is found based on the Taylor extension [234]. For the multivariate functions the process is started by estimating the value of the function as a random starting point using the following Eq. (5.6) based on the Taylor extension:

$$f(x) = f(x_k) + (\nabla f(x_k))^T \Delta x + \frac{1}{2}(\Delta x)^T \nabla^2 f(x_k)\Delta x + \cdots \tag{5.6}$$

In order to minimise $f(x)$, the derivative of the above expression is taken with respect to Δx which is the solution of the derived expression. It results in the following Eq. (5.7) for Δx:

$$\Delta x = -\frac{\nabla f(x_k)}{\nabla^2 f(x_k)} \tag{5.7}$$

So that value of the new location will be as Eq. (5.8):

$$x = x_k - H^{-1}\nabla f(x_k) \tag{5.8}$$

In which H is the Hessian matrix, which is defined as Eq. (5.9):

$$H(x) = \nabla^2 f(x) = \begin{pmatrix} \frac{\partial^2 f}{\partial x_1^2} & \cdots & \frac{\partial^2 f}{\partial x_1 \partial x_n} \\ \vdots & \ddots & \vdots \\ \frac{\partial^2 f}{\partial x_n \partial x_1} & \cdots & \frac{\partial^2 f}{\partial x_n^2} \end{pmatrix} \tag{5.9}$$

The iteration normally starts from the initial random location, $x^{(0)}$, leading to the kth iteration value of, as shown by Eq. (5.10):

$$x^{(k+1)} = x^{(k)} - H^{-1}(x^{(k)})\nabla f(x^{(k)}) \tag{5.10}$$

As explained in general explanation of the optimisation problem in section 5.2.1, the step size is needed to increase the speed and accuracy of the convergence. The step size is in the range of (0-1) which can be added to the Newton's method as Eq. (5.11):

$$x^{(k+1)} = x^{(k)} - \alpha H^{-1}(x^{(k)})\nabla f(x^{(k)}) \tag{5.11}$$

A Quasi-Newton is the simplified Newton's method in which the Hessian matrix is replaced with the $n \times n$ identity matrix. The reason for this replacement is mainly due to complexity and time-consuming derivative calculations in the Hessian matrix when the objective function has higher dimensions. The expression for the kth iteration is expressed as Eq. (5.12):

$$x^{(k+1)} = x^{(k)} - \alpha I^{-1}\nabla f(x^{(k)}) \tag{5.12}$$

The method is called steepest descent when it is aimed to minimise the objective function while it is called hill-climbing method if the maximisation is the case. In these two methods, the amount of step size is calculated which can be time consuming in functions with high nonlinearity. However, as long as the correct direction of descent is identified, the exact amount of step size is not important. The line search method is used when the relatively small step size is selected.

5.2.3. Conjugate Gradient Method

The steepest descent and Newton's methods have some disadvantages requiring an innovative solution. For instance, the steepest descent method is time-consuming in terms of convergence and the Newton's method becomes complex as inverse of the Hessian matrix is needed to be calculated which increases the cost of computations. The conjugate gradient method is introduced in 1950s [232], [235] in order to solve a linear problem by minimising a function as Eq. (5.13):

$$f(u) = \frac{1}{2}u^T A u - b^T u + v \qquad (5.13)$$

Where A is a symmetric matrix, and v is a constant value. Taking the derivative of the above expression with respect to u will lead to the following Eq. (5.14):

$$\nabla f(u) = 0 \rightarrow Au = b \qquad (5.14)$$

The one important requirement of the method is that the matrix should be normal which indicates that $A^T A = AA^T$. The method can be expressed by the following Krylov subspace-based Eq. (5.15):

$$\mathcal{K}_k(A, b) = \{Ib, Ab, A^2 b, \dots, A^{n-1}b\} \qquad (5.15)$$

The residual for the solution of the $Au = b$ through an iteration procedure is as Eq. (5.16):

$$r_k = b - Au_k \qquad (5.16)$$

In addition, the direction vector of the gradient in the conjugate gradient method is expressed as Eq. (5.17):

$$d_{k+1} = d_k - \frac{d_k^T A r_k}{d_k^T A d_k} d_k \qquad (5.17)$$

The solution is found by the common iterative process as Eq. (5.18):

$$u_{k+1} = u_k + \alpha_k d_k, r_{k+1} = r_k - \alpha_k A d_k, d_{k+1} = r_{k+1} + \beta_k d_k \qquad (5.18)$$

Where,

$$\alpha_k = \frac{r_k^T r_k}{d_k^T A d_k}, \beta_k = \frac{r_{k+1}^T r_{k+1}}{r_k^T r_k} \qquad (5.19)$$

5.2.4. Stochastic Gradient Descent

The stochastic gradient descent is a well-known optimisation method in DL in which the objective function can be expressed using a parameter vector called weights vector [236]. For the minimisation optimisation problem, the objective function can be expressed by Eq. (5.20):

$$E(w) = \frac{1}{m} \sum_{i=1}^{m} [u_i(x_i, w) - \bar{y}_i]^2 \qquad (5.20)$$

Where $\bar{y}_i$ represents the real data points, u_i is the predicted values using the x_i as the input of the model, m represents the number of data points, and w stands for the weight vector which is commonly used in the NN models and can be expressed as Eq. (5.21):

$$w = (w_1, w_2, \dots, w_K)^T \qquad (5.21)$$

In such standard gradient problems, the weight vector is updated over an iterative process as Eq. (5.22):

$$w^{t+1} = w^t - \frac{\eta}{m} \sum_{i=1}^{m} \nabla f_i \qquad (5.22)$$

Where η stands for the learning rate (step size), and ∇f_i is the gradient of f with respect to w which requires the calculations of m gradients. It is proven [236] that the stochastic gradient descent will definitely converge when (Eq. (5.23)):

$$\sum_t \eta_t = \infty, \sum_t {\eta_t}^2 < \infty \tag{5.23}$$

Where η_t represents the learning rate at iteration t. The learning rate should gradually

decrease which the decreasing learning rate is normally represented by the following

Eq. (5.24):

$$\eta_t = \frac{1}{1+\beta_t} \tag{5.24}$$

Where β is the hyperparameter of the method which is always greater than zero. The

method is called stochastic as the initial values are selected randomly which can vary

in each iteration. The method is called Stochastic Gradient Descent (SGD) when it is

aimed to minimise the objective function while it is called Stochastic Gradient Ascent

(SGA) when the objective function is needed to get maximised. In addition, it is worth

mentioning that the term descent refers to the average decrease rather than direct

descent. This is one important reason that this method is used in complex DL methods

which will lead to average descent.

5.2.5. Nature-inspired optimisations

The traditional optimisation methods, such as aforementioned common methods, have

been inefficient over the past decades mainly because of increasing complexity in

nonlinear problems. Nonlinearity prevents the traditional optimisation techniques

from finding the global minimum or maximum. As a consequence, new optimisation

methods are needed to deal with the complex linearity in the optimisation problems to

identify the global solutions. Therefore, the modern nature-inspired optimisation

algorithms are introduced to replace the traditional methods.

The traditional optimisation methods are mostly deterministic while the nature

inspired algorithms are stochastic. In general, the stochastic algorithms are categorized

into two types, i.e., heuristic and metaheuristic. The heuristic algorithms are based on

trial and errors which mostly lead to acceptable solutions. However, in some cases, the heuristic algorithms are unable to find the optimal solutions. The progress in heuristic algorithms resulted in invention of metaheuristic algorithms which normally outperform the heuristic algorithms. All stochastic algorithms that have randomization and local search fall into the metaheuristic categorization. Owing to the randomization, the metaheuristic algorithms are suitable for the global optimization. The principle of the metaheuristic algorithms is based on diversification and intensification. Diversification contributes to finding the diverse solutions while the intensification is focusing on region of the current solution which will result in finding the best solution. Finding the best solution alongside the diversification through the randomisation contribute to finding the global solution rather than remaining in the local optimal solutions [137].

Figure 5.2 shows different types of metaheuristic classifications in which the population-based and trajectory-based algorithms are the most common metaheuristics. Most of the common metaheuristic algorithms such as GA and PSO are population-based algorithms.
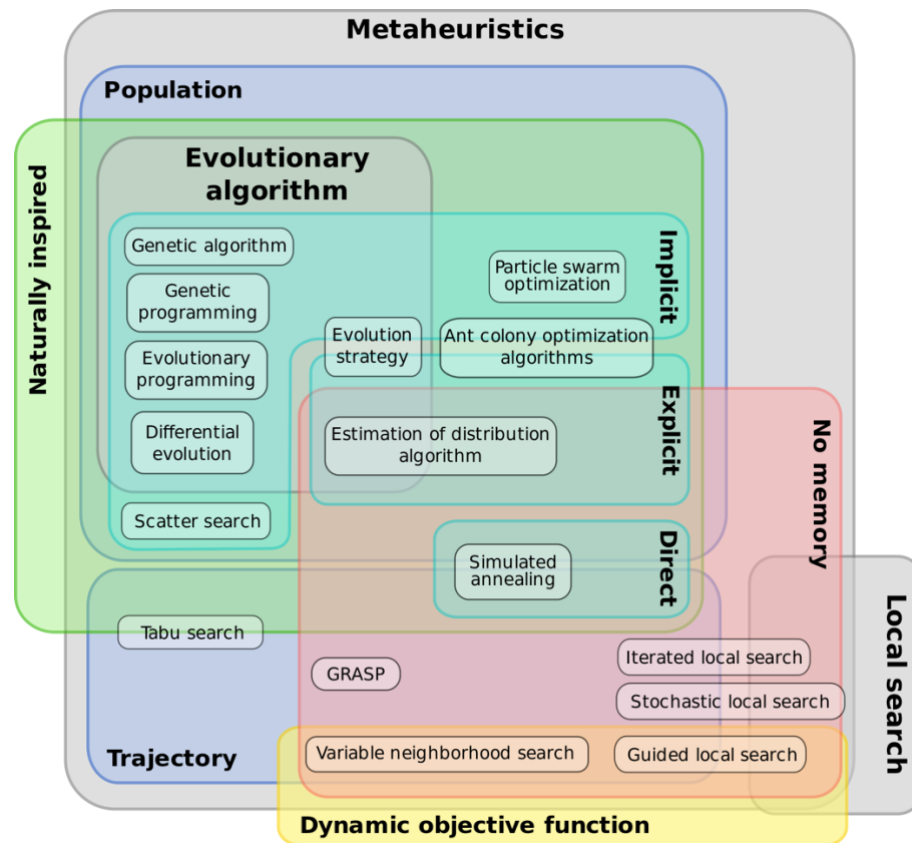
Figure 5.2: Euler diagram for different metaheuristic algorithms [237]

The first ever study which is resulted in development of non-deterministic algorithms is carried out by Alan Turing in 1940s [238], [239]. Darwin theory of evolution has a significant contribution to developing the evolutionary solutions and GA in 1960s. For instance, the GA is developed by John Holland in which the principles of the Darwin theory, i.e., crossover, mutation and selection were used in operation of the algorithm [240]. Similar studies were conducted based on Darwin theory which resulted in introduction of evolutionary programming. As a consequence, all aforementioned endeavours led to invention of a broader method called Evolutionary Algorithms (EAs) which belong to the heuristic algorithms [241], [242]. The progress on development of new algorithms is continued which led to introduction of simulated annealing in 1983 [243], and Tabu search in 1986 [244]. Another method called an Ant Colony Optimisation (ACO) is developed by Marco Dorigo in which

specifications of social ant are used to conduct the optimisation [245]. PSO which is inspired by swarming of fish and birds, is developed in 1995 [246]. The PSO is claimed to outperform many traditional algorithms in which the particles swarm around different search spaces and starts searching for the current best solution from a random guess. Then, it compares different solutions and finds the global best. In 1997, Differential Evolutionary (DE) algorithm is developed which was vector-based by Rainer Storm and Kenneth Price [247]. Later on, in 1997, a new idea is introduced which was saying that it is not possible to find an algorithm which can universally perform well. This development which is called No-Free-Lunch (NFL) decreased the hopes to find an ideal algorithm for all problems [248][249]. The NFL evaluates the performance of the algorithms based on the algorithms' average performance in all problems. However, this idea is rejected by numerous researchers as the aim of research studies was to find a method that can work well on particular problems. Therefore, the studies continued with a particular focus on the nature-inspired algorithms. A honeymoon algorithm was developed in 2004 [250], bees algorithm and virtual bee algorithm [251], and Artificial Bee Colony (ABC) [252] developed in 2005 which were all based on foraging behaviour of bees. Firefly Algorithm (FA) [137], and Cuckoo Search (CS) [253] algorithm were developed in 2008 and 2009 respectively which are proved in being more efficient than previous metaheuristic algorithms. The CS algorithm was based on brood parasitism of the reproduction strategies of cuckoos and the FA was developed based on the flashing behaviour of tropic fireflies. The progress in improving the nature-inspired algorithms continued by introduction of Bat Algorithm (BA) which was based on echolocation of microbats [254]. The FA, CS, and BA are all categorized as swarm intelligence based algorithms [255][256] owing to the fact that all of them are based on the social interactions and

their biologically inspired rules. Some other algorithms such as music-inspired algorithm [257], Gravitational Search Algorithm (GSA) [258], Flower Pollination Algorithm (FPA) [259], are developed in the past decades which are all considered as population-based algorithms.

In this study, three algorithms, i.e., GA, PSO and Slime Mould Algorithm (SMA) are used to firstly identify the optimum operating and design conditions of the GIDPC, and secondly, to compare the results derived from three selected algorithms. The GA and PSO are mainly chosen owing to their proved success and popularity in different applications while pioneering in employing the novel SMA is mainly undertaken to compare the performance of the method with GA and PSO. The main difference between the selected methods is the way they approach the solution.

5.2.6 Weather data creation

In this study, it is decided to conduct the optimisations in all climates around the world in which the GIDPC are needed. Therefore, the air properties, i.e., air temperature and relative humidity, of different climates are needed. In this regard, according to the Koppen–Geiger's climate classification [223] and considering the defined ranges for the GIDPC, hourly temperature and relative humidity in 2020 and 2050 are forecasted for the selected climates. The reason for selecting these years lies in the fact that the operation life of each GIDPC is estimated to be around 30 years. In addition, to meet the carbon neutrality targets in 2050, it would beneficial to have the optimisation results in 2050. Furthermore, it is revealed that the impact of global warming will be more sensible from 2050 onwards [260] .

Based on the operating ranges of the GIDPC, four different climates with one representative city for each climate are chosen to firstly, compare the GIDPC performance in base and optimized designs, and secondly, to investigate the power

saving potential of the optimized systems. Beijing with hot summer continental climate (Dwa), Doha with arid climate (BWh), Miami with tropical rainforest climate (Af), and Rome with Mediterranean hot summer climate (Csa) are the chosen cities. The four suitable classifications and their representative climates and cities as well as the operating months in 2020 which will be used in MOEO models are all shown in **Figure 5.3**.
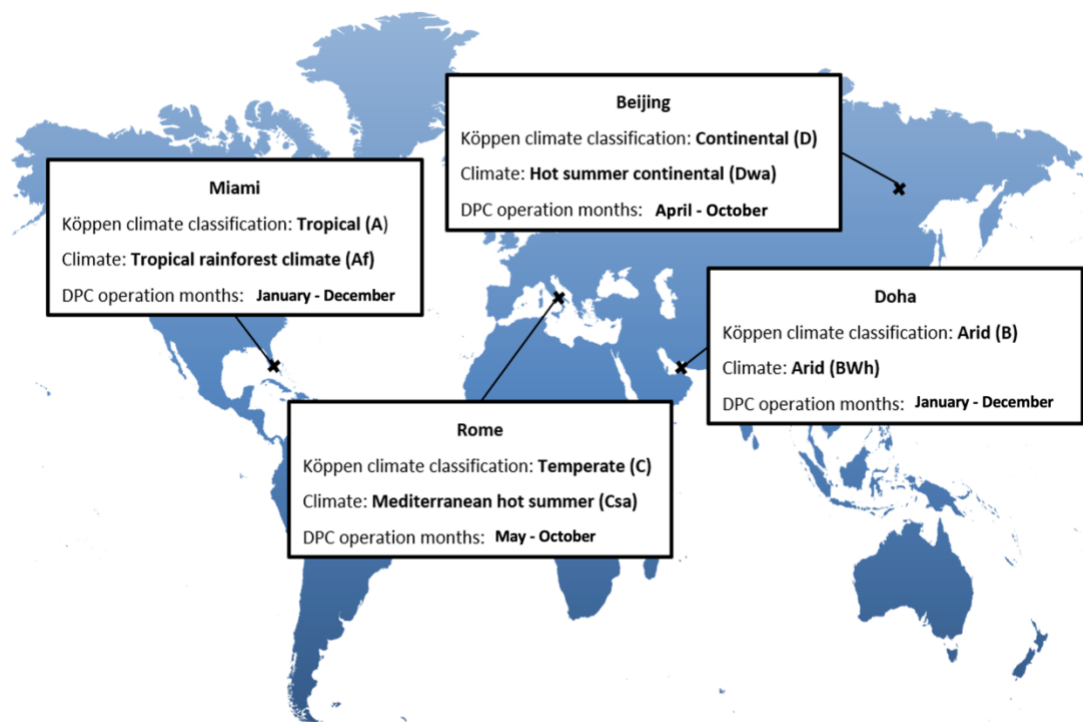
Figure 5.3: Selected climates and their representative cities (operating months are for 2020)

The Intergovernmental Panel for Climate Change (IPCC) developed a quantity of probable scenarios of future greenhouse gas emissions based on the socio-economic data and scenarios to predict the future climate variations for impact and adaptation assessment [261] . A number of emission scenarios is presented through the Special Report on Emission Scenarios (SRES). **Table 5.1** depicts the difference between scenarios in terms of greenhouse gas emissions.

Table 5.1: SRES weather scenarios and associated descriptions

SRES scenario	Description of emissions
A1F1	High end of SRES range
A1B	Intermediate case
A1T	Intermediate/low case
A2	High case
B1	Low end of SRES range
B2	Intermediate/low case

In this study, IPCC's SRES A2 climate scenario that represents high emission future scenario is considered in order to calculate the operating hours for GIDPC in both 2020 and 2050. Meteonorm software [262] is used in this study to generate the hourly temperature and relative humidity data for the selected cities. In this study, based on the operating ranges of the GIDPC, the temperatures above 25 °C are selected as the operating conditions in order to calculate the operating hours.

Figure 5.4 shows the number of operating hours for all climates in 2020 and 2050. According to the results, in all climates, the number of operating hours are increased by 2050 as a result of global warming. In hot summer continental and Mediterranean hot summer, the GIDPC is not needed in winter (December-February) while in other two climates, it is needed to operate in all seasons.
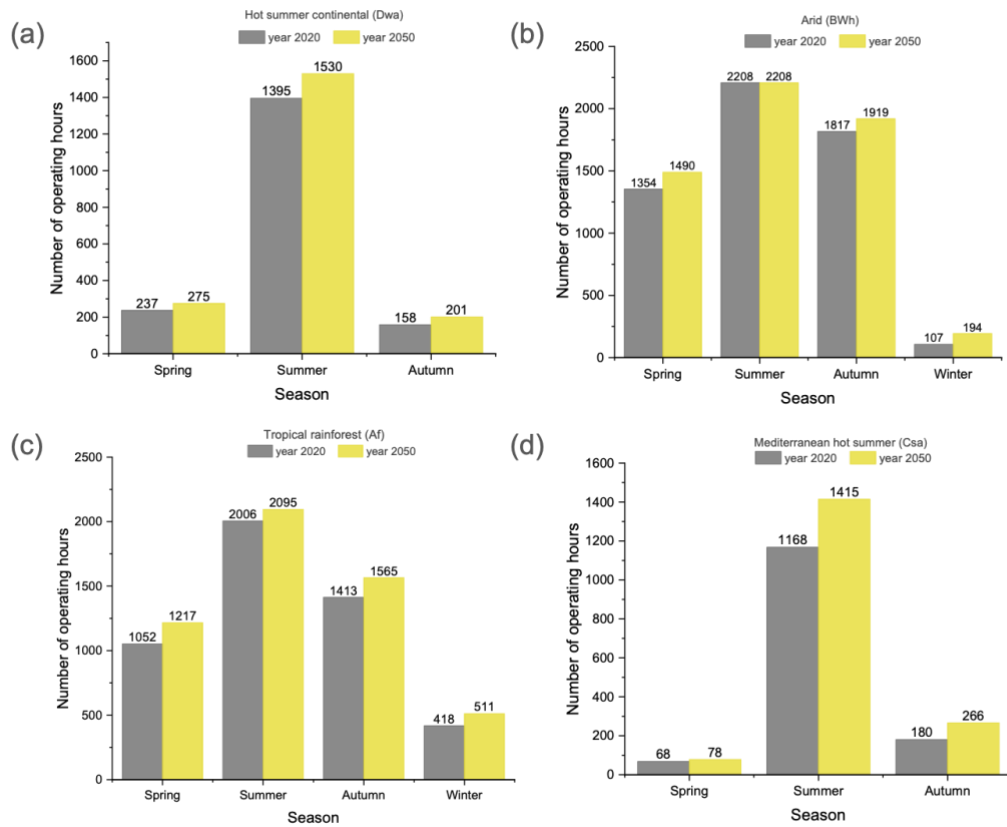
Figure 5.4: Number of operating hours: (a): hot summer continental; (b): arid; (c): tropical rainforest; (d): Mediterranean hot summer.

Average hourly climate data in 2020, are taken to operate all MOEOs in order to identify the optimum decision variables in each city. The reason for taking the average data instead of monthly data is because a single GIDPC unit with optimum operating and design parameters will be introduced for each representative city. The optimisation algorithms are operated for different weight values, which have the total value of one, in order to choose the best possible cost function. In this study, the priority is to choose the best approach in which the majority of the objectives can hold better values than the base system.

5.3. Method I: Genetic Algorithm

5.3.1. Overview

The GA is the first optimisation algorithm which is selected to optimise the performance of the GIDPC in this study. The GA is considered as the most common and widely used algorithm as a random-based classical EA. It means that in order to find a solution using the GA, random changes are applied to the current solutions in order to generate new ones. Although the method is not new but owing to the population-based feature, it has been the basis of modern methods which is originated from fundamental genetic operators. The population-based indicates that GA operates based on a population in which the size of population determines the number of solutions. Each solution represents an individual which has a chromosome. A set of parameters in chromosome defines the individuals. A set of genes form a chromosome which is represented by strings of 0s and 1s.

The algorithm is introduced by John Hollan in 1960s [263] when they were working on a model of biological evolution which is based on the Darwin's theory of natural selection. The strategy of the GA is developed around a few genetic operators which is the backbone of the method. These genetic operators are crossover, recombination, mutation and selection which are all used together for the first time in GA. The GA is used in numerous applications which indicate its popularity and applicability in many optimisation problems. It has been used for graph colouring, pattern recognition, discrete systems, continuous systems, financial market, etc.

As stated in previous section, the metaheuristic algorithms have numerous advantages over the traditional methods. The two advantages of GA over the previous traditional algorithms are the parallelism and the ability of the model in solving the complex problems [264]. The advantages are gained owing to the ability of the GA in solving

all types of objective functions which defines the optimisation problem. The GA is able to handle the stationary and non-stationary, linear and nonlinear, continuous and discontinuous, and with random noise objective functions. This feature makes the GA and in general metaheuristic algorithms more applicable among the users.

In GA, multiple agents are represented by multiple offspring within the population. The population or any small group searches the space in more than one direction simultaneously which makes the processes to parallelise the algorithm for operation. In addition, the ability to simultaneously manipulate various parameters and group of strings is put the GA in a leading position among the other methods. Like other methods, despite the aforementioned advantages, the GA has some disadvantages which are mainly related to appropriate parameter selection [265]. For instance, the type of objective function is one of the important key players in converging the model. Additionally, the size of population is another parameter which plays a key role in determining the speed of convergence and most importantly the accuracy of the results [266]. Determining the key parameters such as rate of mutation and crossover, and basis of selecting new populations are also the key steps which should be taken carefully to converge the problem properly. Otherwise, the GA will bring about senseless results and it will be difficult for the model to converge. Many different GAs are formed based on the aforementioned principles [267].

In order to represent the chromosomes, the objective function is needed to be coded as arrays of bits or by adjusting strings. In addition, the strings are needed to be manipulated by genetic operators, and selection is required to be undertaken based on the fitness quality. As a consequence, the following steps are needed for finding the solutions:

    1) Determining the objective functions or the cost function by encoding them.

2) Defining/choosing the fitness function and selection metrics.

3) Creation of population and its individuals and corresponding fitness evaluation.

4) Developing the population based on evaluation of the individuals' fitness and replacing them by new generations which are created using genetic operators, i.e., crossover, mutation, fitness proportionate reproduction.

5) Decoding the results to represents the optimisation solutions.

The repetitive process in generating new population is carried out using numerous iterations which each of them is called a generation. The lengths of character strings in most GAs is assumed to be constant. However, various lengths for the character strings have been considered in many research studies. Generally, in adaptive GAs, the objective functions are coded as binary or real-valued arrays.

As depicted in **Figure 5.5**, the GA process is triggered by a population which is formed by a set of individuals which are the solutions of the problem. In addition, a set of genes which characterises the individuals are represented by a string, forms the chromosomes. In general, the genes are encoded by strings of 0s and 1s. Having created the required population, a fitness function will determine how fit the current individuals are based on a fitness score which is assigned to each individual. The fitness score determines if an individual (parent) is appropriate to be in next reproduction or not. This is simply called a selection phase.
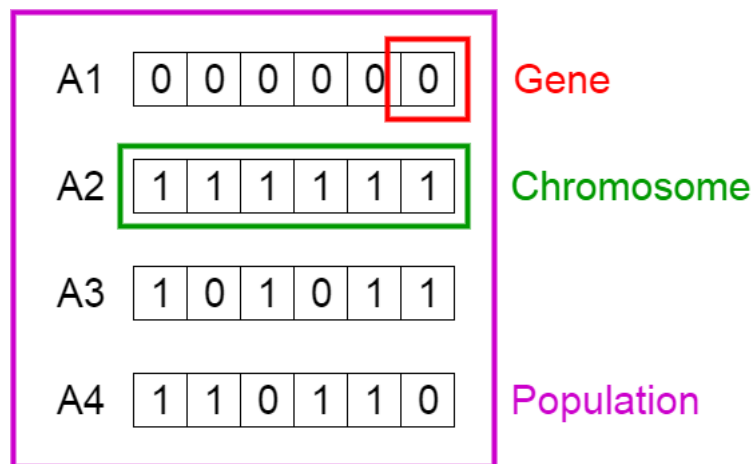
Figure 5.5: Demonstration of a sample population for a GA

The next phase is cross over in which the genes between two parents are exchanged to create offspring which will be added to the population. This genes exchange is done until the crossover point which is shown by red colour in **Figure 5.6**.
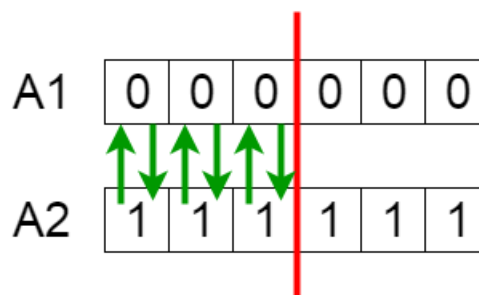
Figure 5.6: Demonstration of the crossover phase

The next genetic operator is mutation which is mainly done to give a genetic diversity within the population as shown in **Figure 5.7**. The genetic algorithm ends if the offspring production can't lead to significantly different parents in the population. It is worth mentioning that the population size is fixed so that continuation of the

aforementioned processes will remove the parents with the least fitness score and will

keep/add better parents to the solution.

Figure 5.7: Demonstration of the mutation phase

5.3.2. GA Development process

In this study, the GA as the first optimization algorithm is developed to reach the

maximum potential of the GIDPC by identifying the optimum values of operating and

design parameters. It can deal with system nonlinearity and ignores the local

minimums of the problem. GA is developed in MATLAB and its correctness was

validated in different studies [268], [269]. The convergence of the GA is investigated

through the cost versus number of iterations.

The cooling capacity, COP, wet-bulb efficiency and surface area of the layers are

selected as objectives as they inherently consider the economic and engineering

characteristics of the system simultaneously. The reason for selecting the cooling

capacity and COP is to maximise the cooling performance and minimise the power

consumption of the system simultaneously. Although the cooling capacity is included

in the COP calculations but considering the COP only, will lead to irrational results as

the focus may be only on reducing the power consumption only. Moreover,

maximising the wet-bulb efficiency minimises the supply air temperature of the

GIDPC. Eventually, minimising the surface area of the layers will lead to lower production cost. Considering a single objective can result in irrational solutions by ignoring crucial trade-offs in identifying the optimum values. For instance, the cooling capacity of a GIDPC can be improved by increasing the length of the channels whereas longer channels can lead to lower COP and higher pressure drop (more fan power) [270]. Thus, a MOEO is necessary to find the best optimum balance between the objectives.

The optimization function is defined by fitness function and the constraint function. The trained DNN in chapter 4, is the fitness function to be optimized which sets the variables of the problem and the optimization objectives. The constraint function implements the parameters defined ranges as restrictions on the fitness function.

In the present GA method, the input parameters are assumed as genotype and output parameters are considered as phenotype. Out of seven input parameters in the developed DNN model, the temperature and relative humidity of the intake air vary by climates but the remaining five input parameters are chosen as decision variables. Hence, for each specific climate, a GA is performed, which will result in a unique optimum design for that climate.

In each generation, selection functions pick the most valuable genes which are chosen as the parents of the next generation and then the multi point crossover procedure is performed on them. Among these, the random genes are added to the population as mutation functions and this procedure is repeated until ultimate criteria are established. Different conditions can be set to stop this process in which reaching the maximum iterations of 200 is selected in this study.

The flowchart of the GA process is shown in **Figure 5.8**. In addition, configured settings and parameters for the proposed optimization are summarized in **Table 5.2**.

194

The trial-and-error is the most common way to select the listed parameters. However, the plot of cost versus iterations, system's nonlinearity, number of inputs were the main factors in selecting these parameters. The cost function in this study is considered as Eq. (5.25):

$$J\left(T_{dry,in}, RH_{dry,in}, U_{dry,in}, \varphi, H, G, N_L\right) = W_1 \frac{Q_{cooling}}{RQ_{cooling}} + W_2 \frac{COP}{RCOP} + W_3 \frac{\varepsilon_{wb}}{R\varepsilon_{wb}} + W_4 \frac{RA_s}{A_s} \qquad (5.25)$$

Where $T_{dry,in}$ and $RH_{dry,in}$ are predefined based on the climates, W is the weights for each objective, $RQ_{cooling}$, RCOP, $R\varepsilon_{wb}$, and RA_s are used to normalize the output values or objectives.

Table 5.2: Genetic Algorithm settings

Type of parameter	Rate or type of consideration
Population Size	40
Iteration or Decades	200
Percentage of Mutations	35%
Type of Mutations	Random Number Generation
Percentage of Crossover	50%
Type of Crossover	2 Point Crossing Over
Percentage of Recombination	15%
Type of Selection	Random Selection

Genetic Algorithm
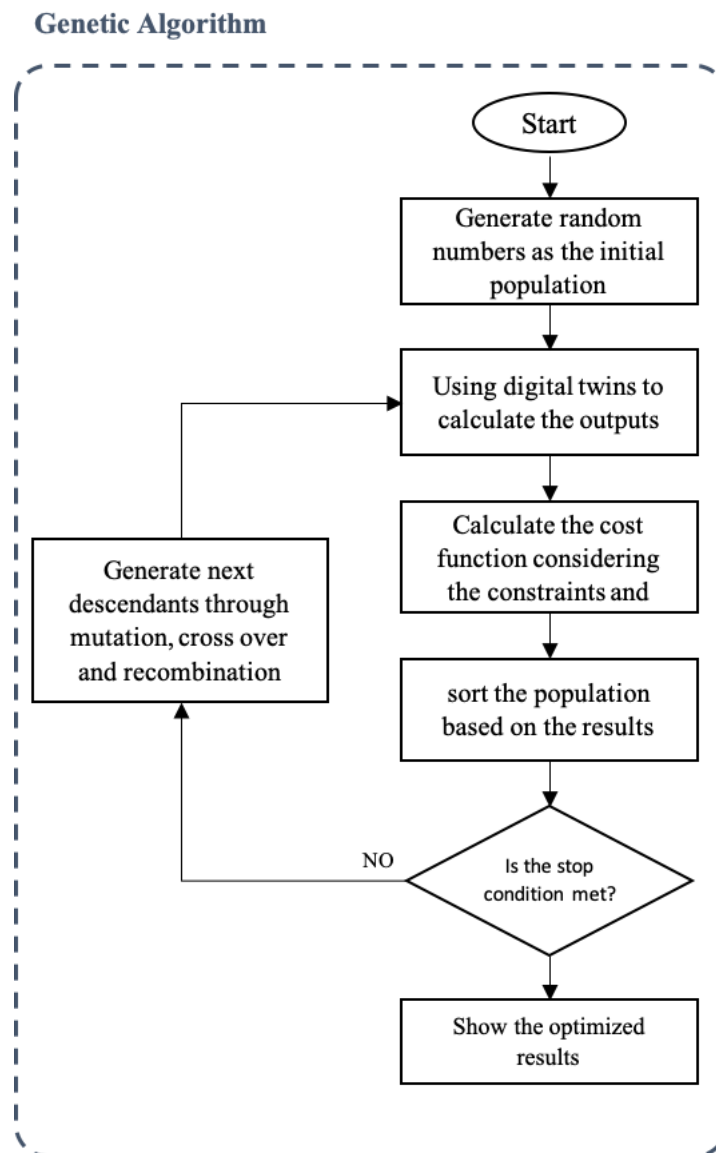
Figure 5.8: Flowchart of the GA process

5.3.4. Results derived from GA: weight distributions

The optimisation results for GA are listed in **Table 5.3** which include the optimum

values of the operating and design parameters in each climate. It is revealed that out

of five considered weight distributions (i.e., equal weights for each objective, and

dominant weights for each of the four considered objectives), the equally distributed

weights (i.e., 0.25) are the most desired condition for optimising the GIDPC

performance in which the COP and surface area values are significantly improved and the cooling capacity and wet bulb efficiency are almost same as the base system. But, considering the cooling capacity as the dominant objective (W1=0.85), results in significantly lower COP and higher surface area values. Considering the COP as the dominant objective (W2=0.85), has caused in low cooling capacity and wet bulb efficiency. Taking the wet bulb efficiency as the dominant objective (W3=0.85), has led to significantly low COP and cooling capacity values. Although considering the surface area as the dominant weight (W4=0.85) gives desired values for COP and efficiency but compared to the equal weights, the cooling capacity is substantially lower. Consequently, the equally distributed weights are chosen as the best solution for optimising the system performance. However, the cooling capacity and efficiency values are sacrificed due to the improved COP and surface area values.

Table 5.3: Optimisation results by GA

	Method: Multi Objective Genetic Algorithm (GA)												
	Climate: Hot summer continental (Dwa) / Beijing												
	Design weights				Decision variables						Objectives		
No.	W1	W2	W3	W4	$U_{dry,in}$ (m/s)	φ (-)	H (m)	G (m)	N_L (-)	$Q_{cooling}$	COP	ε_{wb}	A_s
1	0.25*	0.25*	0.25*	0.25*	2.00	0.23	0.84	0.006	159.85	1.23	34.20	0.85	52.76
2	0.85	0.05	0.05	0.05	2.72	0.24	2.54	0.007	159.93	2.37	14.66	0.89	161.32
3	0.05	0.85	0.05	0.05	2.00	0.17	0.80	0.007	100.5	0.85	40.52	0.67	31.80
4	0.05	0.05	0.85	0.05	2.00	0.30	1.36	0.004	100.13	0.77	17.52	1.42	54.24
5	0.05	0.05	0.05	0.85	2.00	0.22	0.80	0.005	102.32	0.82	36.35	0.86	31.92
	Base system				3.00	0.44	1.00	0.005	160.00	1.60	13.60	1.00	62.49
No.	Climate: Arid (BWh) / Doha												
1	0.25*	0.25*	0.25*	0.25*	2.00	0.25	0.81	0.005	159.92	1.97	51.88	0.99	51.13
2	0.85	0.05	0.05	0.05	2.75	0.22	2.25	0.007	159.95	3.71	25.20	0.85	143.01
3	0.05	0.85	0.05	0.05	2.00	0.16	0.80	0.007	105.28	1.43	64.73	0.67	32.33
4	0.05	0.05	0.85	0.05	2.01	0.28	1.43	0.004	100.27	1.20	26.26	1.38	57.23
5	0.05	0.05	0.05	0.85	2.00	.204	0.83	0.005	100.21	1.26	53.08	0.94	31.94
	Base system				3.00	0.44	1.00	0.005	160.00	2.22	18.88	1.00	62.49
No.	Climate: Tropical rainforest (Af) / Miami												

No.													
1	0.25*	0.25*	0.25*	0.25*	2.00	0.21	0.80	0.006	159.82	1.04	30.42	0.83	50.57
2	0.85	0.05	0.05	0.05	2.93	0.23	2.78	0.007	159.97	2.17	10.68	0.89	126.86
3	0.05	0.85	0.05	0.05	2.00	0.16	0.81	0.007	100.28	0.74	35.36	0.69	31.81
4	0.05	0.05	0.85	0.05	2.00	0.28	1.27	0.004	100.09	0.67	16.48	1.47	50.04
5	0.05	0.05	0.05	0.85	2.00	0.21	0.82	0.006	100.15	0.72	32.23	0.86	31.87
Base system					3.00	0.44	1.00	0.005	160.00	1.21	10.25	1.01	62.49
No.	Climate: Mediterranean hot summer (Csa) / Rome												
1	0.25*	0.25*	0.25*	0.25*	2.00	0.21	0.82	0.006	159.82	0.93	26.58	0.84	51.65
2	0.85	0.05	0.05	0.05	2.70	0.24	2.66	0.007	159.84	1.80	10.88	0.91	169.82
3	0.05	0.85	0.05	0.05	2.00	0.17	0.80	0.007	100.04	0.65	31.30	0.70	31.77
4	0.05	0.05	0.85	0.05	2.00	0.28	1.24	0.004	100.11	0.59	15.17	1.43	48.64
5	0.05	0.05	0.05	0.85	2.00	0.20	0.80	0.006	101.74	0.64	29.12	0.84	31.89
Base system					3.00	0.44	1.00	0.005	160.00	1.71	14.52	0.99	62.49

5.3.5. Results derived from GA: Decision variables

Optimum intake air velocity:

The intake air velocity is a factor which has a remarkable impact on system performance as it directly affects the cooling capacity and rate of heat and mass transfer within the HMX. A higher velocity is associated with larger pressure drop which results in more power consumption and consequently less COP values which are not desirable in optimization and performance evaluation of GIDPCs. Thus, calibrating the air velocity is challenging, as investigated by Xu et al. [127], and a robust trade-off considering the effect of several parameters was required to identify the optimum value in each climate. The GA algorithms revealed that the optimum air velocity is almost 2 (m/s) in all climates which is lower than the velocity in the base system which was 3 (m/s). Tendency of the GA to give a lower value for the air velocity was somehow expected as the higher COP values are expected. Hence, it can be concluded that a trade-off by GA has concluded that the lower range of the intake air velocity is weighted more than the maximum allowable value of 3.3 (m/s).

Optimum working air ratio:

198

The working air ratio is defined as the ratio of the exhaust air to the total intake air. Higher working air ratio will lead to less supply airflow and consequently, more temperature drop will occur in intake air which flows inside the HMX dry channels. As a result, at a very high working air ratio, the dew point efficiency will increase but it will lead to lower COP and cooling capacity values. In addition, the low supply airflow will remain as an unfavourable issue. Thus, similar to the air velocity, calibrating the working air ratio is another important challenge in DPC operation which requires a trade-off between the other involved parameters in different climates. The working air fraction in the base system is taken as 0.44 which was based on the experimental study of the M30 (Coolerado USA) DPC 10. GA algorithm revealed that the optimum working air ratio is ranging from 0.21 to 0.25 which are less than 0.44 in operating condition of the base system. It means that less working air and more supply air compared to the base system operation condition leads to better system performance. The optimum working air ratio holds almost the same value of 0.21 in Miami and Rome where it is 0.25 in Doha and 0.23 in Beijing.

Optimum HMX height:

Higher HMX height normally results in better GIDPC performance in terms of cooling capacity by providing more heat transfer area in the HMX sheets but on the contrary it leads to higher pressure drop along the heat exchanger, higher fan power, larger surface area and higher construction costs simultaneously [172]. Therefore, GA needed a trade-off to recognize the optimum height values. The identified optimum HMX height is identified to be in the range 0.80 – 0.84 (m) which are lower than the base value of 1m. It is identified that the DPC had the best performance with the minimum height value of 0.80 (m) in Miami and by the maximum height of 0.84 (m)

in Beijing. The optimum HMX height in Doha and Rome were detected as 0.81 (m) and 0.82 (m) respectively. As a result, it can be seen that the optimum values are less than the maximum constraint which was 3 (m), less than the base system value which was 1 (m), and tend to hold a lower band value of the range.

Optimum channel gap and number of layers:

The smaller channel gap will cause a higher pressure drop and consequently will result in higher fan power and lower COP values. To the contrary, the larger channel gap will lead to higher mass flow rate and higher cooling capacity. Similarly, more layers can be considered as an important factor in increasing the pressure drop, surface area and construction cost. In addition, an increase of these parameters will lead to more evaporation area and more heat transfer from dry channel to wet channel. Therefore, like previous decision variables, a careful trade-off is needed to identify the optimum values in each climate. GA algorithm revealed that the optimum values are higher than the base system with channel gap of 0.005 (m) and number of layers of 160. The optimum value of channel gap is in the narrow range of 0.005-0.006 (m). Similarly, optimum values of the number of layers are almost same in all cities i.e., 159-160. The channel gap multiplied by the number of layers gives the width of the HMX that was 0.8 (m) in the base system but it varies in the range 0.79 to 0.95 (m) in the optimum conditions. Hence, it is concluded that similar to the height of the system, the lower values of channel gap and number of layers are desired as they lead to a substantial decrease in surface area of the layers.

The aforementioned optimum solutions will be used to investigate and compare the performance of the optimised system by GA with the base system over the operating months in each climate in the next chapter.

5.4. Method II: Particle Swarm Optimisation

5.4.1. Overview

PSO is inspired by movements of birds and fishes that congregate in large groups. The PSO is swarm-intelligence-based, approximate, non-deterministic optimisation which is also considered as a population-based stochastic optimisation algorithm and has some outstanding advantages over the traditional algorithms.

For instance, its simple computation processes and the rapid convergency are the most important advantages of the method. In addition, capability of the PSO in global and local searching, and the ability in solving the highly nonlinear functions are placed the PSO as one of the most popular metaheuristic algorithms. Moreover, the fact that implementation of the PSO requires few parameters to adjust, is another important privilege. All aforementioned benefits, has led to extensive implementation of the PSO in human motion tracking and other complex applications with different fitness functions.

The working principle of the PSO can be simulated by a group of birds which randomly search for a piece of food in a specific area. The best idea to quickly find the place of food to start searching randomly and follow the nearest bird to the food. In a similar manner, PSO is initialised with a random group of particles which represent the solutions which are optimised to find the best solution by updating the generations through numerous iterations.

Each particle has a position in the search space, i.e., position, velocity, and individual best position. In each iteration, the particles are updated based on two best values. The first value represents the best value achieved so far which is also called a fitness value. This represents the local/individual best. The second best value is the best solution

201

that has observed so far by any particle within the population. This simply represents the global value.

To implement the PSO algorithm, three main steps are needed as follows:

1) The fitness of each particle must be evaluated.

2) Updating the calculated global and individual best.

3) The velocity and position of each particle must be updated.

Having found global and individual best values, the PSO updates its positions and speed by the following Eq. (5.26) and (5.27):

$$v_i(t + 1) = \omega v_i(t) + c_1 r_1 [\hat{x}_i(t) - x_i(t)] + c_2 r_2 [g(t) - x_i(t)] \qquad (5.26)$$

$$x_i(t + 1) = x_i(t) + v_i(t + 1) \qquad (5.27)$$

Where

- i represents the particle index

- $v_i(t)$ represents the velocity of particle i at time t

- $x_i(t)$ represents the position of particle i at time t

- $\hat{x}_i(t)$ represents the individual best of particle i at time t

- $g(t)$ represents the global best as of time t

- ω is called inertial coefficient: it helps the particles to move in a direction that was originally supposed to move and holds a value between 0.8 and 1.2. The lower values will increase the time of convergence as it contributes to further space search while the higher values lead to quicker convergence.

- c_1 is a cognitive coefficient: it helps the particle to remember its individual best and return when the space search ends, it normally holds a value near 2.

- c_2 is a social component coefficient or global attraction rate: contributes the particle to move towards the global best which normally holds a value around 2.

- r_1 and r_2 are values which are chosen randomly: are used as additional random weights to improve the exploration and prevent trapping on local minimums.

5.4.2. PSO development process

As discussed in previous section, three different behaviours are defined for the particles in this optimization algorithm; (1) The fundamental behaviour is persistence of a particle having a random search in the solution space, (2) Tendency of the particle to redirect towards the best current solution of the whole swarm (Global best), and (3) The self-tendency of the particle to rely on its best own best solution.

Equation 5.27 provides the mathematical behaviour of particles over iteration t. In the current study, ω, the inertial coefficient has been set to hold the value of 1. **Table 5.4** provides the initial settings and **Figure 5.9** shows the flowchart for the PSO algorithm. In addition, the same cost function for GA, as expressed by **Equation 5.25**, is used for PSO algorithm as well.

Table 5.4: Parameter settings for PSO

Parameter	Values
Number of particles	7
Max. Number of Iterations	500
Cognitive attraction rate, c1	2
Global attraction rate, c2	2
Upper inertia	[3.3, 0.9, 3.0, 0.008, 200]
Lower inertia	[2.0, 0.1, 0.8, 0.004, 100]
Velocity limit	Infinite
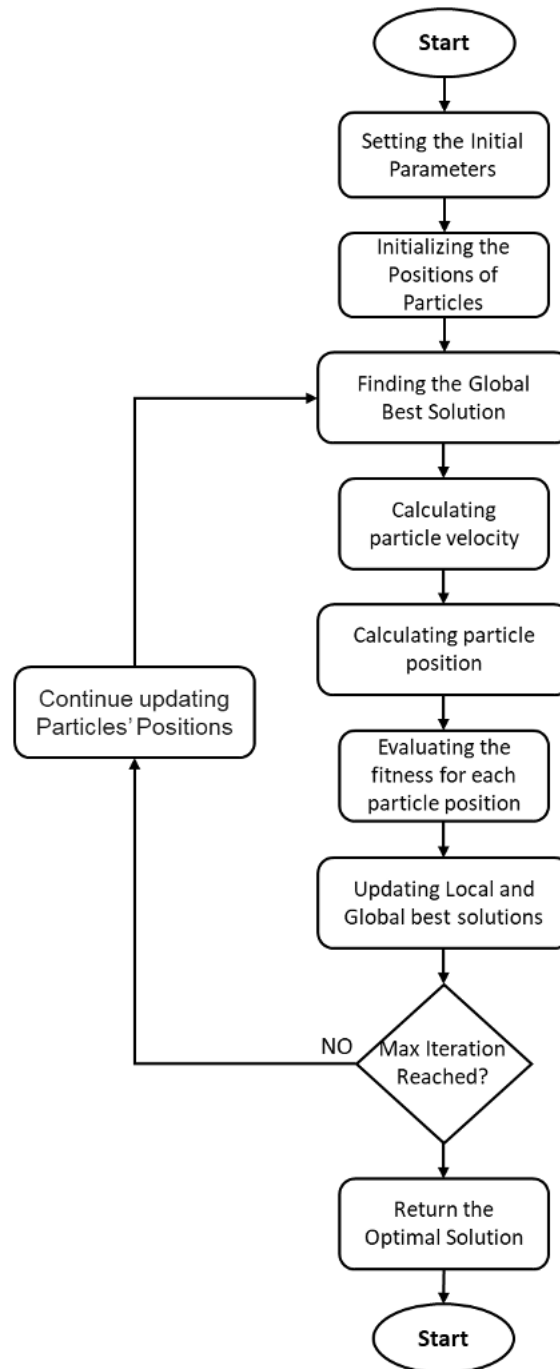
Figure 5.9: Flowchart of the PSO process

5.4.3. Results derived from PSO: weight distributions

The optimum value of the decision variables in each climate is identified by PSO for

the different weight distributions. The results are derived based on the average value

of the air properties, i.e., temperature and relative humidity, over the operating hours in 2020. In a similar manner to GA, this is done because a single optimized unit in each climate is aimed to operate for the next 30 years. Similar to GA, five scenarios are considered for each climate in which different weight distributions are assumed in order to assess and compare different weight distributions over the objectives.

The primary scenario is to equally distribute the weights over selected objectives (multi-objective). It means that importance of objectives for the optimization algorithms is same while in other four scenarios, weight distribution is focused on one objective (single objective). This means that optimization algorithm will mainly focus on maximising/minimising that particular objective. This allows us to observe and compare the performance of the system under each scenario.

The comprehensive results derived from PSO are listed in **Table 5.5**. In addition, the base system properties are listed in the table for better comparison. The results revealed that identified optimum decision variables by PSO are different from the base system. In addition, compared to the base system, the equally distributed weights lead to better results in terms of cooling capacity and COP while other objectives, i.e., wet bulb efficiency and surface area, remain almost same. However, the system performance under other single objective scenarios is not satisfying. Although, the third scenario where COP is considered as the dominant objective ($W3 = 0.85$) leads to convincing results, where COP is maximised and the surface area is lower than the base system, but cooling capacity which is one of the main performance parameters are lower than the base system. This trend is same in scenario 5 where surface area is the dominant objective ($W4 = 0.85$). High surface area in second scenario where cooling capacity is the dominant objective ($W1 = 0.85$) and low cooling capacity in the fourth scenario where wet bulb efficiency is the dominant objective ($W3 = 0.85$) have

made these scenarios unsatisfactory. As a consequence, scenario 1 in PSO method is selected to discuss optimization results and to investigate performance of the optimized systems.

Table 5.5: Optimisation results by PSO

	Method: Multi Objective Particle Swarm Optimization (PSO)												
	Climate: Hot summer continental (Dwa) / Beijing												
	Design weights				Decision variables						Objectives		
No.	W1	W2	W3	W4	$U_{dry,in}$ (m/s)	φ (-)	H (m)	G (m)	N_L (-)	$Q_{cooling}$	COP	ε_{wb}	A_s
1	0.25[*]	0.25[*]	0.25[*]	0.25[*]	2.00	0.26	0.80	0.005	196.29	1.72	39.17	0.87	62.20
2	0.85	0.05	0.05	0.05	2.55	0.25	2.10	0.008	200.00	3.19	21.21	0.85	167.32
3	0.05	0.85	0.05	0.05	2.00	0.18	0.81	0.008	104.62	1.04	47.77	0.65	32.16
4	0.05	0.05	0.85	0.05	2.00	0.32	1.38	0.004	100.09	0.88	19.52	1.40	55.02
5	0.05	0.05	0.05	0.85	2.00	0.23	0.80	0.005	100.00	0.93	41.50	0.86	31.75
	Base system				3.00	0.44	1.00	0.005	160.00	1.60	13.60	1.00	62.49
No.	Climate: Arid (BWh) / Doha												
1	0.25[*]	0.25[*]	0.25[*]	0.25[*]	2.00	0 .27	0.80	0.005	170.11	2.04	51.55	0.94	53.78
2	0.85	0.05	0.05	0.05	2.52	0.25	1.93	0.008	200.00	4.33	31.86	0.84	153.63
3	0.05	0.85	0.05	0.05	2.00	0.18	0.80	0.008	111.49	1.55	66.40	0.65	34.05
4	0.05	0.05	0.85	0.05	2.00	0.34	1.43	0.004	100.00	1.18	25.29	1.38	57.09
5	0.05	0.05	0.05	0.85	2.00	0.24	0.80	0.005	100.00	1.26	53.86	0.92	31.75
	Base system				3.00	0.44	1.00	0.005	160.00	2.22	18.88	1.00	62.49
No.	Climate: Tropical rainforest (Af) / Miami												
1	0.25[*]	0.25[*]	0.25[*]	0.25[*]	2.00	0.24	0.80	0.006	200.00	1.39	31.96	0.83	63.38
2	0.85	0.05	0.05	0.05	2.53	0.24	2.20	0.008	200.00	2.48	16.12	0.87	175.00
3	0.05	0.85	0.05	0.05	2.00	0.17	0.80	0.008	100.00	0.79	38.01	0.67	31.75
4	0.05	0.05	0.85	0.05	2.00	0.30	1.31	0.004	100.00	0.71	16.84	1.44	51.84
5	0.05	0.05	0.05	0.85	2.00	0.21	0.80	0.006	100.00	0.75	34.35	0.85	31.75
	Base system				3.00	0.44	1.00	0.005	160.00	1.21	10.25	1.01	62.49
No.	Climate: Mediterranean hot summer (Csa) / Rome												
1	0.25[*]	0.25[*]	0.25[*]	0.25[*]	2.00	0.27	0.80	0.005	199.43	1.83	40.78	0.88	63.21
2	0.85	0.05	0.05	0.05	2.51	0.26	2.09	0.008	200	3.35	23.08	0.85	165.91
3	0.05	0.85	0.05	0.05	2.00	0.18	0.80	0.008	107.69	1.12	50.05	0.64	32.80
4	0.05	0.05	0.85	0.05	2.00	0.35	1.40	0.004	100.00	0.91	19.82	1.39	55.81
5	0.05	0.05	0.05	0.85	2.00	0.24	0.80	0.005	100.00	0.98	43.12	0.85	31.75
	Base system				3.00	0.44	1.00	0.005	160.00	1.71	14.52	0.99	62.49

5.4.4. Results derived from PSO: Optimised decision variables

As listed in **Table 5.5**, in all climates, the optimum velocity of the intake air derived by PSO is 2 (m/s) which is lower than the velocity in base system, i.e., 3 (m/s). This is resulted from a robust trade-off by the optimization algorithms as higher velocity leads to higher pressure drop and to lower COP values which are not preferred but could lead to more heat and mass transfer rate within the HMX. This low value was expected as the higher COP was aimed.

The optimum working air ratio by PSO methods in all four climates are in the range of 0.24 – 0.27 which are lower than the working air ratio in base system, i.e., 0.44. The working air ratio is proportional to the exhaust air to intake air which its higher value will lead to higher temperature drop, higher efficiencies but will bring down the COP and cooling capacity. The identified working air ratio by PSO method in hot summer, typical rainforest, Mediterranean hot summer, and Arid climates are same which are 0.26, 0.24, 0.27 and 0.27 respectively.

The optimum HMX height identified by PSO is 0.80 (m) which is lower than the base system height, i.e., 1 (m). A GIDPC with longer HMX has better performance in terms of cooling capacity but it brings up negative effects by increasing the surface area, pressure drop and fan power consumption [33]. Therefore, although it provides the users with more efficient system but it can't be an economical choice. As a consequence, over a trade-off, it is concluded by both optimization methods that the optimum HMX height is 0.8 (m) in all climates.

The channel gap in the base system is 0.005 (m) while it is revealed that the optimum values are different. Base on the PSO method, the optimum channel gap in tropical rainforest climate is 0.006 (m) while it is same as the base system in other climates. High pressure drop can be recorded in smaller channel gap values which require higher

fan power consumption while a larger channel gap can lead to better cooling capacity values.

Higher number of layers will bring about more power consumption as a result of higher pressure drop and add up to the construction and running cost. However, it can improve the system performance in terms of cooling capacity. The number of layers in the base system is 160 while the optimum numbers in PSO range from 170.11 to 200.00.

The PSO results will be used to investigate and compare the performance of the optimised GIDPC in different climates over the operating month in the next chapter in order to report the impact of the PSO.

5.5. Method III: Slime Mould Algorithm

5.5.1. Overview

The state-of-the-art metaheuristic optimisation algorithm, called Slime Mould Algorithm (SMA), is used to compare its performance with two selected common algorithms (PSO and GA). The considered SMA optimisation is inspired by the behaviour and constructional change in slime mould in foraging in which the slime mould simply refers to Physarum polycephalum. Slime mould is considered as a eukaryote that can be found in cold and humid climates. Its main nutritional phase is called Plasmodium in which the organic matter search for food and surrounds it to let the enzymes to digest it [271].

Figure 5.10 demonstrates the foraging process of the slime mould. As seen, due to the unique pattern, they can be fed by different food sources through a venous network. Very few studies have been conducted on the slime mould so far that let us recognize that a propagating wave, which is produced by the bio-oscillator when a vein goes for

a food source, produces cytoplastic flow via the vein [272]. In addition, it is unveiled that the faster cytoplasm leads to thicker veins. Eventually, the slime tries to find the best/optimal way to reach the food sources. This feature caused the slime mould to be modelled and applied in a few research studies [273], [274].
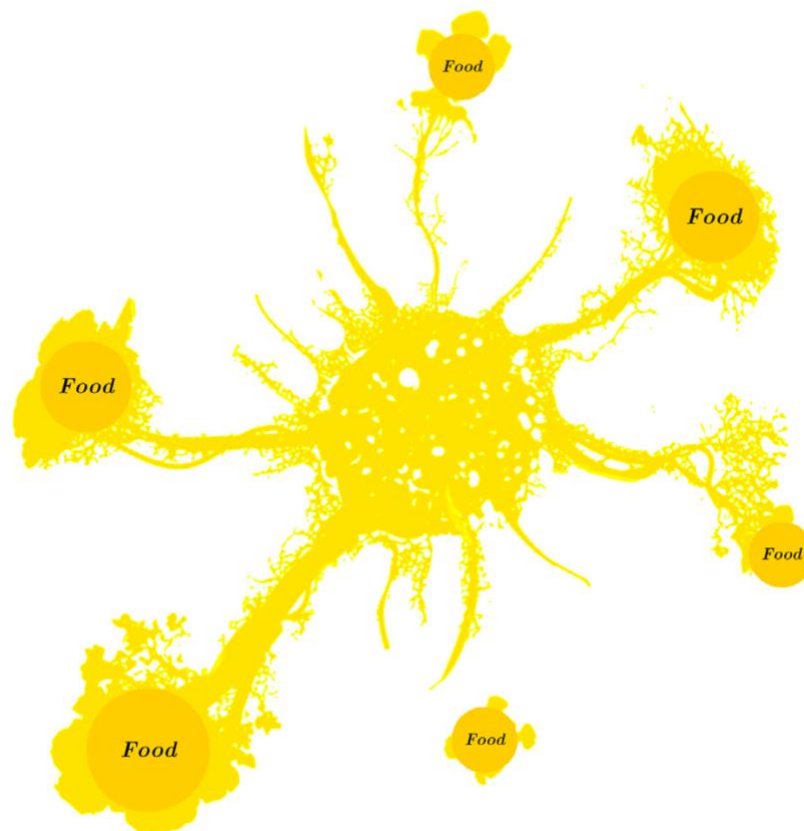
Figure 5.10: Foraging of slime mould [275]

The correlations between the contraction mode and structural changes in the venous shaping are as follows:

-   The contraction frequency change from outside to inside leads to the vein construction.

-   The anisotropy happens when the contraction mode is not stable.

-   The venous is not present when the contraction is independent of space and time.

It can be concluded that like previous algorithms, the concentration and focus of the slime mould is on the region where the solution can be found. It means that the slime mould focuses on a region where the food concentration is high by building a robust root. The root is powered by increasing the diameter of the veins when the cytoplasm flow increases and when it decreases, the diameter of the veins decreases [275].

The aforementioned features have made the researchers consider the slime mould as an optimisation algorithm [276] which resulted in introduction of SMA. In a quite similar way with PSO, the slime mould, searches for the food with higher concentration/quality with a need to choose the appropriate speed and risk in foraging process. In addition, the slime mould needs to know when is the best time to get away from a food source which one supportive way would be to follow the heuristic and empirical rules [277]. One superior feature of slime mould is that it can consume and be fed by different food sources at the time even when it finds more than one good food sources [278]. Moreover, the slime mould can adjust or optimise the searching pattern based on the quality of the food source using a method called region-limited search [279]. If the quality of the currently exploring food source is not satisfying, the slime mould would get away from that particular source to approach the other source [280].

All aforementioned features of the slime mould are used in development of the SMA method which makes it competitive with the previously discussed methods (GA and PSO).

5.5.2. SMA development process

As stated, the SMA has three phases including approach food, wrap food and grabble food. In the approach food, Eq. (5.28) can be used as a mathematical model for approaching behaviour of slime mould.

$$\overrightarrow{X(t+1)} = \begin{cases} \overrightarrow{X_b(t)} + \overrightarrow{vb} \cdot \left(\overrightarrow{W} \cdot \overrightarrow{X_A(t)} - \overrightarrow{X_B(t)} \right), r < tanh|S(i) - DF| \\ \overrightarrow{vc} \cdot \overrightarrow{X(t)}, r \geq tanh|S(i) - DF| \end{cases} \quad (5.28)$$

where $|S(i) - DF|$ stands for the distance between the fitness of $\vec{X}$ and the fitness achieved in all iterations ($i \in 1,2, ..., n$), $\overrightarrow{vb}$ is an internal vector in SMA with the range defined based on Eq. (5.29), $\overrightarrow{vc}$ is another vector that linearly decreases from one to zero, t stands for current iteration number. The location of a point with the highest rate of odour concentration that currently is found can be represented by $\overrightarrow{X_b}$, and current location of the slime mould is represented by $\vec{X}$. In each iteration, two individuals are randomly selected from the swarm as $\overrightarrow{X_A}$ and $\overrightarrow{X_B}$ and their distance will be gained by weight of slime mould as $\overrightarrow{W}$.

$$\overrightarrow{vb} = [-arctanh\left(-\left(\frac{t}{max\_t}\right) + 1\right), arctanh\left(-\left(\frac{t}{max\_t}\right) + 1\right)] \quad (5.29)$$

Weight of slime mould $\overrightarrow{W}$ can be calculated by Eq. (5.30) in which "Smell Index" is a sorted version of fitness vector.

$$\overrightarrow{W(SmellIndex(i))} = \begin{cases} 1 + r \cdot log\left(\frac{bF - S(i)}{bF - wF} + 1\right), & \text{condition} \\ 1 - r \cdot log\left(\frac{bF - S(i)}{bF - wF} + 1\right), & \text{others} \end{cases} \quad (5.30)$$

where r is a uniformly distributed random number with the range of [0, 1], the ranked first half of the population is indicated by $S(i)$, bF and wF denote the best and the worst fitness values in each iteration respectively. In the wrap food phase, the location of the slime mould can be formulated using Eq. (5.31) as follows:

$$\vec{X^*} = \begin{cases} \text{rand} \cdot (\text{UB} - \text{LB}) + \text{LB}, \text{rand} < z \\ \overrightarrow{X_b(t)} + \overrightarrow{vb} \cdot \left(W \cdot \overrightarrow{X_A(t)} - \overrightarrow{X_B(t)} \right), r < p \\ \overrightarrow{vc} \cdot \overrightarrow{X(t)}, r \geq p \end{cases} \tag{5.31}$$

where upper bound and lower bound of the search algorithm can be defined by UB and LB, respectively. Both rand and r are the uniformly distributed random numbers which range from 0 to 10.

In the grabble food phase which is generated through a random oscillation procedure with the bound of $[-a, a]$, and a negative gain, $\overrightarrow{vb}$ which gradually tends to zero over the iterations. Similarly, $\overrightarrow{vc}$ value is generated through a random oscillation procedure with the bound of [-1,1] and a negative gain that eventually approaches zero in the final iteration. The flowchart of the SMA is illustrated in **Figure 5.11** and the initial parameters are listed in **Table 5.6**.

Table 5.6: Parameter settings for SMA

Parameter	Values
Max. Number of Iterations	500
Slime Mould Dimension Size	7
Number of Search Agents	30
Upper Bound Vector (UB)	[3.3, 0.9, 3.0, 0.008, 200]
Lower Bound Vector (LB)	[2.0, 0.1, 0.8, 0.004, 100]

The following Multi-Objective (MO) cost function, Eq. (5.32), is same as the cost function for GA and PSO in which seven dimensions are associated, i.e., intake air temperature ($T_{dry,in}$), intake air relative humidity ($RH_{dry,in}$), intake air velocity ($U_{dry,in}$), working air ratio (φ), HMX height (H), gap (G), and number of layers in HMX structure (N_L). Noted that $T_{dry,in}$ and $RH_{dry,in}$ are predefined based on the

climates. It means that the decision variables of the optimization algorithm are intake air velocity, working air ratio, channel gap and number of layers. In addition, the objective of the optimization is to maximise the cooling capacity ($Q_{cooling}$), COP and wet bulb efficiency (ε_{wb},), and to minimise the surface area of the layers (A_s,) [33].

$$\left(T_{dry,in}, RH_{dry,in}, U_{dry,in}, \varphi, H, G, N_L\right) = W_1 \frac{Q_{cooling}}{RQ_{cooling}} + W_2 \frac{COP}{RCOP} + W_3 \frac{\varepsilon_{wb}}{R\varepsilon_{wb}} + W_4 \frac{RA_s}{A_s} \qquad (5.32)$$

where W_i represent the weights for each objective, $RQ_{cooling}$, RCOP, $R\varepsilon_{wb}$, and RA_s are typical values of $Q_{cooling}$, COP, ε_{wb}, and A_s, respectively.
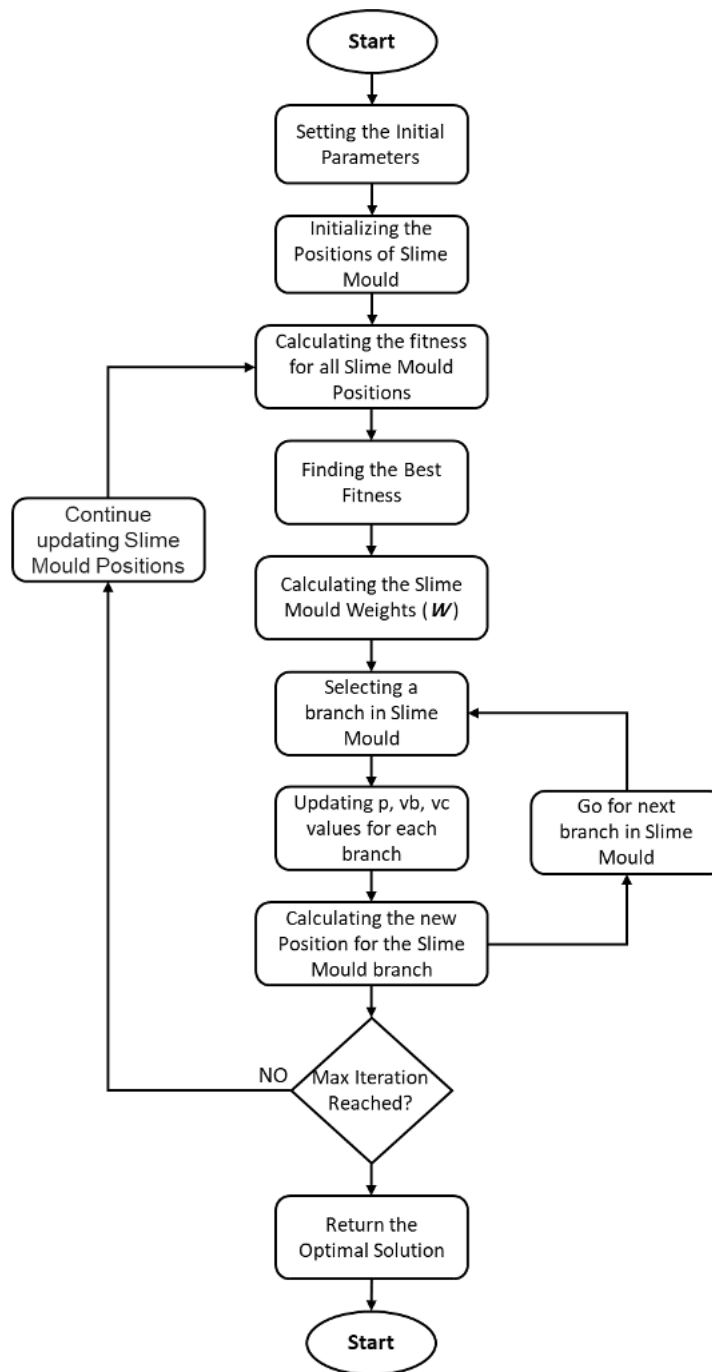
Figure 5.11: Flowchart of SMA method

5.5.3. Results derived from SMA: Weight distributions

In a similar way to GA and PSO, the optimum value of the decision variables in each

climate is identified by SMA. It is worth repeating that the results are derived based

on the average value of the air properties, i.e., temperature and relative humidity, over the operating hours in 2020. This is done because a single optimized unit in each climate is aimed to operate for the next 30 years. The same five scenarios are considered for each climate in which different weight distributions are assumed to make the comparison more sensible. The comprehensive results derived from SMA are listed in **Table 5.7**.

Compared to the base system, the equally distributed weights lead to better results in terms of cooling capacity and COP while other objectives, i.e., wet bulb efficiency and surface area, remain almost same. However, the system performance under other single objective scenarios is not satisfying. Although, the third scenario where COP is considered as the dominant objective ($W3 = 0.85$) leads to convincing results, where COP is maximised and the surface area is lower than the base system, but cooling capacity which is one of the main performance parameters are lower than the base system. This trend is same in scenario 5 where surface area is the dominant objective ($W4 = 0.85$). High surface area in second scenario where cooling capacity is the dominant objective ($W1 = 0.85$) and low cooling capacity in fourth scenario where wet bulb efficiency is the dominant objective ($W3 = 0.85$) have made these scenarios unsatisfactory. As a consequence, similar to the previous methods, scenario 1 in SMA method is selected to discuss optimization results and to investigate performance of the optimized systems.

Table 5.7: Optimisation results by SMA

Method: Slime Mould Algorithm (SMA)		
Climate: Hot summer continental (Dwa) / Beijing		
Design weights	Decision variables	Objectives

No.	W1	W2	W3	W4	$U_{dry,in}$ (m/s)	φ (-)	H (m)	G (m)	N_L (-)	$Q_{cooling}$	COP	ε_{wb}	A_s
1	0.25*	0.25*	0.25*	0.25*	2.00	0.26	0.80	0.004	128.03	1.06	33.12	1.07	40.70
2	0.85	0.05	0.05	0.05	2.30	0.24	1.60	0.008	200.00	2.72	28.35	0.81	126.79
3	0.05	0.85	0.05	0.05	2.00	0.18	0.81	0.008	103.34	1.03	47.79	0.65	31.99
4	0.05	0.05	0.85	0.05	2.00	0.32	1.41	0.004	100.00	0.88	19.30	1.40	56.28
5	0.05	0.05	0.05	0.85	2.00	0.22	0.80	0.005	100.00	0.93	41.23	0.86	31.75
Base system					3.00	0.44	1.00	0.005	160.00	1.60	13.60	1.00	62.49
No.					**Climate: Arid (BWh) / Doha**								
1	0.25*	0.25*	0.25*	0.25*	2.00	0.22	0.80	0.004	141.36	1.65	48.54	0.98	44.99
2	0.85	0.05	0.05	0.05	3.02	0.22	1.40	0.008	200.00	4.26	27.27	0.67	111.59
3	0.05	0.85	0.05	0.05	2.00	0.18	0.80	0.008	110.21	1.53	66.38	0.65	33.58
4	0.05	0.05	0.85	0.05	2.00	0.34	1.41	0.004	100.00	1.18	25.56	1.38	56.25
5	0.05	0.05	0.05	0.85	2.00	0.24	0.80	0.004	100.00	1.16	44.82	1.08	31.75
Base system					3.00	0.44	1.00	0.005	160.00	2.22	18.88	1.00	62.49
No.					**Climate: Tropical rainforest (Af) / Miami**								
1	0.25*	0.25*	0.25*	0.25*	2.00	0.24	0.80	0.006	199.86	1.40	32.83	0.79	63.33
2	0.85	0.05	0.05	0.05	2.28	0.23	2.22	0.008	200.00	2.33	18.93	0.90	176.89
3	0.05	0.85	0.05	0.05	2.00	0.16	0.80	0.008	100.00	0.79	38.04	0.67	31.75
4	0.05	0.05	0.85	0.05	2.00	0.29	1.32	0.004	100.00	0.71	16.80	1.44	52.27
5	0.05	0.05	0.05	0.85	2.00	0.21	0.80	0.005	100.96	0.75	33.49	0.88	31.79
Base system					3.00	0.44	1.00	0.005	160.00	1.21	10.25	1.01	62.49
No.					**Climate: Mediterranean hot summer (Csa) / Rome**								
1	0.25*	0.25*	0.25*	0.25*	2.00	0.27	0.82	0.006	158.41	1.52	42.34	0.84	51.19
2	0.85	0.05	0.05	0.05	2.23	0.27	1.89	0.008	200	3.00	28.84	0.88	150.16
3	0.05	0.85	0.05	0.05	2.00	0.18	0.80	0.008	104.96	1.10	50.03	0.65	32.21
4	0.05	0.05	0.85	0.05	2.00	0.34	1.39	0.004	100.00	0.91	19.90	1.39	55.41
5	0.05	0.05	0.05	0.85	2.00	0.21	0.80	0.006	100.00	1.01	46.57	0.76	31.75
Base system					3.00	0.44	1.00	0.005	160.00	1.71	14.52	0.99	62.49

5.5.4. Results derived from SMA: Optimised decision variables

In all climates optimum velocity of the intake air derived by SMA is 2 (m/s) which is lower than the velocity in base system, i.e., 3 (m/s). The optimum working air ratio by SMA method in all four climates are in the range of 0.22 – 0.27 which are lower than the working air ratio in base system, i.e., 0.44. The identified working air ratio by both methods in Arid, hot summer, typical rainforest and Mediterranean hot summer climates are same which are 0.22, 0.26, 0.24 and 0.27 respectively. The optimum HMX height identified by SMA is in narrow range of 0.80-0.82 (m) which is lower

than the base system height, i.e., 1 (m). The channel gap in the base system is 0.005 (m) while it is revealed that the optimum values are different. Based on SMA results, it holds the optimum value of 0.004 (m) in hot summer continental and arid climates, and 0.006 (m) in tropical rainforest and Mediterranean hot summer climates. The number of layers in the base system is 160 while the optimum numbers in SMA it is in the range of 128.03-199.86.

The results derived in SMA will be used to investigate/compare the performance of the optimised system by SMA with other optimised systems (by PSO and GA) and base system in different climates in the next chapter to discuss the impact of optimisations.

5.6. Comparison and assessment of the optimisation methods

In this section, the methods to assess the accuracy and correctness of the developed optimisation methods, i.e., GA, PSO and SMA, are summarised. It is followed by comparison of the models in terms of efficiency and convergence speed to reveal the pros and cons of each method.

In general, there are different ways to check the correctness and accuracy of the implemented optimisation models which are all derived in MATLAB. However, The following common and most effective approaches to check the correctness and efficiency of the optimization models are provided as follows [268]:

Comparison with classical approaches: In some problems it can be possible to run both classical approach and multi-variate GA to make sure the results are correct and accurate. However, in this paper, because of mathematical complexity using a classical approach for comparison is not possible.

Using Well-known Benchmarks: The correctness of the code can be also proven through the existing benchmarks. The used algorithm has been validated via 23 well-known benchmarks [281].

Using Expert Idea: An expert of the system can check the results and their rationality. The authors of this paper have implemented the system and they have the experimental experience with the system. Therefore, they all agree that the final results are logical.

Convergence: The convergence of the implemented multi-objective genetic algorithm can be easily observed through the plot of cost vs. iterations. There are also other factors such as roundoff errors and local extrema that have the same perspective.

Domination Factor: The implemented multi-objective genetic algorithm has the function to separate dominant results from non-dominant one. So, all final results are dominant and with a proper initial population it is very rare to be trapped by a local minimum. For more information regarding the domination please check.

Although in general the common GA and PSO methods have similar efficiencies but PSO is more efficient in terms of computations in which fewer functions are used. Exploration and exploitation are considered as two important stages in the metaheuristic algorithms which are needed to be balanced. As it was mentioned the No-Free-Lunch (NFL) theory has proven that none of the substantially improved metaheuristic algorithms, can assure to find the global optimum. As a result, the endeavours in introducing the new efficient algorithms are led to introduction of new methods which the SMA is one of them. It is proved that the SMA makes a superb balance between the explorations and exploitations which can lead to better statistical performance than the PSO.

It has concluded that the SMA has the following advantages over the PSO and GA:

I)   It is novel optimization algorithm with no application/study in engineering.

II)   The SMA is fast and it diverges to an optimal solution quickly.

III)   The algorithm has low computational complexity.

However, it is thought that the efficiency and applicability of the SMA may be refused as it is a new method which is not implemented in different fields yet. Thus, the PSO and GA algorithms as well-known optimization algorithms are used in parallel to make sure that the SMA performs well in our field of research.

To this end, apart from the acceptable results derived by SMA, **Figures 5.12-5.14** are provided to show the quicker convergence in SMA than the PSO and GA. The methods are comparable as the cost function, fitness function, objective functions and all decision variables are identical in all of them. Therefore, it can be concluded that in terms of efficiency and convergence speed, SMA outperforms the PSO and GA. However, in the next chapter, the performance of the optimised systems by all of the three methods will be assessed in order to disclose which method leads to better GIDPC performance.
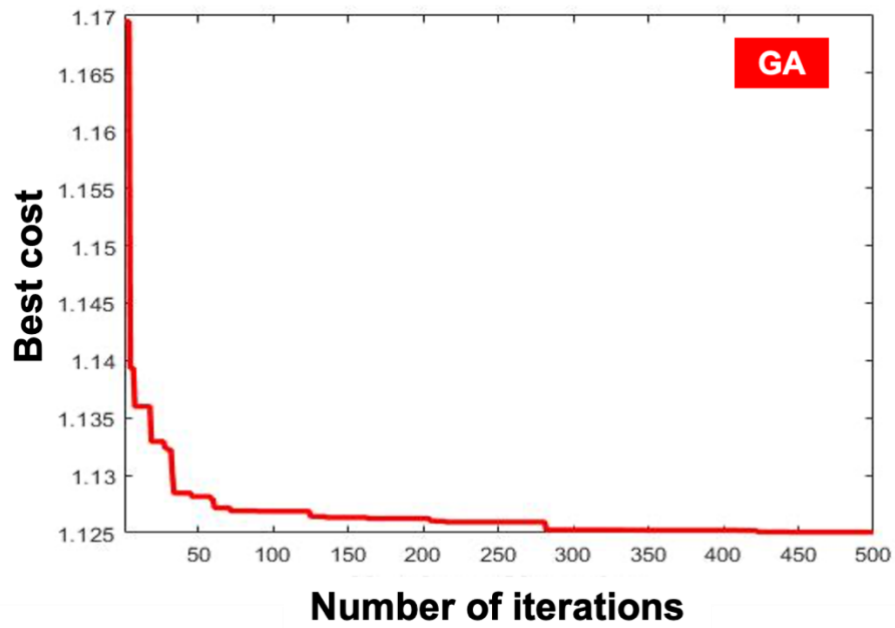
Figure 5.12: GA convergence
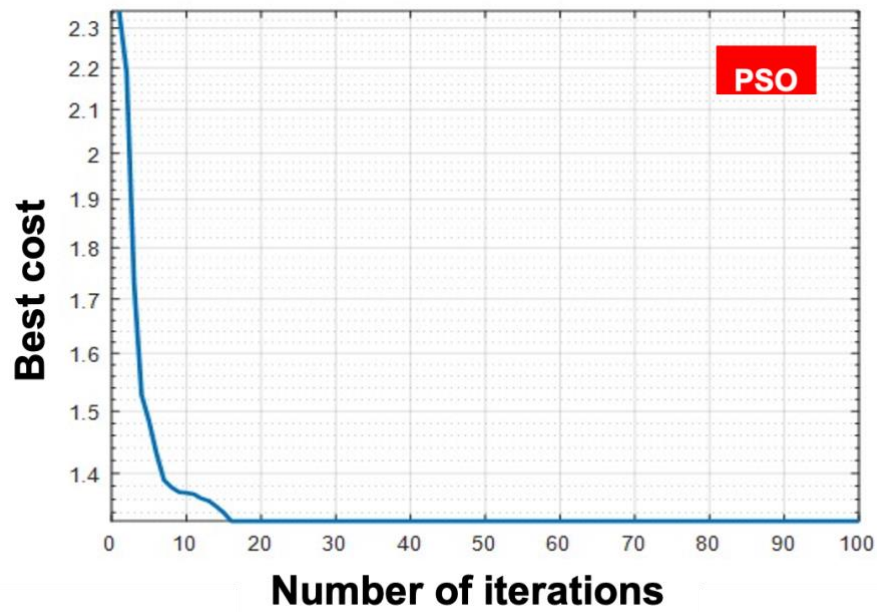
Figure 5.13: PSO convergence
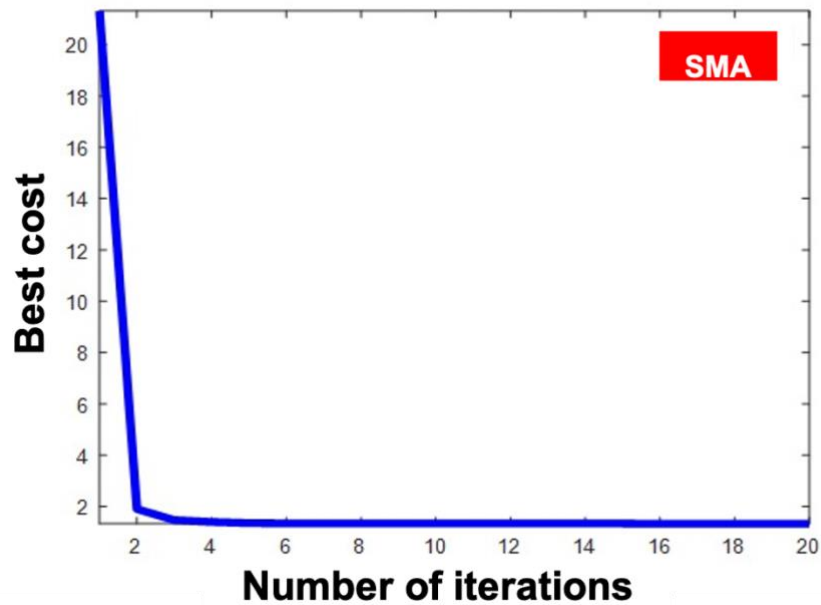
Figure 5.14: SMA convergence

5.7. Summary

In this chapter, firstly a review is carried out over the development of the optimisation algorithms. It is narrated that the heuristic optimisation algorithms are more preferred owing to their outstanding superiority over the traditional optimisation algorithms. Being robust in considering the highly nonlinear functions and swift calculation process is the main advantage of the heuristic optimisations over the traditional ones. Three nature-inspired optimisation algorithms including the popular Genetic Algorithm (GA) and Particle Swarm Optimisation (PSO) as well as a state-of-the-art Slime Mould Algorithm (SMA), are all developed to identify the optimum operating and design parameters of the GIDPC. This is made in four different climatic conditions which are suitable for operation of the GIDPC during their warm months. The results revealed that the identified operating and design parameters by all algorithms are relatively similar, however, there are slight differences in some decision variables. The performance of the base system is compared with the optimised systems and it is

revealed that the optimised systems outperform the base system in terms of COP and surface area. However, other performance parameters are unchanged or differed slightly. Eventually, the comparison-based analysis is conducted to assess the performance of the developed models. It is revealed that the SMA is fast in operation and also in diverging to an optimal solution and has less computational complexity.

CHAPTER 6: APPLICATIONS AND ENERGY SAVING ASSESSMENT OF THE GIDPC

6.1. Introduction

In this chapter, firstly, sample applications for the developed ML models are presented to show how the ML models can predict the performance of the GIDPC. Afterwards, the second and major objective of this chapter which is comparing the performance of the optimized GIDPCs in diverse climates, is presented. This is carried out to show the performance and impact of the optimization algorithms on the system's operation. As of the MPR application, the monthly performance of a GIDPC in Arid climate, i.e., Doha city, in 2020 is predicted using the MPR model. Then, owing to the increased cooling demand in Data Centres (DCs), as a result of growing internet and cloud computing needs, GIDPC is introduced as potential cooling systems in DCs. As a consequence, an application of a DNN model is presented in which the ability of the GIDPC in removing the dissipated heat from the IT room of a small assumed DC is discussed. This is conducted by predicting the supply air temperature of the GIDPC in different climates.

Eventually, the performance of the base GIDPC is compared with three optimized GIDPCs in four selected climates, i.e., Hot summer continental, Arid, tropical rainforest, and Mediterranean hot summer, in 2020 and 2050. This is carried out by comparing the hourly COP of the systems during the operating hours in all climates. Moreover, the average values of other performance parameters such as cooling capacity and wet-bulb efficiency for all systems are provided. This is followed by annual energy saving analysis of the optimized systems in which the rate of power consumption by all systems is selected as the basis of the calculations.

6.2. MPR application: Performance prediction of the GIDPC

6.2.1. MPR initial settings

In this section, an application of the developed MPR model is presented to demonstrate its capability in GIDPC performance prediction. In this regard, the comprehensive **Equation 4.16** is needed to be adjusted. In order to initialise the adjustment, the appropriate polynomial coefficients for the 8th degree polynomial equations, as listed in Table 4.7, are needed to be replaced in general/comprehensive equations. Therefore, GIDPC's design (geometric set) and operating conditions are needed to be selected accordingly. In this application, the geometric set 2 in which the HMX height is 1(m), the HMX gap is 0.004(m), and the number of layers is 200, is selected. As a result of considering the aforementioned conditions and applying the 8th degree polynomial powers from Table 4.6 in the general equations, the following Eq. (6.1) is achieved which will be used for the performance prediction of the selected GIDPC.

$$\begin{bmatrix} Q_{cooling} \\ COP \\ \varepsilon_{wb} \\ \varepsilon_{dp} \\ \Delta P \end{bmatrix} =$$

$$\begin{bmatrix} Q_{cooling} \\ COP \\ \varepsilon_{wb} \\ \varepsilon_{dp} \\ \Delta P \end{bmatrix} = \begin{bmatrix} +3.118e+03 \\ -2.287e+03 \\ -1.661e+02 \\ +3.661e+02 \\ -3.839e+01 \end{bmatrix} + \begin{bmatrix} +1.048e+03 & +1.092e+02 & \dots & -6.689e+04 \\ +5.186e+02 & +5.186e+02 & \dots & -4.727e+03 \\ +1.046e+02 & +1.046e+02 & \dots & +5.501e+01 \\ -8.634e+01 & -8.634e+01 & \cdots & \vdots \\ +8.032e+00 & +8.032e+00 & \cdots & +4.384e+00 \end{bmatrix} \times \begin{bmatrix} T^1 \times RH^0 \times U^0 \times \varphi^0 \\ T^2 \times RH^0 \times U^0 \times \varphi^0 \\ T^3 \times RH^0 \times U^0 \times \varphi^0 \\ \vdots \\ T^0 \times RH^0 \times U^0 \times \varphi^8 \end{bmatrix} \quad (6.1)$$

6.2.2. GIDPC operating conditions

As explained in chapter 5, a high emission scenario defined by the Intergovernmental Panel for Climate Change (IPCC) is used to generate the weather data in this research study. It is worth reviewing that the IPCC's SRES A2 climate scenario in Meteonorm software is used to create the hourly temperature and relative humidity in the selected

cities. The selected cities represent the four operating climates in which the GIDPC is eligible (or needed) to operate based on the predefined operating ranges and weather properties.

In this section, the developed MPR model is employed to predict the GIDPC monthly performance in Arid climate, i.e., Doha city. To this end, the monthly average temperature and relative humidity values in 2020 are calculated in Doha. The monthly temperature and relative humidity of the operating months are listed in Table 6.1. The reason for selecting Doha is mainly because of its warmest conditions and highest number of operating hours among the other selected cities. The geometric set 2 GIDPC in MPR model is selected for the performance predictions while the working air velocity is set 3(m/s) and the working air ratio of 0.44 is selected.

Table 6.1: Average monthly weather properties in Doha 2020

Month	Average T (°C)	Average RH (-)
January	25.62	0.49
February	26.59	0.48
March	27.32	0.46
April	29.02	0.47
May	32.61	0.42
June	34.96	0.39
July	36.3	0.45
August	35.75	0.51
September	33.25	0.62
October	30.51	0.61
November	27.79	0.62

December	26.31	0.58

6.2.3. Monthly performance prediction

In **Figure 6.1**, three performance parameters of the GIDPC, i.e., cooling capacity, COP, and wet-bulb efficiency are shown for Doha from January to June in 2020. As seen, the cooling capacity in the selected operating months ranges from 3.68kW in January to 5.63kW in June. Similarly, the COP is in the range of 16.01-24.75, wet-bulb efficiency is in the range of 0.90-0.94.

Although the main ML model in this study is DNN, but this application revealed that the MPR is capable of making the predictions despite being weak compared to the DNN. The main weakness of MPR is that the design parameters are limited to the determined geometric sets which substantially decrease the efficiency and flexibility of the model. In addition, it covers limited ranges of the operating parameters which again this issue decreases the comprehensiveness of the model.
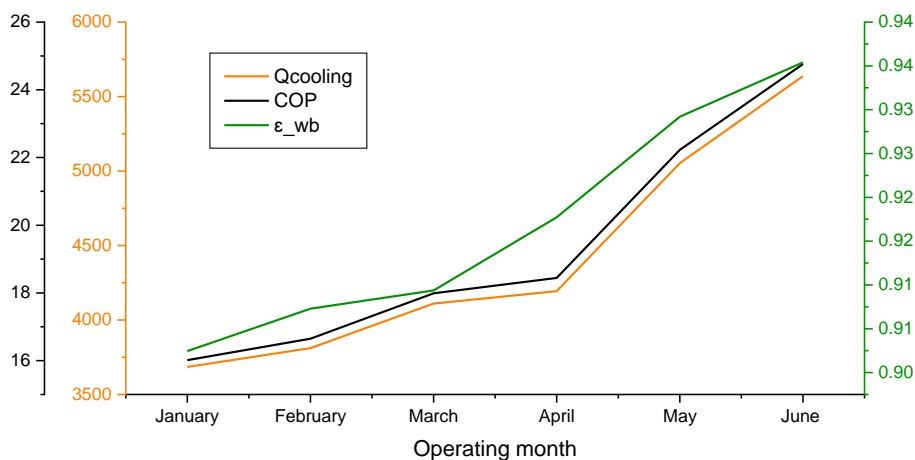
Figure 6.1: MPR application: Monthly performance parameters prediction in Doha 2020

6.3. DNN application: The GIDPCs in a Small Data Centre

6.3.1. Design requirement and operating conditions

Over the past few years, the cooling demand of commercial and industrial buildings has increased significantly which led to a rapid increase in size and number of the Data Centres (DCs) to satisfy the growing the internet and cloud computing needs [282]. DCs usually operate 24/7 all along the year, which leads to intensive power usage levels [283]–[286] (e.g., Google with 300 million and Facebook with 60 MW of power usage [287]. The equipment used in DCs produces a massive amount of heat [288], which has to be removed from the server rooms using the cooling systems [289]. While the power densities of DCs is varied from 0.5 to 10 $kW.m^{-2}$ [290], cooling systems are responsible for almost 40% of total energy consumption in DCs [291]. Moreover, cooling costs form around 30% of the total energy expenditure in DCs, which has caused the DCs to operate at higher temperatures to reduce cooling costs [222]. The cooling systems' main tasks in DCs are: removing the dissipated heat from the IT Equipment (ITE) and distributing cold air into the DCs [289]. The efficient cooling systems are required to run the DCs in a more economically and efficiently way.

In general, the cooling systems in DCs comprises two parts, i.e., a CRAC unit and a dedicated air distribution system [292] in which the CRAC unit includes the main cooling systems and the air distribution system comprises the ducting system which distribute the produced supply air by the cooler to the IT room of the DC.

Figure 6.2 illustrates the power consumption breakdown in DCs. As seen from **Figure 6.2**, the power consumption is categorized in three different groups, i.e., space cooling,

electrical losses and powering the server equipment in which the majority of the power delivered to the DCs is consumed for the space cooling. This is 15% more than the electricity needed for powering the server equipment which is considered as the core part of the DCs. Moreover, it can be seen that the electrical losses are 35% less than the power required for space cooling. This information indicates that the need for efficient cooling systems in DCs is vital. This can happen by proposing the new methods and strategies for cooling the DCs which can replace the current traditional cooling systems. Traditional cooling systems are based on energy intensive mechanical vapour compression. The energy intensiveness of the traditional cooling systems is worsened because of the following reasons [293]:

1. The cooling systems are needed to operate all along the year even in the coldest seasons as the heat dissipation by the ITE continues.

2. In the traditional DCs, the air distribution was unable to stop the cold and hot air streams from mixing that was leading more need for the cooling system operation.

3. In some cooling systems, e.g., water side cooling systems, due to the size and floor plan of the DCs, long ducting pipes. The required fans and pumps which are needed to transport the air/water increases the power consumption of the whole cooling system.

One simple solution to improve the efficiency of the cooling systems in DCs and to solve the second and the third aforementioned problems is reducing or even eliminating the need for the ducting pipes. Several solutions are proposed through different research studies to mitigate this problem in DCs. For instance, employing rack backdoor coolers, ceiling coolers, specific rack arrangement, etc. [294], [295]. However, the first problem is now solved by implementing the free air-cooling

technology which is also called an economizer cycle. This technology reduces or in some cases removes the need for CRAC units which can results in substantial power saving in DCs [296]–[300]. The free air-cooling technology has three types, as below:

- **Airside economizer:** The airside economizer free air-cooling technology simply decreases the operating temperature of the DCs by making the air to directly flow into the IT room of the DC or by to indirectly make the air to flow into the room. In the indirect mode, auxiliary components such as fin and tube heat exchanger, rotary wheel and the air to air heat exchanger are needed.

- **Waterside economizer:** The waterside economizer employs different technologies, e.g., water pump, cooling tower, to transfer and then circulate the water in the CRAC

- **Heat pipe systems:** Heat pipe is used to transfer the heat based on the thermal conductivity and phase transition.
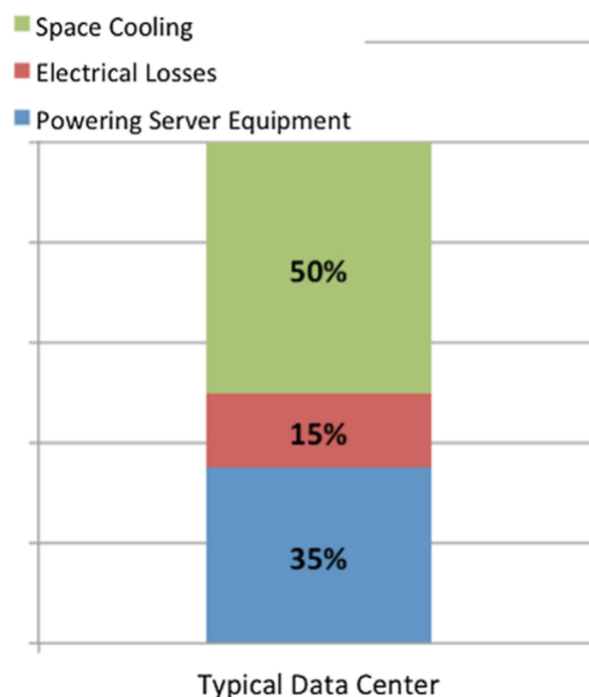
Figure 6.2: Hot/Cold aisle cooling configuration in DCs [301]

Although the free air-cooling technology is efficient enough but in order to employ them in the DCs, the following effective factors must take into considerations:

- **The geographic location:** The airside free cooling technology is limited to mild/cold climates and it underperforms in hot and humid climates.

- **DC operating range:** Although the operating ranges were tight in the DCs but it then updated by ASHRAE which let the free air-cooling technology to operate in more hours [302]. The most updated classification and corresponding operating ranges are shown in **Figure 6.3**.

- **Air distribution system:** The most concerning issue in the traditional DCs was mixing the hot and cold airflows within the IT room which could lead to inefficient cooling. This problem is solved by separating the hot and cold airflows in order to avoid them from mixing.
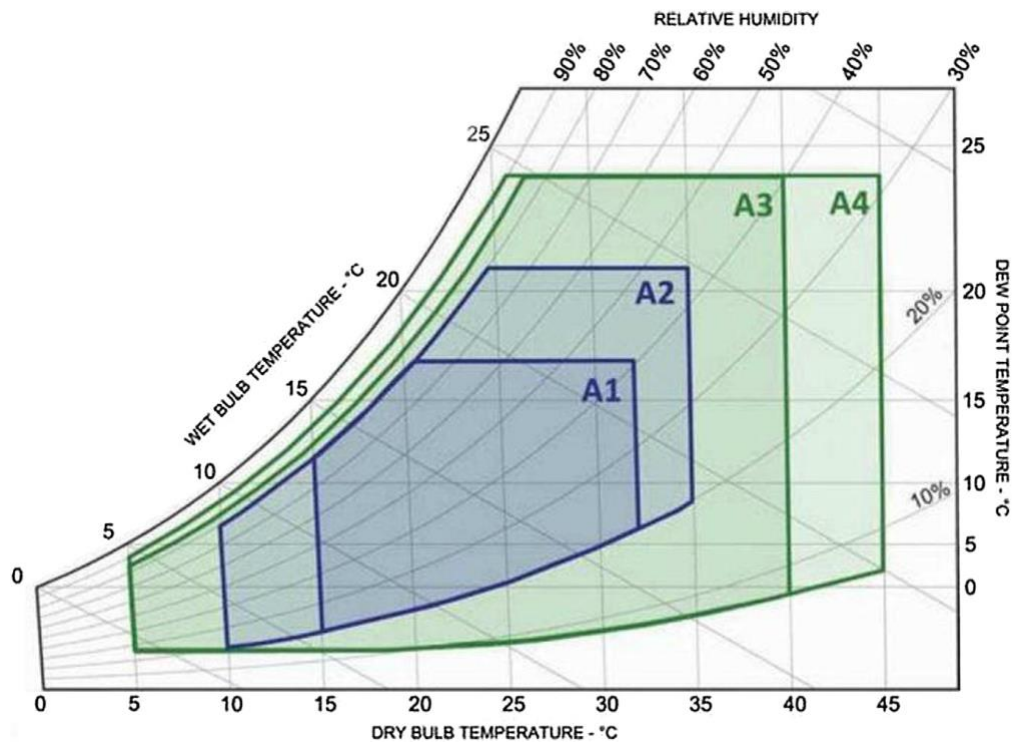
Figure 6.3: ASHRAE classification for data centres

The cooled air with the required temperature is supplied into the DC through the dedicated air distribution system to remove the dissipated heat from the ITE [303]. Although there are numerous containments which are used in DCs to separate the cold and hot air streams as shown in **Figure 6.4,** there are two common cold/hot aisle containment in DCs in which the cold airstreams and hot air streams are kept separated. The supply air for the cooling systems is transferred to the cold aisle in order to reject the heat dissipated by the ITE through the hot aisle. The positions of the hot and cold aisle can be either between the racks or insides which depend on design factors in DCs.
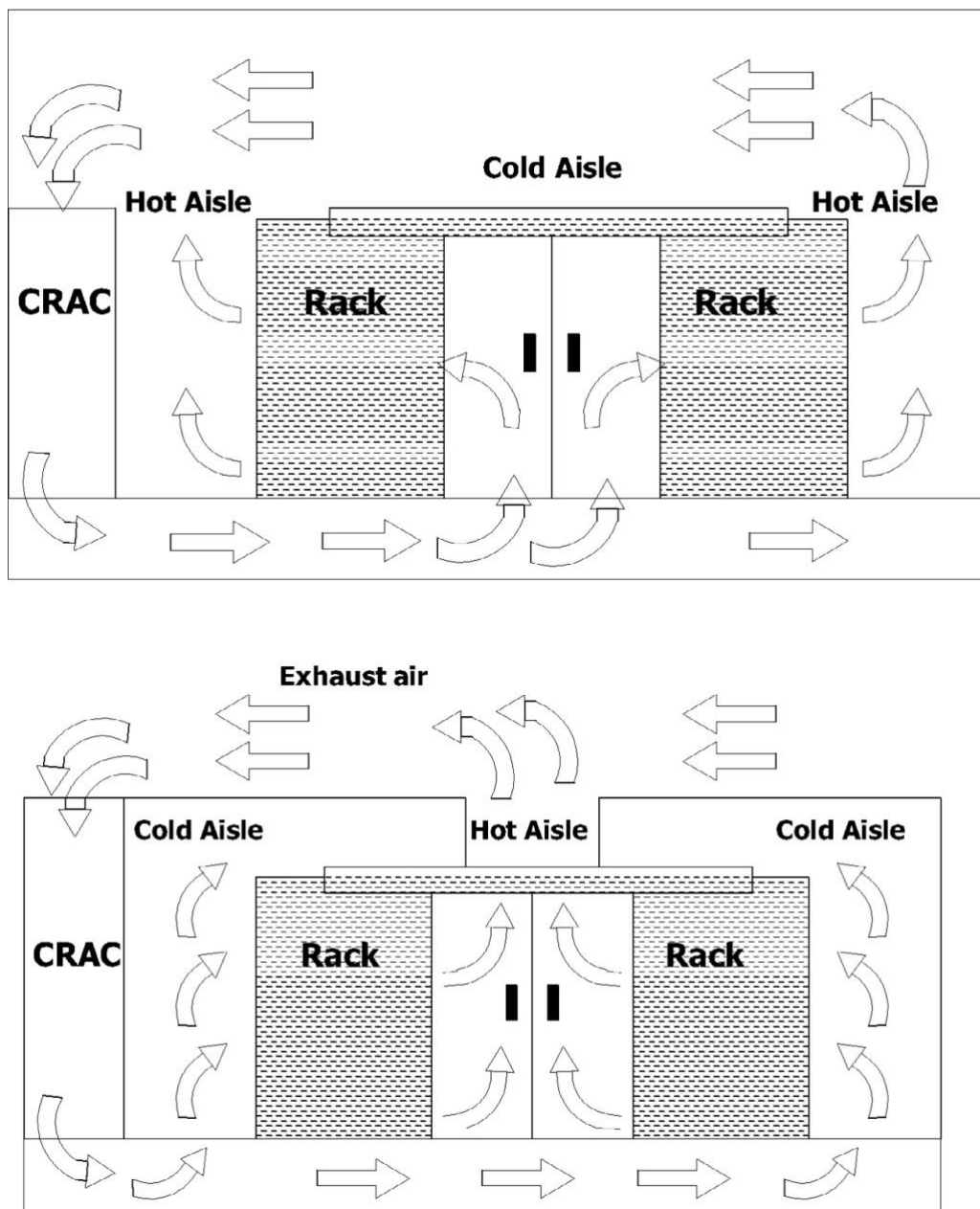
Figure 6.4: Two commonly used cold/hot aisle containment in DCs [304]

As seen in **Figure 6.4**, the supply air produced by the cooling system is transferred to the IT room from under the floor. This is called and Underfloor Air Distribution (UFAD) system which is identified as the most efficient method to transfer the supply/cooled airflow into the ITE room within the DCs [305]. However, the efficiency of the cooling system in DCs significantly depends on the airflow distribution system within the ITE room.

The hot/cold aisle airflow distribution is identified as the most efficient configuration in the modern DCs as shown in **Figure 6.5**. The main advantage of this configuration is that it keeps the cooled and warm air separated, resulting in better cooling efficiency. This configuration prevents the cooled and warm from being mixed and assures that the cooled air arrives the cold aisle in its original condition and without being affected by the warm air to the high temperature ITE. Therefore, this leads to the more efficient cooling process and less power consumption within the DCs.

Based on the ASHRAE thermal guidelines for DCs (2016), *ASHRAE TC9.9-Data Centre Power Equipment Thermal Guidelines and Best Practices*, DCs are classified into six classes based on reliability and their uptime. The recommended operating temperature and relative humidity ranges for all classes regardless of climate/region are 18-27˚C and 20-80% respectively. It means that the temperature and relative humidity of cold air delivered to the DCs (supply air temperature of GIDPC) should be in the aforementioned ranges to assure the efficient cooling down process for the ITE of the DC.

6.3.2. Assumed Data Centre

In this section, an application of operating GIDPC as the main cooling system in the ITE room of a small DC is provided to report the energy saving potential of the technology by predicting the performance of GIDPC using the DNN model. Thus, to fulfil this goal, a small DC is assumed to operate when the GIDPC is its main cooling technology.

Based on the potential of the current GIDPC [38], [127], [171] and the performance of the technology in the current study, it is concluded that the supply air temperature of the GIDPC which will be delivered to the ITE room of the DC (cold aisle temperature), should reach a value of less than 22˚C. This will help the GIDPC to reach its highest cooling capacity and to satisfy the all classes of the DC according to the aforementioned ranges suggested by ASHRAE. However, the lower values are in favour as they will lead to more heat removal capacity and consequently more cooling efficiency. According to the ASHRAE thermal guidelines for DCs, the average exhaust temperature rise is 15 ˚C which is mainly because of the heat transfer from the ITE to the cold aisle which is cooled by the supply air of the GIDPC. This value represents the temperature difference between the cold and aisle of the ITE room within the DC. Having considered the cold aisle temperature of below 22˚C, and the average temperature rise of 15 ˚C, the hot aisle temperature will have a value of below 37˚C. Furthermore, it is established that the dissipated heat from the traditional DCs ranges from 430 to 861W.m^{-2} [290].

Having considered all of the aforementioned information, in this study a small 100 m^2 DC is considered to report the potential of the GIDPC in removing the dissipated heat from the ITE room of it. The upper bound, i.e., 861 W.m^{-2}, heat dissipation is considered as the cooling load density of the DC which led to the heat dissipation of 86.1 kW.
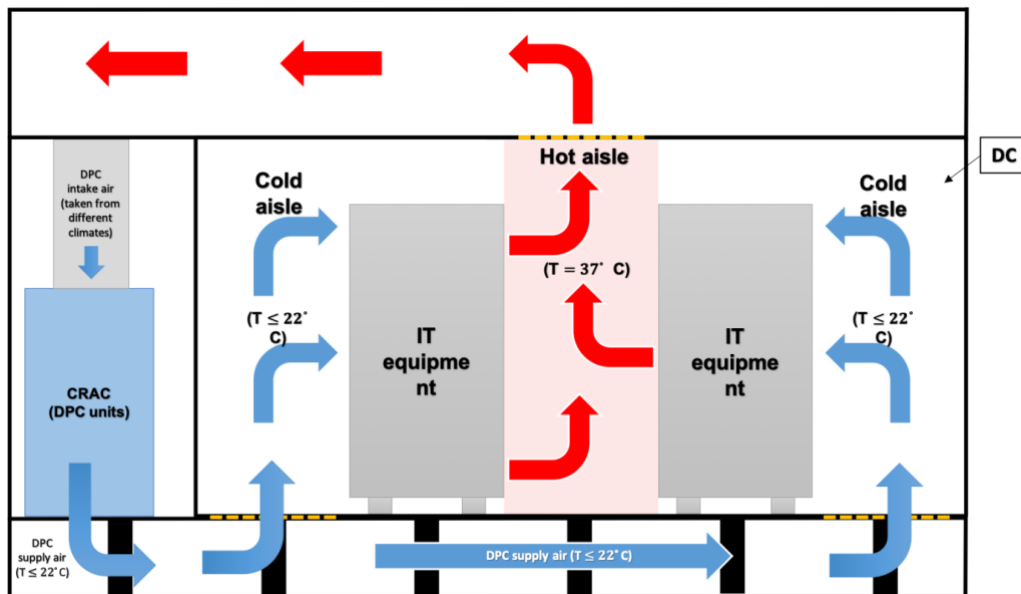
Figure 6.5: Hot/Cold aisle cooling configuration in DCs

6.3.3. Effect of GIDPC on DC indoor environment

It is aimed to observe the GIDPC ability in decreasing the temperature and removing the dissipated heat from the ITE room of the selected DC in operating months of four selected climates. The results revealed that the performance of the system in the DC is varied owing to the different temperature and relative humidity values. It is worth mentioning that the base GIDPC, i.e., with intake air velocity of 3(m/s), working air ratio of 0.44, HMX height of 1(m), HMX gap of 0.004(m), and the number of layers of 200, is selected in the current application. The monthly average temperature and relative humidity values (in operation hours) in 2020 are listed in Table 6.2.

Table 6.2: Monthly weather properties in the selected cities in 2020

City	Beijing		Doha		Miami		Rome	
month	T(°C)	RH	T(°C)	RH	T(°C)	RH	T(°C)	RH
January	-	-	25.62	0.49	26.93	0.54	-	-

February	-	-	26.59	0.49	27.01	0.55	-	-
March	-	-	27.32	0.46	27.11	0.58	-	-
April	26.85	0.31	29.02	0.47	27.35	0.59	-	-
May	28.51	0.41	32.61	0.42	28.10	0.66	26.71	0.49
June	29.59	0.55	34.96	0.39	28.72	0.74	28.16	0.55
July	29.70	0.70	36.30	0.46	29.14	0.74	29.07	0.58
August	28.88	0.69	35.75	0.52	29.16	0.75	29.10	0.59
September	28.18	0.50	33.25	0.63	28.51	0.77	27.29	0.61
October	25.68	0.38	30.51	0.61	27.96	0.70	25.74	0.52
November	-	-	27.79	0.62	27.27	0.63	-	-
December	-	-	26.31	0.58	26.87	0.57	-	-

Figure 6.6 (a) shows the temperature difference between the cold aisle and hot aisle of the selected DC, and **Figure 6.6 (b)** gives the corresponding indoor cooling capacities caused by the GIDPC. The cold aisle and the GIDPC supply air temperatures were assumed to be identical and the hot aisle temperature is assumed 37°C. The aforementioned temperature difference is the base factor in illustrating the GIDPC heat removal capacity from the IT room. The higher temperature difference leads to higher heat removal capacity which is identical with the indoor cooling capacity. It is also assumed that the 160mm circular ducts are assumed to be used for the airflow streams in the DCs. This is inspired from the experimental studies [38] on the GIDPC prototype which leads to the airflow rate of 868.14 m³/hr.

The results revealed that the temperature difference is in the range of 15.20-25.57°C, and the indoor cooling capacity for one DPC is varied between 6.41 and 7.49 kW. In Beijing, the lowest temperature difference and indoor cooling capacity, i.e., 23.92°C and 7.01 kW, respectively, occurred in July whereas the highest values are recorded in October as 25.57 °C and 7.49 kW, respectively. Similarly, the maximum

temperature difference in Doha, Miami and Rome (i.e., 25.57, 25.04 and 25.51˚C) happened in January, December and October, which led to the maximum corresponding indoor capacities (7.49, 7.34, and 7.48kW, respectively). Furthermore, the corresponding minimum temperature differences (i.e., 21.89, 24.10, and 24.17˚C) and minimum indoor cooling capacities (i.e., 6.41, 7.06, and 7.08kW) occurred in July, August and August.
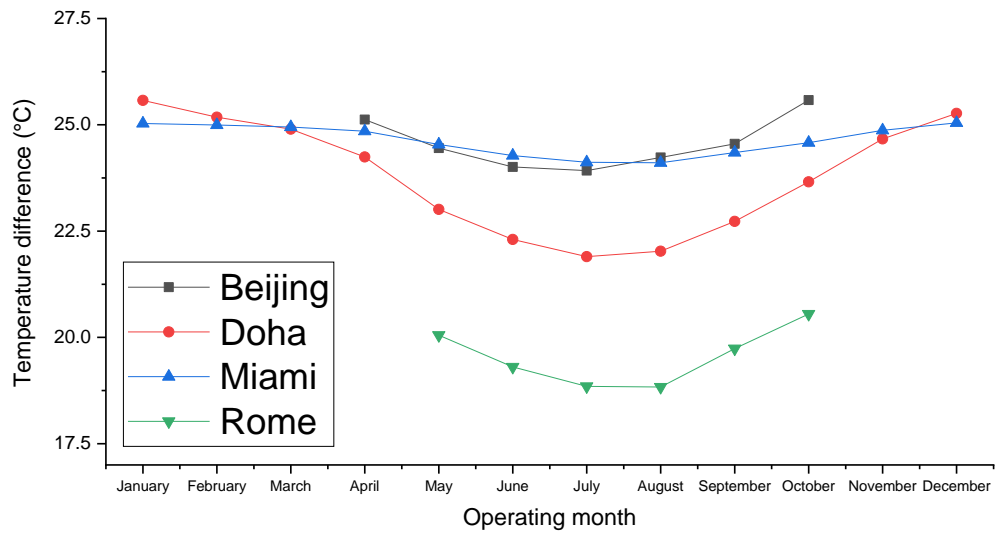
(a)
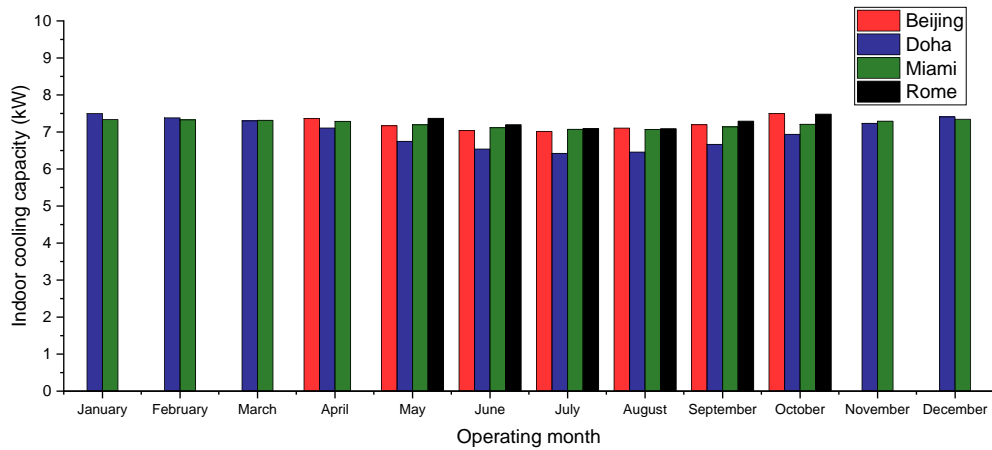
(b)

Figure 6.6: (a): Monthly temperature difference between cold aisle and hot aisle (b): Monthly

indoor cooling capacity

6.4. Performance comparison of the optimised GIDPCs

In this section, the performance of the base GIDPC with three optimised systems are compared to reveal the impact of optimisation algorithm on the efficiency of the systems. This is done by comparing the hourly COP of the all aforementioned systems in four selected climates over the operating hours in 2020 and 2050. This is followed by the energy saving analysis which will report the power consumption of the systems in both years.

6.4.1. Operating conditions

The hourly weather data in 2020 and 2050 with a temperature above 25 °C are selected as the operating conditions of the GIDPC. Four identified climates and their representative cities as wells as operating months were all illustrated in **Figure 5.7** in chapter 5. In the following section, these hourly data in each city for both aforementioned years are taken to compare the hourly COP of the base system with

three optimized GIDPCs. In addition, the annual cooling capacity and wet-bulb efficiency are provided for both base and three optimized systems.

6.4.2. Hourly performance of the optimized systems in 2020 and 2050

In this section, the hourly COP of the base system is compared with all of the optimized systems by GA, PSO and SMA in all climates in years 2020 and 2050. It is worth repeating that the selected 4-kW GIDPC prototype is called the base system in this study which its dimensions are inspired from the authors' previous study and listed in the upcoming sections of the current study. In addition, the average value of the cooling capacity, COP and wet bulb efficiency in operating hours are compared for all systems. The performance of the base system is calculated based on the base system properties which were listed in Chapter 5 i.e., air velocity of 3 (m/s), working air ratio of 0.44, HMX height of 1(m), Gap of 0.005 (m) and the number of layers of 160. Furthermore, the performance of the GA, SMA and PSO systems are calculated using the identified optimum decision variables from the previous Chapter.

The results revealed that in general, the COP of the GA, PSO and SMA systems are superior to the base system while the identified decision variables by GA, SMA and PSO play the key role in introducing the superior optimisation methods. The differences between the GA, SMA and PSO are the results of robust trade-offs made by the optimisation methods by considering the advantages and disadvantages of the identified optimum decision values.

Figure 6.7-6.10 shows the hourly COP of four systems over the operating hours in each climate. Although due to the high number of operating hours and in order to

clearly visualise the results, the first 250 hours of operation are shown in the figures but the discussions are provided for the whole operating hours. As shown in **Figure 6.7 (a)**, the COP of the systems in hot summer continental climate is demonstrated over 250 hours of operation. As expected, the optimised system outperforms the base system. However, COP in GA outperforms PSO and SMA in both years which is mainly due to the differences in working air ratio, i.e., 0.23 in GA versus 0.26 in both PSO and SMA, HMX height, i.e., 0.84(m) in GA versus 0.80(m) in both PSO and SMA, number of layers, i.e., 159.85 in GA, 196.29 in PSO and 128.03 in SMA. Additionally, HMX gap was slightly different in three optimised systems.

In 2020, the COP of the base system is in the range of 2.28-33.16 while the COP of the improved system by GA, ranges from 8.41 to 96.64, by PSO ranges from 7.14 to 85.53, and by SMA is in the range of 7.22-70.39. The trend is similar in 2050 where the COP of the base system varies from 2.32 to 36.87 while in GA it is in the range of 8.16-107.75, in PSO it ranges from 6.89 to 95.46 and in SMA it is in the range of 7.05-78.26.
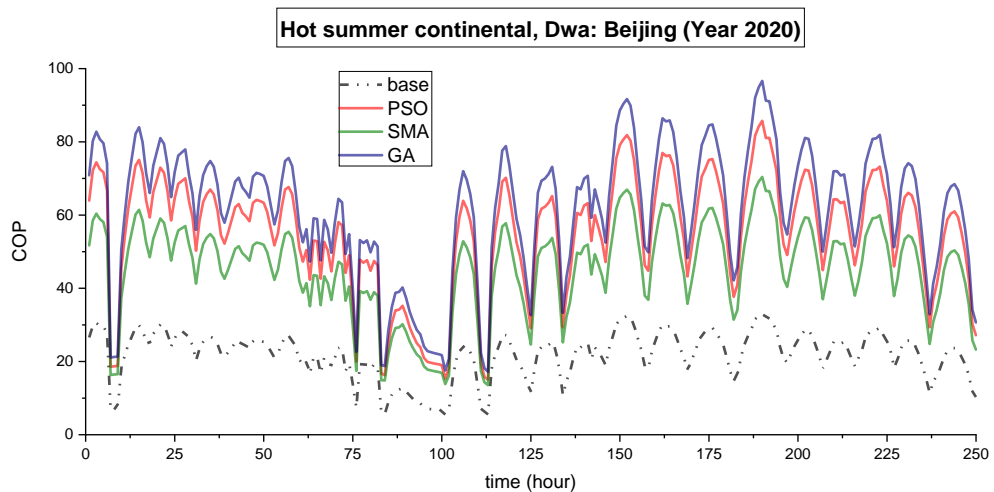
(a)
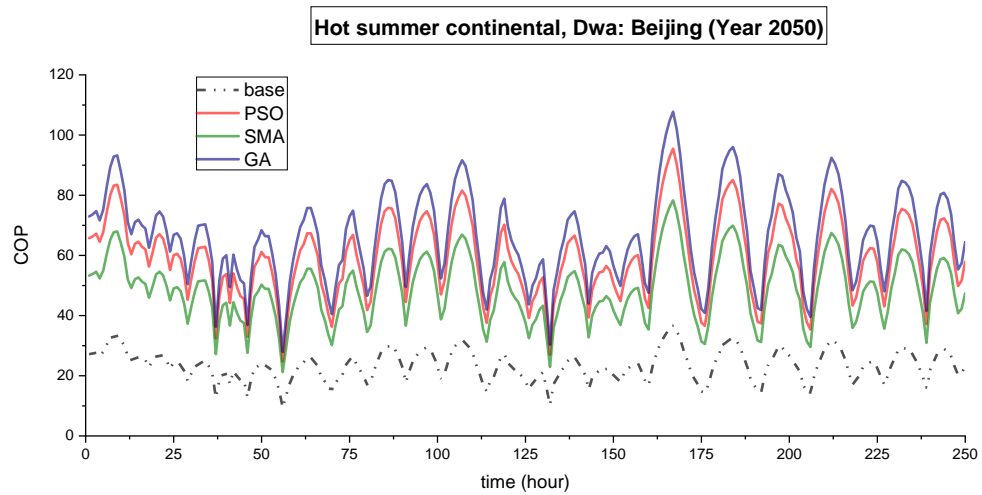
(b)

Figure 6.7: First 250 hours hourly COP values in hot summer continental climate: (a): 2020, total hours: 1790 ; (b): 2050, total hours: 2006

As seen in **Figure 6.8**, the system behaviour in Arid climate is similar to the hot summer continental climate where GA outperforms the PSO, SMA and base system in both years. This is because of the higher working air ratio, a larger gap in GA which have led to slightly better COP values. In 2020, the COP of the base system is in the range of 2.39-43.74. This range is significantly improved when the optimized systems are in operation. The COP ranges from 8.60 to 135.39 in GA, and ranges from 7.37 to 116.78 in PSO system and it is in the range of 7.95-100.61 in SMA system. This trend continues in 2050 when the COP of the base system is in the range of 2.47-45.72 while in GA it is in the range of 9.06-142.14, in SMA it is in the range of 8.45-105.37 and in PSO the COP varies from 7.73 to 122.38.
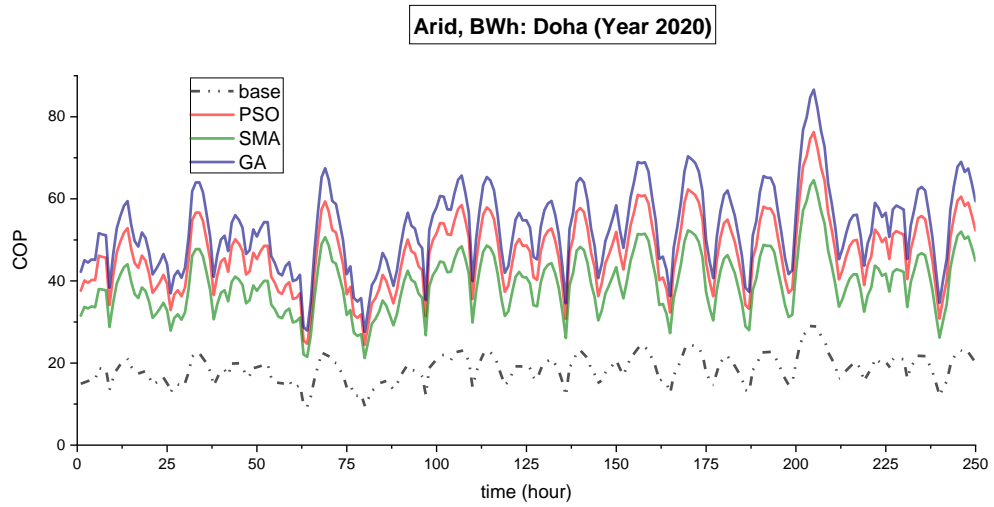
(a)
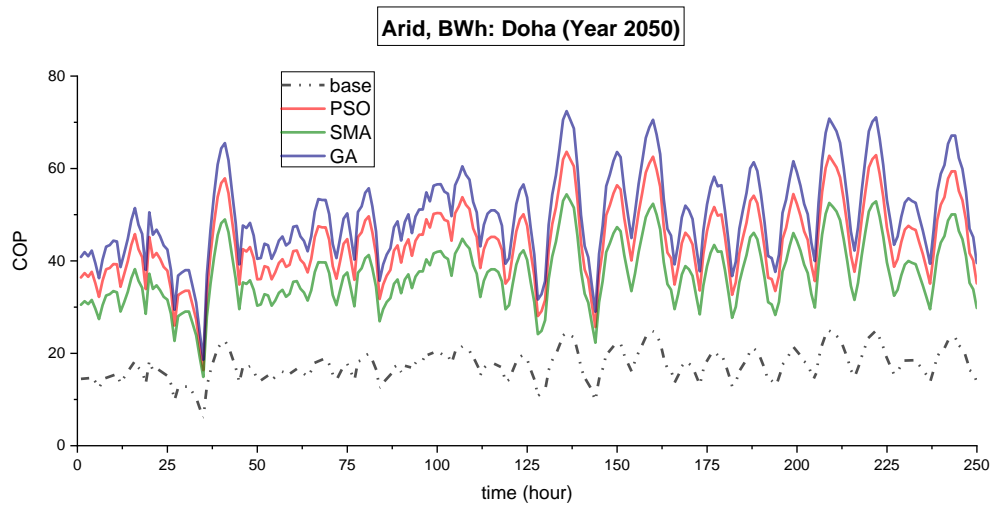
(b)

Figure 6.8: First 250 hours hourly COP values in Arid climate: (a): 2020, total hours: 5486 ; (b): 2050, total hours: 5811

As seen in **Figure 6.9**, the overall COP values of the optimized systems in tropical rainforest climate are improved compared with the base system in both years. However, owing to the identical/similar optimum parameters derived by all methods, the performance of systems are almost same. In 2020, the COP of the base system is in the range of 2.31-25.13 while in GA it is in the range of 8.09-71.51, and in PSO and

242

SMA systems, it is in the similar range of 7.61-72.73. The similar behaviour in both optimized systems was expected due to the extremely similar identified optimum operating and design parameters. In 2050, the COP of the base system varies from 2.31 to 24.37 while in GA it is in the range of 8.06-69.16 , and by PSO and SMA, it is in the similar range of 7.58-70.37.
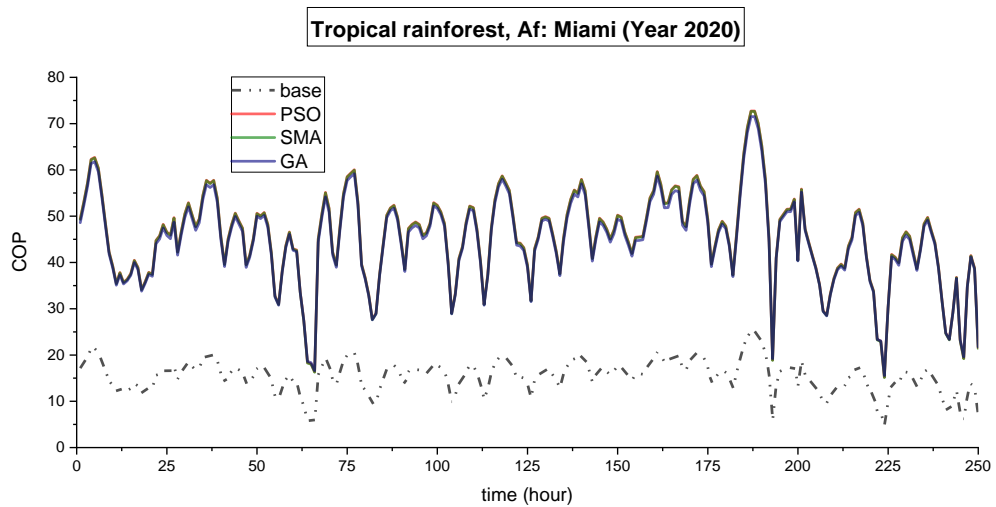
(a)
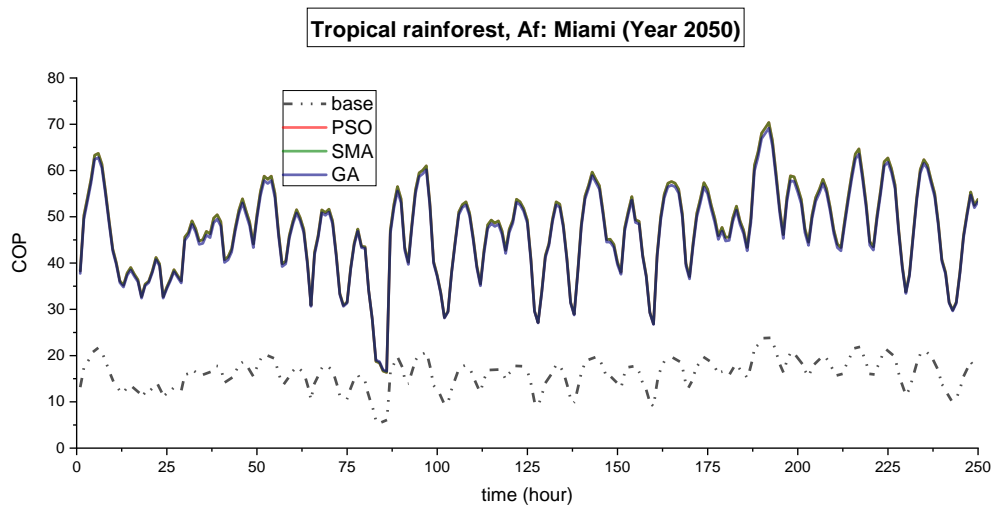
(b)

Figure 6.9: First 250 hours hourly COP values in tropical rainforest climate: (a): 2020, total hours: 4889 ; (b): 2050, total hours: 5388

In Mediterranean hot summer the optimized systems outperform the base system in terms of COP where the GA and SMA outperform PSO in both 2020 and 2050. This is because of the differences in optimum values of three parameters, i.e., HMX height, gap and number of layers by both methods. As seen in **Figure 6.10**, in 2020, the COP of the base system was in the range of 2.83-28.37 while it is improved to the ranges of 8.10-71.23 by PSO, 9.09-79.01 by SMA, and 9.68-80.25 by GA. Same behaviour occurs in 2050 when the COP of the base system was in the range of 2.39-27.85 while the GA, SMA and PSO have increased the ranges to 8.60-85.15, 7.97-82.41 and 7.06-73.94 respectively.
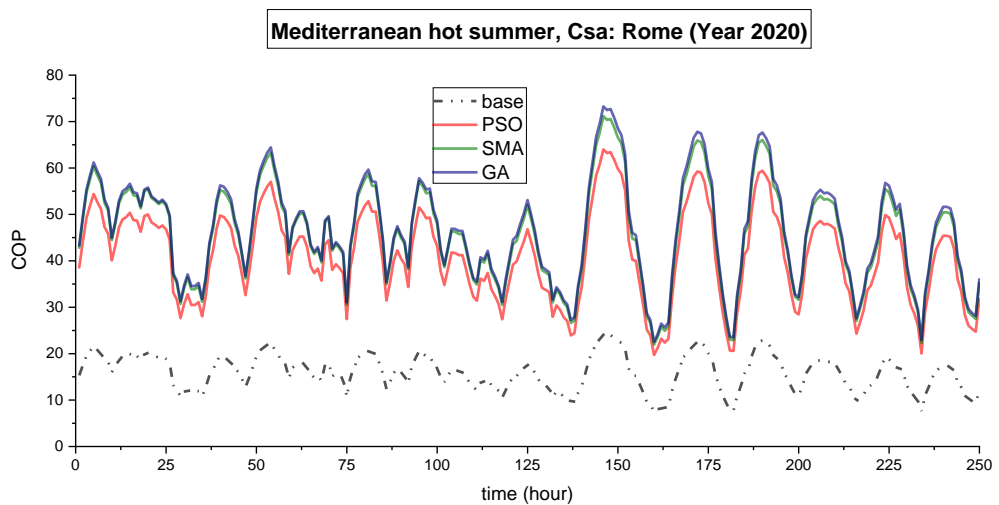
(a)
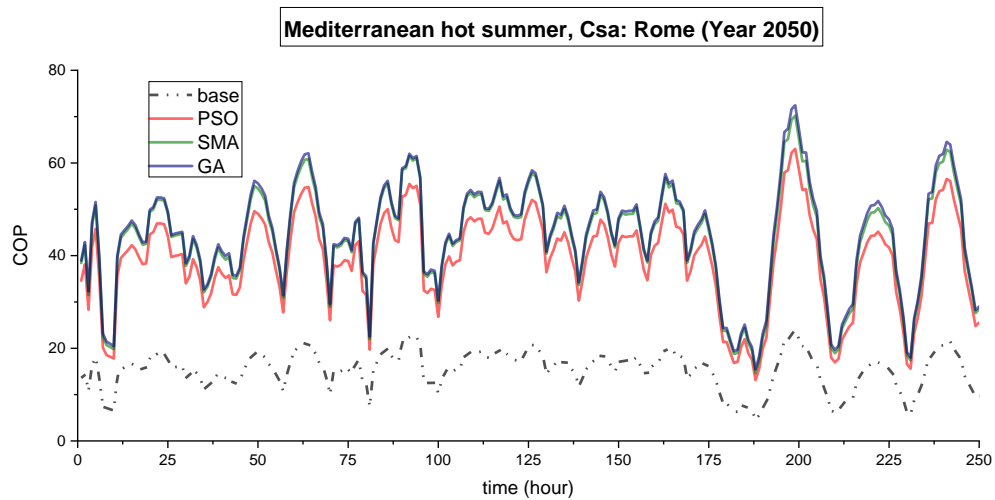
(b)

Figure 6.10: First 250 hours hourly COP values in Mediterranean hot summer climate: (a):

2020, total hours: 1416 ; (b): 2050, total hours: 1759

In order to further compare the impact of optimization algorithms on the system performance, the average value of three objectives, i.e., cooling capacity, COP and wet bulb efficiency, over the operating hours are summarized in **Table 6.3 and 6.4**. In terms of COP, the performance of the optimized systems has significantly improved by both GA, PSO and SMA methods. However, in terms of cooling capacity and wet bulb efficiency, the changes are not same.

For instance, in 2020, the cooling capacity of the PSO system in hot summer continental, tropical rainforest and Mediterranean is better than the base system while it is almost unchanged in Arid climate. However, for the optimized system by SMA, except in tropical rainforest where the cooling capacity is better than the base system, in other climates the cooling capacity is lower than the base system. Although the

245

operating hours in 2050 has increased in all climates but the behaviour of the systems remains exactly the same as in 2020.

In terms of wet bulb efficiency, the performance of the systems follows the same trend in both 2020 and 2050. In hot summer continental, arid and Mediterranean climates, the wet bulb efficiency of the optimized system by PSO is slightly decreased (almost unchanged) but in the tropical rainforest it is decreased by 16% by reaching the average value of 0.86. The performance of the SMA system, compared with the base system, outperforms in hot summer continental and Arid climates while it holds the lower average values in tropical rainforest and Mediterranean hot summer climates.

Table 6.3: Average value of performance parameters in the base and optimized systems - Year 2020

Year	Climate	Hot summer continental (Dwa)				Arid (BWh)			
	objective	Base	PSO	SMA	GA	Base	PSO	SMA	GA
	$Q_{cooling}$ (kW)	1.68	1.71	1.06	1.53	2.31	2.08	1.61	2.14
	COP	14.27	37.56	31.69	42.44	19.57	51.78	44.92	59.28
2020	ε_{wb}	1.01	0.98	1.23	0.86	1.00	0.97	1.07	0.83
	Climate	Tropical rainforest (Af)				Mediterranean hot summer (Csa)			
	objective	Base	PSO	SMA	GA	Base	PSO	SMA	GA
	$Q_{cooling}$ (kW)	1.26	1.41	1.41	1.17	1.74	1.78	1.54	1.58
	COP	10.73	32.70	32.70	32.63	14.80	38.55	42.86	43.85
	ε_{wb}	1.02	0.86	0.86	0.89	0.99	0.95	0.85	0.82

Table 6.4: Average value of performance parameters in the base and optimized systems - Year 2050

Year	Climate	Hot summer continental (Dwa)				Arid (BWh)			
	objective	Base	PSO	SMA	GA	Base	PSO	SMA	GA
	$Q_{cooling}$ (kW)	1.67	1.72	1.06	1.52	2.32	2.10	1.64	2.17
	COP	14.21	37.51	31.67	42.41	19.66	52.30	45.52	60.02
	ε_{wb}	1.01	0.98	1.23	0.86	1.00	0.98	1.08	0.84
2050	objective	Tropical rainforest (Af)				Mediterranean hot summer (Csa)			
	$Q_{cooling}$ (kW)	1.26	1.42	1.41	1.17	1.60	1.65	1.42	1.46
	COP	10.68	32.71	32.71	32.68	13.61	35.71	39.73	40.74
	ε_{wb}	1.03	0.86	0.87	0.89	1.00	0.97	0.87	1.33

As shown in chapter 5, the surface area of the base system with 200 layers is 62.49 (m^2) whereas the optimized systems have lower values in some climates. For instance, in the selected scenario (No.1), for GA, the surface area has decreased in all climates but for SMA system, except tropical rainforest climate in which the surface area is same as the base system, in all other climates, owing to a smaller number of layers, it has decreased. However, in the PSO system, the surface area is only decreased in Arid climate, i.e., 53.78 (m^2) while in all other climates it is almost unchanged.

6.4.3. Energy saving potential of the optimized systems

The power consumption of the GIDPC considering the forecasted operating hours in 2020 and 2050 is analysed to assess the energy saving potential of the optimized systems. The power consumption values are calculated for the three existed systems, i.e., base, optimized by GA, PSO and optimized by SMA. The basis of the calculations

is the rate of power consumption for each system which is calculated considering the system performance in terms of cooling capacity and COP. The rate of power consumption for the base system is around 117.5W while it is 36W for GA, around 45W for the PSO system and around 33W for SMA system. The values are in line with the presented cooling capacity and COP values for each of the four systems.

Based on the operating hours in each climate, the total power consumption is calculated in both 2020 and 2050. As seen in **Figure 6.11 (a)**, in the hot summer continental climate in 2020, the power consumption is 211.00 (kWh) for the base system whereas it has reduced to 80.55 (kWh), 64.44(kWh), and 59.07 (kWh) for PSO, GA and SMA respectively. In spite of higher operating hours in 2050, the trend is same and the optimized systems perform economically. The power consumption of the base system is 236.46 (kWh) whereas it is 90.27 (kWh) for the PSO, 72.21 (kWh) for the GA, and 66.19 (kWh) for the SMA systems. This means that in both years the power savings of 61.82% and 72.00% can occur by the PSO and SMA respectively.

In the arid climate, as shown in **Figure 6.11 (b)**, the same story is predicted where the power consumption of the base system in 2020 with 5486 operating hours is 647.34(kWh) while   PSO system consumes 66.10% less energy, GA consumes 69.39% less, and the SMA consumes 69.49% less energy. In 2050, the power consumption by the base system is estimated to be 685.69(kWh) while the PSO, GA and SMA systems are estimated to consume 453.25(kWh), 475.47(kWh),   and 476.49(kWh) less power respectively.

Owing to the similar optimum operating and design parameters, the power consumption by both optimized systems in tropical rainforest climate is almost same. As seen in **Figure 6.11 (c)**, the power consumption by the base system in 2020 is 572.01(kWh) while it holds the value of 176.15 (kWh) by GA, and 63.24% less power is consumed by PSO and SMA systems. In 2050 the power consumption by the base system is 635.75(kWh) while for GA system is 194.26 kWh, and for both SMA and PSO systems is 233.73 (kWh).

As seen in **Figure 6.11 (d)**, in Mediterranean hot summer climate in 2020, the power consumption of the base system is estimated to be 165.67(kWh) whereas it has reduced to 65.13 (kWh), 51 (kWh), and 50.83(kWh) for PSO, GA and SMA systems respectively. In 2050, the base system is estimated to consume 205.80(kWh) power while PSO, GA and SMA systems consume 80.91(kWh), 63.38 (kWh), and 63.25(kWh) power respectively.

The aforementioned explanations revealed that in general, the power consumption of all systems will increase by 2050 which is mainly due to the more operating hours caused by global warming. Although this increase is valid for both optimized systems but the optimization has resulted in significant power saving.

Hot summer continental (Dwa): Beijing

(a)
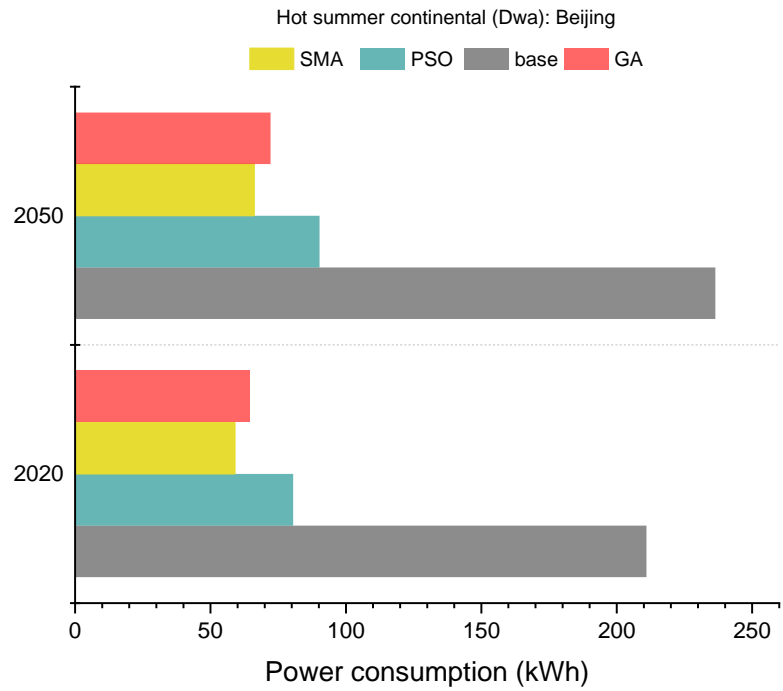
Arid (BWh): Doha
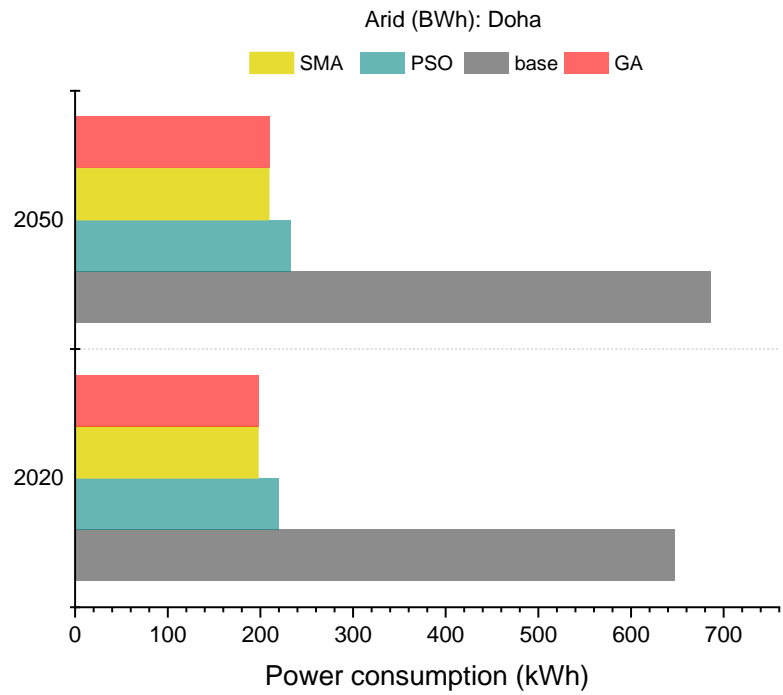
(b)
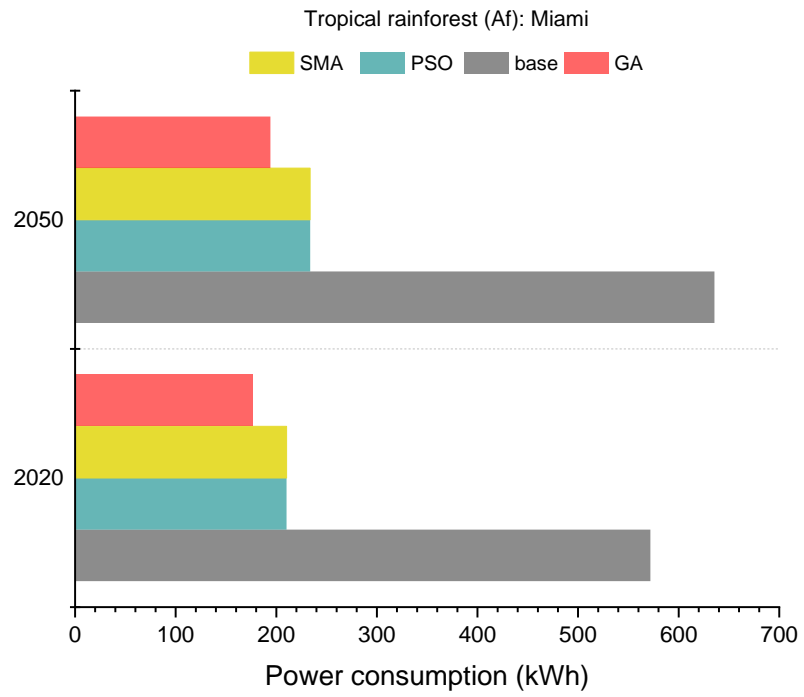
(c)
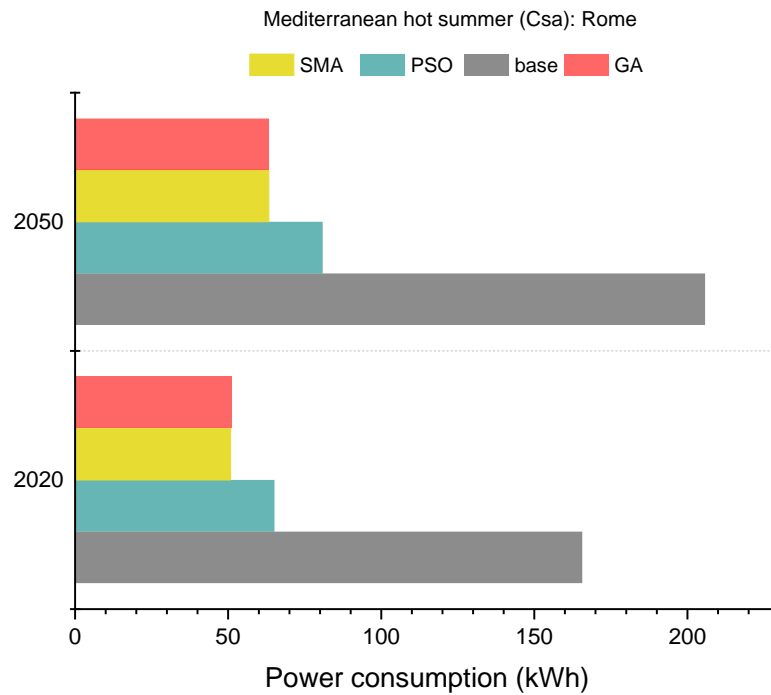
(d)

Figure 6.11: Annual Power consumption in 2020 and 2050: (a): hot summer continental; (b): arid; (c): tropical rainforest; (d): Mediterranean hot summer

6.5. Summary

In this chapter, an example application for each developed ML model is presented. For MPR model, the monthly cooling capacity, COP, and wet-bulb efficiency of the GIDPC is predicted in the city of Doha in 2020. Then the DNN application is presented by shifting the focus towards the cooling technologies in DCs. DNN is used to predict the supply air temperature of the GIDPC when it flows into the IT room of a small DC leading the significant temperature drop, i.e., ranges from 21.89 °C to 25.57 °C, between the cold and hot aisle in the IT room. Furthermore, the indoor cooling capacity as a result of aforementioned temperature differences is calculated.

Furthermore, the hourly COP of the base system is compared with three optimised systems. The results revealed that in general, the performance of the optimized systems in terms of COP outperform the base system in all climates in both 2020 and 2050. Although the optimised system by GA has the best COP in hot summer continental, Arid and Mediterranean hot summer climates but in Tropical rainforest climate, the COP of all optimised systems are roughly same. It is also reported that the surface area of the optimized systems is also decreased in the majority of the climates. Eventually, it is reported that by operating the optimised systems, the energy savings of up to 72% can be achieved.

CHAPTER 7: CONCLUSION AND FUTURE WORKS

7.1. Introduction

This chapter is provided to summarise the work conducted in this PhD research study. The study is considered the state-of-the-art counter-flow GIDPC to mainly assess and optimise the system performance in various operating conditions using the ML and MOEO algorithms. The chapter outlines the justification and objectives of the research which were set to achieve. In addition, the main results and conclusions derived from the study is summarised in this chapter. Moreover, the future work which can be undertaken by implementing the achievements of the current study in the real world is described.

7.2. Overview of the objectives

The study is aimed to firstly conduct a detailed literature review for research studies on the ECs. The objective of the literature review was to chronologically overview the main achievements of the research studies which were conducted to present the advancements made on this technology over the years. As a consequence, the existed gaps, which are mainly the lack of robust ML and optimisation algorithms for the GIDPC, are identified.

In this regard, firstly, it is aimed to pioneer in development of ML based predictive tools for performance prediction of the GIDPC, and secondly, to develop nature-inspired MOEO models for performance optimisation of the system. To this end, a big dataset comprising the major operating, design and performance parameters of the GIDPC was needed. It is aimed to conduct an experiment to both investigate the system performance in diverse climates, and to assure the validity of a numerical

model as the main source for data production. Having constructed the big dataset, two ML models are trained in order to predict and analyse the system performance. The models are compared in terms of accuracy, efficiency and flexibility in predictions and the advanced model is selected.

Afterwards, it is aimed to use the selected model as the fitness function of the MOEO models to optimise the system performance. Different nature-inspired optimisation algorithms are developed in order to compare the performance of the methods in terms of efficiency and convergence speed.

Eventually, applications of the developed ML models are presented by shifting the focus towards comparing the performance of the optimised GIDPCs in diverse climates. This is led to reporting the energy savings that can occur by operating the optimised systems instead of the base system.

7.3. Summary of the main conclusions

The critical and in-depth literature review on the ECs technology revealed that in spite of substantial research-based endeavours to improve the technology but some significant gaps are in existence. It is disclosed that the majority of the studies were focused on the experimental and numerical simulations. After introducing the M-cycle HMXs, which was considered as a technical breakthrough for the ECs, further improvements were struggling by analysing the same traditional cross-flow and counter flow DPCs. The outstanding breakthrough in performance improvement of the DPC is provided by introducing the novel DPC with new corrugated HMX which is called GIDPC. The GIDPC was introduced through the experimental and numerical simulation-based studies in which the great improvement in COP and thermal efficiencies are achieved. However, the GIDPC technology suffered from lack of

further operation and assessments in real life. In addition, although there are limited AI based studies for the traditional DPCs but so far, no data-driven model is developed for the GIDPC. Furthermore, it is revealed that the GIDPC technology is suffering from lack of optimisation-based studies which is essential for performance improvement of the technology. Eventually, it is aimed to investigate the energy saving potential of the optimised systems compared to the based system (4kW-GIDPC prototype) over the annual operation in the four selected climates.

7.3.1. Dataset construction: Experiment and numerical model

A 4-kW GIDPC prototype was tested in a lab to assess the monthly performance of the system in four different climates. This was a pioneer study for the GIDPC in which the monthly cooling capacities of the GIDPC were reported to be in the range of 1.6-4.65 kW, and the monthly COP values were varied between 17.7 and 51.38. In addition, the wet-bulb and dew point efficiencies were in the range of 68.57%–126.47% and 35.29 %- 90.2%, respectively. The numerical model is validated by comparing the monthly COP of the system in one climate in which it is proved that the maximum discrepancies between the experimental and numerical results were as low as 5.24%. Afterwards, a big dataset comprising the major operating parameters, i.e., temperature, relative humidity, and velocity of intake air, and working air ratio, and major design parameters, i.e., HMX height, gap, and the number of layers, and performance parameters, i.e., cooling capacity, COP, supply air temperature, pressure drop, wet-bulb and dew point efficiency, and surface area of the layers, is constructed. It is worth mentioning that the predefined ranges for the operating and design parameters are considered for having a realistic dataset.

7.3.2. Machine Learning models

Two ML models based on MPR and DNN algorithms were developed to predict the performance of the GIDPC. Such kind of effort in bringing the MPR and DNN into the GIDPC technology added important scientific values to characterization of the engineering process of the GIDPC. The models explored the constructed big dataset and produced predictive tools which were able to directly correlate the selected major parameters of the technology. The MPR model was classified in different geometric sets by considering the channel height, channel interval and number of layers in the HMX as the geometric characteristics. The model is also assessed by three common metrics i.e., R2, MSE and MRE by considering different polynomial degrees which led to selection of the 8th degree polynomial model. The selected 8th degree model can predict the performance of the GIDPC with discrepancies of 6.1%, 7.54%, 0.07%, 3.53% and 2.53% for cooling capacity, COP, pressure drop, dew point and wet-bulb effectiveness respectively. The presented regression model is swift in operation and can be used in prediction, optimization and design of the GIDPC to commercialize this technology.

The second ML model is based on the DNN algorithm which is more flexible, accurate and efficient compared to the MPR. Ten different models are compared by calibrating the hyperparameters of the models and the one with MSE of 0.04 and R2 of 1 was selected. The structure of the selected DNN model had one input layer which contained seven operating and design parameters, two hidden layers with 45 neurons in each layer and one output layer which contained six performance parameters of the GIDPC. Eventually, the supply air temperature of the GIDPC in the selected climates are compared with the numerical results to examine the efficiency of the model.

In addition, this research is pioneered in bringing XAI to the GIDPC research studies by employing the game theory based SHAP method. For the newly evolving XAI, this is considered as a preliminary approach which is conducted using the SHAP method to demonstrate the features (performance and design parameters) contributions on the predicted parameters throughout the force plots which is based on the DNN model.

7.3.3. Evolutionary optimisations

Three different models based on GA, PSO and SMA as the metaheuristic optimisations are used to optimise the system performance in 2020 and 2050. Four climates with one representative city for each are selected to compare the performance of the base system with the optimized systems. The climate data revealed that in general, the operating hours increase from 2020 to 2050 as a result of global warming. However, it is possible to reduce power consumption through the optimisation.

The main outcomes of this study are summarised as follows:

The results revealed that the optimum intake air velocity by all three methods was 2 (m/s) in all climates which was lower than the velocity in the base system, i.e., 3 (m/s). Moreover, the optimum working air ratio derived by GA was in the range of 0.21-0.25, the height and channel gap were in the ranges of 0.80-0.84, 0.005-0.006 respectively while the optimum number of layers held the same value of 160 in all climates. The optimum working air ratio by PSO methods in all four climates was in the range of $0.24 - 0.27$ which were lower than the working air ratio in the base system, i.e., 0.44. The optimum HMX height identified by PSO is 0.80 (m) which was lower than the base system height, i.e., 1 (m). Base on the PSO method, the optimum channel gap in tropical rainforest climate was 0.006 (m) while it was same as the base system, i.e., 0.005(m), in other climates. The number of layers in the base system was 160

while the optimum numbers in PSO ranged from 170.11 to 200.00. The optimum working air ratio by SMA method in all four climates were in the range of 0.22 – 0.27 which were lower than the working air ratio in the base system, i.e., 0.44. The optimum HMX height identified by SMA was in the narrow range of 0.80-0.82 (m) which was lower than the base system height, i.e., 1 (m). Based on SMA results, the HMX gap held the optimum value of 0.004 (m) in hot summer continental and arid climates, and 0.006 (m) in tropical rainforest and Mediterranean hot summer climates. The number of layers in the base system was 160 while the optimum numbers in SMA were in the range of 128.03-199.86.

The optimization results revealed that in general, performance of the optimized system in terms of COP outperform the base system in all climates in both 2020 and 2050. The surface area of the optimized system by GA has decreased in all climates. However, in the SMA's selected scenario (No.1) it was same as the base system in the tropical rainforest climate whereas it has decreased to the values of 40.70(m^2), 44.99(m^2), and 51.19(m^2) in hot summer, arid and tropical Mediterranean climates respectively. But in the optimized system by PSO, it has only decreased in the Arid climate, i.e., 53.78(m^2) and it is almost unchanged in all other climates.

In spite of more operating hours in 2050, the power consumption of the optimized systems was estimated to substantially decrease. The power consumption of the base system in all climates was in the range of 165.67- 647.34 (kWh) while it has reduced to the ranges of 51-210.22 (kWh), 65.13-234.09 (kWh) and 50.83-209.46 (kWh) by GA, PSO and SMA systems respectively. This has resulted in power savings of up to 72%, 69.49%, 63.24%, and 69.21% in hot summer, Arid, tropical rainforest and tropical Mediterranean climates respectively, compared to the base system in the same operating conditions.

The comparison of the models proved that the SMA has the following advantages over the PSO and GA: I) It is a novel optimization algorithm, II) The SMA is fast and it diverges to an optimal solution quickly, and III) The algorithm has low computational complexity.

7.4. Future studies

The identified gap in the literature is now filled by, firstly, experimental investigation of the monthly performance of the GIDPC in diverse climates, secondly, by developing the ML and optimisation models which could identify the optimum operating and design parameters of the GIDPC. Several studies can be undertaken to further complete and challenge the outcomes of this study which are explained below.

7.4.1. Improvement of Machine Learning models

The final selected DNN model can be challenged by a new superior model. The superior model can include data from real operation of the GIDPC in different applications. This can contribute to improving the accuracy of the developed models which will lead to more realistic predictions. The constructed dataset in the current study is mainly based on the numerical data. This is because the GIDPC is not commercialised yet and there was no real time data to be considered. By commercialising the GIDPC and operating it over time, in different regions, the volume of the real data will increase which can build a massive dataset comprising the real operating conditions. As a consequence, more robust ML models will be required to get trained through the new comprehensive and real data. Apart from this, owing to

the rapid progress in the field of data science, new algorithms can be developed which can outperform the current models by removing the current limitations.

7.4.2. Construction of new GIDPCs

In regard to the results derived from the optimisation algorithms, new prototypes with optimum operating and design conditions can be constructed to challenge the achieved results in this study. This will be more economical to commercialise the system by considering the optimisation results. As there is no GIDPC in operation with the derived optimisation results, therefore, it would be beneficial to examine the outcomes of this study by investigating the performance of the GIDPC practically. Furthermore, similar to the ML models, the outcome of the current study can be challenged using the new optimisation algorithms. Superior ML models can be used in the optimisation algorithms as the fitness function to observe the results of the new methods and compare them with the current algorithms.

REFERENCES

[1]   C. Yap *et al.*, "Air-con system efficiency primer: a summary."

[2]   L. Lecamwasam, J. Wilson, and D. Chokolich, "Guide to best practice maintenance & operation of HVAC systems for energy efficiency," 2012.

[3]   B. E.-B. plc: London, undefined UK, and undefined 2018, "BP Energy Outlook," *oilandgasforum.ru*, Accessed: Aug. 07, 2020. [Online]. Available: http://oilandgasforum.ru/data/files/Presentations/III NNF/Derbentsov.pdf.

[4]   S. UNFCCC, "Report of the Conference of the Parties on its twenty-first session, held in Paris from 30 November to 13 December 2015. Addendum. Part two: Action," 2015.

[5]   U. Secretariat, . "Part Two: Action Taken by the Conference of the Parties at Its Twenty-First Session. United Nations Framework Convention on Climate Change, Geneva," 2015.

[6]   D. Bosseboeuf, L. Gynther, B. Lapillonne, K. P.-O.-M. project, and undefined 2015, "Energy efficiency trends and policies in the household and tertiary sectors an analysis based on the ODYSSEE and MURE databases."

[7]   Z. Duan *et al.*, "Indirect evaporative cooling: Past, present and future potentials," *Renewable and Sustainable Energy Reviews*, vol. 16, no. 9. Elsevier Ltd, pp. 6823–6850, Dec. 01, 2012, doi: 10.1016/j.rser.2012.07.007.

[8]   T. Abergel, B. Dean, J. D.-U. E. and I. E. Agency, and undefined 2017, "Towards a zero-emission, efficient, and resilient buildings and construction sector: Global Status Report 2017."

[9]   P. Xu, "Investigation of a super performance dew point air cooler and its application in buildings," 2017.

[10]   L. Pérez-Lombard, J. Ortiz, and C. Pout, "A review on buildings energy

REFERENCES

consumption information," *Energy Build.*, vol. 40, no. 3, pp. 394–398, 2008, doi: 10.1016/j.enbuild.2007.03.007.

[11] A. E. Kabeel and M. Abdelgaied, "Numerical and experimental investigation of a novel configuration of indirect evaporative cooler with internal baffles," *Energy Convers. Manag.*, vol. 126, pp. 526–536, Oct. 2016, doi: 10.1016/j.enconman.2016.08.028.

[12] S. Anisimov, D. Pandelidis, and J. Danielewicz, "Numerical analysis of selected evaporative exchangers with the Maisotsenko cycle," *Energy Convers. Manag.*, vol. 88, pp. 426–441, Dec. 2014, doi: 10.1016/j.enconman.2014.08.055.

[13] "2004 ASHRAE HANDBOOK HVAC Systems and Equipment I-P Edition Supported by ASHRAE Research." Accessed: Jun. 29, 2020. [Online]. Available: http://www.ashrae.org.

[14] H. Caliskan, I. Dincer, and A. Hepbasli, "Exergoeconomic, enviroeconomic and sustainability analyses of a novel air cooler," in *Energy and Buildings*, Dec. 2012, vol. 55, pp. 747–756, doi: 10.1016/j.enbuild.2012.03.024.

[15] K. J. Chua, S. K. Chou, W. M. Yang, and J. Yan, "Achieving better energy-efficient air conditioning - A review of technologies and strategies," *Applied Energy*, vol. 104. Elsevier Ltd, pp. 87–104, Apr. 01, 2013, doi: 10.1016/j.apenergy.2012.10.037.

[16] P. Glanville, A. Kozlov, and V. Maisotsenko, "Dew Point Evaporative Cooling: Technology Review and Fundamentals."

[17] L. E. gas and electric Company, "Laboratory Evaluation of the Coolerado cooler indirect evaporative cooling unit," 2006.

[18] V. Maisotsenko, L. Gillan, … T. H.-U. P., and undefined 2003, "Method and

plate apparatus for dew point evaporative cooler," 2003. Accessed: Jun. 02, 2020. [Online]. Available: https://patents.google.com/patent/US6581402B2/en.

[19] R. Tariq, C. Zhan, N. Ahmed Sheikh, and X. Zhao, "Thermal Performance Enhancement of a Cross-Flow-Type Maisotsenko Heat and Mass Exchanger Using Various Nanofluids," *Energies*, vol. 11, no. 10, p. 2656, Oct. 2018, doi: 10.3390/en11102656.

[20] J. Lin, D. T. Bui, R. Wang, and K. J. Chua, "The counter-flow dew point evaporative cooler: Analyzing its transient and steady-state behavior," *Appl. Therm. Eng.*, vol. 143, pp. 34–47, Oct. 2018, doi: 10.1016/j.applthermaleng.2018.07.092.

[21] S. K. Jha, J. Bilalovic, A. Jha, N. Patel, and H. Zhang, "Renewable energy: Present research and future scope of Artificial Intelligence," *Renewable and Sustainable Energy Reviews*, vol. 77. Elsevier Ltd, pp. 297–317, Sep. 01, 2017, doi: 10.1016/j.rser.2017.04.018.

[22] S. T. Smith, V. I. Hanby, and C. Harpham, "A probabilistic analysis of the future potential of evaporative cooling systems in a temperate climate," *Energy Build.*, vol. 43, no. 2–3, pp. 507–516, Feb. 2011, doi: 10.1016/j.enbuild.2010.10.016.

[23] H. El-Dessouky, H. Ettouney, and A. Al-Zeefari, "Performance analysis of two-stage evaporative coolers," *Chem. Eng. J.*, vol. 102, no. 3, pp. 255–266, Sep. 2004, doi: 10.1016/j.cej.2004.01.036.

[24] O. Amer, R. Boukhanouf, and H. G. Ibrahim, "A Review of Evaporative Cooling Technologies," *Int. J. Environ. Sci. Dev.*, vol. 6, no. 2, pp. 111–117, 2015, doi: 10.7763/ijesd.2015.v6.571.

REFERENCES

[25] R. Z. Wang and T. S. Ge, *Advances in Solar Heating and Cooling*. 2016.

[26] "Vapor-compression refrigeration - Wikipedia." https://en.wikipedia.org/wiki/Vapor-compression_refrigeration (accessed Oct. 01, 2020).

[27] S. and P. C. in S. C. Patients, B. A. R. Hassan, Z. B. M. Yusoff, M. A. H. and S. Bin Othman, A. information is available at the end of the Chapter, and Http://dx.doi.org/10.5772/55358, "Thermal Analysis of an Absorption and Adsorption Cooling Chillers Using a Modulating Tempering Valve," *Intech*, p. 13, 2012, doi: 10.1016/j.colsurfa.2011.12.014.

[28] M. Kilic and M. Anjrini, "Comparative performance analysis of a combined cooling system with mechanical and adsorption cycles," *Energy Convers. Manag.*, vol. 221, p. 113208, Oct. 2020, doi: 10.1016/j.enconman.2020.113208.

[29] K. Daou, R. Z. Wang, and Z. Z. Xia, "Desiccant cooling air conditioning: A review," *Renewable and Sustainable Energy Reviews*, vol. 10, no. 2. pp. 55–77, Apr. 2006, doi: 10.1016/j.rser.2004.09.010.

[30] H. R. Goshayshi, J. F. Missenden, and R. Tozer, "Cooling tower - an energy conservation resource," *Appl. Therm. Eng.*, vol. 19, no. 11, pp. 1223–1235, Nov. 1999, doi: 10.1016/S1359-4311(98)00119-7.

[31] Q. Chen, K. Yang, M. Wang, N. Pan, and Z. Y. Guo, "A new approach to analysis and optimization of evaporative cooling system I: Theory," *Energy*, vol. 35, no. 6, pp. 2448–2454, Jun. 2010, doi: 10.1016/j.energy.2010.02.037.

[32] Q. Chen, N. Pan, and Z. Y. Guo, "A new approach to analysis and optimization of evaporative cooling system II: Applications," *Energy*, vol. 36, no. 5, pp. 2890–2898, May 2011, doi: 10.1016/j.energy.2011.02.031.

[33] Y. Golizadeh Akhlaghi *et al.*, "A constraint multi-objective evolutionary optimization of a state-of-the-art dew point cooler using digital twins," *Energy Convers. Manag.*, 2020, doi: 10.1016/j.enconman.2020.112772.

[34] X. Zhao, J. M. Li, and S. B. Riffat, "Numerical study of a novel counter-flow heat and mass exchanger for dew point evaporative cooling," *Appl. Therm. Eng.*, vol. 28, no. 14–15, pp. 1942–1951, Oct. 2008, doi: 10.1016/j.applthermaleng.2007.12.006.

[35] C. Zhan, Z. Duan, X. Zhao, S. Smith, H. Jin, and S. Riffat, "Comparative study of the performance of the M-cycle counter-flow and cross-flow heat exchangers for indirect evaporative cooling - Paving the path toward sustainable cooling of buildings," *Energy*, vol. 36, no. 12, pp. 6790–6805, Dec. 2011, doi: 10.1016/j.energy.2011.10.019.

[36] S. Delfani, J. Esmaeelian, H. Pasdarshahri, and M. Karami, "Energy saving potential of an indirect evaporative cooler as a pre-cooling unit for mechanical cooling systems in Iran," *Energy Build.*, vol. 42, no. 11, pp. 2169–2176, Nov. 2010, doi: 10.1016/j.enbuild.2010.07.009.

[37] G. P. Maheshwari, F. Al-Ragom, and R. K. Suri, "Energy-saving potential of an indirect evaporative cooler," *Appl. Energy*, vol. 69, no. 1, pp. 69–76, May 2001, doi: 10.1016/S0306-2619(00)00066-0.

[38] P. Xu, X. Ma, X. Zhao, and K. Fancey, "Experimental investigation of a super performance dew point air cooler," *Appl. Energy*, vol. 203, pp. 761–777, Oct. 2017, doi: 10.1016/j.apenergy.2017.06.095.

[39] "ASHRAE 133-2008." https://www.techstreet.com/standards/ashrae-133-2008?product_id=1590625 (accessed May 29, 2020).

[40] "ASHRAE 143-2015." https://www.techstreet.com/standards/ashrae-143-

2015?product_id=1891325 (accessed May 29, 2020).

[41] Standards Association of Australia., *Evaporative airconditioning equipment.* Standards Australia, 2000.

[42] M. H. Saidi, B. Sajadi, and P. Sayyadi, "Energy consumption criteria and labeling program of wet cooling towers in Iran," *Energy Build.*, vol. 43, no. 10, pp. 2712–2717, Oct. 2011, doi: 10.1016/j.enbuild.2011.06.016.

[43] B. of Indian Standards, "IS 3315 (1994): Evaporative Air Coolers (desert coolers)," 1994.

[44] "C22.2 No.104-M1983 | Standards Council of Canada - Conseil canadien des normes." https://www.scc.ca/en/standardsdb/standards/2806 (accessed May 29, 2020).

[45] S. B. Riffat and J. Zhu, "Mathematical model of indirect evaporative cooler using porous ceramic and heat pipe," *Appl. Therm. Eng.*, vol. 24, no. 4, pp. 457–470, Mar. 2004, doi: 10.1016/j.applthermaleng.2003.09.011.

[46] "Australian Standard 2913-1987: Evapourative Air-Conditioning Equipment : 9780726244278." .

[47] A. H.-I. . Atlanta, U. GA, and USA, "American society of heating, refrigerating and air-conditioning engineers," 2009.

[48] F. Yuan, Q. C.- Energy, and undefined 2012, "A global optimization method for evaporative cooling systems based on the entransy theory," *Elsevier*, Accessed: Aug. 09, 2020. [Online]. Available: https://www.sciencedirect.com/science/article/pii/S0360544212002733?casa_token=ssscbPmO3JkAAAAA:8DK0wjDDnsSBEO5I8MmjOn_9ebp77pJwB YjHk6fS7UwUyUqcAvRdzJKatY-NIGFIf9hbZv9ltFyO.

[49] J. Santos, G. Barros, … J. G.-I. J. of, and undefined 2013, "Energy and exergy

REFERENCES

analysis applied to the evaporative cooling process in air washers," *Elsevier*, Accessed: Aug. 09, 2020. [Online]. Available: https://www.sciencedirect.com/science/article/pii/S0140700712003556?casa_token=HD3j7h3XX6wAAAAA:XfQvIxawuNZHTEeHMbjAIxXFrQdQvaPcVs1-3u3d_aXdL3doXuAvDlLPcoCdpTY42urGh_CJz5tX.

[50] M. Farmahini-Farahani, S. Delfani, J. E.- Energy, and undefined 2012, "Exergy analysis of evaporative cooling to select the optimum system in diverse climates," *Elsevier*, Accessed: Aug. 09, 2020. [Online]. Available: https://www.sciencedirect.com/science/article/pii/S0360544212000904?casa_token=jIev2ZN455QAAAAA:x_MoUNzV9OJcYfxSq4SW7TzHrFFwYXX7uggA9_uc3eM2xRf1MxZk2NVEkY7RrlQ2c8uCDOe0zLAx.

[51] H. Caliskan, I. Dincer, A. H.-E. and buildings, and undefined 2011, "Exergetic and sustainability performance comparison of novel and conventional air cooling systems for building applications," *Elsevier*, Accessed: Aug. 09, 2020. [Online]. Available: https://www.sciencedirect.com/science/article/pii/S0378778811000508?casa_token=23K3J3CV7zwAAAAA:xL-DXvuKE0czYyq_KWf8pJ9KKgiv1gjiHv22KgvsPQOnkag8KzPIH_Mo9NYNUKx-F_d8xEmRDohA.

[52] T. Zhang, X. Liu, H. Tang, J. Liu, Y. J.-E. and Buildings, and undefined 2016, "Exergy and entransy analyses in air-conditioning system part 1—Similarity and distinction," *Elsevier*, Accessed: Aug. 09, 2020. [Online]. Available: https://www.sciencedirect.com/science/article/pii/S037877881630665X?casa_token=ryURoc17YY8AAAAA:K2IJ_7BSUApPPtOnt1YNiS31wNjzhSp0Sa4nzk2mSi0XQvAXJqYsZxfwtDJKbooTikZVCD39UQwg.

REFERENCES

[53] T. Zhang, X. Liu, J. Liu, H. Tang, Y. J.-E. and Buildings, and undefined 2017, "Exergy and entransy analyses in air-conditioning system part 2—Humid air handling process," *Elsevier*, Accessed: Aug. 09, 2020. [Online]. Available: https://www.sciencedirect.com/science/article/pii/S0378778817300117?casa_token=eSR5g92Up_QAAAAA:izF_-0ewBBh4yYe1ds2Otr2-N3r-ghB0p-MJHFiPP8L1AzpfKkwf5wXCLbXjPtseXwm7wKB22u0V.

[54] T. Zhang, X. Liu, X. Xiang, J. Liu, Y. J.-E. and Buildings, and undefined 2017, "Performance investigation of terminal handling process in air-conditioning system from the perspective of entransy dissipation," *Elsevier*, Accessed: Aug. 09, 2020. [Online]. Available: https://www.sciencedirect.com/science/article/pii/S0378778816318795?casa_token=IV_8huijO3cAAAAA:H1cyhZV946icTp1qMx9HRqIg1KPdoAz5Sh2c0xwwzrqRXmNwzRgR3He688etXGCRdDFxyUnEc4Lz.

[55] Y. Jiang, X. X.-S. Energy, and U. 2010, "Theoretical and testing performance of an innovative indirect evaporative chiller," *Elsevier*.

[56] R. Armbruster and J. Mitrovic, "Evaporative cooling of a falling water film on horizontal tubes," *Exp. Therm. Fluid Sci.*, vol. 18, no. 3, pp. 183–194, Nov. 1998, doi: 10.1016/S0894-1777(98)10033-X.

[57] F. J. R. Martínez, E. V. Gómez, R. H. Martín, J. M. Gutiérrez, and F. V. Diez, "Comparative study of two different evaporative systems: An indirect evaporative cooler and a semi-indirect ceramic evaporative cooler," in *Energy and Buildings*, Jul. 2004, vol. 36, no. 7, pp. 696–708, doi: 10.1016/j.enbuild.2003.10.010.

[58] E. V. Gómez, F. J. R. Martínez, F. V. Diez, M. J. M. Leyva, and R. H. Martín, "Description and experimental results of a semi-indirect ceramic evaporative

cooler," *Int. J. Refrig.*, vol. 28, no. 5, pp. 654–662, Aug. 2005, doi: 10.1016/j.ijrefrig.2005.01.004.

[59] V. Vakiloroaya, B. Samali, A. Fakhar, and K. Pishghadam, "A review of different strategies for HVAC energy saving," *Energy Convers. Manag.*, vol. 77, pp. 738–754, Jan. 2014, doi: 10.1016/j.enconman.2013.10.023.

[60] Y. Huang and J. lei Niu, "A review of the advance of HVAC technologies as witnessed in ENB publications in the period from 1987 to 2014," *Energy Build.*, vol. 130, pp. 33–45, Oct. 2016, doi: 10.1016/j.enbuild.2016.08.036.

[61] R. Best and W. Rivera, "A review of thermal cooling systems," *Appl. Therm. Eng.*, vol. 75, pp. 1162–1175, Jan. 2015, doi: 10.1016/j.applthermaleng.2014.08.018.

[62] A. Tejero-González, M. Andrés-Chicote, P. García-Ibáñez, E. Velasco-Gómez, and F. J. Rey-Martínez, "Assessing the applicability of passive cooling and heating techniques through climate factors: An overview," *Renewable and Sustainable Energy Reviews*, vol. 65. Elsevier Ltd, pp. 727–742, Nov. 01, 2016, doi: 10.1016/j.rser.2016.06.077.

[63] S. P. Jain, S. D. Suryawanshi, T. M. Chordia, N. Nenwani, H. Bawaskar, and S. Yambal, *Efficient Technique of Air-Conditioning Suraj Yambal Efficient Technique of Air-Conditioning*. 2011.

[64] R. Pacheco, J. Ordóñez, and G. Martínez, "Energy efficient design of building: A review," *Renewable and Sustainable Energy Reviews*, vol. 16, no. 6. Pergamon, pp. 3559–3573, Aug. 01, 2012, doi: 10.1016/j.rser.2012.03.045.

[65] F. Kojok, F. Fardoun, R. Younes, and R. Outbib, "Hybrid cooling systems: A review and an optimized selection scheme," *Renewable and Sustainable Energy Reviews*, vol. 65. Elsevier Ltd, pp. 57–80, Nov. 01, 2016, doi:

REFERENCES

10.1016/j.rser.2016.06.092.

[66]   H. M. Daraghmeh and C. C. Wang, "A review of current status of free cooling in datacenters," *Appl. Therm. Eng.*, vol. 114, pp. 1224–1239, Mar. 2017, doi: 10.1016/j.applthermaleng.2016.10.093.

[67]   M. Rafique, P. Gandhidasan, … S. R.-… and S. E., and undefined 2015, "A review on desiccant based evaporative cooling systems," *Elsevier*, Accessed: Aug.   11,   2020.   [Online].   Available: https://www.sciencedirect.com/science/article/pii/S1364032115000611?casa_ token=uclypWCoXDQAAAAA:77F64_BJuIe6XL8cuTZZ5Qw32kkmYk7Z7 AsyW4DMu4NBYTI6URxFLY70lrPVm3lMH7OQlp0Df6H-.

[68]   Z. Han *et al.*, "Simulation study on the operating characteristics of the heat pipe for combined evaporative cooling of computer room air-conditioning system," *Energy*, vol. 98, pp. 15–25, Mar. 2016, doi: 10.1016/j.energy.2016.01.009.

[69]   Y. S. H. Najjar and A. M. Abubaker, "Indirect evaporative combined inlet air cooling with gas turbines for green power technology," *Int. J. Refrig.*, vol. 59, pp. 235–250, Nov. 2015, doi: 10.1016/j.ijrefrig.2015.07.001.

[70]   M. Farmahini-Farahani and G. Heidarinejad, "Increasing effectiveness of evaporative cooling by pre-cooling using nocturnally stored water," *Appl. Therm.   Eng.*,   vol.   38,   pp.   117–123,   May   2012,   doi: 10.1016/j.applthermaleng.2012.01.023.

[71]   C. Cianfrini, M. Corcione, E. Habib, and A. Quintino, "Energy performance of air-conditioning systems using an indirect evaporative cooling combined with a cooling/reheating treatment," *Energy Build.*, vol. 69, pp. 490–497, Feb. 2014, doi: 10.1016/j.enbuild.2013.11.030.

[72]   H. T. El-Dessouky, H. M. Ettouney, and W. Bouhamra, "A novel air

conditioning system: Membrane air drying and evaporative cooling," *Chem. Eng. Res. Des.*, vol. 78, no. 7, pp. 999–1009, Oct. 2000, doi: 10.1205/026387600528111.

[73]   S. M. Huang and L. Z. Zhang, "Researches and trends in membrane-based liquid desiccant air dehumidification," *Renewable and Sustainable Energy Reviews*, vol. 28. Pergamon, pp. 425–440, Dec. 01, 2013, doi: 10.1016/j.rser.2013.08.005.

[74]   Z. Chen, J. Zhu, H. Bai, Y. Yan, and L. Zhang, "Experimental study of a membrane-based dehumidification cooling system," *Appl. Therm. Eng.*, vol. 115, pp. 1315–1321, Mar. 2017, doi: 10.1016/j.applthermaleng.2016.10.153.

[75]   O. Labban, T. Chen, A. F. Ghoniem, J. H. Lienhard, and L. K. Norford, "Next-generation HVAC: Prospects for and limitations of desiccant and membrane-based dehumidification and cooling," *Appl. Energy*, vol. 200, pp. 330–346, Aug. 2017, doi: 10.1016/j.apenergy.2017.05.051.

[76]   B. Yang, W. Yuan, Y. Shang, J. Wang, and Bin Wei, "Numerical and experimental study of a novel three-fluid membrane dehumidification method applied to spacecraft humidity control," *J. Memb. Sci.*, vol. 530, pp. 112–124, May 2017, doi: 10.1016/j.memsci.2017.02.022.

[77]   D. B. Jani, M. Mishra, and P. K. Sahoo, "Solid desiccant air conditioning - A state of the art review," *Renewable and Sustainable Energy Reviews*, vol. 60. Elsevier Ltd, pp. 1451–1469, Jul. 01, 2016, doi: 10.1016/j.rser.2016.03.031.

[78]   K. S. Rambhad, P. V. Walke, and D. J. Tidke, "Solid desiccant dehumidification and regeneration methods - A review," *Renewable and Sustainable Energy Reviews*, vol. 59. Elsevier Ltd, pp. 73–83, Jun. 01, 2016, doi: 10.1016/j.rser.2015.12.264.

[79]   L. Pistocchini, S. Garone, and M. Motta, "Air dehumidification by cooled adsorption in silica gel grains. Part I: Experimental development of a prototype," *Appl. Therm. Eng.*, vol. 107, pp. 888–897, Aug. 2016, doi: 10.1016/j.applthermaleng.2016.06.103.

[80]   L. Pistocchini, S. Garone, and M. Motta, "Air dehumidification by cooled adsorption in silica gel grains. Part II: Theoretical analysis of the prototype testing results," *Appl. Therm. Eng.*, vol. 110, pp. 1682–1689, Jan. 2017, doi: 10.1016/j.applthermaleng.2016.06.104.

[81]   J. Woods and E. Kozubal, "A desiccant-enhanced evaporative air conditioner: Numerical model and experiments," *Energy Convers. Manag.*, vol. 65, pp. 208–220, Jan. 2013, doi: 10.1016/j.enconman.2012.08.007.

[82]   A. T. Mohammad, S. Bin Mat, M. Y. Sulaiman, K. Sopian, and A. A. Al-Abidi, "Historical review of liquid desiccant evaporation cooling technology," *Energy and Buildings*, vol. 67. Elsevier, pp. 22–33, Dec. 01, 2013, doi: 10.1016/j.enbuild.2013.08.018.

[83]   M. H. Kim, J. Y. Park, S. W. Ham, and J. W. Jeong, "Energy conservation benefit of water-side free cooling in a liquid desiccant and evaporative cooling-assisted 100% outdoor air system," *Energy Build.*, vol. 104, pp. 302–315, Aug. 2015, doi: 10.1016/j.enbuild.2015.07.029.

[84]   M. S. Buker, B. Mempouo, and S. B. Riffat, "Experimental investigation of a building integrated photovoltaic/thermal roof collector combined with a liquid desiccant enhanced indirect evaporative cooling system," *Energy Convers. Manag.*, vol. 101, pp. 239–254, Jun. 2015, doi: 10.1016/j.enconman.2015.05.026.

[85]   A. H. Abdel-Salam and C. J. Simonson, "State-of-the-art in liquid desiccant air

conditioning equipment and systems," *Renewable and Sustainable Energy Reviews*, vol. 58. Elsevier Ltd, pp. 1152–1183, May 01, 2016, doi: 10.1016/j.rser.2015.12.042.

[86] F. Fakhrabadi and F. Kowsary, "Optimal design of a hybrid liquid desiccant-regenerative evaporative air conditioner," *Energy Build.*, vol. 133, pp. 141–154, Dec. 2016, doi: 10.1016/j.enbuild.2016.09.048.

[87] H. J. Kim, S. J. Lee, S. H. Cho, and J. W. Jeong, "Energy benefit of a dedicated outdoor air system over a desiccant-enhanced evaporative air conditioner," *Appl. Therm. Eng.*, vol. 108, pp. 804–815, Sep. 2016, doi: 10.1016/j.applthermaleng.2016.07.185.

[88] M. H. Kim, H. W. Dong, J. Y. Park, and J. W. Jeong, "Primary energy savings in desiccant and evaporative cooling-assisted 100% outdoor air system combined with a fuel cell," *Appl. Energy*, vol. 180, pp. 446–456, Oct. 2016, doi: 10.1016/j.apenergy.2016.08.004.

[89] X. She, Y. Yin, Y. Dong, and X. Zhang, "Investigation on air flow patterns of evaporative cooling and dehumidification process for a hybrid refrigeration system," *Appl. Therm. Eng.*, vol. 95, pp. 79–94, Feb. 2016, doi: 10.1016/j.applthermaleng.2015.11.044.

[90] X. Cui, M. R. Islam, B. Mohan, and K. J. Chua, "Theoretical analysis of a liquid desiccant based indirect evaporative cooling system," *Energy*, vol. 95, pp. 303–312, Jan. 2016, doi: 10.1016/j.energy.2015.12.032.

[91] J. H. Lee, G. H. Ro, Y. T. Kang, Y. S. Chang, S. C. Kim, and Y. L. Kim, "Combined heat and mass transfer analysis for LiCl dehumidification process in a plate type heat exchanger," *Appl. Therm. Eng.*, vol. 96, pp. 250–257, Mar. 2016, doi: 10.1016/j.applthermaleng.2015.11.040.

[92] S. J. Lee, H. J. Kim, H. W. Dong, and J. W. Jeong, "Energy saving assessment of a desiccant-enhanced evaporative cooling system in variable air volume applications," *Appl. Therm. Eng.*, vol. 117, pp. 94–108, May 2017, doi: 10.1016/j.applthermaleng.2017.02.007.

[93] H. W. Dong, S. J. Lee, D. S. Yoon, J. Y. Park, and J. W. Jeong, "Impact of district heat source on primary energy savings of a desiccant-enhanced evaporative cooling system," *Energy*, vol. 123, pp. 432–444, Mar. 2017, doi: 10.1016/j.energy.2017.02.005.

[94] F. Zhang, Y. Yin, and X. Zhang, "Performance analysis of a novel liquid desiccant evaporative cooling fresh air conditioning system with solution recirculation," *Build. Environ.*, vol. 117, pp. 218–229, May 2017, doi: 10.1016/j.buildenv.2017.03.015.

[95] F. Bruno, "On-site experimental testing of a novel dew point evaporative cooler," *Energy Build.*, vol. 43, no. 12, pp. 3475–3483, Dec. 2011, doi: 10.1016/j.enbuild.2011.09.013.

[96] E. Gómez, A. González, F. M.-A. Energy, and U. 2012, "Experimental characterisation of an indirect evaporative cooling prototype in two operating modes," *Elsevier*.

[97] X. Zhao, S. Liu, and S. B. Riffat, "Comparative study of heat and mass exchanging materials for indirect evaporative cooling systems," *Build. Environ.*, vol. 43, no. 11, pp. 1902–1911, Nov. 2008, doi: 10.1016/j.buildenv.2007.11.009.

[98] N. Shrivastava, R. Gandhi, P. Vishwavidyalaya, and V. Shrivastava, "Performance Evaluation of Alternative Evaporative Cooling Media Performance evaluation of double pass solar air heater with storage effect View

project," 2014. Accessed: Aug. 11, 2020. [Online]. Available: https://www.researchgate.net/publication/305351539.

[99] R. K. Kulkarni and S. P. S. Rajput, "COMPARATIVE PERFORMANCE ANALYSIS OF EVAPORATIVE COOLING PADS OF ALTERNATIVE CONFIGURATIONS AND MATERIALS," 2013.

[100] N. Soponpongpipat and S. Kositchaimongkol, "Recycled High-Density polyethylene and rice husk as a wetted pad in evaporative cooling system," *Am. J. Appl. Sci.*, vol. 8, no. 2, pp. 186–191, 2011, doi: 10.3844/ajassp.2011.186.191.

[101] F. Al-Sulaiman, "Evaluation of the performance of local fibers in evaporative cooling," *Energy Convers. Manag.*, vol. 43, no. 16, pp. 2267–2273, Nov. 2002, doi: 10.1016/S0196-8904(01)00121-2.

[102] B. Niyomvas and B. Potakarat, "Performance study of cooling pads," in *Advanced Materials Research*, 2013, vol. 664, pp. 931–935, doi: 10.4028/www.scientific.net/AMR.664.931.

[103] Pescod D, "Unit air cooler using plastic heat exchanger with evaporatively cooled plates," *Aust. Refrig. Air Cond. Heat.*, 1969.

[104] A. Malli, H. R. Seyf, M. Layeghi, S. Sharifian, and H. Behravesh, "Investigating the performance of cellulosic evaporative cooling pads," *Energy Convers. Manag.*, vol. 52, no. 7, pp. 2598–2603, Jul. 2011, doi: 10.1016/j.enconman.2010.12.015.

[105] J. K. Jain and D. A. Hindoliya, "Experimental performance of new evaporative cooling pad materials," *Sustain. Cities Soc.*, vol. 1, no. 4, pp. 252–256, Dec. 2011, doi: 10.1016/j.scs.2011.07.005.

[106] M. Barzegar, M. Layeghi, G. Ebrahimi, Y. Hamzeh, and M. Khorasani,

"Experimental evaluation of the performances of cellulosic pads made out of Kraft and NSSC corrugated papers as evaporative media," *Energy Convers. Manag.*, vol. 54, no. 1, pp. 24–29, Feb. 2012, doi: 10.1016/j.enconman.2011.09.016.

[107] P. Xu, X. Ma, X. Zhao, and K. S. Fancey, "Experimental investigation on performance of fabrics for indirect evaporative cooling applications," *Build. Environ.*, vol. 110, pp. 104–114, Dec. 2016, doi: 10.1016/j.buildenv.2016.10.003.

[108] I. Maclaine-Cross and P. Banks, "A general theory of wet surface heat exchangers and its application to regenerative evaporative cooling," 1981.

[109] N. Stoitchkov, G. D.-I. journal of Refrigeration, and U. 1998, "Effectiveness of crossflow plate heat exchanger for indirect evaporative cooling: Efficacité des échangeurs thermiques à plaques, à courants croises pour," *Elsevier*.

[110] J. Alonso, F. Martinez, … E. G.-E. and, and U. 1998, "Simulation model of an indirect evaporative cooler," *Elsevier*.

[111] D. Pescod, "A heat exchanger for energy saving in an air-conditioning plant," 1979.

[112] P. Erens, A. D.-I. journal of heat and mass Transfer, and U. 1993, "Modelling of indirect evaporative air coolers," *Elsevier*.

[113] B. H.-R. générale de thermique and U. 1998, "A general mathematical model of evaporative cooling devices," *Elsevier*.

[114] R. H. Poppe M, "Berechnung von Ru¨cku¨hlwerken: VDI-Wa¨rmeatlas," *Mi 1–Mi 15.*, 1991.

[115] F. Merkel, "Verdunstungsku¨hlung: VDI-Zeitchrift," *pp. 123-128*, 1925.

[116] C. Kettleborough and C. Hsieh, "The thermal performance of the wet surface

plastic plate heat exchanger used as an indirect evaporative cooler," 1983.

[117] X. Guo, T. Z.-I. communications in heat and mass Transfer, and U. 1998, "A parametric study of an indirect evaporative air cooler," *Elsevier*.

[118] C. Ren and H. Yang, "An analytical model for the heat and mass transfer processes in indirect evaporative cooling with parallel/counter flow configurations," *Int. J. Heat Mass Transf.*, vol. 49, no. 3–4, pp. 617–627, 2006, doi: 10.1016/j.ijheatmasstransfer.2005.08.019.

[119] H. Hettiarachchi, M. Golubovic, W. W.-A. Thermal, and U. 2007, "The effect of longitudinal heat conduction in cross flow indirect evaporative air coolers," *Elsevier*.

[120] T. R. Tulsidasani, R. L. Sawhney, S. P. Singh, and M. S. Sodha, "Recent research on an indirect evaporative cooler (IEC) Part 1: optimization of the COP," *Int. J. Energy Res.*, vol. 21, no. 12, pp. 1099–1108, Oct. 1997, doi: 10.1002/(SICI)1099-114X(19971010)21:12<1099::AID-ER311>3.0.CO;2-S.

[121] D. J.-B. and Environment and U. 2007, "Development and testing of two-stage evaporative cooler," *Elsevier*.

[122] B. Costelloe, D. F.-E. and Buildings, and U. 2007, "Thermal effectiveness characteristics of low approach indirect evaporative cooling systems in buildings," *Elsevier*.

[123] R. A. Davis, "Pacific Gas and Electric Company PY2005 Emerging Technologies Program Application Assessment Report #0402 Laboratory Evaluation of the Coolerado Cooler™ Indirect Evaporative Cooling Unit," 2006.

[124] B. Riangvilaikul and S. Kumar, "An experimental study of a novel dew point evaporative cooling system," *Energy Build.*, vol. 42, no. 5, pp. 637–644, May

2010, doi: 10.1016/j.enbuild.2009.10.034.

[125] M. Jradi and S. Riffat, "Experimental and numerical investigation of a dew-point cooling system for thermal comfort in buildings," *Appl. Energy*, vol. 132, pp. 524–535, Nov. 2014, doi: 10.1016/j.apenergy.2014.07.040.

[126] D. Pandelidis and S. Anisimov, "Numerical analysis of the heat and mass transfer processes in selected M-Cycle heat exchangers for the dew point evaporative cooling," *Energy Convers. Manag.*, vol. 90, pp. 62–83, Jan. 2015, doi: 10.1016/j.enconman.2014.11.008.

[127] P. Xu *et al.*, "Numerical investigation of the energy performance of a guideless irregular heat and mass exchanger with corrugated heat transfer surface for dew point cooling," *Energy*, vol. 109, pp. 803–817, Aug. 2016, doi: 10.1016/j.energy.2016.05.062.

[128] J. Lin, R. Z. Wang, M. Kumja, T. D. Bui, and K. J. Chua, "Multivariate scaling and dimensional analysis of the counter-flow dew point evaporative cooler," *Energy Convers. Manag.*, vol. 150, pp. 172–187, Oct. 2017, doi: 10.1016/j.enconman.2017.08.003.

[129] J. Lin, D. T. Bui, R. Wang, and K. J. Chua, "On the fundamental heat and mass transfer analysis of the counter-flow dew point evaporative cooler," *Appl. Energy*, vol. 217, pp. 126–142, May 2018, doi: 10.1016/j.apenergy.2018.02.120.

[130] Y. Wan, J. Lin, K. J. Chua, and C. Ren, "Similarity analysis and comparative study on the performance of counter-flow dew point evaporative coolers with experimental validation," *Energy Convers. Manag.*, vol. 169, pp. 97–110, Aug. 2018, doi: 10.1016/j.enconman.2018.05.043.

[131] J. Lin, S. M. Huang, R. Wang, and K. J. Chua, "Thermodynamic analysis of a

hybrid membrane liquid desiccant dehumidification and dew point evaporative cooling system," *Energy Convers. Manag.*, vol. 156, pp. 440–458, Jan. 2018, doi: 10.1016/j.enconman.2017.11.057.

[132] Y. Wan, J. Lin, K. J. Chua, and C. Ren, "A new method for prediction and analysis of heat and mass transfer in the counter-flow dew point evaporative cooler under diverse climatic, operating and geometric conditions," *Int. J. Heat Mass Transf.*, vol. 127, pp. 1147–1160, Dec. 2018, doi: 10.1016/j.ijheatmasstransfer.2018.07.142.

[133] Y. Liu, Y. G. Akhlaghi, X. Zhao, and J. Li, "Experimental and numerical investigation of a high-efficiency dew-point evaporative cooler," *Energy Build.*, vol. 197, 2019, doi: 10.1016/j.enbuild.2019.05.038.

[134] Y. Liu, J. M. Li, X. Yang, and X. Zhao, "Two-dimensional numerical study of a heat and mass exchanger for a dew-point evaporative cooler," *Energy*, vol. 168, pp. 975–988, Feb. 2019, doi: 10.1016/j.energy.2018.11.135.

[135] R. Mitchell, J. Michalski, and T. Carbonell, *An artificial intelligence approach*. 2013.

[136] Ibrahim Dincer and Marc A. Rosen, *Optimization of Energy Systems*. 2019.

[137] X. S. Yang, *Nature-Inspired Optimization Algorithms*. Elsevier Inc., 2014.

[138] X. Li and R. Yao, "A machine-learning-based approach to predict residential annual space heating and cooling loads considering occupant behaviour," *Energy*, vol. 212, p. 118676, Dec. 2020, doi: 10.1016/j.energy.2020.118676.

[139] H. Sun, H. V. Burton, and H. Huang, "Machine Learning Applications for Building Structural Design and Performance Assessment: State-of-the-Art Review," *J. Build. Eng.*, p. 101816, Sep. 2020, doi: 10.1016/j.jobe.2020.101816.

REFERENCES

[140] T. Hong, Z. Wang, X. Luo, and W. Zhang, "State-of-the-art on research and applications of machine learning in the building life cycle," *Energy and Buildings*, vol. 212. Elsevier Ltd, p. 109831, Apr. 01, 2020, doi: 10.1016/j.enbuild.2020.109831.

[141] Y. Zhou, S. Zheng, and G. Zhang, "A state-of-the-art-review on phase change materials integrated cooling systems for deterministic parametrical analysis, stochastic uncertainty-based design, single and multi-objective optimisations with machine learning applications," *Energy and Buildings*, vol. 220. Elsevier Ltd, p. 110013, Aug. 01, 2020, doi: 10.1016/j.enbuild.2020.110013.

[142] J. G. Koomey, "GROWTH IN DATA CENTER ELECTRICITY USE 2005 TO 2010," 2011. Accessed: Oct. 05, 2020. [Online]. Available: http://www.koomey.comhttp//www.analyticspress.com/datacenters.html.

[143] J. Gao and R. Jamidar, "Machine Learning Applications for Data Center Optimization," *Google White Pap.*, pp. 1–13, 2014.

[144] https://www.menerga-adria.com/, "DATA CENTERS, COOLING AND AI." .

[145] Https://deepmind.com/, "DeepMind AI Reduces Google Data Centre Cooling Bill by 40%." .

[146] S. Yang, M. P. Wan, W. Chen, B. F. Ng, and S. Dubey, "Model predictive control with adaptive machine-learning-based model for building energy efficiency and comfort optimization," *Appl. Energy*, vol. 271, no. January, p. 115147, 2020, doi: 10.1016/j.apenergy.2020.115147.

[147] D. Pandelidis and S. Anisimov, "Application of a statistical design for analyzing basic performance characteristics of the cross-flow Maisotsenko cycle heat exchanger," *Int. J. Heat Mass Transf.*, vol. 95, pp. 45–61, Apr. 2016, doi: 10.1016/j.ijheatmasstransfer.2015.11.060.

[148] A. Sohani, H. Sayyaadi, and S. Hoseinpoori, "Modélisation et optimisation à objectifs multiples d'un refroidisseur évaporatif indirect à écoulements croisés à cycle M en utilisant le réseau neuronal de type GMDH," *Int. J. Refrig.*, vol. 69, pp. 186–204, Sep. 2016, doi: 10.1016/j.ijrefrig.2016.05.011.

[149] H. Jafarian, H. Sayyaadi, and F. Torabi, "Modeling and optimization of dew-point evaporative coolers based on a developed GMDH-type neural network," *Energy Convers. Manag.*, vol. 143, pp. 49–65, Jul. 2017, doi: 10.1016/j.enconman.2017.03.015.

[150] A. Sohani, H. Sayyaadi, and N. Mohammadhosseini, "Comparative study of the conventional types of heat and mass exchangers to achieve the best design of dew point evaporative coolers at diverse climatic conditions," *Energy Convers. Manag.*, vol. 158, pp. 327–345, Feb. 2018, doi: 10.1016/j.enconman.2017.12.042.

[151] A. Sohani, H. Sayyaadi, and M. Zeraatpisheh, "Optimization strategy by a general approach to enhance improving potential of dew-point evaporative coolers," *Energy Convers. Manag.*, vol. 188, pp. 177–213, May 2019, doi: 10.1016/j.enconman.2019.02.079.

[152] A. Pakari and S. Ghani, "Regression models for performance prediction of counter flow dew point evaporative cooling systems," *Energy Convers. Manag.*, vol. 185, pp. 562–573, Apr. 2019, doi: 10.1016/j.enconman.2019.02.025.

[153] J. Lin, R. Wang, C. Li, S. Wang, J. Long, and K. J. Chua, "Towards a thermodynamically favorable dew point evaporative cooler via optimization," *Energy Convers. Manag.*, vol. 203, p. 112224, Jan. 2020, doi: 10.1016/j.enconman.2019.112224.

REFERENCES

[154] W. van der Aalst and W. van der Aalst, "Data Science in Action," in *Process Mining*, Springer Berlin Heidelberg, 2016, pp. 3–23.

[155] F. Provost and T. Fawcett, "Data Science and its Relationship to Big Data and Data-Driven Decision Making," *Big Data*, vol. 1, no. 1, pp. 51–59, Mar. 2013, doi: 10.1089/big.2013.1508.

[156] L. L. Pipino, Y. W. Lee, and R. Y. Wang, "Data Quality Assessment," *Commun. ACM*, vol. 45, no. 4, pp. 211–218, Apr. 2002, doi: 10.1145/505248.506010.

[157] undefined KPMG, "Now or Never: 2016 Global CEO Outlook," 2016.

[158] T. Schutz, "The 2016 Global Data Management Benchmark Report," 2016.

[159] P. Amaral, J. Dinis, P. Pinto, L. Bernardo, J. Tavares, and H. S. Mamede, "Machine learning in software defined networks: Data collection and traffic classification," in *Proceedings - International Conference on Network Protocols, ICNP*, Dec. 2016, vol. 2016-December, doi: 10.1109/ICNP.2016.7785327.

[160] Y. Roh, G. Heo, and S. E. Whang, "A Survey on Data Collection for Machine Learning: A Big Data - AI Integration Perspective," *IEEE Trans. Knowl. Data Eng.*, pp. 1–1, Oct. 2019, doi: 10.1109/tkde.2019.2946162.

[161] D. A. Keim, "Visual Exploration of Large Data Sets," *Commun. ACM*, vol. 44, no. 8, pp. 38–44, Aug. 2001, doi: 10.1145/381641.381656.

[162] "Feature Engineering for Machine Learning: Principles and Techniques for Data ... - Alice Zheng, Amanda Casari - Google Books." .

[163] L. Ehrlinger, V. Haunschmid, D. Palazzini, and C. Lettner, "A DaQL to Monitor Data Quality in Machine Learning Applications," in *Lecture Notes in Computer Science (including subseries Lecture Notes in Artificial Intelligence*

and Lecture Notes in Bioinformatics), Aug. 2019, vol. 11706 LNCS, pp. 227–237, doi: 10.1007/978-3-030-27615-7_17.

[164] H. Foidl and M. Felderer, "Risk-based data validation in machine learning-based software systems," in *MaLTeSQuE 2019 - Proceedings of the 3rd ACM SIGSOFT International Workshop on Machine Learning Techniques for Software Quality Evaluation, co-located with ESEC/FSE 2019*, Aug. 2019, vol. 19, pp. 13–18, doi: 10.1145/3340482.3342743.

[165] Z. Li, X. Ma, and H. Xin, "Feature engineering of machine-learning chemisorption models for catalyst design," *Catal. Today*, vol. 280, pp. 232–238, Feb. 2017, doi: 10.1016/j.cattod.2016.04.013.

[166] "Feature Engineering for Machine Learning and Data Analytics - Google Books." .

[167] J. Heaton, "An empirical analysis of feature engineering for predictive modeling," in *Conference Proceedings - IEEE SOUTHEASTCON*, Jul. 2016, vol. 2016-July, doi: 10.1109/SECON.2016.7506650.

[168] Y. G. Akhlaghi, X. Zhao, S. Shittu, A. Badiei, M. E. G. V. Cattaneo, and X. Ma, "Statistical investigation of a dehumidification system performance using Gaussian process regression," *Energy Build.*, vol. 202, 2019, doi: 10.1016/j.enbuild.2019.109406.

[169] "Machine Learning Benchmarks and Random Forest Regression." .

[170] A. Balaji and A. Allen, "Benchmarking Automatic Machine Learning Frameworks," Aug. 2018, Accessed: Aug. 14, 2020. [Online]. Available: http://arxiv.org/abs/1808.06492.

[171] Y. G. Akhlaghi, X. Ma, X. Zhao, S. Shittu, and J. Li, "A statistical model for dew point air cooler based on the multiple polynomial regression approach,"

REFERENCES

Energy, vol. 181, 2019, doi: 10.1016/j.energy.2019.05.213.

[172] Y. Chen, H. Yang, and Y. Luo, "Parameter sensitivity analysis and configuration optimization of indirect evaporative cooler (IEC) considering condensation," *Appl. Energy*, vol. 194, pp. 440–453, May 2017, doi: 10.1016/j.apenergy.2016.06.121.

[173] Y. Bi, W. Yang, and X. Zhao, "Numerical investigation of a solar/waste energy driven sorption/desorption cycle employing a novel adsorbent bed," *Energy*, vol. 149, pp. 84–97, Apr. 2018, doi: 10.1016/j.energy.2018.02.021.

[174] Weather and Climate, "Climate and average monthly weather in Beijing, Rome, Las Vegas, Riyadh," 2019. .

[175] O. Zienkiewicz and P. Morice, *The finite element method in engineering science*. 1971.

[176] O. Zienkiewicz, R. Taylor, R. Taylor, and R. Taylor, *The finite element method: solid mechanics*. 2000.

[177] K. Huebner, D. Dewhirst, D. Smith, and T. Byrom, *The finite element method for engineers*. 2001.

[178] J. Jin, *The finite element method in electromagnetics*. 2015.

[179] O. C. Zienkiewicz, R. L. Taylor, and J. Z. Zhu, "The Finite Element Method: Its Basis and Fundamentals Sixth edition," 2005. Accessed: Aug. 14, 2020. [Online]. Available: www.cimne.upc.es.

[180] G. E. Fasshauer, "Newton iteration with multiquadrics for the solution of nonlinear PDEs," *Comput. Math. with Appl.*, vol. 43, no. 3–5, pp. 423–438, Feb. 2002, doi: 10.1016/S0898-1221(01)00296-6.

[181] S. García, J. Luengo, and F. Herrera, *Data preprocessing in data mining*. 2015.

[182] S. Kotsiantis, D. Kanellopoulos, P. P.-I. J. of, and undefined 2006, "Data

preprocessing for supervised leaning," 2006. Accessed: Aug. 14, 2020. [Online]. Available: http://citeseerx.ist.psu.edu/viewdoc/download?doi=10.1.1.104.8413&rep=rep 1&type=pdf.

[183] S. García, S. Ramírez-Gallego, J. Luengo, J. M. Benítez, and F. Herrera, "Big data preprocessing: methods and prospects," *Big Data Anal.*, vol. 1, no. 1, Dec. 2016, doi: 10.1186/s41044-016-0014-0.

[184] P. Cichosz, *Data Mining Algorithms*. John Wiley & Sons, Ltd, 2015.

[185] S. Chaudhary, N. Singh, A. Pathak, and A. K. Vatsa, "Energy Efficient Techniques for Data aggregation and collection in WSN," *Int. J. Comput. Sci. Eng. Appl.*, vol. 2, no. 4, 2012, doi: 10.5121/ijcsea.2012.2405.

[186] "Principles of Artificial Intelligence - Nils J. Nilsson - Google Books." .

[187] E. Charniak, "Introduction to artificial intelligence," 1985, doi: 10.2514/6.1986-163.

[188] A. Bundy, "Preparing for the future of Artificial Intelligence," *AI Soc.*, vol. 32, no. 2, pp. 285–287, May 2017, doi: 10.1007/s00146-016-0685-0.

[189] B. Goertzel, "Artificial General Intelligence: Concept, State of the Art, and Future Prospects," *J. Artif. Gen. Intell.*, vol. 5, no. 1, pp. 2013–2015, 2014, doi: 10.2478/jagi-2014-0001.

[190] B. Goertzel, P. W.-A. in artificial general intelligence, and undefined 2007, "A foundational architecture for artificial general intelligence," *books.google.com*, Accessed: Aug. 14, 2020. [Online]. Available: https://books.google.com/books?hl=en&lr=&id=t2G5srpFRhEC&oi=fnd&pg =PA36&dq=Artificial+General+Intelligence+&ots=hA2SnXQLR6&sig=mlD LvM2dH4zQusWXcrXe-km-05I.

[191] K. S. Gill, "Artificial super intelligence: beyond rhetoric," vol. 31, pp. 137–143, 2016, doi: 10.1007/s00146-016-0651-x.

[192] M. Mohri, A. Rostamizadeh, and A. Talwalkar, *Foundations of machine learning*. 2018.

[193] I. Goodfellow, Y. Bengio, A. Courville, and Y. Bengio, *Deep learning*. 2016.

[194] Y. LeCun, Y. Bengio, G. H.- nature, and undefined 2015, "Deep learning," *nature.com*, Accessed: Aug. 14, 2020. [Online]. Available: https://idp.nature.com/authorize/casa?redirect_uri=https://www.nature.com/articles/nature14539&casa_token=vuW5I1MNVU0AAAAA:t9gnwV9hsAeIZZpAu6wIYF4pLfAW8woHg352IV39TSSm-BCPyDqSd52idNS4VIxaynsr4N5S_B3Yky23VVQ.

[195] Ö. Genç, "Notes on Artificial Intelligence, Machine Learning and Deep Learning for curious people," *Towards data science*, 2019. .

[196] T. M.-B. Ridge, I. M. Hill, and undefined 1997, "Machine learning. 1997."

[197] Alpaydin Ethem, "Introduction to Machine Learning - Ethem Alpaydin - Google Books," *Massachusetts Institute of Technology*, 2020. .

[198] Dietterich Thomas G, "Machine-learning research: Four current directions," *AI Mag.*, vol. 18, no. 4, pp. 97–136, Dec. 1997, doi: 10.1609/aimag.v18i4.1324.

[199] P. Lison, "An introduction to machine learning." Accessed: Aug. 14, 2020. [Online]. Available: http://folk.uio.no/plison/pdfs/talks/machinelearning.pdf.

[200] H. Anandakumar and K. Umamaheswari, "Supervised machine learning techniques in cognitive radio networks during cooperative spectrum handovers," *Cluster Comput.*, vol. 20, no. 2, pp. 1505–1515, Jun. 2017, doi: 10.1007/s10586-017-0798-3.

[201] S. Chatterjee and A. Hadi, *Regression analysis by example*. 2015.

[202] T. Ryan, *Modern regression methods*. 2008.

[203] W. Y. Loh, "Classification and regression trees," *Wiley Interdiscip. Rev. Data Min. Knowl. Discov.*, vol. 1, no. 1, pp. 14–23, 2011, doi: 10.1002/widm.8.

[204] https://www.javatpoint.com/, "Regression vs. Classification in Machine Learning." .

[205] Z. Ghahramani, "Unsupervised learning," *Lect. Notes Comput. Sci. (including Subser. Lect. Notes Artif. Intell. Lect. Notes Bioinformatics)*, vol. 3176, pp. 72–112, 2004, doi: 10.1007/978-3-540-28650-9_5.

[206] H. B. Barlow, "Unsupervised Learning," *Neural Comput.*, vol. 1, no. 3, pp. 295–311, Sep. 1989, doi: 10.1162/neco.1989.1.3.295.

[207] C. W. Nathan Landman, Hannah Pang, "k-Means Clustering," *https://brilliant.org/*. .

[208] L. Pack Kaelbling, M. L. Littman, A. W. Moore, and S. Hall, "Reinforcement Learning: A Survey," 1996. Accessed: Aug. 14, 2020. [Online]. Available: https://www.jair.org/index.php/jair/article/view/10166.

[209] R. Sutton and A. Barto, *Reinforcement learning: An introduction*. 2018.

[210] Y. LeCun, Y. Bengio, G. H.- nature, and undefined 2015, "Deep learning," *nature.com*, Accessed: Aug. 14, 2020. [Online]. Available: https://idp.nature.com/authorize/casa?redirect_uri=https://www.nature.com/articles/nature14539&casa_token=cuuFvm1WfJwAAAAA:auvbbPollV_--IHrGjusNl8OGhfmq-l0LOSpHfrkxJeom2DoTef0ERD517P9RIGBron9euxyCG-WlZlkmGM.

[211] K. Willems, "Keras Tutorial: Deep Learning in Python," *https://www.datacamp.com/*, 2019. .

[212] S. Lawrence, C. Giles, A. T.-… on neural networks, and undefined 1997, "Face

recognition: A convolutional neural-network approach," *ieeexplore.ieee.org*, Accessed: Aug. 14, 2020. [Online]. Available: https://ieeexplore.ieee.org/abstract/document/554195/?casa_token=OImORgF Ffr4AAAAA:QlLq9DEd0gdyWaa5S0l1tRGw4hV9NsqId8PhQtEIoJ0jzQKk AihbKueHb9H2ZGWKkR6yp6MG4YjdDp8.

[213] S. Weisberg, *Applied Linear Regression Third Edition*. 2005.

[214] S. Ruder, "An overview of gradient descent optimization algorithms," Sep. 2016, Accessed: Aug. 14, 2020. [Online]. Available: http://arxiv.org/abs/1609.04747.

[215] A. Pant, "Introduction to Linear Regression and Polynomial Regression," *https://medium.com/*, 2019. .

[216] S. Chatterjee and A. Hadi, *Regression analysis by example*. 2015.

[217] D. Tarkhov and A. Vasilyev, *Semi-empirical Neural Network Modeling and Digital Twins Development*. 2019.

[218] P. Ramachandran, B. Zoph, and Q. V Le Google Brain, "SEARCHING FOR ACTIVATION FUNCTIONS." Accessed: Aug. 14, 2020. [Online]. Available: https://arxiv.org/abs/1710.05941.

[219] Y. Chauvin and D. Rumelhart, *Backpropagation: theory, architectures, and applications*. 1995.

[220] H. O.-A. neural networks-models and applications and undefined 2016, "Bayesian regularized neural networks for small n big p data," *books.google.com*, Accessed: Aug. 14, 2020. [Online]. Available: https://books.google.com/books?hl=en&lr=&id=1G-QDwAAQBAJ&oi=fnd&pg=PA27&dq="Bayesian+regularized+neural+netw orks+for+small+n+big+p+data,"+Artificial+Neural+Networks-

Models+and+Applications&ots=nJgzGfG8lF&sig=X41aUR2d2f3HnGQcNG
_cmCmLghw.

[221] Y. Yang, "Information Theory, Inference, and Learning Algorithms," *J. Am. Stat. Assoc.*, vol. 100, no. 472, pp. 1461–1462, Dec. 2012, doi: 10.1198/jasa.2005.s54.

[222] ASHERE, "Design Considerations for datacom equipment centers," *Atlanta Am. Soc. Heating. Refrig. Air-Conditioning Eng.*, 2009.

[223] M. Kottek, J. Grieser, C. Beck, B. Rudolf, and F. Rubel, "World Map of the Köppen-Geiger climate classification updated," *Meteorol. Zeitschrift*, vol. 15, no. 3, pp. 259–263, 2006, doi: 10.1127/0941-2948/2006/0130.

[224] D. Gunning, "Explainable Artificial Intelligence (XAI)," 2017. Accessed: Sep. 09, 2020. [Online]. Available: http://listverse.com/.

[225] A. Preece, D. Harborne, D. Braines, R. Tomsett, and S. Chakraborty, "Stakeholders in Explainable AI," Sep. 2018.

[226] A. Barredo Arrieta *et al.*, "Explainable Explainable Artificial Intelligence (XAI): Concepts, taxonomies, opportunities and challenges toward responsible AI," *Inf. Fusion*, vol. 58, pp. 82–115, Jun. 2020, doi: 10.1016/j.inffus.2019.12.012.

[227] S. M. Lundberg, P. G. Allen, and S.-I. Lee, "A Unified Approach to Interpreting Model Predictions," 2020.

[228] E. Štrumbelj and I. Kononenko, "Explaining prediction models and individual predictions with feature contributions," *Knowl. Inf. Syst.*, vol. 41, no. 3, pp. 647–665, Nov. 2014, doi: 10.1007/s10115-013-0679-x.

[229] A. Roth, *The Shapley value: essays in honor of Lloyd S. Shapley*. 1988.

[230] S. Lundberg, B. Nair, M. Vavilala, and … M. H.-N. biomedical, "Explainable

machine-learning predictions for the prevention of hypoxaemia during surgery," *nature.com*, 2918.

[231] A. J. Kulkarni and S. C. Satapathy, *Optimization in Machine Learning and Applications*, no. January. 2020.

[232] S. Boyd, S. Boyd, and L. Vandenberghe, *Convex optimization*. 2004.

[233] X. Yang, *Optimization techniques and applications with examples*. 2018.

[234] X.-S. Yang and X.-S. He, "Introduction to Optimization," 2019, pp. 1–20.

[235] W. H. Press, S. A. Teukolsky, H. A. Bethe, W. T. Vetterling, and B. P. Flannery, "NUMERICAL RECIPES The Art of Scientific Computing Third Edition," 2007. Accessed: Jul. 29, 2020. [Online]. Available: https://books.google.com/books?hl=en&lr=&id=1aAOdzK3FegC&oi=fnd&pg=PA1&dq=Press+WH,+Teukolsky+SA,+Vetterling+WT,+Flannery+BP+(2007)+Numerical+recipes:+the+art+of+scientific+computing,+3rd+edn.+Cambridge+University+Press,+Cambridge&ots=3kVmCeFmlj&sig=fhLpJT1W1mSHl4vW1sCxm_S7Lz0.

[236] L. Bottou, "Large-Scale Machine Learning with Stochastic Gradient Descent," in *Proceedings of COMPSTAT'2010*, Physica-Verlag HD, 2010, pp. 177–186.

[237] Wikipedia, "Metaheuristic," [Online]. Available: https://en.wikipedia.org/wiki/Metaheuristic#cite_note-nojhan07-8.

[238] B. Copeland, "The Essential Turing: Seminal Writing in Computing, Logic, Philosophy, Artificial Life Plus the Secrets of Enigma," 2004.

[239] Alan Turing, "Intelligent machinery," *Natl. Phys. Lab. Tech. Report, Teddingt.*, 1948.

[240] J. Holland, "1975, Adaptation in Natural and Artificial Systems, University of Michigan Press, Ann Arbor."

[241] L. Fogel, A. Owens, and M. Walsh, "Artificial intelligence through simulated evolution," 1966, Accessed: Jul. 29, 2020. [Online]. Available: https://cds.cern.ch/record/107769.

[242] J. P.- Reading, undefined MA, and undefined 1984, "Heuristics Addison-Wesley."

[243] S. Kirkpatrick, C. D. Gelatt, and M. P. Vecchi, "Optimization by simulated annealing," *Science (80-.).*, vol. 220, no. 4598, pp. 671–680, May 1983, doi: 10.1126/science.220.4598.671.

[244] F. Glover, "FUTURE PATHS FOR INTEGER PROGRAMMING AND LINKS TO AR TIFI CIAL INTELLI G EN CE," 1986. Accessed: Jul. 30, 2020. [Online]. Available: http://leeds-faculty.colorado.edu/glover/fred pubs/174 - Future Paths for Integer Programming TS.pdf.

[245] M. D.-P. Thesis, P. di Milano, and undefined 1992, "Optimization, learning and natural algorithms," *ci.nii.ac.jp*, Accessed: Jul. 30, 2020. [Online]. Available: https://ci.nii.ac.jp/naid/10000136323/.

[246] R. E.-95-I. C. on N. Kennedy, J and U. 1995, "Particle swarm optimization," *ieeexplore.ieee.org*, 1995, Accessed: Jul. 30, 2020. [Online]. Available: https://ieeexplore.ieee.org/abstract/document/488968/?casa_token=6KlWRe3J ydMAAAAA:pZYKP0Uz137TlaFK5-H8US0xZPZegvMFU8YKevhxbqm9ypocPyGiASuv5_D_27lkDIAsiUvupaos -F4.

[247] R. Storn and K. Price, "Differential Evolution - A Simple and Efficient Heuristic for Global Optimization over Continuous Spaces," *J. Glob. Optim.*, vol. 11, no. 4, pp. 341–359, 1997, doi: 10.1023/A:1008202821328.

[248] T. Joyce and J. M. Herrmann, "A review of no free lunch theorems, and their

implications for metaheuristic optimisation," in *Studies in Computational Intelligence*, vol. 744, Springer Verlag, 2018, pp. 27–51.

[249] D. Wolpert, W. M.-I. transactions on Evolutionary, and U. 1997, "No free lunch theorems for optimization," *ieeexplore.ieee.org*, 1997.

[250] S. Nakrani and C. Tovey, "On honey bees and dynamic server allocation in internet hosting centers," in *Adaptive Behavior*, 2004, vol. 12, no. 3–4, pp. 223–240, doi: 10.1177/105971230401200308.

[251] X. S. Yang, "Engineering optimizations via nature-inspired virtual bee algorithms," in *Lecture Notes in Computer Science*, 2005, vol. 3562, no. PART II, pp. 317–323, doi: 10.1007/11499305_33.

[252] D. Karaboga, "AN IDEA BASED ON HONEY BEE SWARM FOR NUMERICAL OPTIMIZATION," 2005. Accessed: Jul. 30, 2020. [Online]. Available: https://pdfs.semanticscholar.org/015d/f4d97ed1f541752842c49d12e429a7854 60b.pdf.

[253] X. Yang, S. D.-& biologically inspired computing (NaBIC), and undefined 2009, "Cuckoo search via Lévy flights," *ieeexplore.ieee.org*, Accessed: Jul. 30, 2020. [Online]. Available: https://ieeexplore.ieee.org/abstract/document/5393690/?casa_token=r1Z77g5k 8jIAAAAA:BkEPLO3o8RtPN-kkOQtQ4XP8haRu8k_Ce3N3_I-Yf7OnmnNo2_08YFfZrwBaC09IfPyTaa4uhup_LzU.

[254] X.-S. Yang, "A New Metaheuristic Bat-Inspired Algorithm, in: Nature Inspired Coop-erative Strategies for Optimization," Springer, 2010. Accessed: Jul. 30, 2020. [Online]. Available: https://link.springer.com/chapter/10.1007/978-3-642-12538-6_6.

[255] J. Altringham, T. McOwat, L. H.-N. York, and undefined 1996, "Bats: Biology and Behaviour: Oxford University Press."

[256] W. B.-S. behaviour and undefined 1991, "The behavioural ecology of finding resources," *... and Hall Anim. Behav. Ser.*

[257] Z. W. Geem, J. H. Kim, and G. V. Loganathan, "A New Heuristic Optimization Algorithm: Harmony Search," *Simulation*, vol. 76, no. 2, pp. 60–68, 2001, doi: 10.1177/003754970107600201.

[258] E. Rashedi, H. Nezamabadi-Pour, S. S.-I. sciences, and undefined 2009, "GSA: a gravitational search algorithm," *Elsevier*, Accessed: Jul. 30, 2020. [Online]. Available: https://www.sciencedirect.com/science/article/pii/S0020025509001200?casa_token=ppPvj1uPZZAAAAAA:iL0aT94DIZ4DL7JRubvk6HV0o7_tTk1wBhYbAjqFU9Vt5kwt6_0MgqXXcH7lSD-RsjLG-cjFX6vf.

[259] X. S. Yang, "Flower pollination algorithm for global optimization," in *Lecture Notes in Computer Science (including subseries Lecture Notes in Artificial Intelligence and Lecture Notes in Bioinformatics)*, 2012, vol. 7445 LNCS, pp. 240–249, doi: 10.1007/978-3-642-32894-7_27.

[260] J. N. Kang, Y. M. Wei, L. C. Liu, R. Han, B. Y. Yu, and J. W. Wang, "Energy systems for climate change mitigation: A systematic review," *Applied Energy*, vol. 263. Elsevier Ltd, p. 114602, Apr. 01, 2020, doi: 10.1016/j.apenergy.2020.114602.

[261] I. Adopted, "Climate Change 2014 Synthesis Report," 2014, Accessed: Aug. 05, 2020. [Online]. Available: ftp://atitlan.ethz.ch/docs/afischli/for-srinivasan/TS-01978822-Can't suppress pdf indexing during imports/Attached PDFs/Ip096.pdf.

[262] A. Moazami, V. Nik, S. Carlucci, S. G.-A. Energy, and U. 2019, "Impacts of future weather data typology on building energy performance–Investigating long-term patterns of climate change and extreme weather conditions," *Elsevier*.

[263] J. Holland and J. Holland, "Adaptation in natural and artificial systems: an introductory analysis with applications to biology, control, and artificial intelligence," 1975.

[264] M. Dowd, "A simple model for genetic algorithm convergence," *Int. J. Pure Appl. Math.*, 2010.

[265] "Genetic algorithms in search, optimization, and machine learning," *Choice Rev. Online*, 1989, doi: 10.5860/choice.27-0936.

[266] S. Forrest, "Genetic algorithms," in *Computer Science Handbook, Second Edition*, 2004.

[267] D. G.- Optimization, and MachineLearning, and undefined 1989, "Genetic algorithms in search," *ci.nii.ac.jp*, Accessed: Aug. 03, 2020. [Online]. Available: https://ci.nii.ac.jp/naid/10000038763/.

[268] M. Elarbi, S. Bechikh, A. Gupta, … L. S.-I. transactions on, and undefined 2017, "A new decomposition-based NSGA-II for many-objective optimization," *ieeexplore.ieee.org*, Accessed: Aug. 04, 2020. [Online]. Available:

https://ieeexplore.ieee.org/abstract/document/7866900/?casa_token=TvzZMhr

RPYkAAAAA:sW-bq2T8wvk-

yAXltniEBPipN82XjFGcS1QEV7VAvp43p0fyykZqZ6NE9dNXOXfmdXZ

WW0v1Z4EcJXY.

[269] X.-S. Yang, "Test Problems in Optimization," Aug. 2010, Accessed: Aug. 04,

2020. [Online]. Available: http://arxiv.org/abs/1008.0549.

[270] C. Zhan, X. Zhao, S. Smith, S. R.-B. and Environment, and undefined 2011, "Numerical study of a M-cycle cross-flow heat exchanger for indirect evaporative cooling," *Elsevier*, Accessed: Aug. 04, 2020. [Online]. Available: https://www.sciencedirect.com/science/article/pii/S0360132310002817?casa_ token=y5EZFnZxvmoAAAAA:l5BILHOR0tZwlFxgapznQO5qY_zU1n0Dpv JI1-xO-8xMiXfihOTTyONGvToQGkjamJlGoeOm4GJh.

[271] D. KESSLER, "Plasmodial Structure and Motility," in *Cell Biology of Physarum and Didymium*, Elsevier, 1982, pp. 145–208.

[272] T. Nakagaki, H. Yamada, and T. Ueda, "Interaction between cell shape and contraction pattern in the Physarum plasmodium," *Biophys. Chem.*, vol. 84, no. 3, pp. 195–204, May 2000, doi: 10.1016/S0301-4622(00)00108-3.

[273] M. B.-2015 I. I. C. on Systems and undefined 2015, "On the efficiency of nature-inspired algorithms for generation of fault-tolerant graphs," *ieeexplore.ieee.org*, Accessed: Aug. 05, 2020. [Online]. Available: https://ieeexplore.ieee.org/abstract/document/7379424/?casa_token=BstQwsp UIOsAAAAA:arBL6ZCkTpIx4HKRvC8hLUUyIx0i_DZvLLtFELIpSybIotbx hr9LDBVYSB9mxph3Bmjdud6WFyOJViY.

[274] V. Šešum-Čavić, E. Kühn, and D. Kanev, "Bio-inspired search algorithms for unstructured P2P overlay networks," *Swarm Evol. Comput.*, vol. 29, pp. 73–93, Aug. 2016, doi: 10.1016/j.swevo.2016.03.002.

[275] S. Li, H. Chen, M. Wang, A. A. Heidari, and S. Mirjalili, "Slime mould algorithm: A new method for stochastic optimization," *Futur. Gener. Comput. Syst.*, vol. 111, pp. 300–323, Oct. 2020, doi: 10.1016/j.future.2020.03.055.

[276] T. Latty and M. Beekman, "Food quality and the risk of light exposure affect

patch-choice decisions in the slime mold Physarum polycephalum," *Ecology*, vol. 91, no. 1, pp. 22–27, Jan. 2010, doi: 10.1890/09-0358.1.

[277] T. Latty and M. Beekman, "Speed–accuracy trade-offs during foraging decisions in the acellular slime mould *Physarum polycephalum*," *Proc. R. Soc. B Biol. Sci.*, vol. 278, no. 1705, pp. 539–545, Feb. 2011, doi: 10.1098/rspb.2010.1624.

[278] M. Beekman and T. Latty, "Brainless but Multi-Headed: Decision Making by the Acellular Slime Mould Physarum polycephalum," *Journal of Molecular Biology*, vol. 427, no. 23. Academic Press, pp. 3734–3743, Nov. 20, 2015, doi: 10.1016/j.jmb.2015.07.007.

[279] P. Kareiva and G. Odell, "Swarms of predators exhibit 'preytaxis' if individual predators use area-restricted search.," *Am. Nat.*, vol. 130, no. 2, pp. 233–270, 1987, doi: 10.1086/284707.

[280] T. Latty, M. B.-B. Ecology, and undefined 2009, "Food quality affects search strategy in the acellular slime mould, Physarum polycephalum," *academic.oup.com*, Accessed: Aug. 05, 2020. [Online]. Available: https://academic.oup.com/beheco/article-abstract/20/6/1160/199575.

[281] J. G. Digalakis and K. G. Margaritis, "On benchmarking functions for genetic algorithms," *Int. J. Comput. Math.*, 2001, doi: 10.1080/00207160108805080.

[282] H. Chen, Y. hang Peng, and Y. ling Wang, "Thermodynamic analysis of hybrid cooling system integrated with waste heat reusing and peak load shifting for data center," *Energy Convers. Manag.*, vol. 183, pp. 427–439, Mar. 2019, doi: 10.1016/j.enconman.2018.12.117.

[283] S. Dong, E. Kremers, M. Brucoli, R. Rothman, and S. Brown, "Techno-enviro-economic assessment of household and community energy storage in the UK,"

Energy Convers. Manag., vol. 205, p. 112330, Feb. 2020, doi: 10.1016/j.enconman.2019.112330.

[284] V. Depoorter, E. Oró, and J. Salom, "The location as an energy efficiency and renewable energy supply measure for data centres in Europe," *Appl. Energy*, vol. 140, pp. 338–349, Feb. 2015, doi: 10.1016/j.apenergy.2014.11.067.

[285] E. Oró, V. Depoorter, A. Garcia, and J. Salom, "Energy efficiency and renewable energy integration in data centres. Strategies and modelling review," *Renewable and Sustainable Energy Reviews*, vol. 42. Elsevier Ltd, pp. 429–445, Feb. 01, 2015, doi: 10.1016/j.rser.2014.10.035.

[286] C. Dupont, G. Giuliani, F. Hermenier, T. Schulze, and A. Somov, "An energy aware framework for virtual machine placement in cloud federated data centres," in *Proceedings of the 3rd International Conference on Future Energy Systems: "Where Energy, Computing and Communication Meet", e-Energy 2012*, 2012, doi: 10.1145/2208828.2208832.

[287] K. Ebrahimi, G. F. Jones, and A. S. Fleischer, "A review of data center cooling technology, operating conditions and the corresponding low-grade waste heat recovery opportunities," *Renewable and Sustainable Energy Reviews*, vol. 31. Elsevier Ltd, pp. 622–638, Mar. 01, 2014, doi: 10.1016/j.rser.2013.12.007.

[288] A. M. Haywood, J. Sherbeck, P. Phelan, G. Varsamopoulos, and S. K. S. Gupta, "The relationship among CPU utilization, temperature, and thermal power for waste heat utilization," *Energy Convers. Manag.*, vol. 95, pp. 297–303, May 2015, doi: 10.1016/j.enconman.2015.01.088.

[289] H. Moazamigoodarzi, P. J. Tsai, S. Pal, S. Ghosh, and I. K. Puri, "Influence of cooling architecture on data center power consumption," *Energy*, vol. 183, pp. 525–535, Sep. 2019, doi: 10.1016/j.energy.2019.06.140.

[290] D. L. Beaty, "Internal IT load profile variability," *ASHRAE J.*, vol. 55, no. 2, pp. 72–75, Feb. 2013, Accessed: Aug. 13, 2020. [Online]. Available: https://go.gale.com/ps/i.do?p=AONE&sw=w&issn=00012491&v=2.1&it=r&id=GALE%7CA348647991&sid=googleScholar&linkaccess=fulltext.

[291] M. Salim, R. T.-A. transactions, and undefined 2010, "Data Centers' Energy Auditing and Benchmarking-Progress Update.," *search.ebscohost.com*, Accessed: Aug. 13, 2020. [Online]. Available: http://search.ebscohost.com/login.aspx?direct=true&profile=ehost&scope=site&authtype=crawler&jrnl=00012505&AN=50842468&h=oELHxGzcvRD720BbFFEFgABgmqW96ZP%2BEXD9GrLP69adSa1iPcRnfeIvqKWGuB%2FrxShObCjbBlkCCVJ8kgnDUQ%3D%3D&crl=c&casa_token=PVEQxziF4_sAAAAA:Jf89zUu-aVK24MixR5PJOz82mB8joXlQhLBz5cSfBwaynp_Y_Rdm4Ymf9Hx4JZCZl7w7z1MjXZctN4ke.

[292] J. Cho, T. Lim, and B. S. Kim, "Measurements and predictions of the air distribution systems in high compute density (Internet) data centers," *Energy Build.*, vol. 41, no. 10, pp. 1107–1115, Oct. 2009, doi: 10.1016/j.enbuild.2009.05.017.

[293] J. Dai, D. Das, and M. Pecht, "Prognostics-based risk mitigation for telecom equipment under free air cooling conditions," *Appl. Energy*, vol. 99, pp. 423–429, Nov. 2012, doi: 10.1016/j.apenergy.2012.05.055.

[294] A. Almoli, A. Thompson, N. Kapur, J. Summers, H. Thompson, and G. Hannah, "Computational fluid dynamic investigation of liquid rack cooling in data centres," *Appl. Energy*, vol. 89, no. 1, pp. 150–155, Jan. 2012, doi: 10.1016/j.apenergy.2011.02.003.

[295] C. Patel, C. Bash, C. Belady, … L. S.-P. of, and undefined 2001, "Computational fluid dynamics modeling of high compute density data centers to assure system inlet air specifications," *hpl.americas.hp.net*, Accessed: Aug. 13, 2020. [Online]. Available: http://www.hpl.americas.hp.net/research/papers/power.pdf.

[296] E. Oró, V. Depoorter, N. Pflugradt, and J. Salom, "Overview of direct air free cooling and thermal energy storage potential energy savings in data centres," *Appl. Therm. Eng.*, vol. 85, pp. 100–110, Jun. 2015, doi: 10.1016/j.applthermaleng.2015.03.001.

[297] J. Dai, M. M. Ohadi, D. Das, and M. G. Pecht, *Optimum cooling of data centers: Application of risk assessment and mitigation techniques*. Springer New York, 2014.

[298] H. Zhang, S. Shao, H. Xu, H. Zou, and C. Tian, "Free cooling of data centers: A review," *Renewable and Sustainable Energy Reviews*, vol. 35. Elsevier Ltd, pp. 171–182, Jul. 01, 2014, doi: 10.1016/j.rser.2014.04.017.

[299] M. O. A.-C. Engineers, undefined Inc., undefined Atlanta, undefined GA, and undefined 2001, "Ashrae Fundamental Handbook."

[300] M. Pawlish and A. S. Varde, "Free cooling: A paradigm shift in data centers," in *Proceedings of the 2010 5th International Conference on Information and Automation for Sustainability, ICIAfS 2010*, 2010, pp. 347–352, doi: 10.1109/ICIAFS.2010.5715685.

[301] "Blog - Rocky Mountain Institute." https://rmi.org/rmi-insights/blog/ (accessed Aug. 11, 2020).

[302] ASHRAE, "Data center power equipment thermal guidelines and best practices. Wiretapper created by ASHRAE Technical Committee (TC) 9.9 Mission

Critical FacilitiesData Centers, Technology Spaces, and Electronic Equipment," 2016.

[303] ASHER, "Design Considerations for datacom equipment centers," *Atlanta Am. Soc. Heating. Refrig. Air-Conditioning Eng.*, 2009.

[304] J. Niemann, "Impact of Hot and Cold Aisle Containment on Data Center Temperature and Efficiency Revision 2." Accessed: Aug. 12, 2020. [Online]. Available: https://www.researchgate.net/publication/265533396.

[305] J. Ni and X. Bai, "A review of air conditioning energy performance in data centers," *Renewable and Sustainable Energy Reviews*, vol. 67. Elsevier Ltd, pp. 625–640, Jan. 01, 2017, doi: 10.1016/j.rser.2016.09.050.